

NASA CONTRACTOR
REPORT



NASA CR-847

NASA CR-847

LUNAR ORBITER I

PHOTOGRAPHY

Prepared by
THE BOEING COMPANY
Seattle, Wash.
for Langley Research Center

FACILITY FORM 602	N67-32334	
	(ACCESSION NUMBER)	(THRU)
	125	1
	(PAGES)	(CODE)
	CR-847	31
	(NASA CR OR TMX OR AD NUMBER)	(CATEGORY)

LUNAR ORBITER I

PHOTOGRAPHY

Distribution of this report is provided in the interest of information exchange. Responsibility for the contents resides in the author or organization that prepared it.

Issued by Originator as D2-100727-2

Prepared under Contract No. 1-3800 by
THE BOEING COMPANY
Seattle, Wash.

for Langley Research Center

NATIONAL AERONAUTICS AND SPACE ADMINISTRATION

For sale by the Clearinghouse for Federal Scientific and Technical Information
Springfield, Virginia 22151 - CFSTI price \$3.00

CONTENTS

Section *	Page No
2.0 PHOTOGRAPHY	1
2.1 PHOTOGRAPHIC MISSION	1
2.1.1 PHOTOGRAPHIC SUBSYSTEM FUNCTIONS	1
2.1.1.1 CAMERA	3
2.1.1.2 PROCESSOR - DRYER	5
2.1.1.3 READOUT SCANNER	5
2.1.1.4 GROUND RECONSTRUCTION SYSTEM	6
2.1.1.5 REASSEMBLY PROCESS	6
2.1.2 MISSION PHOTOGRAPHY	6
2.1.3 PHOTOGRAPHIC OBJECTIVES	8
2.1.4 PHOTOGRAPHIC SITES	8
2.1.4.1 SITE SELECTION CRITERIA	9
2.1.4.2 SITE LOCATION	9
2.2 MISSION PHOTOGRAPHS	11
2.2.1 DESCRIPTION PHOTOGRAPHS	11
2.2.1.1 GENERAL MISSION PHOTOGRAPHS	11
2.2.1.2 SITE PHOTOGRAPHS	17
2.2.1.3 OTHER PHOTOGRAPHS	33
2.2.2 RECONSTRUCTED RECORD	33
2.2.3 REASSEMBLED RECORD	34
2.2.4 STEREO COVERAGE	37
2.3 PHOTOGRAPHIC SUPPORTING DATA	38
2.4 PHOTOGRAPHIC SUBSYSTEM CALIBRATION	57
2.5 PHOTOGRAPHIC MISSION ANALYSIS	61
2.6 LANGLEY RESEARCH CENTER OPERATIONS	117
2.7 HIGH-RESOLUTION FILM SMEAR ANALYSIS	118

*The section number 2 signifies only that this report is the second in a series of numbered volumes submitted by the contractor on the Lunar Orbiter I Project. Publication of the complete series by NASA is not necessarily contemplated.

	Figures	Page No
Figure	2.1-1: Lunar Orbiter Photographic System	2
Figure	2.1-2 Camera Subsystem Schematic Diagram	3
Figure	2.1-3 Photographic Overlap and Coverage for Sequencing Modes	3
Figure	2.1-4: Film Format and Placement of Frames	4
Figure	2.1-5: Edge Data Format	4
Figure	2.1-6 Characteristics of Type SO-243 Film (H&D Curve)	5
Figure	2.1-7: Readout Subsystem Schematic	6
Figure	2.1-8 Reassembly Sequence	7
Figure	2.1-9 Mission I Primary Site Locations	9
Figure	2.2-1: Processor Stop Line	13
Figure	2.2-2 Bimat Supply Separation Line	14
Figure	2.2-3: Double Mark by Bimat Metering Roller	15
Figure	2.2-4 Examples of Processing Marks	16
Figure	2.2-5 Example of 610-mm and 80-mm Photography Site 1-2	18
Figure	2.2-6 Detail in 610-mm Photograph Frame 85 Dionysius	19
Figure	2.2-7: Noise Pattern	20
Figure	2.2-8 Site I-0 Coverage	21
Figure	2.2-9 Site I-1 Coverage	22
Figure	2.2-10 Site I-1 High Resolution Photo	23
Figure	2.2-11: Site 1-2 Coverage	24
Figure	2.2-12 Site 1-3 Coverage	25
Figure	2.2-13 Site I-4 Coverage	26
Figure	2.2-14: Site 1-5 Coverage	27
Figure	2.2-15 Site 1-6 Coverage	28
Figure	2.2-16: Site 1-6 Photographs -- Example of 610-mm and 80-mm Photography	29
Figure	2.2-17: Site 1-7 Coverage	30
Figure	2.2-18 Site 1-8.1 Coverage	31
Figure	2.2-19 Site 1-9.2 Coverage	32
Figure	2.2-20: Priority Readout Diagram	35
Figure	2.2-21: Reassembly Process Diagram	36
Figure	2.3-1: Photo Supporting - Data Flow	37
Figure	2.3-2 EVAL Program Tabulation (Sample)	43
Figure	2.3-3 Photographic Geometry	44
Figure	2.3-4 Corner Coordinate Designation Convention	46

	Figures (cont'd)	Page No
Figure 2.41:	Modulation Transfer Function- 80-mm Lens	58
Figure 2.42:	Lens Transmission - - 80-mm and 610-mm Lenses	58
Figure 2.43:	Radial and Tangential Distortion - 80-mm Lens	59
Figure 2.5-1:	Design of Earth-Moon Photograph Orbit 16	65
Figure 2.5-2:	Earth-Moon Geometry	66
Figure 2.5-3:	Earth-Moon-Spacecraft Geometry at Time of Photography	67
Figure 2.5-4:	Camera Axis Positioning	68
Figure 2.55:	Spacecraft Maneuvers	69
Figure 2.5-6:	Design of Earth-Moon Photograph Orbit 27	70
Figure 2.5-7:	Representation of Earth in Orbit 27 Photograph	70
Figure 2.5-8:	Camera Axis Positioning	71
Figure 2.5-9:	Reduction of Resolving Power Due to Multiple Reproduction	72
Figure 2.5-10:	Tone Reproduction	73
Figure 2.5-11:	1-N to 3-N Tone Reproduction	73
Figure 2.5-12:	1-N to 2-P Reproduction	73
Figure 2.5 13	V/H Ratio Site I-0	77
Figure 2.5-14:	V/H Ratio Test Site	77
Figure 2.5-15:	V/H Ratio Site I-1	78
Figure 2.5-16:	V/H Ratio Site I-2	78
Figure 2.5-17:	V/H Ratio Site I-3	78
Figure 2.5-18:	V/H Ratio Site I-4	78
Figure 2.5-19:	V/H Ratio Site I-5	78
Figure 2.5 20	V/H Ratio Site I-6	78
Figure 2.5-21:	V/H Ratio Site I-7	79
Figure 2.5-22:	V/H Ratio Site I-8.1	79
Figure 2.5-23:	V/H Ratio Site I-9.2a	79
Figure 2.5-24:	V/H Ratio Site I-9.2b	79
Figure 2.5-25:	Frequency Plot: Processor-off Duration	81
Figure 2.5-26:	Simultaneous Recording During Priority Readout	84
Figure 2.5-27:	Edge-Data Step Nine Density - Mission I	85
Figure 2.5-28:	Edge Data Densities - Effect of Video Gain Change	86
Figure 2.529:	Edge Data Densities - Final Readout	86
Figure 2.5-30:	Position of Processor Lines	87

	Figures (cont'd)	Page No
Figure 2.5-31:	Edge Data Densities, DSS-12	87
Figure 2.5-32:	Edge Data Densities, DSS-61 Before Masking	87
Figure 2.5-33:	Edge Data Densities, DSS-61 After Masking	88
Figure 2.5-34:	Nominal Edge Data Densities	88
Figure 2.5-35:	Effect of Bimat Dryout	88
Figure 2.5-36:	Edge Data Densities Readout Sequence 121	89
Figure 2.5-37:	Milgo Plot of Telemetry During Readout	90
Figure 2.5-38:	GRE Sensitometric Processing Curve, Emulsion SO-349-505-3	91
Figure 2.5-39:	GRE Sensitometric Processing Curve, Emulsion SO-349-525-36	91
Figure 2.5-40:	Sensitometric Curve for Stairstep Function	91
Figure 2.5-41:	Gyro Position, Crab Angle, and Maneuver During Photography Site I-0	97
Figure 2.5-42:	Gyro Position, Crab Angle, and Maneuver During Photography Site I-1	98
Figure 2.5-43:	Gyro Position, Crab Angle, and Maneuver During Photography Site I-2	99
Figure 2.5-44:	Gyro Position, Crab Angle, and Maneuver During Photography Site I-3	100
Figure 2.5-45:	Gyro Position, Crab Angle, and Maneuver During Photography Site I-4	101
Figure 2.5-46:	Gyro Position, Crab Angle, and Maneuver During Photography Site I-5	102
Figure 2.5-47:	Gyro Position, Crab Angle, and Maneuver During Photography Site I-6	103
Figure 2.5-48:	Gyro Position, Crab Angle, and Maneuver During Photography Site I-7	104
Figure 2.5-49:	Gyro Position, Crab Angle and Maneuver During Photography Site I-8.1	105
Figure 2.5-50:	Gyro Position, Crab Angle, and Maneuver During Photography Site I-9.2a	106
Figure 2.5-51:	Gyro Position, Crab Angle, and Maneuver During Photography Site I-9.2b	107
Figure 2.5-52:	Reassembly Printer Transfer Characteristic	108
Figure 2.5-53:	H & D Curve for Kodak Aerographic Duplicating Film, Type 5427	108
Figure 2.5-54:	Video Output Waveform	109
Figure 2.5-55:	MTF of GRE Amplifiers with 31 Peaking	110
Figure 2.5-56:	Spot Wobble	110

	Figures (cont'd)	Page No
Figure	2.5-57: Geometry of Kinetube-line Image Production	111
Figure	2.5-58: GRE Camera and Magazine Film-Threading Diagram	111
Figure	2.5-59: H & D Curve for 3 5mm Processor Control SO-349	111
Figure	2.5-60: Composite Signal Generator Waveform Diagrams	112
Figure	2.5-61: Spacecraft Film Density vs. GRE Film Density	113
Figure	2.5-62: Relationship Between N.H. Blue and Visual Densities for Bimat Processed SO-243	113
Figure	2.563: Video Signal Focus Conditions	114
Figure	2.564: Modulation Transfer Function of GRE Camera Lens	115
Figure	2.5-65: Modulation Transfer Function of Eastman Television Recording Film Type 5374	115
Figure	2.566: Reassembly Printer Gating System	115
Figure	2.5-67: Edge Data Test Pattern; Horizontal and Diagonal Groups	116
Figure	2.7-1: Shutter Trigger Positions in the IMC Cycle	118

	Tables	Page No
Table	2.1-1: Summary of Mission Photography	1
Table	2.2-1: Percent Forward Overlap	37
Table	2.3-1: Photographic Maneuver Angles	39
Table	2.3-2: Sources of Image Distortion	42
Table	2.3-3: Photo Supporting Data	47
Table	2.4-1: Photographic Subsystem Tests and Calibrations	57
Table	2.5-1: Predicted Site Albedoes	62
Table	2.5-2: Primary Site Phase Angles and Shutter Speeds	63
Table	2.5-3: Computation of Standard Deviation of Resolution Measurements	72
Table	2.5-4: V/H Sensor Duty Cycle	80
Table	2.5-5: Processing Record	82
Table	2.5-6: Normalization Procedures	92
Table	2.5-7: Site Parameter Summary QUAL Program	94
Table	2.5-8: Postmission QUAL Computations of Image Densities	95
Table	2.5-9: Spacecraft Attitude During Primary Site Photographs	95
Table	2.5-10: Spacecraft Attitude During Film Set	96
Table	2.7-1: Smear and Displacement Data	119

LUNAR ORBITER I

2.0 PHOTOGRAPHY

This volume of the Lunar Orbiter Mission I final report contains a complete description of the photographic results, specifically the reconstructed and reassembled photographic records. All data required to identify and analyze these pictures, including a brief description of the photographic subsystem functions, have been presented to provide a basis for understanding the limitations and constraints on the photography. A detailed description of this subsystem can be found in Photographic Subsystem Reference Handbook for the Lunar Orbiter, Eastman Kodak Company, L-018375-RU, March 15, 1966.

The photographs obtained by Lunar Orbiter I provide data on 262,000 square kilometers of the Moon's nearside to a level of detail over two orders of magnitude better than can be obtained from Earth. One hundred fifty ~~six~~ medium- and high-resolution photographs were taken of nine preselected sites within the principal area of interest, a band ± 5 degrees in lunar latitude and ± 45 degrees in longitude, within which a landing site for Apollo LM must be identified and verified. In addition, 45 medium- and high-resolution frames were exposed of nearside and farside areas of special interest, including an oblique view of the Moon's farside eastern limb with the Earth in the background. In all, over 3,000,000 square kilometers of the farside were photographed at a resolution of 250 meters, of which over 400,000 square kilometers were taken at a resolution of about 30 meters. Operation of the photographic subsystem, including the ground reconstruction and reassembly operations, was satisfactory with one major exception. Incorrect timing of the focal-plane shutter operation degraded the high-resolution photographs taken when the V/H sensor was operated. In some cases, however, qualitative information regarding surface detail down to a few meters in size may be derived from these photographs. Such information may be used to assist interpretation of corresponding areas shown in the 80-mm-lens photographs. Where exposure of the photographs taken by the 80-mm lens was satisfactory, resolution equivalent to 8 meters from the nominal altitude of 46 km was observed within the central area of the photographs. Minimum size of detectable features was larger in photographs overexposed ~~or~~ of low contrast.

2.1 PHOTOGRAPHIC MISSION

On August 14, 1966, the spacecraft was injected into an elliptical orbit about the Moon with a 199-km perilune, an 1850-km apolune, and an inclination of 12.05 ± 0.05 degrees. Four days were scheduled in this ellipse for determination of precise orbital characteristics and for proper target illumination. Photographic operations were initiated during Orbit 25 (August 18, 1966) with a series of camera operations to run ~~off~~ the film leader and move photographic film into the camera. A series of 20 exposures of Site I-0 centered at 92° E longitude, 0° latitude, were made on the next orbit from an altitude of 208 km. ~~This~~ photography was timed to permit read-out at Goldstone (DSIF-12) for early photographic subsystem evaluation, operational control, and special press releases.

The spacecraft was transferred into a second ellipse on August 21, at 09:44:58 GMT during Orbit 44. This ellipse, designed for photography of the specified sites,

had a perilune of 50 km. Site I-1 photography followed nine orbits of planned tracking to provide precise ellipse computation, and to await proper target illumination. Sites I-1, I-2, I-3, I-4, and I-5 were photographed in this ellipse. During Orbit 30, the spacecraft was placed in a third ellipse having an initial perilune of 40.5 km. Perturbations of the orbit by ~~Earth~~ and Moon ~~effects~~ resulted in an increase in perilune altitude to 48 km by completion of photography.

This change was made in an unsuccessful attempt to ~~correct~~ the focal-plane shutter operation. Photography of the remaining target sites, plus certain special nearside and farside exposures, was continued in this ellipse

A tabulation of all target site photography and the special nearside and farside exposures will be found in Table 2.1-1.

Site Photography	Frames Exposed	
I-0	20	
I-1	16	
I-2	16	
I-3	16	
I-4	8	
I-5	16	
I-6	8	
I-7	16	
I-8.1	8	
I-9.2a	16	
I-9.2b	16	
	<u>156</u>	
Other Photographs		
Nearside	17	
Farside	11	
Mission B Sites	15	
Earth	2	
Miscellaneous and Test*	<u>10</u>	
		<u>55</u>
Total Number of Exposures		211

*Includes four with thermal door closed; thus blank.

Table 2.1-1: Summary of Mission Photography

2.1.1 PHOTOGRAPHIC SUBSYSTEM FUNCTIONS

The Lunar Orbiter photographic subsystem shown schematically in Figure 2.1-1 was designed to obtain broad coverage at moderate resolution and limited coverage at high resolution within specific conditions of illumination and contrast. The Earth-based equipment was designed to reconstruct the photographs to close density tolerance and with a minimum resolution loss between copy generations.

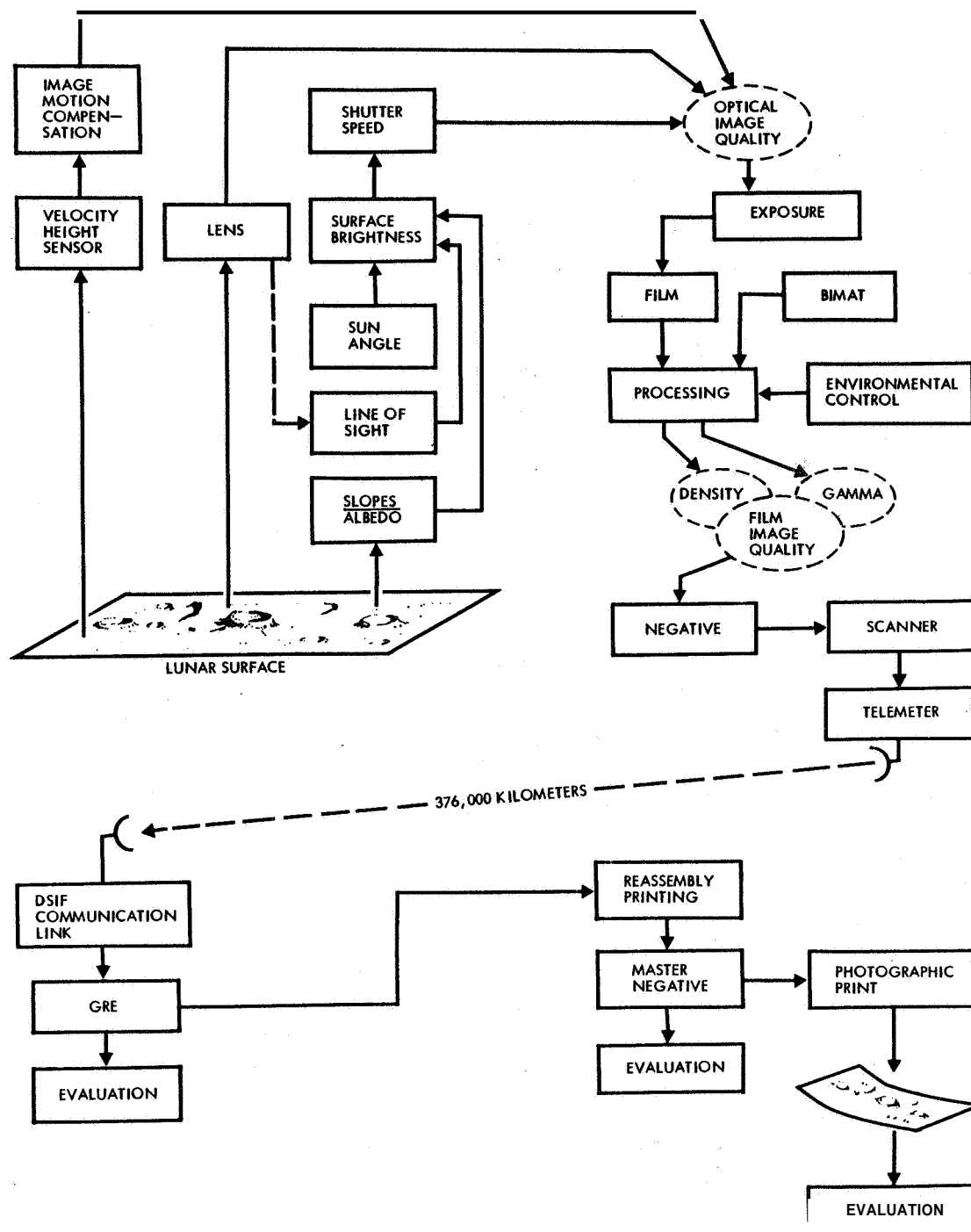


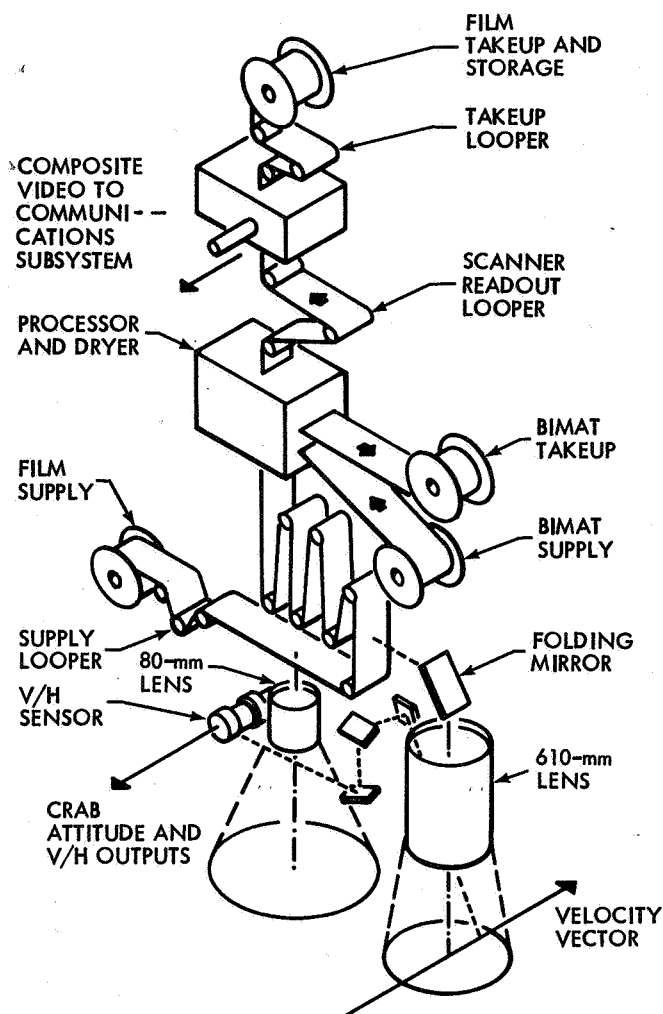
Figure 2.1-1: Lunar Orbiter Photographic System

As shown in Figure 2.1-1, the photographic system is composed of three major elements:

- 1) The spacecraft photographic subsystem;
- 2) The ground reconstruction system;
- 3) The reassembly process.

The subsystem design represents an optimum balance of lens, film, and scanner readout designed to obtain 1-meter and 8-meter-resolution photographs from a nominal altitude of 46 km. The photographic method was selected over the television method for four important reasons:

- 1) Resolution is, essentially, limited only by the granularity of the film and a much larger format at high resolution is provided.



- 2) Power required to process and transmit pictures is significantly lower, because of the time-dispersion of readout
- 3) Film provides a higher data-storage capacity than magnetic tape for a given size and weight.
- 4) Pictures can be read out and transmitted as desired.

2.1.1.1 CAMERA

The camera consists of a dual-lens system that produces both medium- and high-resolution images on 70-millimeter film as shown in Figure 2.1-2. The medium-resolution lens is a Schneider Xenotar 80-millimeter lens, and the high-resolution lens is a Paxoramic 610-millimeter lens made by Pacific Optical Company. Both lenses operate at a fixed aperture of $f/5.6$. A between-the-lens shutter is used with the 80-millimeter lens, a double-curtain focal-plane shutter with the 610-millimeter lens; 1/25-, 1/50-, or 1/100-second shutter speed is selected by commands from mission control. Both shutters operate at the same nominal speed. The film is held in the focal plane by film damps and vacuum that holds the film flat during exposure. The film is advanced approximately 298 millimeters after each exposure. Ground commands select camera operating parameters: number of frames per sequence, time interval between exposures, shutter speed, line-scan tube focus, and video gain.

For a typical orbital velocity of 1.936 km/sec., the photographic target moves 77 meters during the 1/25-second exposure interval; thus, smear caused by this movement must be compensated. The amount of compensation is dependent on velocity and altitude. Experiments have shown that if image motion is less than 60 % of the size of the minimum resolvable detail (0.6 meter in the Lunar Orbiter case), degradation will not cause loss of detection capability. Lunar Orbiter image-motion compensation, accurate to within 0.5%, is designed to reduce smear to 0.33 meter (at 46-km altitude), well within the 0.6-meter limit. This is achieved by moving the platen to follow the image along the direction of flight.

Figure 2.1-2: Camera Subsystem Schematic Diagram

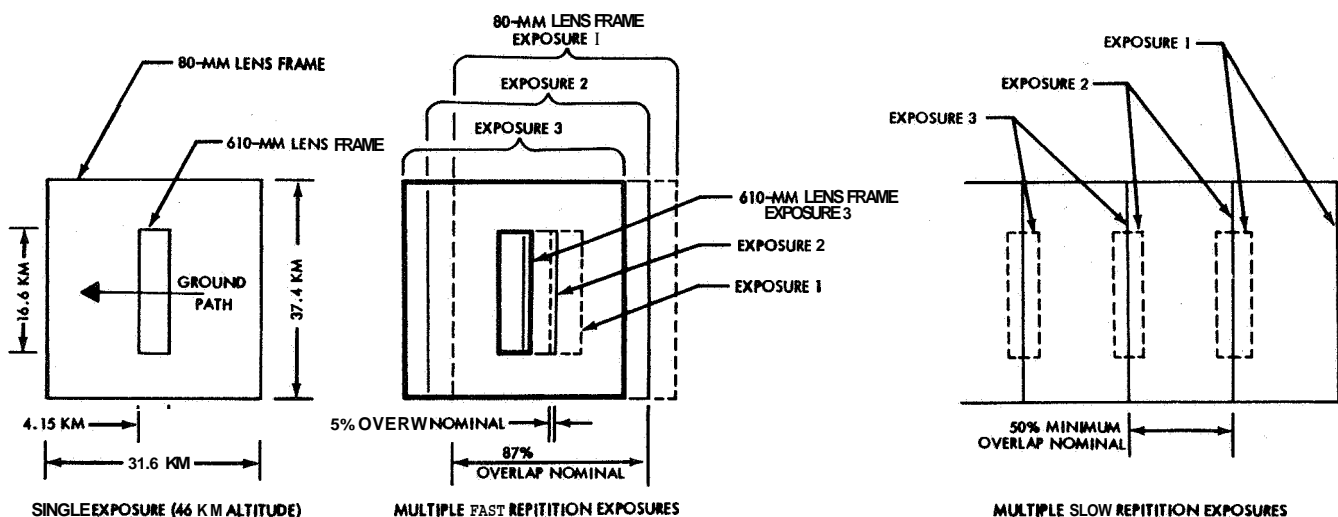


Figure 2.1-3: Photographic Overlap and Coverage for Sequencing Modes

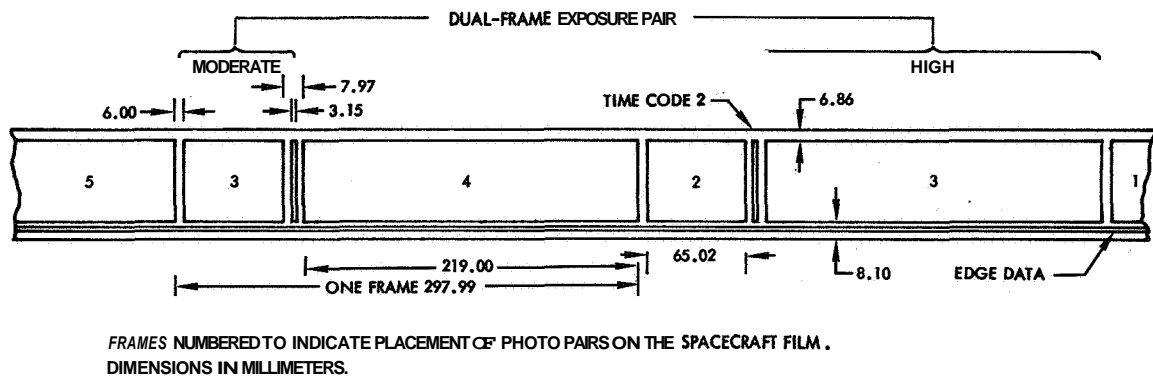


Figure 2.1-4: Film Format and Placement of Frames

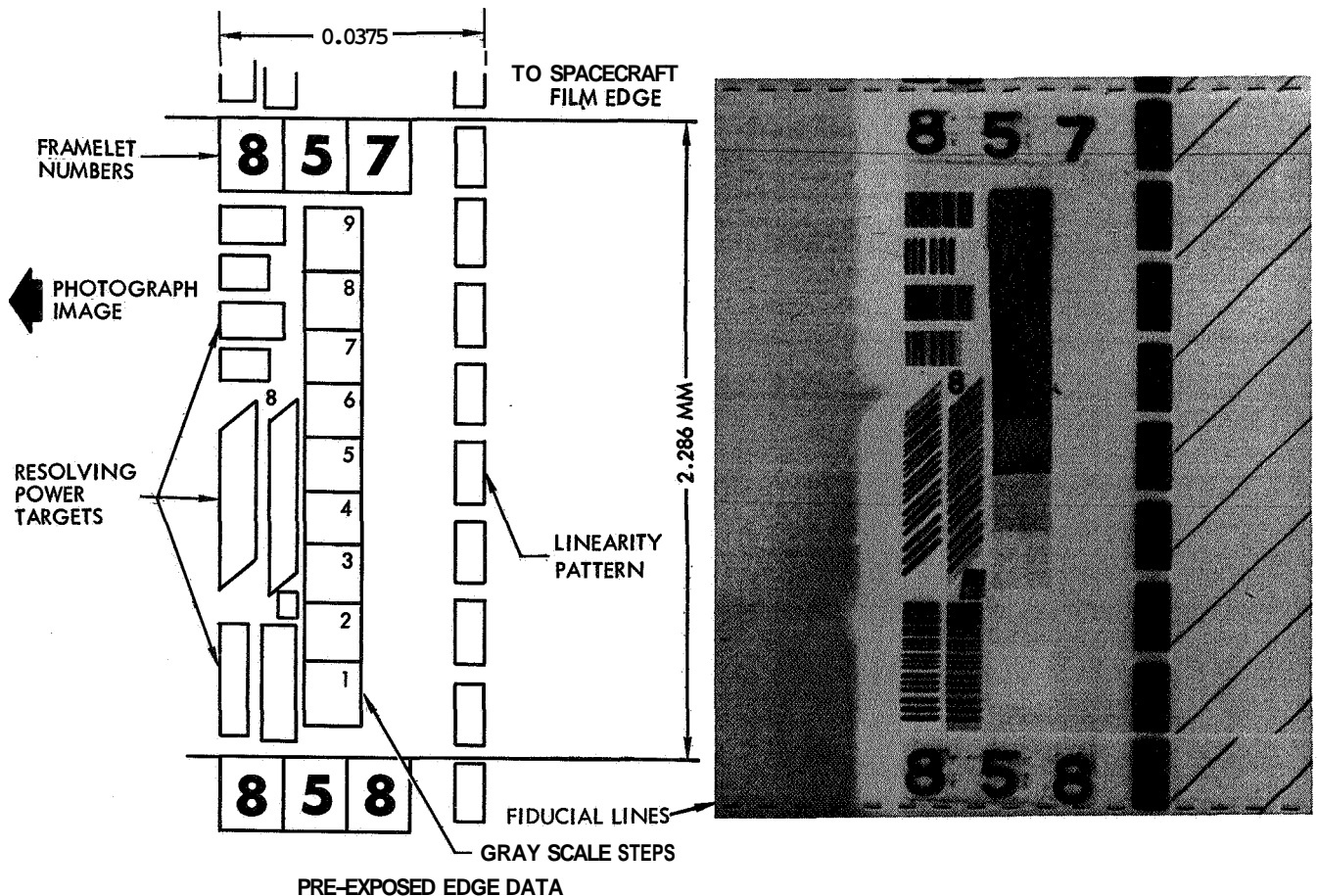


Figure 2.1-5: Edge Data Format

Platen motion is controlled by the velocity-to-height ratio (V/H) sensor that tracks a portion of the 610-mm-lens view of the surface. The V/H sensor also determines the sequencing rate of exposures to obtain proper overlap of the photographic coverage, Figure 2.1-3. Exposures are made as single dual frames, or in automatic sequences of 4, 8, or 16 dual frames on command. A dual frame is one high- and one moderateresolution frame exposed simultaneously. Sequencing rate may be "slow mode," producing 50% overlap of moderateresolution coverage, or "fast mode," which results in conti-

guous coverage by the 610-mm lens and 87% overlap by the 80-mm lens.

The picture formats and their placement on the film are shown in Figure 2.1-4. To provide for control and calibration of the photographs, high- and low-contrast resolution bars, a nine-step gray scale, linearity patterns, and framelet numbers (as shown in Figure 2.1-5) are pre-exposed along one edge of the film. A binary time code indicating spacecraft time of exposure is exposed across the film in the space between formats.

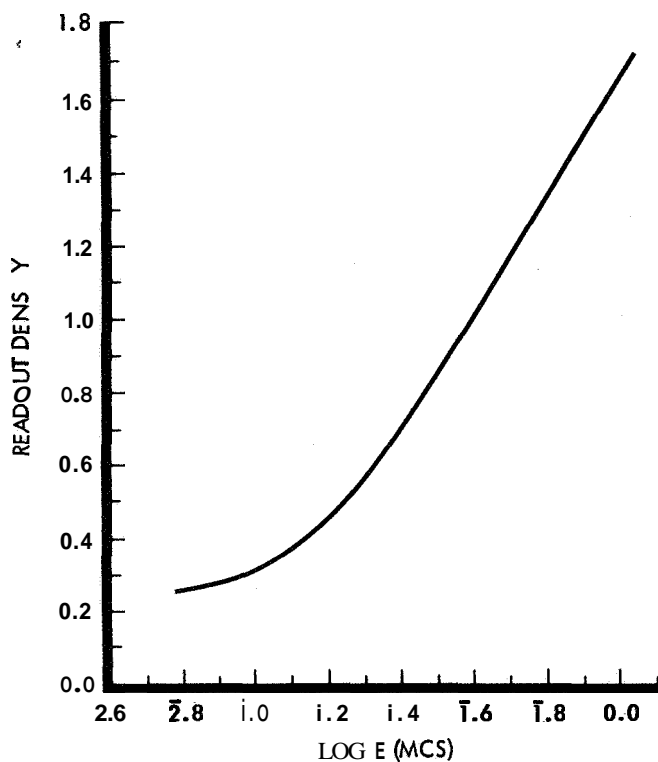


Figure 2.1-6: Characteristics of Type SO-243 Film (H&D Curve)

Film is exposed at a rate much faster than it can be processed. A looper having a capacity of 20 frames takes up the film and holds it until processed.

The film selected for Lunar Orbiter is Eastman Kodak Special High Definition Aerial Film, Type SO-243; characteristics of this film are shown in Figure 2.1-6. Although the film's A.S.A. exposure index of 1.6 is slow compared to more common emulsions, it has an extremely fine grain and exceptionally high resolving power - approximately 250 lines per millimeter. The film's relative insensitivity to radiation is an important reason for its selection. Following a 100-rad radiation dosage, only about one-half of the film capability is lost; this dosage then is the upper limit that the film could tolerate and still give usable (but degraded) photographs. In determining if this 100-rad-dose limit would be exceeded during a Lunar Orbiter mission, radiation from three sources was evaluated

- 1) Galactic cosmic, essentially an omnidirectional flux amounting to about a 5-rad integration radiation;
- 2) Geomagnetically trapped radiation in the Van Allen belts, with an integrated radiation varying between 1 and 6 rads, dependent on the cislunar trajectory;
- 3) Solar flares with radiation levels that can exceed 100 rads (Class 3 and greater flares).

Solar flare radiation presents the most serious threat to

film. The probability of realizing a 100-rad total radiation during a 30-day mission, however, is computed to be only 4%. The spacecraft provides shielding equivalent to 2 grams/cm³, and an additional 2 grams/cm² are installed around the film supply cassette. The resultant shielding reduces the 100-rad-dose probability to less than 1%. A 100-rad radiation dose would change the maximum resolution of the film from 1 to 1.1 meters. During Mission I, no degradation of film was noted.

2.1.1.2 PROCESSOR-DRYER

Eastman-Kodak "Bimat" (SO-111) processing is used to develop the exposed SO-243 film to provide a photographic negative. The process is classed as nonliquid. The Bimat holds a monobath processing solution, P S 485, absorbed in its emulsion. At the completion of processing, the film is merely damp and can be easily dried. The exposed film is laminated to the Bimat film and processing goes to completion in 3.4 minutes of contact time at a temperature of 85°F.

As the film and Bimat leave the processor drum, they are delaminated. The Bimat film is pulled onto a separate takeup spool, and the slightly damp SO-243 film is brought into contact with the dryer drum heated to 95±3°F. Moisture is collected by a mat containing potassium thiocyanate desiccant. Film is processed at a rate of 2.3 inches per minute; all frames exposed during an orbital pass can thus be processed prior to start of the succeeding pass.

Three significant constraints govern operation of the photo subsystem:

- 1) Temperature of the Bimat supply must be kept below 70°F. The Bimat has a 28-day lifetime at 70°F and increases to 56 days at 40°F.
- 2) Film and Bimat must not remain in contact longer than 15 hours or they will laminate permanently.
- 3) The film must not remain "stationary" over the rollers for longer than 8 hours. Beyond this film-set results; the film will not be flat in the platens, thus destroying focus, and excessive power is required to move the film to a subsequent position.

The last two constraints require that film be moved in the system at least once every 8 hours to prevent film set. These are the "film-set" frames. From the dryer, the processed film moves to the film takeup and storage reel where it remains until readout is desired.

2.1.1.3 READOUT SCANNER

Transmission of the photographic image to Earth is accomplished by converting the image density to an electrical video signal, as shown in Figure 2.1-7.

In the linescan tube (LST), a beam from the electron gun moves linearly across a phosphor-covered anode that rotates so that different areas are bombarded on successive scans. A 6.5-micron image of the light spot is focused on the film by the scanner lens. The lens is moved at right angles to the film following each scan. The result is a "framelet" comprising a raster of 16,359 lines - each 2.67-mm-long - across 57 mm of the 70-mm film.

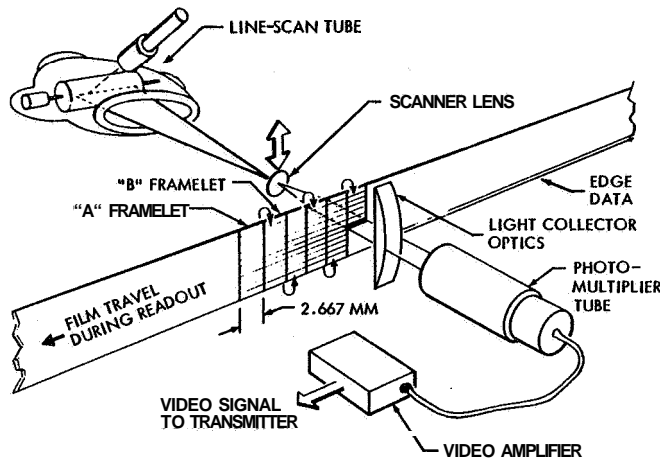


Figure 2.1-7: Readout Subsystem Schematic

Following completion of one framelet, the film is moved 2.54 mm to begin scan of the next framelet -- the scanner lens moves in the opposite direction for this framelet. (The framelets are designated A or B, dependent on the direction the mechanical scan lens was moving during composition of the framelet.) Scanning begins at the edge-data side of the film to produce the A framelet and the B on the return. Marks, scribed on the LST phosphor at each end of the scan line, produce fiducial marks in the composite video signal which provide a calibration of system magnification. A complete dual-exposure frame--298 mm -- requires 117 such framelets.

The light passing through the film, modulated by image density, is sensed by the photomultiplier tube through associated light-collection optics. An analog electrical signal proportional to the intensity of the transmitted light is generated and amplified, and timing and synchronization pulses are added to form the composite video signal, Figure 2.5-54, which is fed to the spacecraft's video transmitter.

Film motion during readout is opposite to that during photography and processing. The processor cannot be reversed until all film has been processed and the Bimat cleared from the processor. A looper having a capacity of four frames, located between the processor and the scanner, permits readouts of up to four frames between photographic orbits and prior to cutting the Bimat. Final readout of all photographs is accomplished only after all photographs have been taken and processed, and the Bimat cut and cleared from the processor.

2.1.1.4 GROUND RECONSTRUCTION SYSTEM

The composite 230-kHz video signal, multiplexed to the spacecraft's 10-MHz S-band rf signal, is received (on

command) at any of the three Deep Space Stations in view. At the DSS, recordings are made on two GRE's and an Ampex FR 900 wideband, rotating-head magnetic tape recorder. The tape records the 10-MHz undetected IF signal. Within the limitations of the reproduction processes, the playback image is nearly identical to that of the original 35-mm film record.

The 35-mm film record is made using the ground reconstruction electronics (GRE) located at each DDS. The 10-MHz signal is demodulated to separate the 230-kHz composite video signal, processed, displayed on a kinescope tube, and recorded by the GRE camera. Two GRE's are located at each DSS.

The films are processed at the DSS and sent to Eastman Kodak at Rochester, New York, where reassembly is completed. The magnetic tapes are delivered to NASA's Langley Research Center as part of the final documentation package. The tapes will provide GRE input for producing additional reconstructed records.

2.1.1.5 THE REASSEMBLY PROCESS

The 35-mm reconstructed record is reassembled by hand or may be reassembled automatically on 9 1/2-inch (24.2 cm) film by photographic projection printing. This machine reassembly reduces the GRE film image by a factor of 0.893 and "A-B" framelet reversal is corrected for proper orientation of high-resolution frames.

Fourteen framelets are reassembled to produce one 9-by-14-inch subframe. Two framelets overlap the adjacent subframe. Approximately three subframes are required for a single moderateresolution photo and seven for each high-resolution photo.

This sequence is diagrammed in Figure 2.1-8.

2.1.2 MISSION PHOTOGRAPHY

Photography during the first ellipse was planned to permit the following:

- 1) Verify and assess subsystem operation prior to transfer into the second ellipse;
- 2) Verify premission exposure predictions;
- 3) Advance the film through the processor to permit readout of selected photographs;
- 4) Satisfy the constraints on time delay between successive camera and processor operations.

On the basis of analysis of the first few frames of Site I-0 photographs, some modifications were made to the premission plans. Additional frames were used for diagnostic purposes, to advance film for test exposures to be read out, and to satisfy film-set constraints. Some were used to photograph the farside of the Moon.

Premission plans to expose the film-set frames without maneuvering the spacecraft were generally followed; however, confidence in spacecraft operation resulted in a decision to maneuver the spacecraft to obtain farside photography - which required an approximately 180-degree roll maneuver - and to obtain photographs of the Earth.

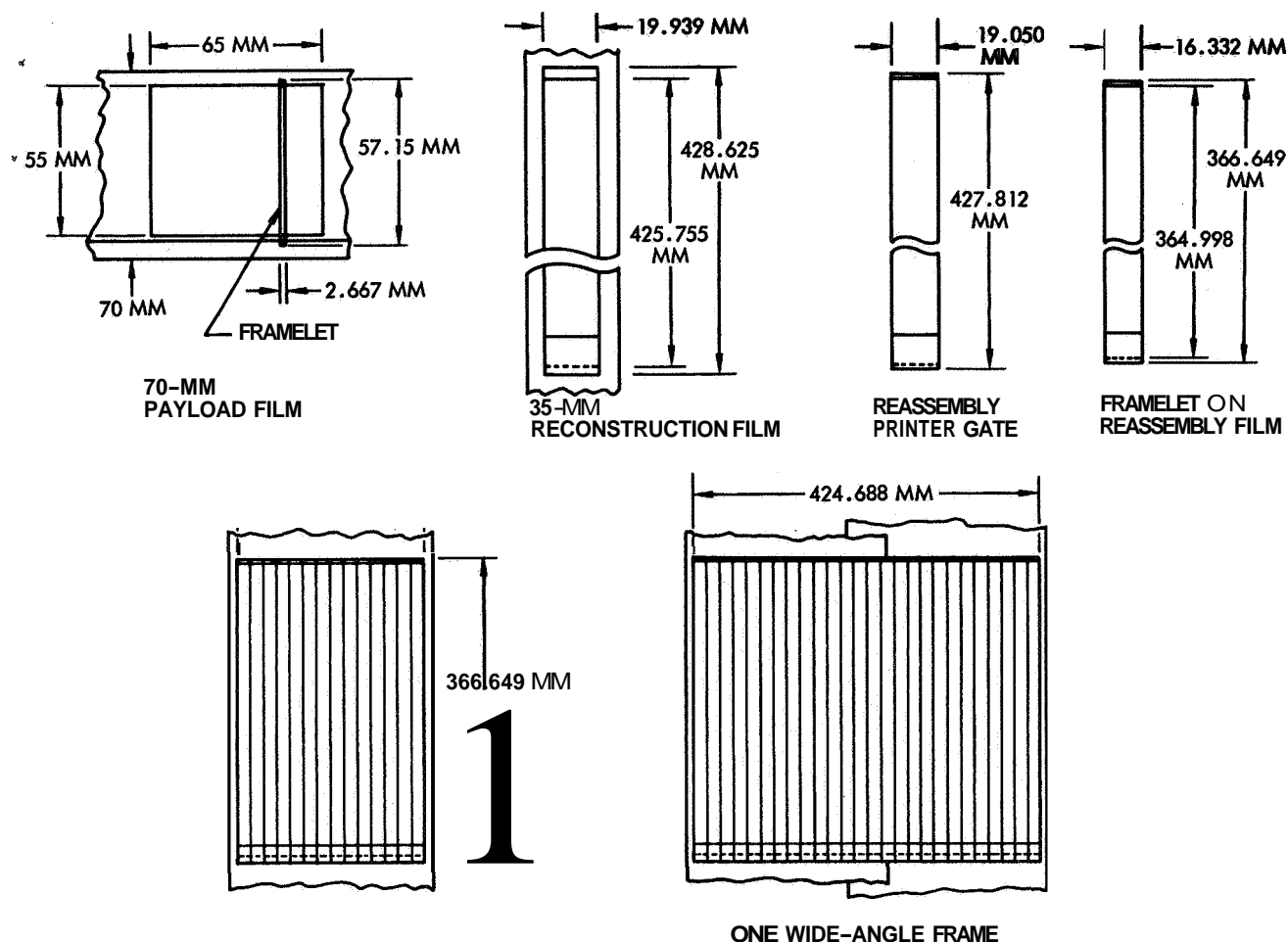


Figure 2.1-8 Reassembly Sequence

The first-ellipse photography was initiated on August 18, 1966 at 12:42:49.9 GMT during Orbit 26 at an altitude of approximately 208 kilometers. Photos of Site I-0 were exposed along the orbit track from 84° 36' E longitude, 1° 40' N latitude, to 98° 12' E longitude, 1° 24' S latitude. The solar phase angle was 62.9 degrees. The area photographed was the vicinity of Mare Smythii and includes both mare and upland types of terrain, providing a range of albedo for exposure check. The premission prediction indicated an albedo of 0.065 for the mare area, requiring an exposure of 0.02 second.

First-ellipse photography included the following:

Site I-0	20 Frames
Nearside Film Set	6 Frames
Test and Film Advance	5 Frames
Farside Photographs	8 Frames
TOTAL	39 Frames

A description and evaluation of these first-ellipse photographs will be found in Paragraph 2.2.1.2.

Target sites representative of the terrain types and combinations of types found within the Apollo landing zone were specified. They included the area where Surveyor I landed. The other sites were distributed over a wide range of longitude for sampling a variety of terrain types. A description of the preselected target sites, obtained by Earth-based observation, is given in Section 2.1.3.

Second-ellipse photography was started August 21, 1966, at 11:28 GMT on Orbit 1, as a film-set exposure. (Orbit numbering was restarted on the second ellipse. Sites I-1 through I-5 were photographed from this ellipse.) On August 27, during Orbit 30, a retrograde velocity maneuver was made to place the spacecraft in a third ellipse having a perilune about 5 to 7 km lower. Photography was completed over Site I-9.2 on August 29 at 1324 GMT. The Bimat web was cut August 30 at 1814 GMT and final readout started. Final readout was completed September 14. All frames, including the pre exposed and processed Goldstone test film, were read out successfully.

2.1.3 PHOTOGRAPHIC OBJECTIVES

The photographic objectives of the mission were:

- 1) Obtain moderate and high-resolution photographs of selected areas of the lunar surface;
- 2) Photograph the area surrounding Surveyor I;
- 3) Provide topographic information that will extend scientific knowledge of the lunar surface characteristics.

Except for the limited area coverage obtained by Rangers VII, VIII, and IX, and Surveyor I, knowledge of lunar topography has been limited to Earth-based observation in which the best resolution, by optical means, has been about 0.5 to 1 kilometer. The requirement for surface resolution for the Apollo landings is approximately 1 meter. Landing sites are desired at a number of locations to fulfill the exploration and scientific objectives of the Apollo program and to provide an adequate launch window to obtain acceptable lighting. Lunar Orbiter mission photography will provide a major contribution to, if not a solution of, these requirements.

The specific photographic objectives of Mission I were lunar areas that, from Earth-based observation, appear to be representative of different terrain types offering candidate sites for Apollo landing. To accomplish this, the mission was designed to:

- 1) Take a series of 16 dual-frame exposures in the fast-sequencing mode over each of the preselected target sites. These exposures were to provide contiguous coverage of high-resolution, and forward overlap of moderate resolution, frames suitable for stereo measurement. The photographs were to be taken from a nominal 46-km altitude.
- 2) Take a series of 16 exposures during the first phase as far east as possible consistent with the lighting constraints and mission design (Site I-0).
- 3) Use the film-set exposures to obtain photographs of proposed Mission B target sites on a non-interference basis with Mission I.
- 4) Read out and transmit to the DSN, selected exposures from the first ellipse phase, prior to injection into the second ellipse, for early evaluation of photo subsystem and system performance.
- 5) Read out and transmit selected photographs to the DSN between photo orbits for mission control and system operational validation.
- 6) Following the completion of photography, read out and transmit to the DSN all of the photographs obtained for the entire mission.

2.1.4 PHOTOGRAPHIC SITES

The selection and specification of the sites to be photographed was made by the NASA Lunar Orbiter Project Office (LOPO) prior to the mission.

Ten target sites were chosen for this mission. Of necessity, selection of the sites was based upon telescopic observation from Earth and thus subject to many uncertainties.

A set of ground rules was established by LOPO to guide and direct selection of appropriate target sites. The ground rules, as stated in Lunar Orbiter Mission A Description, NASA LOTD-102-1, as approved by the Ad Hoc Surveyor/Orbiter Utilization Committee, September 29, 1965, (Amended June 1, 1966), were:

- 1) Obtain several samples of significant terrain types.
- 2) Samples of like terrain types shall be reasonably distributed for Apollo launch window considerations.
- 3) Concentrate on the most promising areas within the Apollo zone of $\pm 5^\circ$ latitude, -45° longitude.
- 4) Examine promising Surveyor sites.
- 5) Perturb site selection if additional information becomes available and time permits.

A number of mission constraints were imposed, as follows:

- 1) Minimize attitude control gas consumption by limiting photography to a single photo pass over each target, except for the two 16-frame sequences at the Surveyor I site.
- 2) Photo readout between sites for reliability and mission control.
- 3) Maximum of nine equatorial sites within Apollo zone.
- 4) Maximum photographic coverage at each site, using one pass.
- 5) The orbit inclination will be 11 to 12 degrees.
- 6) Lighting conditions and altitude must be adequate for:
 - a) Detection of features equivalent to a cone having a 2-meter-diameter base and a 0.5-meter height;
 - b) Detection of a 7-degree slope of an area 7 by 7 meters.

NOTE This requirement resulted in premission prediction limiting the phase angle to between 50 and 80 degrees and a nominal perilune altitude of 46 km.

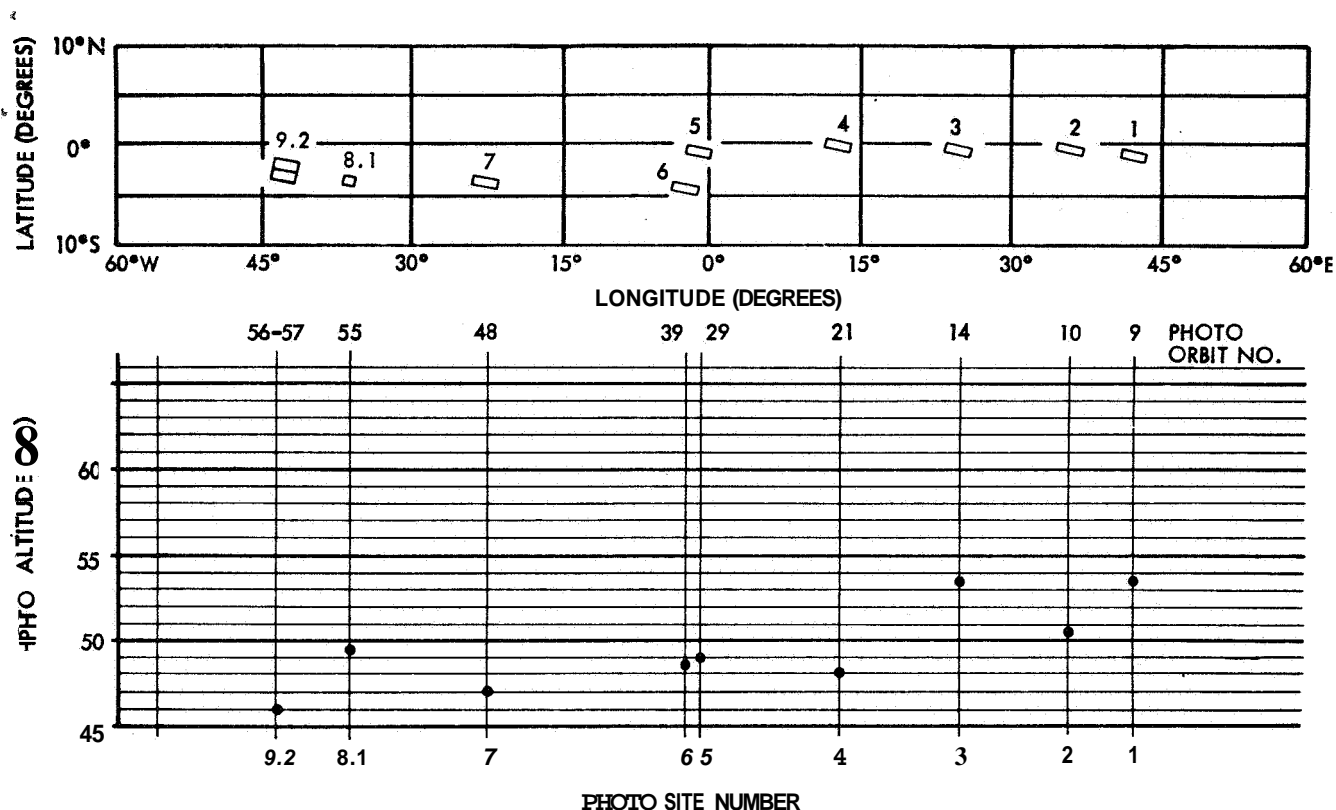


Figure 2.1-9 Mission I Primary Site Locations

2.1.4.1 SITE SELECTION CRITERIA

A detailed account of the target site selection for the mission is contained in the reference given above (NASA LOTD-102-1).

Target area selection was based on the 1:1,000,000-scale U. S. Geological Survey lunar terrain map of the equatorial zone. Lunar surface morphology for this map was derived from quantitative data which included slope component studies, relative relief studies, and crater density studies. Sources of qualitative data were:

- 1) A.C.I.C Lunar Atlas and other charts.
- 2) Earth-based photography.
- 3) The U.S.G.S. 1:1,000,000-scale geological maps.
- 4) Ranger VII, VIII, and IX photography

These studies included extensive work carried out by the U.S.G.S. on photometrically derived slope measurements

and slope frequencies. The results of Ranger VII, VIII, and IX missions contributed a great deal of supporting data.

Surface roughness is of primary concern from the standpoint of landing requirements for Apollo Landing Module (LM). This factor has been used as a major parameter in site analysis. Terrain units considered critical for terrain calibration purposes were established on the basis of slopes at 1-kilometer resolution.

Possible information of scientific value, as well as of direct value to the Apollo mission, was also considered in selection of the target sites.

2.1.4.2 SITE LOCATION

The location of each site, its description based on pre-mission information, and its evaluation as given in NASA LOTD-102-1 are summarized below. A plot indicating the approximate locations of the sites within the lunar equatorial regional is shown in Figure 2.1-9.

LUNAR ORBITER SITE EVALUATIONS

MISSION I

Site I-1 0° 50' S, 42° 20' E

Rating **A**: Inclusion of dark mare, moderately light mare, and uplands in ~~this~~ site make it a valuable terrain calibration area. The 1-meter relative roughness of the ~~two~~ mare types is of special interest. The possible detection of genetic relationships at the contact of the upland and dark mare is of particular importance scientifically. The maria units are potential Apollo landing sites.

Site I-2 0° 10' S, 36° 00' E

Rating **B** Significant terrain calibration data is anticipated at this site for the upland units II-A and II-B, and the mare. Potential Apollo landing sites may be revealed here.

Site I-3 0° 20' N, 24° 50' E

Rating **B**: ~~Useful~~ data concerning small scale roughness and morphology of this area should be obtained. It is a potential Surveyor and Apollo landing site.

Site I-4 0° 00', 12° 50' E

Rating **A**: It is anticipated that high-resolution photography of terrain units II-A, II-B, II-C, and II-D will provide the data necessary to define the 1-meter resolution roughness of the upland areas. This site is a potential Surveyor and Apollo landing area.

Site I-5 0° 25' S, 1° 20' W

Rating **B**: This is an especially good example of smooth mare with low subdued ridge structures, which are important in the evaluation of mare origin and development. It has high potentiality as an Apollo and Surveyor landing site.

Site I-6 4° 00' S, 2° 50' W

Rating **A**: This area is particularly important to terrain calibration, because it provides high-resolution photography of upland unit II-D, as well as the deformed crater ~~floor~~ 111-B-2. The crater floor is a previously selected Surveyor landing site. It is anticipated that this coverage will be of high value when bearing strength data becomes available for the major terrain types.

Site I-7 3° 45' S, 22° 45' W

Rating **B** ~~This~~ is a moderately good example of mare that has low sinuous ridges, small craters, and a light ray covering. It should provide important information regarding the development of older mare surfaces and their characteristic morphology. It is a previously selected Surveyor landing site (16-50).

Site I-8.1 3° 00' S, 36° 30' W

Rating **A**: This is a superior example of a relatively linear mare ridge system, which is especially important in the definition of 1-meter scale roughness. It provides an excellent opportunity to investigate the genetic processes concerned in the development of this type of mare morphology. It is a highly rated Surveyor landing site (11-50).

Site I-9.1 2° 21' S, 43° 22' W

Surveyor I landing site.

NOTE The location of this site was changed on the basis of later refinement of the position of Surveyor I. In addition, the area was photographed on ~~two~~ successive orbits. The designation of the site was therefore changed to Site A-9.2a and Site A-9.2b.

2.2 MISSION PHOTOGRAPHS

This section will cover the mission photographic quality and characteristics of the ground reconstructed record and reassembled film. The photographs consist of the original 35-mm GRE film (one from each of two GRE's at each DSIF site) and the following copies:

- 1) 35-mm negative transparencies (35-IN);
- 2) 35-mm positive transparencies (35-2P);
- 3) 9 1/2-inch reassembled positive transparency (SF-2P);
- 4) 9 1/2-inch reassembled negative transparency (SF-3N);
- 5) 9 1/2-inch paper positive prints (SF-4P).

2.2.1 DESCRIPTION PHOTOGRAPHS

The half of film processing and photograph reconstruction resulted in: a) a set of characteristics of Lunar color photography; b) the framelet line; c) a series of unavoidable distortions; d) a by-product of the X-ray exposure problems were also explained because of uncertain luminance data, e) data on the effect of light from hard shadows to bright light, which is a system limitation. Some unexpected functional are: f) the effect of the photographic quality on information content of the photographs.

photographic sites, or differences in illumination, albedo, topography, or differences in altitude, or the inability of the system to deal with a wide range of variables or other conditions far less than ordinarily encountered in the field.

The descriptions are limited to a qualitative, or a preliminary assessment. They are based on the examination of a standard reference copy of the 35-mm GRE reconstructed record. All photographs did not be made by this method because of a large amount of film record needed by the mission. A sampling program was used. From the original dual-frames distributed over contact were selected. The initial selection was prepared from easenilm negative frames of each reel. Overlap, illumination exposure variation, processing effects, and overall quality

2.2.1.1 GENERAL MISSION PHOTOGRAPHS

The quality of site photographs obtained with the 80-mm lens varied irregularly because of exposure problems. Sites 1-5 and 11-9 were of good quality, but the exposure of 10 remaining sites from moderate to poor. Features approaching 8 meters in size were detected at all sites. Detection of features in the rocks or block field was difficult. In a number of instances, illumination produced high contrast. In a number of instances, where the photograph was taken by the 610-mm lens, the image was smeared and the image (IMC direction), and the orientation of the features was difficult to discern. This information may assist interpretation of corresponding features in the 80-mm-lens photographs.

Coverage of the specified sites changed during the mission at three sites where eight exposures were made, rather than the planned 16. At two of these sites - Sites 1-4 and 1-6 - coverage was greater because the slow sequencing mode was used and overlap decreased to about 50%. Only at Site 1-8.1, where fast sequencing was used, was coverage reduced, but coverage of the specified target position was accomplished

Photographic Characteristics

Use of film-set frames for additional photography, together with most of the frames required for diagnosis of the shutter problem, produced 45 moderate-resolution and some high-resolution photographs of outstanding scientific interest. These include photographs of the lunar farside and of the Earth.

The most obvious characteristic of the reassembled photographs is that they are made up of narrow strips. This is inherent in the system. While tolerances are held to a minimum, junction lines are unavoidable and accepted because of marked advantages of the resolution capability of the LST scanning technique.

Light Transmission Characteristics

The two lenses of the camera have different light transmission properties, as discussed in Paragraph 2.4.1.1. Both operated at a fixed aperture of $f/5.6$. The difference in light transmission, however, resulted in each producing a different exposure on the film. The 80-mm lens, with an on-axis transmission of 92%, produces a greater exposure than the 610-mm lens with an on-axis transmission of 68%. Equal image densities could not, therefore, be possible with both shutters operating at the same speed. The difference in exposure between the 610- and 80-mm lens - - due to the difference in lens transmission - - has, in effect, increased the luminance latitude of the system. Good detail is present in the 80-mm photographs of darker mare areas and poorly illuminated slopes where information may well have been lost. The 610-mm-lens photographs show the presence of much recognizable fine detail in brighter areas such as slopes' facing the Sun, and the higher-albedo uplands where detail may be obscured in corresponding 80-mm photographs. It follows also that, in areas of low luminance, severe underexposure with accompanying loss of data will occur in the 610-mm photographs while data loss occurs in bright areas overexposed in the 80-mm photographs.

Lunar Surface Photometric Characteristics

The lunar surface has a unique reflection characteristic of backscatter, which can produce large changes in apparent brightness as a function of the geometry of illumination and observation. This characteristic has no counterpart in terrestrial photography. The variable geometry over the field of view, coupled with the lunar photometric characteristic, results in a nonuniform brightness within the area of a photograph. This effect is accentuated by a normal lens, which has reduced light transmission with angular distance from the optical axis.

Imperfections

The mission photographs contain some imperfections. Where a blemish occurs on an 80-mm photograph that is one of a sequence, the area covered by the blemish ordinarily will be included on one or more other frames of the

sequence because of overlapping coverage. Data loss will occur only at the start or end of a sequence where no overlap is obtained, within 610-mm coverage (except for the 5% overlap), and in single-frame exposures. Imperfections related to the intermittent processing were anticipated and recognized as inherent in the system. Those not expected are mostly of minor extent that become apparent only by critical examination.

Imperfections in the photographs are described in the following paragraphs as a means of identification. With few exceptions they are scattered through many frames. The significance of the imperfections and the extent of their effect on photographic quality is strongly dependent upon the use made of the photographs.

Development Imperfections

It was a recognized and accepted characteristic of the processing method that each time the processor was stopped, distribution of the imbibant in the Bimat would be affected, and thus affect processing in limited areas of the film. Partial dryout of the Bimat occurred in the diffusion channel between the Bimat supply and processor. Pressure exerted against the Bimat by a roller in the processor mechanism altered the imbibant distribution between each processing period. When processing was resumed, the altered Bimat produced a narrow strip of incorrectly processed film. An example is shown in Figure 2.2-1. Other types of imperfection (Figure 2.2-2) also related to intermittent processing originated at the line where the Bimat separated from the supply roll at the start of a processing period. A double mark (Figure 2.2-3) caused by pressure of the Bimat metering roller during stop periods also occurred.

Blemishes present in the photographs processed during the latter part of the mission appear as lobate loops or as patches of small rounded spots within which the image is lost. Partial dry-out of the Bimat with resulting incomplete processing or poor contact with the film that impairs diffusion of the processing solution is presumably the cause. In some cases, the appearance of the marks suggests formation of small droplets of the imbibant on the Bimat. Examples of these marks are shown in Figure 2.2-4.

Small particles separated from the Bimat and adhered to the film. This occurrence increased toward the end of photography, indicating some deterioration of the Bimat. These particles may be the source of some very

small scratches that appear on the spacecraft film, as they would tend to collect on the platens and film handling equipment.

Restricted Density Latitude

It should be noted that the maximum density latitude of the reassembled record corresponds to a restricted luminance range in the original scene. The primary reason for this restriction was the need for maintaining a high signal-to-noise ratio throughout the information handling channel. This was accomplished by restricting readout to a density range of 0.3 to 1.3 on the Type SO-243 film aboard the spacecraft. The lunar surface will frequently exhibit a range of brightness that will produce image densities exceeding the above range, thus a photograph unavoidably may include both underexposed and overexposed areas. Exposure was selected on the basis of predicted brightness of the terrain type of interest within the area. Limited areas such as highlighted slopes, the area of bright rayed craters, and other areas of higher albedo thus may be overexposed. Steeper slopes facing away from the Sun may be underexposed. Hard shadows invariably result in complete loss of information within their confines.

Density Variations

Some density variations are related to reconstruction of the individual framelets. One type occurs across the width of framelets and is due primarily to variation of focus of the line-scan tube in the spacecraft. Modification of line-scan tube and GRE focus partially compensated for this difficulty during readout in the latter part of the mission. In some photographs, a density variation appears longitudinally on alternate framelets. This has been attributed to too slow an extinction or halo glow of the phosphor of certain GRE kinescope tubes. A masking technique developed during the mission resulted in significant improvement. Small-scale longitudinal streaking that is attributed to phosphor granularity is also present in many of the photographs. This effect is characteristic of the individual GRE kinescope tubes and varies with each particular GRE. A density anomaly appearing in the moderate resolution photographs consists of a slight flare along the center of the edge adjacent to the time code and extends across the first one or two framelets. It may be caused by stray light from the time-code lights; however, this has not been confirmed.

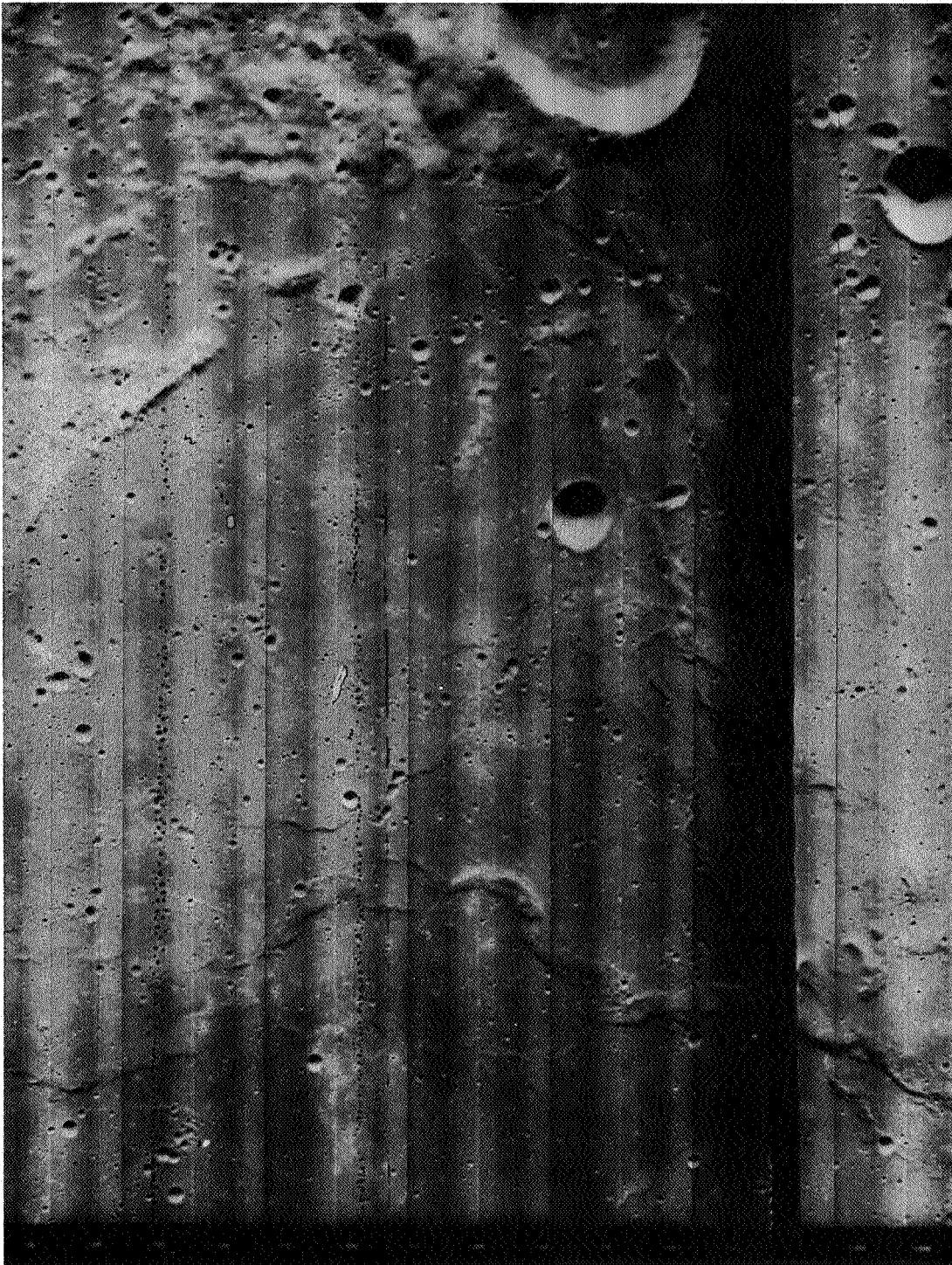


Figure 2.2-1: Processor Stop Line

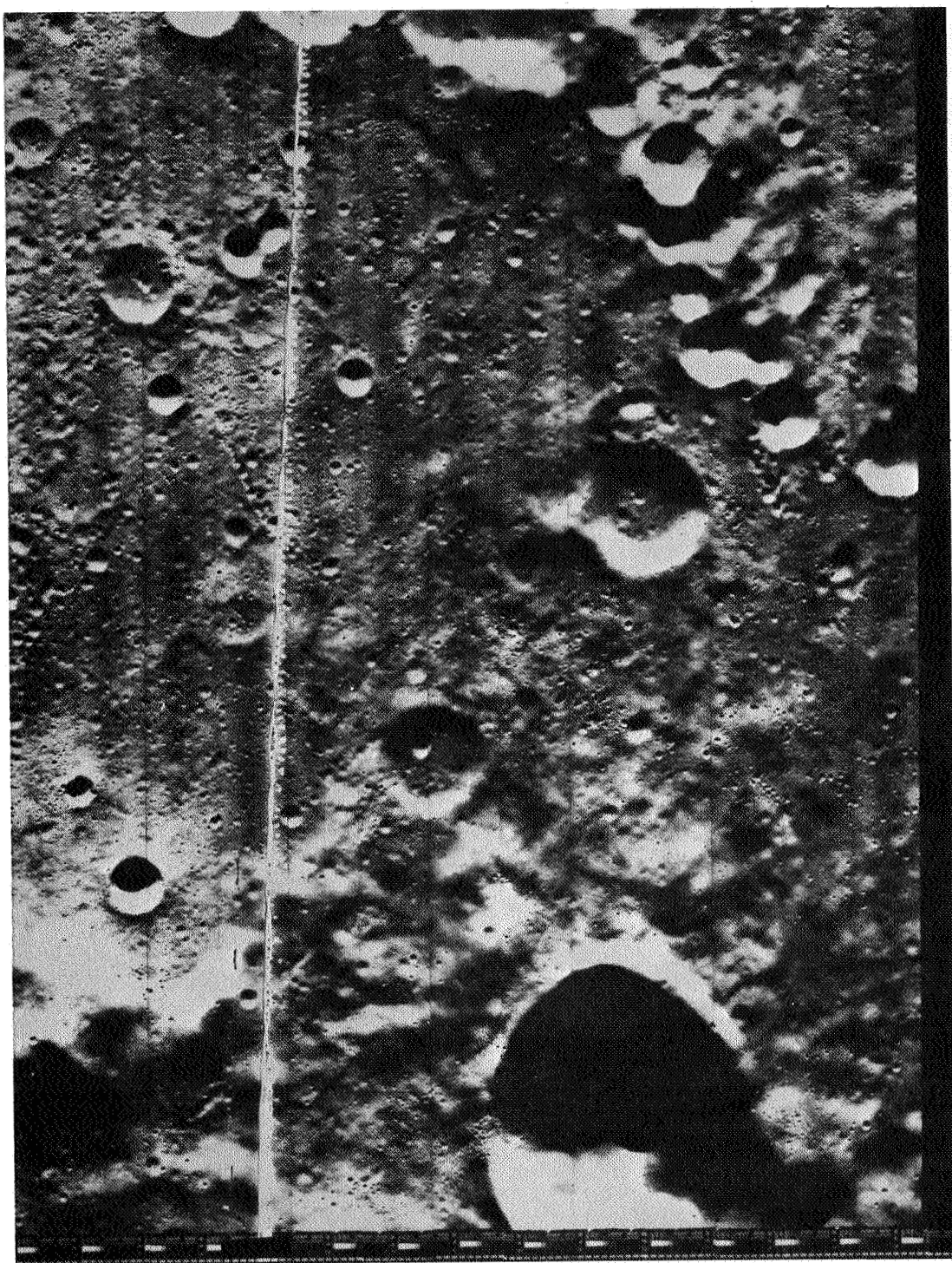


Figure 2.2-2 Bimat Supply Separation Line

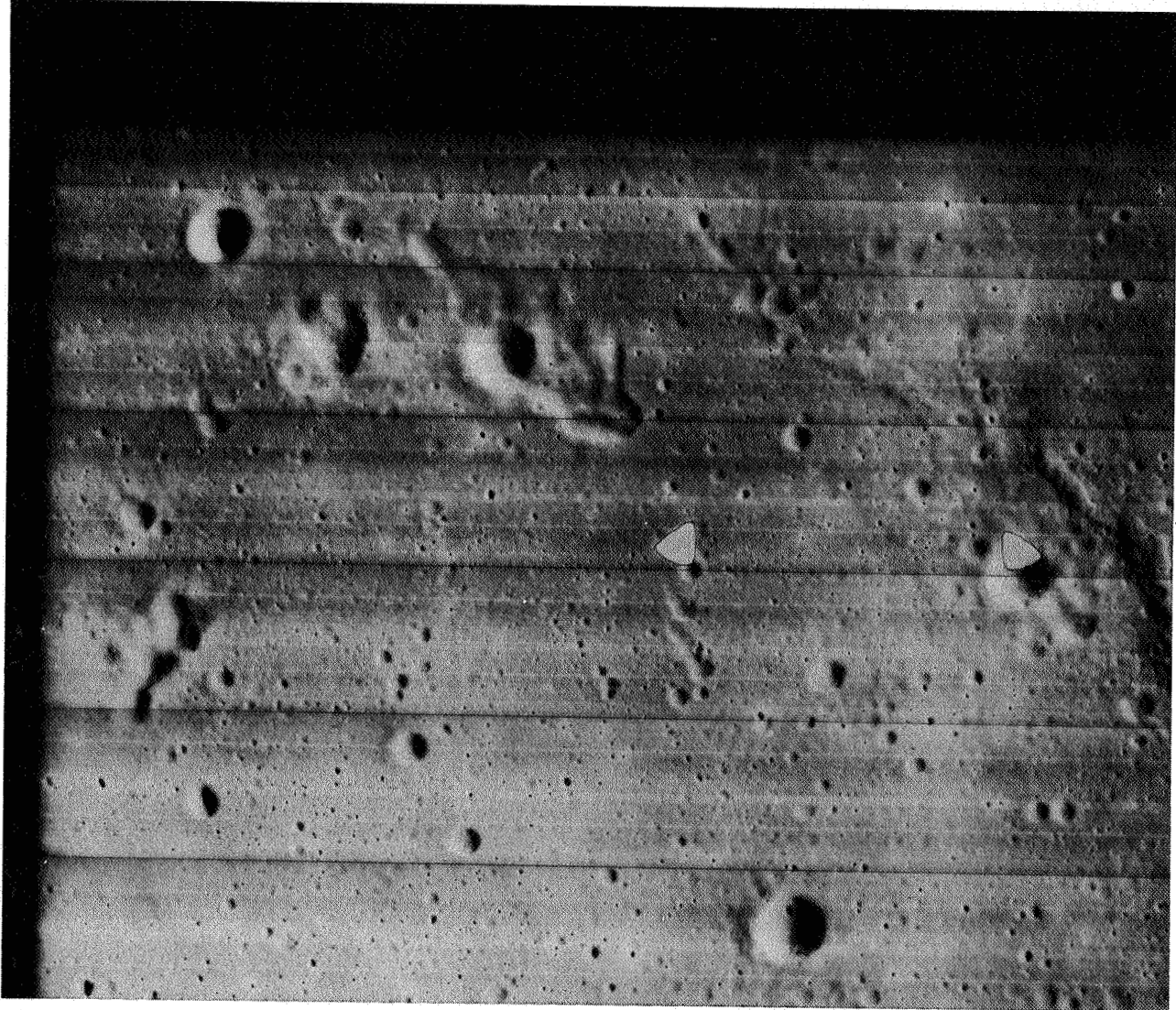


Figure 2.23: Double Mark by Bimat Metering Roller

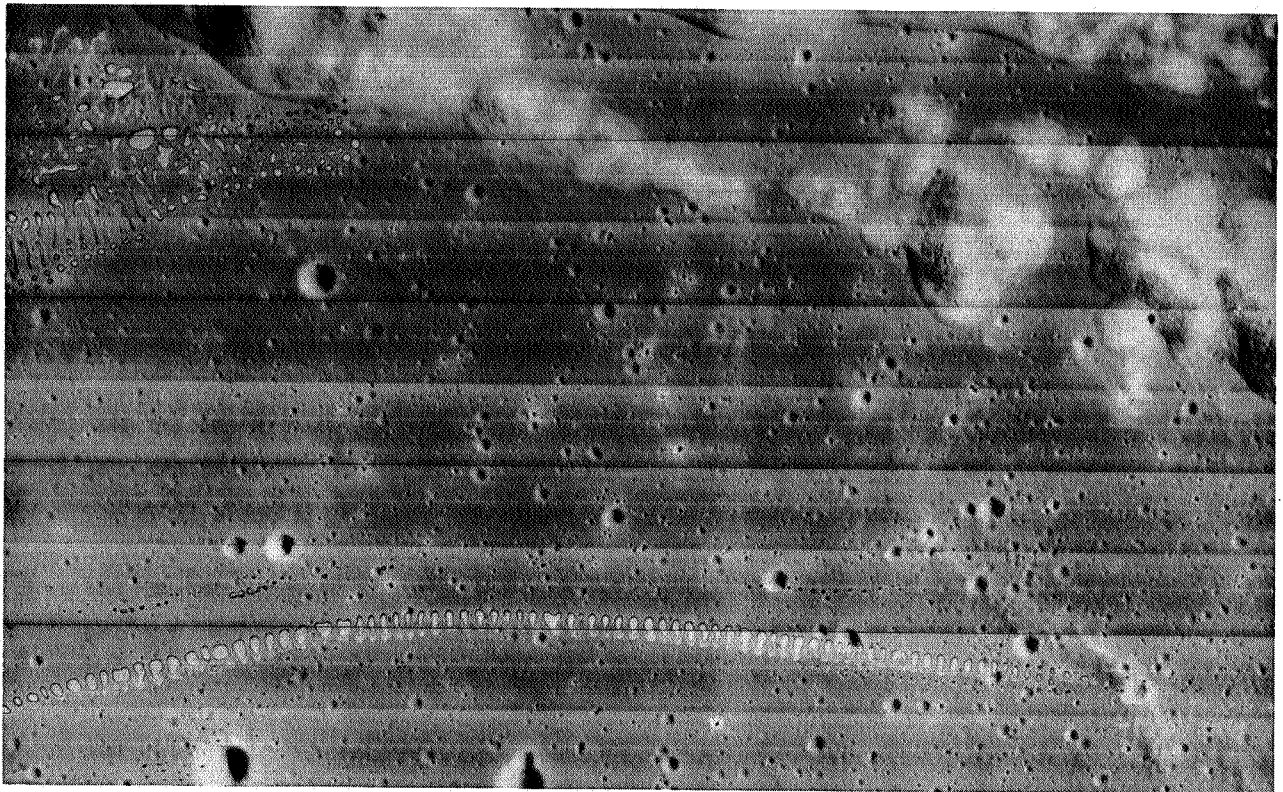
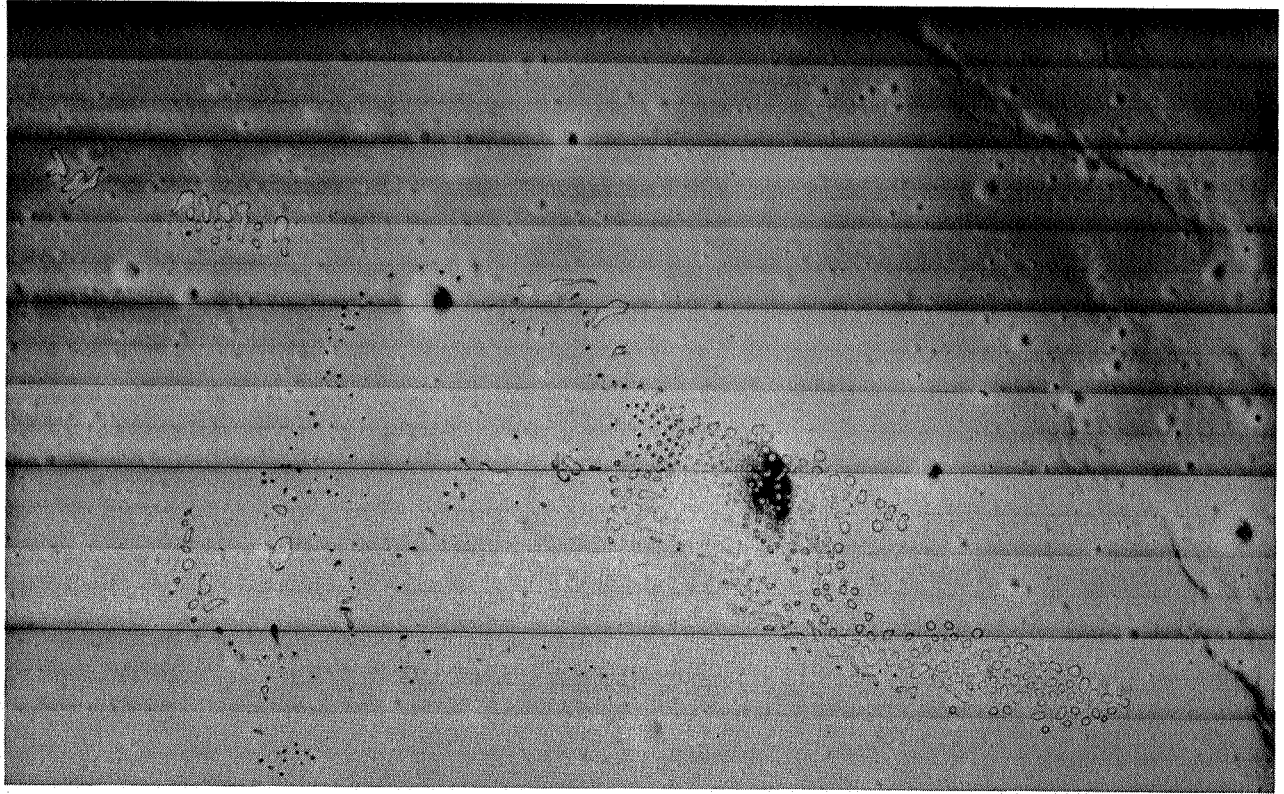


Figure 2.2-4: Examples of Processing Marks

Smear

Photographs obtained when the V/H sensor was not operating were of good quality. These are typified by the Earth-Moon photograph. Photographs taken with the V/H sensor on, however, including those of the target sites, were smeared as a result of improper focal-plane shutter actuation. The image smear appears in three directions: IMC, film advance, and a combination of the two. Those photographs smeared in the IMC direction only may contain significant information in spite of this effect. This is readily apparent in Figures 2.2-5 and 2.2-6. Small surface features are easily recognized and their size and relative locations evident from the width of the image and its position. Presence of even smaller detail is indicated by the occurrence of fine striations of the smeared image. While the photographs obtained with the 610-mm lens in many cases provide information that may be of value in conjunction with that obtained by the 80-mm lens, it is of a qualitative nature because of degraded resolution and photometric properties.

As the mission progressed and it became apparent that the problem with the focal-plane shutter could not be corrected, better exposure of the moderate-resolution photographs then was a prime consideration in selection of shutter speed. This action tended to accentuate the already near-minimum exposure by the 610-mm lens resulting from its lower light transmission. An analysis of the image smear is given in Paragraph 2.7.

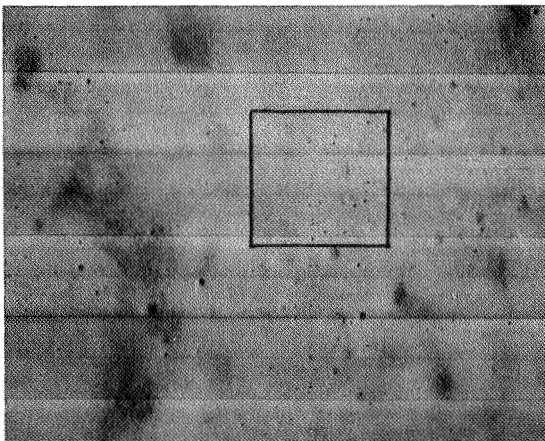
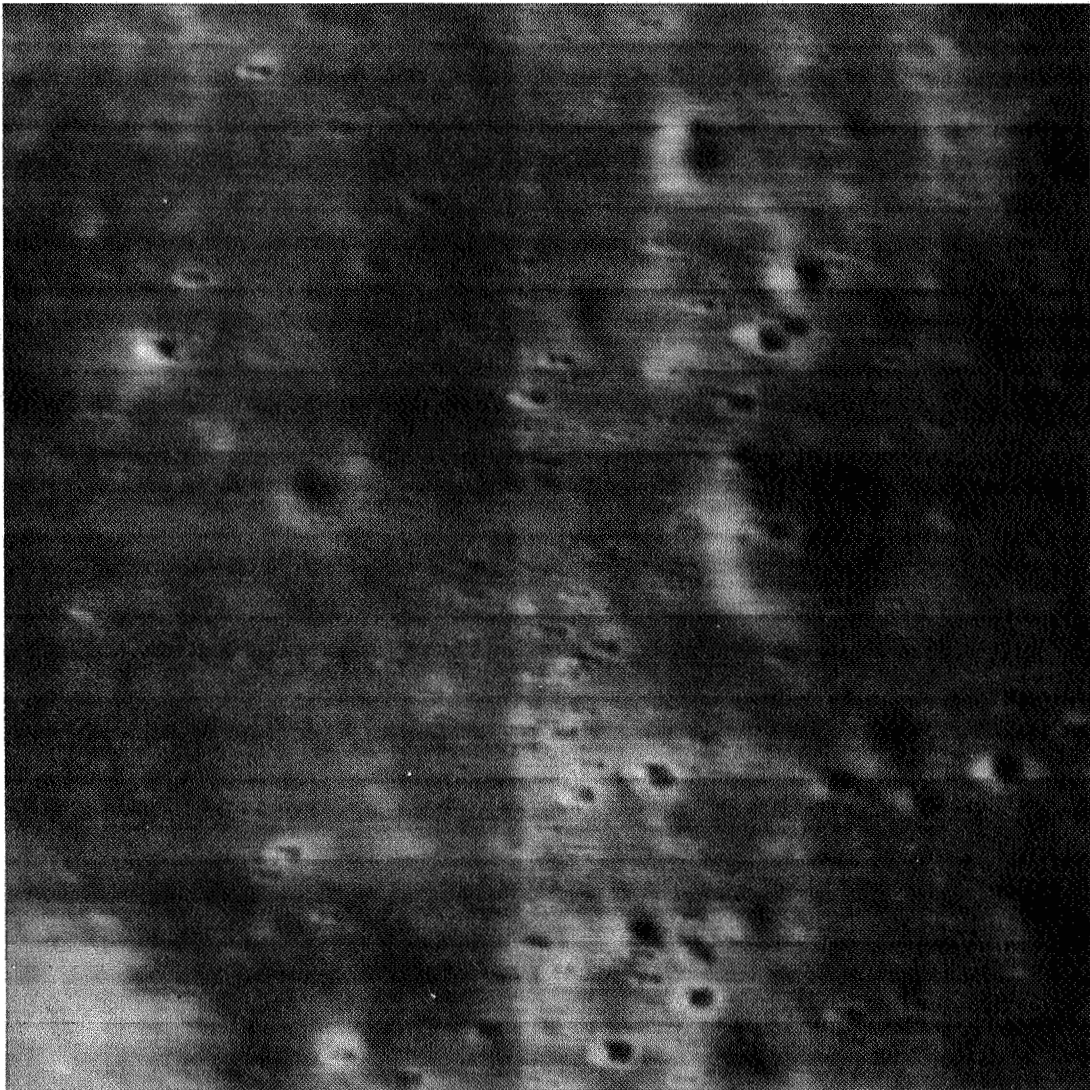
Noise Pattern

Examination of the 35-mm GRE film under a magnification of 15 to 30 diameters - - the equivalent of up to 225 times enlargement of the spacecraft film - - has revealed the presence of a small-scale density variation that resembles an extremely fine reticulation pattern (see Figure 2.2-7). The cause of this noise pattern has not been established. This pattern must be recognized by the user, when examining the 35-mm GRE film under magnification, to avoid its interpretation as a very small lunar surface structure. The size of the pattern is nearly the size of the theoretical system resolution limit.

2.2.1.2 SITE PHOTOGRAPHS

Variation in the quality of photographs obtained at each site was anticipated because of the difference in character of the surface and terrain features, the illumination, and uncertainties in premission data on these and other factors critical to photography. While the brightness and character of the target areas varied over a wide range, photographic quality was dependent upon selection of the best of only three shutter speeds. Optimum exposure could not, therefore, always be achieved.

Data specifically defining the location of each photograph and the conditions under which it was taken are tabulated in Paragraph 2.3.



**Figure 2.2-5: Example of 610-mm and
SO-mm Photography
Site 1-2**

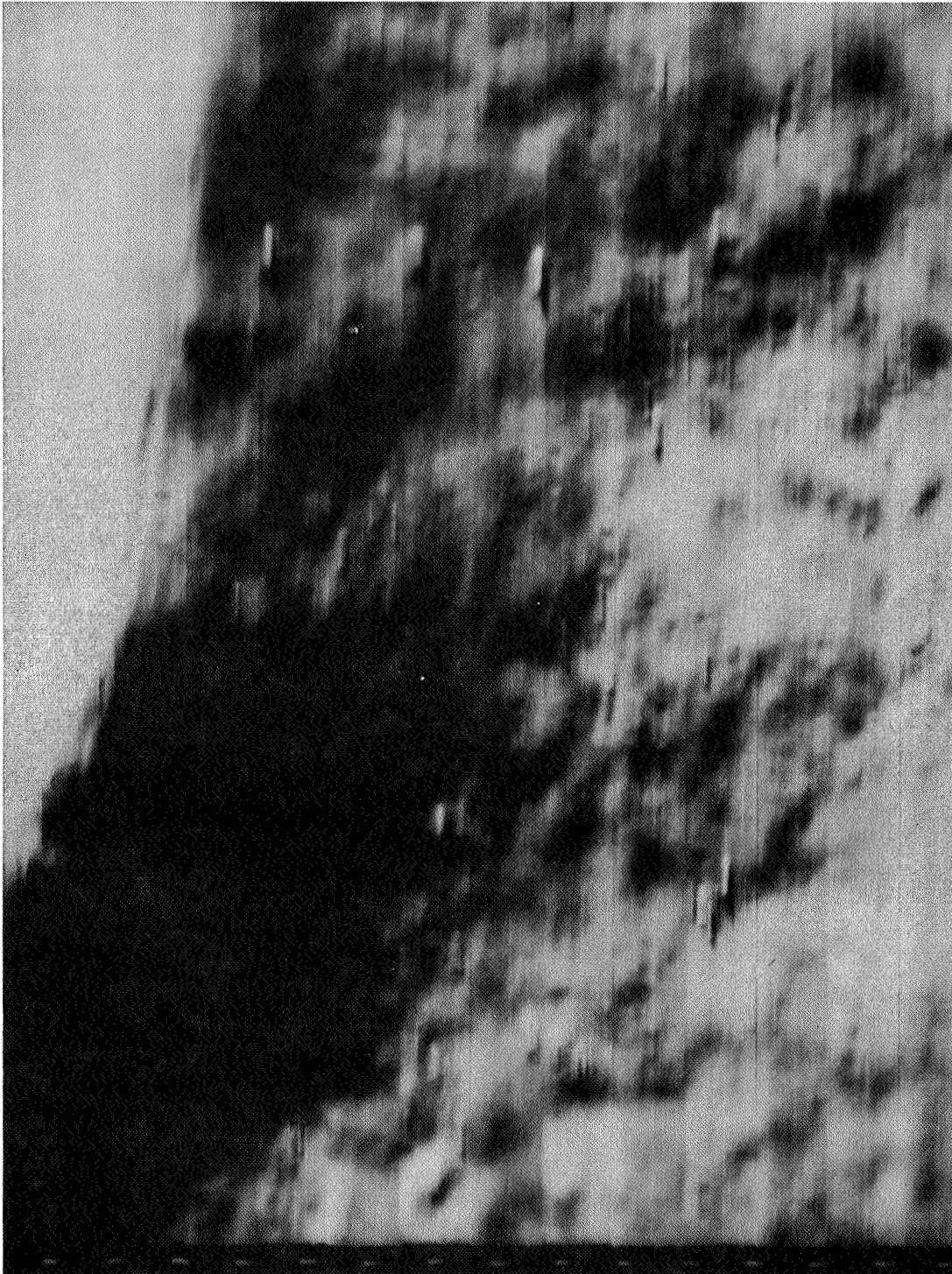


Figure 2.2-6 Detail in 310-mm Photograph Frame 85 Dionysius

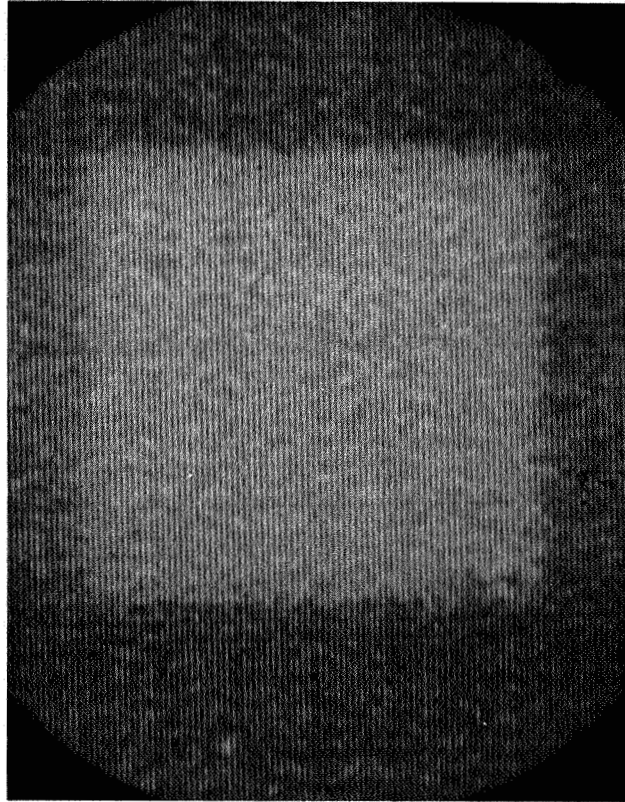


Figure 2.2-7: Noise Pattern

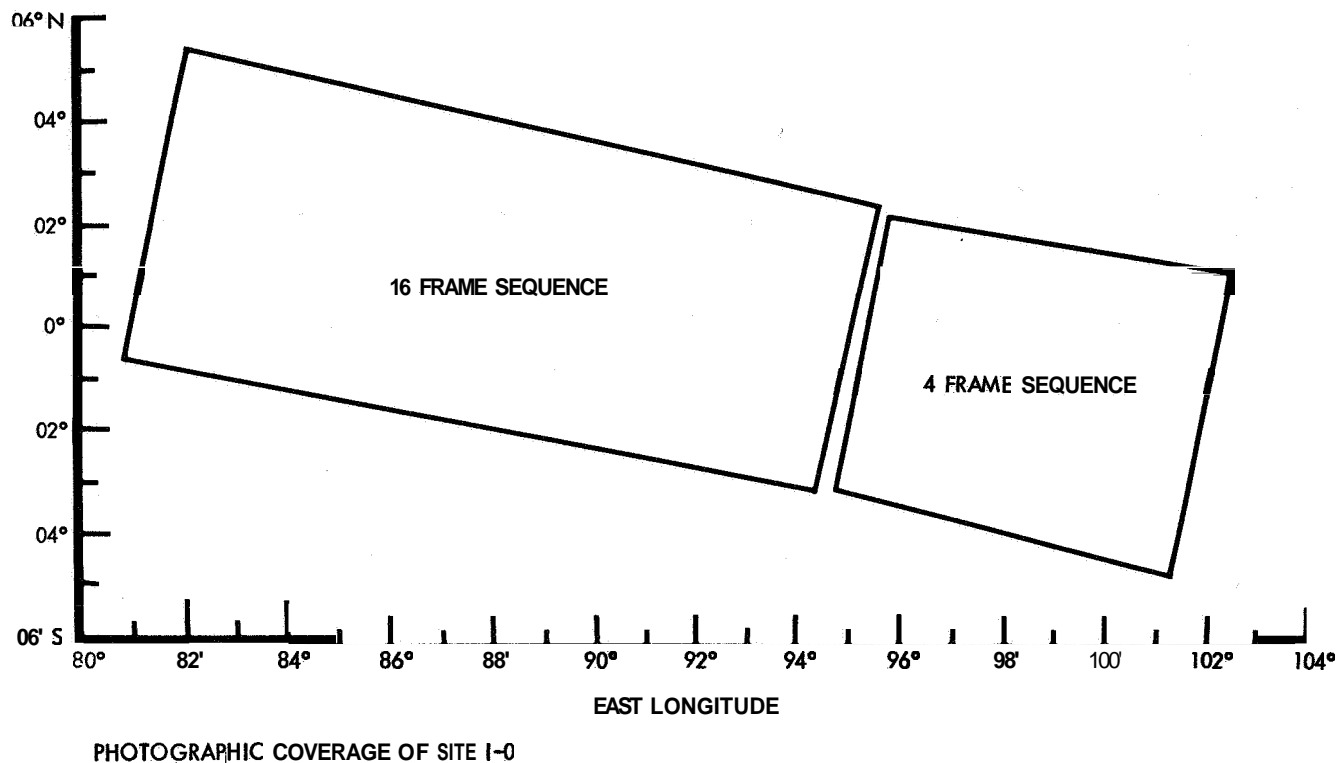


Figure 2.2-8: Site I-0 Coverage

Site I-0, Figure 2.2-8, was photographed during first-ellipse Orbit 26 from an altitude of 208 km. This area, including upland terrain and Mare Smythii, lies close to the eastern limb as observed from Earth. Because of its location, data regarding surface character was uncertain or unknown. This included its albedo. The mare surface was the principal target area, and an albedo of 0.065 was assumed, based on comparison with apparently similar terrain types.

The moderate-resolution photographs show that the selection of a shutter speed of 0.02 second was satisfactory for the mare area although somewhat less would have been more nearly optimum. Since exposure selection was based upon a mare-type albedo, the upland areas to the west and east of Mare Smythii exceeded the desirable exposure. Because of improper focal-plane shutter operation, approximately 25 to 30% of each moderate-resolution frame included an overlapping exposure from the 610-mm lens.

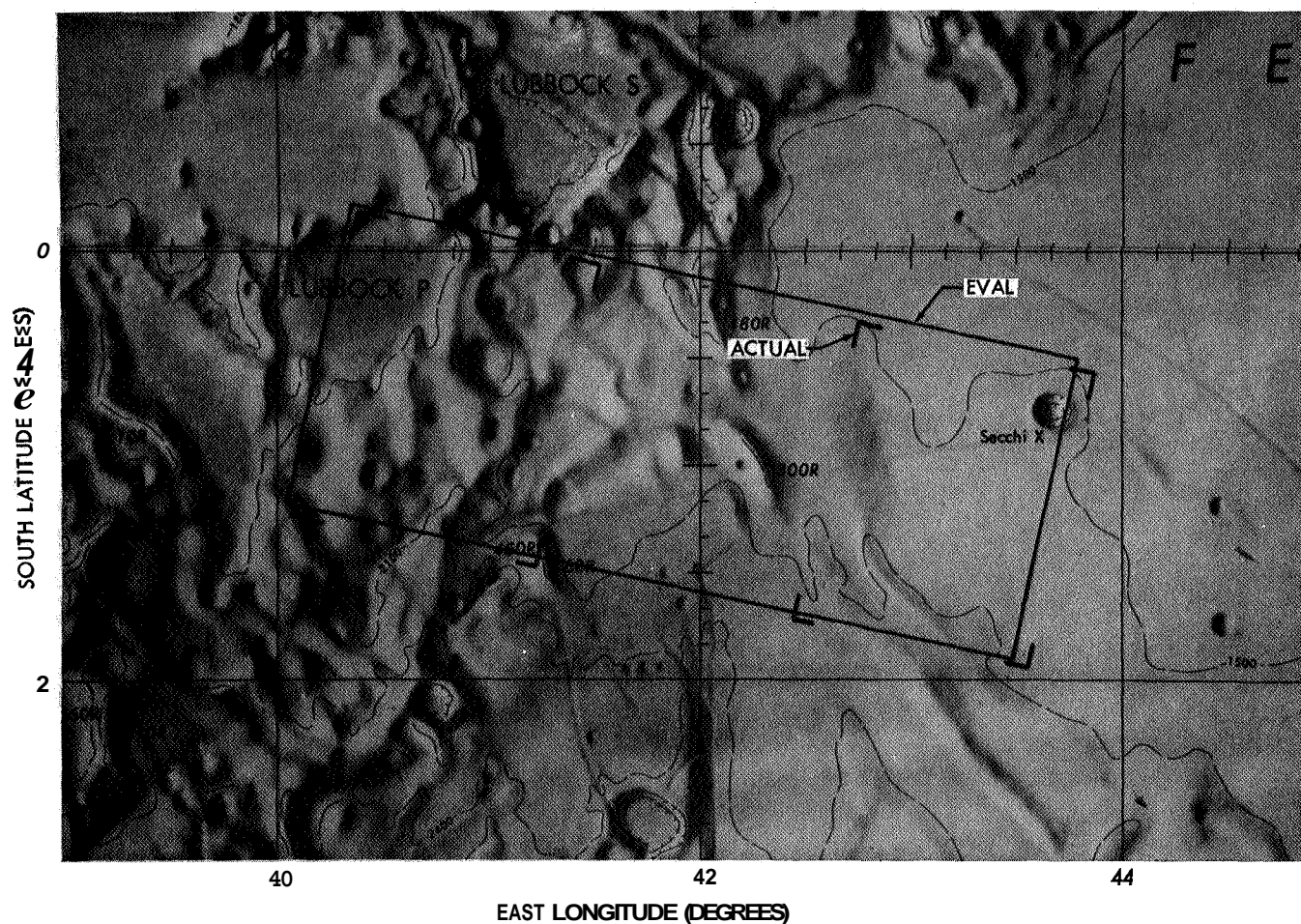


Figure 2.2-9 Site I-1 Coverage

Site I-1 (Figure 2.2-9) photographs cover the area extending from the old flooded crater, Lubbock P, across a 45-km isthmus of upland terrain, and into Mare Fecunditatis to the crater Secchi X. The area thus contains both bright upland area and darker mare area of low surface relief. Significant areas of hard shadow occur only on some of the larger upland ridges and the interior of Secchi X. A few of the upland slopes facing the Sun exceeded the brightness latitude of the system. The shutter speed of 0.02 second was correct for best representation of surface detail. Craters 8 to 9 meters in diameter can be detected in level areas, although the

combination of bright surfaces and smaller illumination and phase angles resulted in images of low contrast. Small craters and projections of this size can be discerned quite easily when they are located on slopes, crater edges, or ridges where contrasts are greater.

In Figure 2.2-4 and following site coverage diagrams, the coverage, as determined by photograph corner coordinates computed by the EVAL program, is outlined. The approximate corners of the first and last photographs of the sequence, as found by comparison of the photographs with the chart, are shown labeled "ACTUAL." Refer to Paragraph 2.3.3.

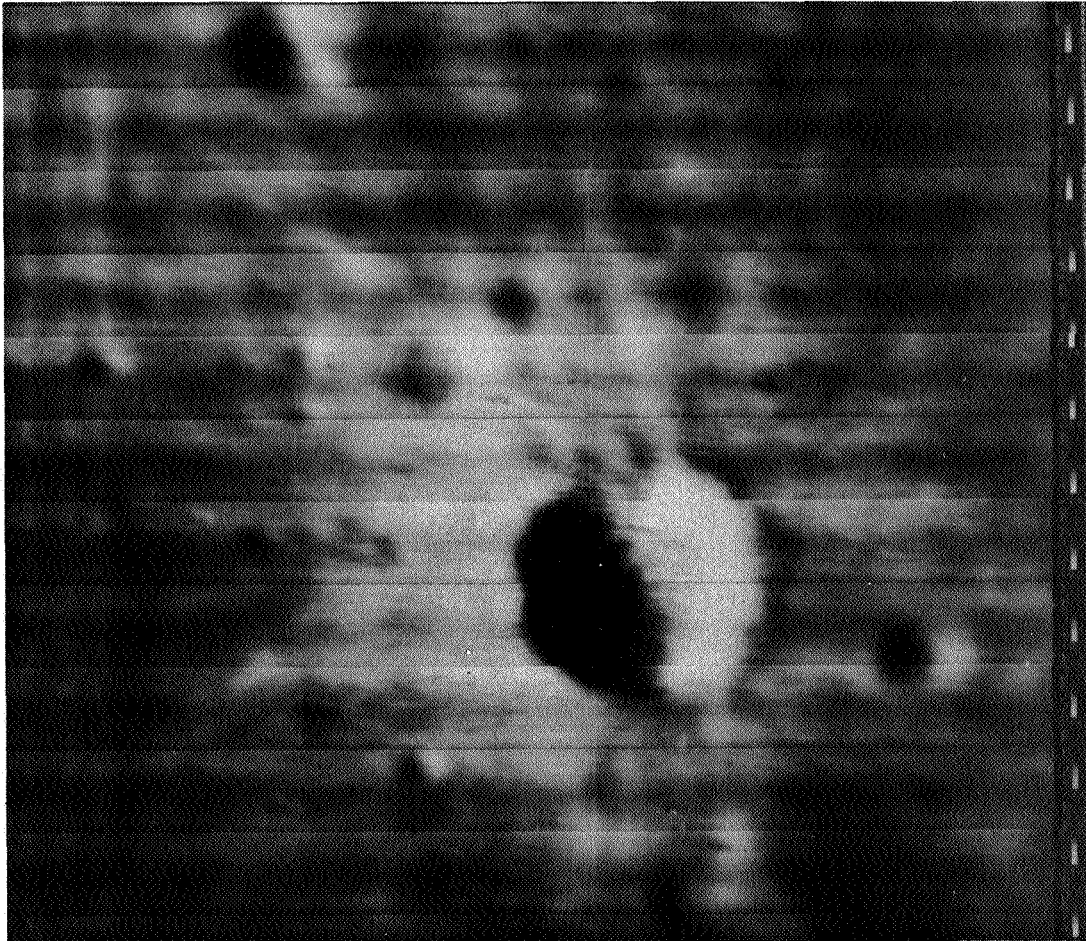


Figure 2.2-10: Site I-1 High-Resolution Photo

Significant information is present in photographs of Site I-1 obtained with the 610-mm lens, since smear occurred **only** in the IMC direction. Some determination can be made of the frequency and location of craters and fea-

tures smaller than readily detectable in the 80-mm photographs. An example is shown in Figure 2.2-10. The framelet widths in this photograph are **220** meters.

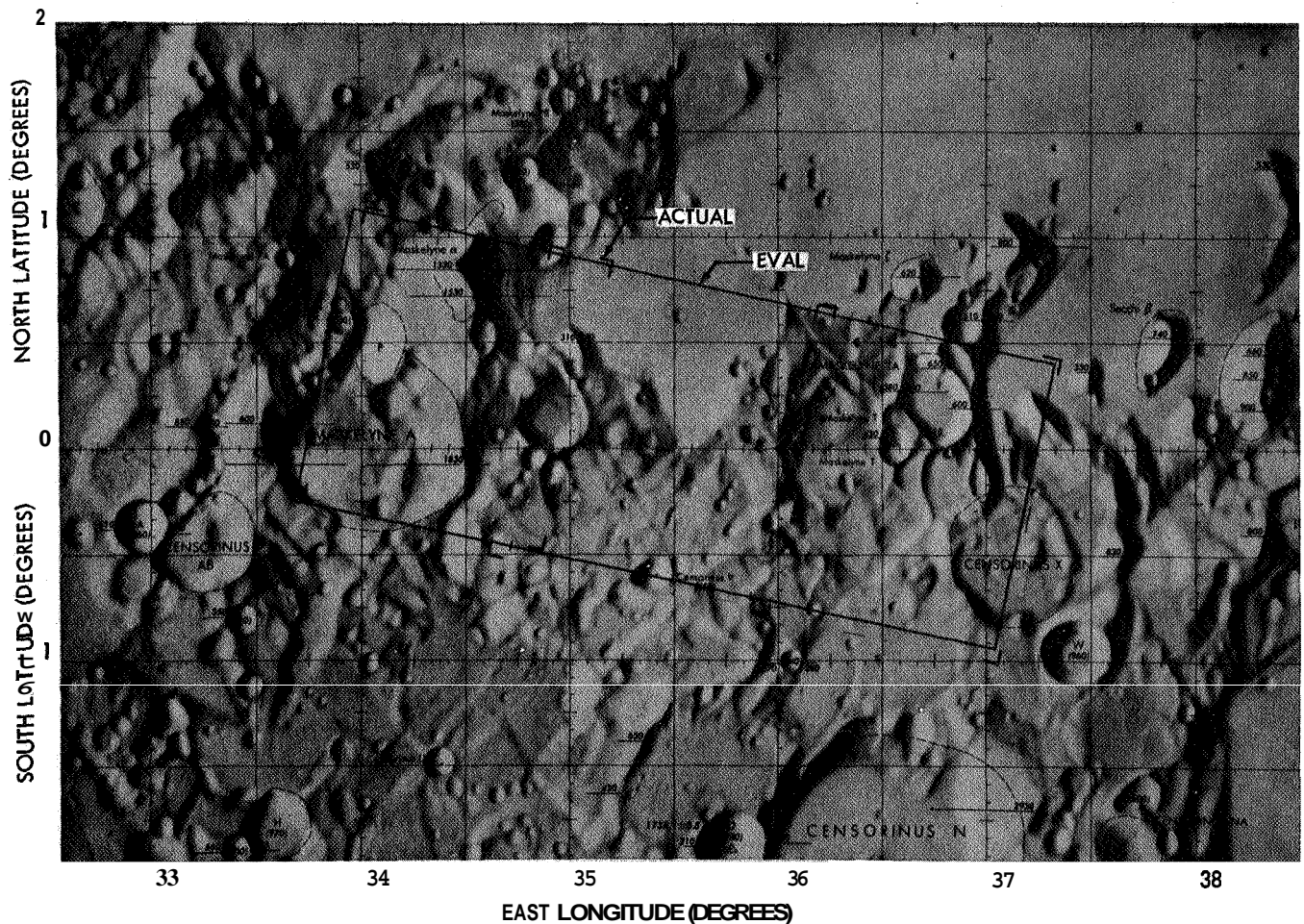


Figure 2.2-11: Site 1-2 Coverage

Site 1-2 (Figure 2.2-11) is predominantly upland terrain between the craters Maskelyne A and Censorinus X. The only mare-type area is a portion of a bay on the southern edge of Mare Tranquillitatis. The western part of the area includes rugged terrain associated with Maskelyne A. Because of steeper slopes of the topography, the range of surface luminance exceeded the system latitude. A shutter speed of 0.02 was selected on the basis of phase angle and albedo of the mare. Site 1-2 photography was accomplished on the orbit following photography of Site I-1. Therefore, data from the previous site was not available as a guide to exposure, and the predicted shutter speed was used. A shutter speed of 0.01 second would have been suitable for the bright upland area, but at the expense of detail in the mare area,

This illustrates the difficulty of photographing an area including widely different character. Features at limiting resolution are detectable in the mare area. In the uplands, most features have a *soft*, rounded appearance without well-defined boundaries that makes detection of small objects difficult.

The 610-mm photographs, with the exception of the first frame, had good exposure, and as in the case of Site I-1, provide some qualitative information regarding the occurrence of surface features. The presence of features smaller than readily apparent in the 80-mm photographs is indicated by the narrow streaks in some areas of the smeared image.

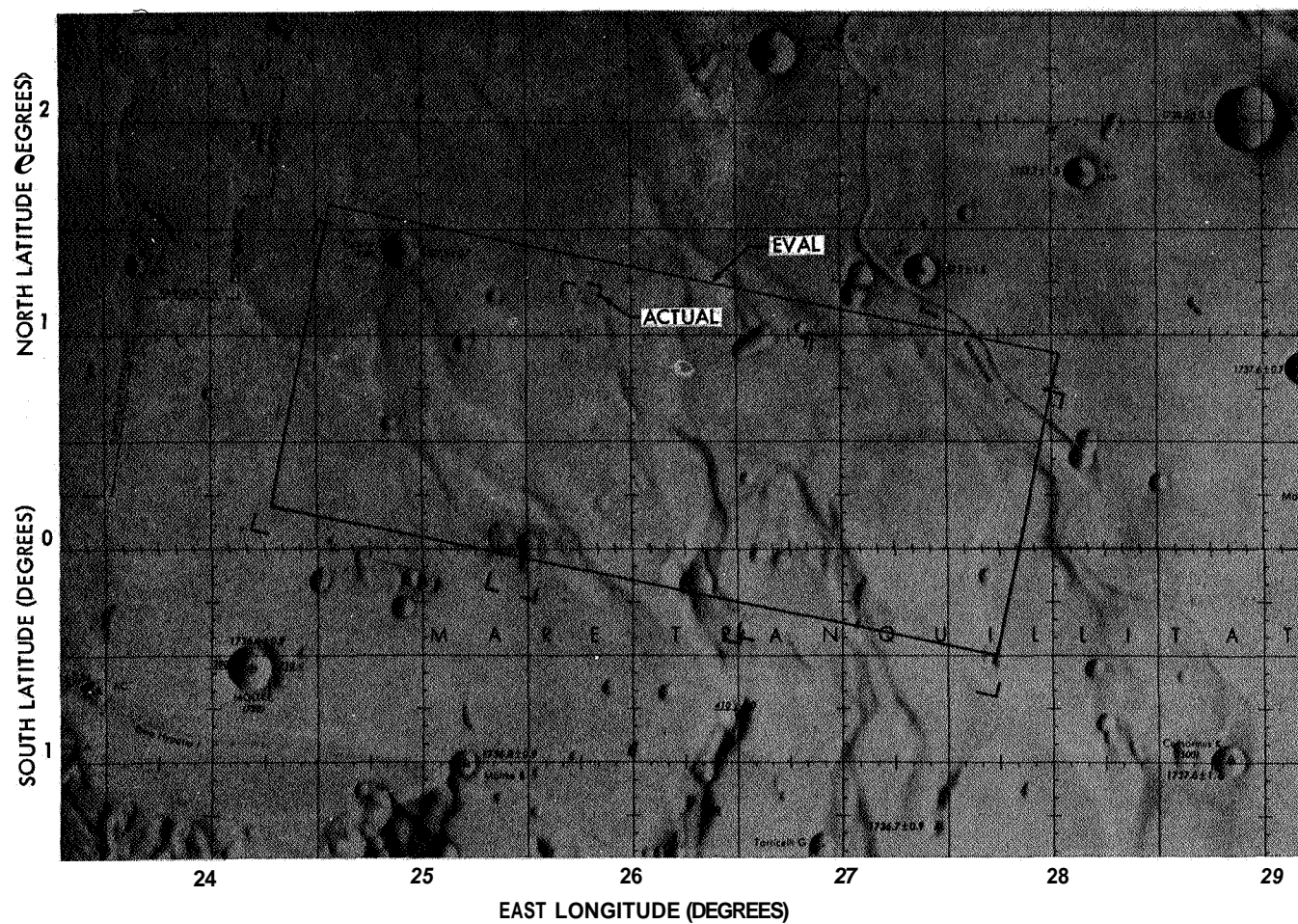


Figure 2.2-12: Site 1-3 Coverage

The quality of the moderateresolution photographs obtained at Site 1-3 (Figure 2.2-12) was satisfactory. The exposure time of 0.04 second resulted in photographs with acceptable overall density. However, flat terrain resulted in low contrast in the areas of interest, thus increasing the difficulty of detecting small features whose size is near the system resolution limit

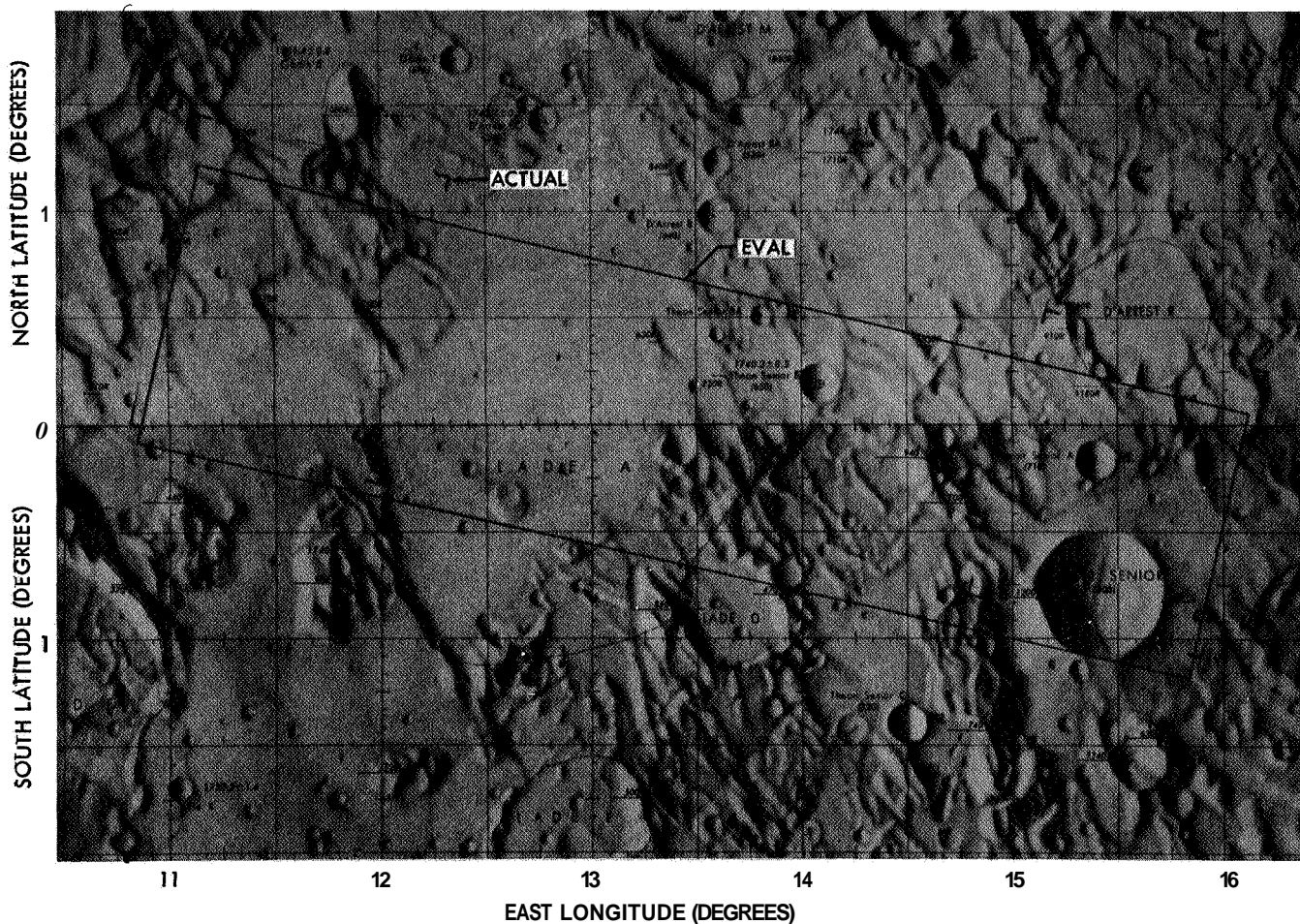


Figure 2.2-13 Site I-4 Coverage

Eight frames were exposed at Site I-4 (Figure 2.2-13). Because the slow sequencing mode was used, resulting in 50% overlap of the moderate resolution frames, the area photographed is larger than planned. The area is predominantly low-relief upland terrain, but includes some mare in the western central portion. The range of surface brightness is increased at this site also by inclusion of both upland and mare, and increased further by the ridges and slopes. The shutter speed of 0.02 second, indicated by a phase angle of 68.3 degrees and an albedo of 0.135, was used. Consideration was given to the mare area even though marginal overexposure was

anticipated in the uplands. Analysis of the photographs has shown that an exposure of 0.01 second would have been more satisfactory.

As in the photographs of Site I-2, the 610-mm photographs of this site provide some qualitative information, particularly in areas where the surface luminance was high and the 80-mm photographs were overexposed. Utility of the 610-mm photographs for aiding interpretation of bright areas was lowered by the techniques developed by personnel at Langley Research Center for enhancing the overexposed 80-mm photographs. Refer to Paragraph 2.6-3.

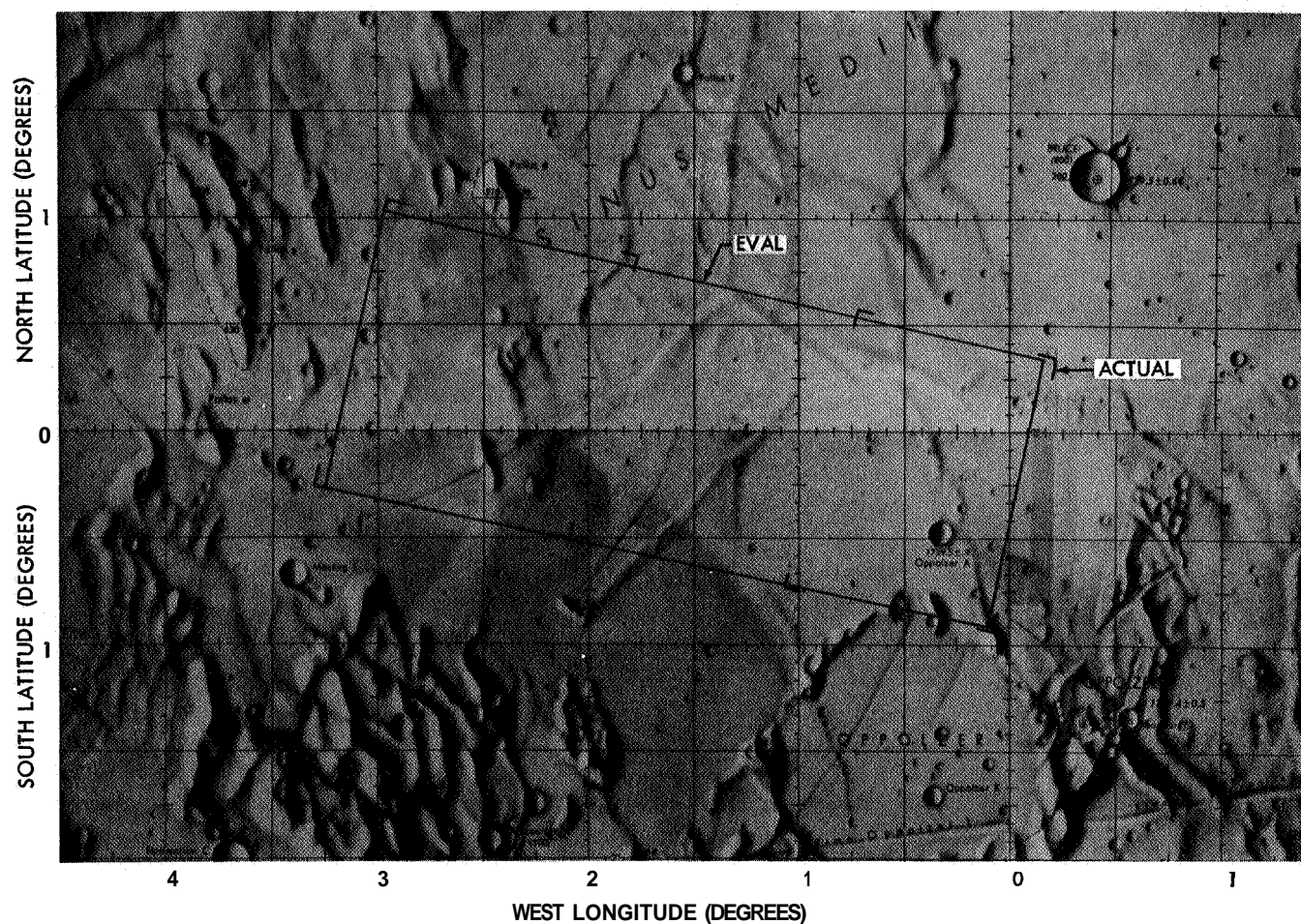


Figure 2.2-14 Site 1-5 Coverage

The photographs of Site 1-5 (Figure 2.2-14) show the area to be almost entirely a flat mare surface with few large topographic features. The moderate-resolution photographs of this site are of exceptionally high quality on the basis of exposure, resolution, and aesthetic appearance. Exposure at this site is considered to be nearly optimum.

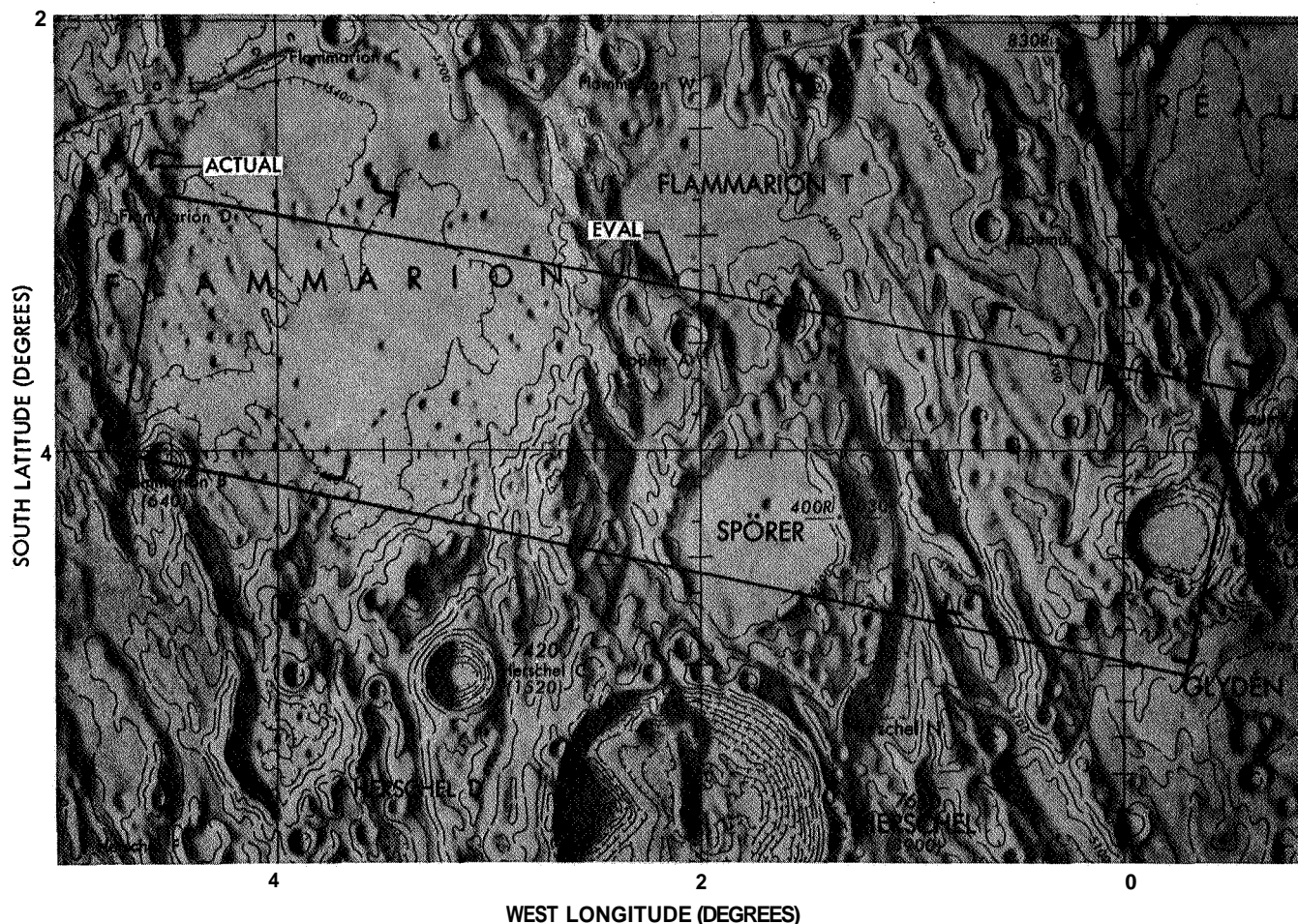


Figure 2.2-15 Site 1-6 Coverage

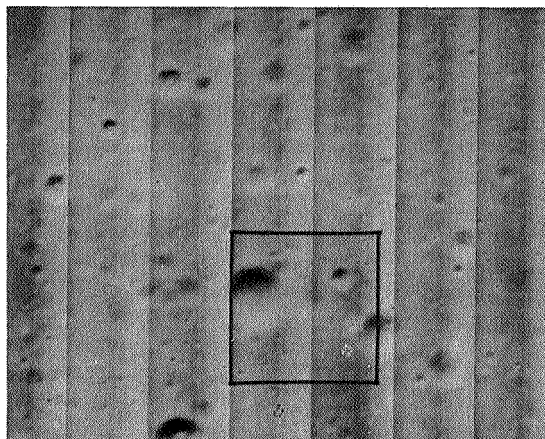
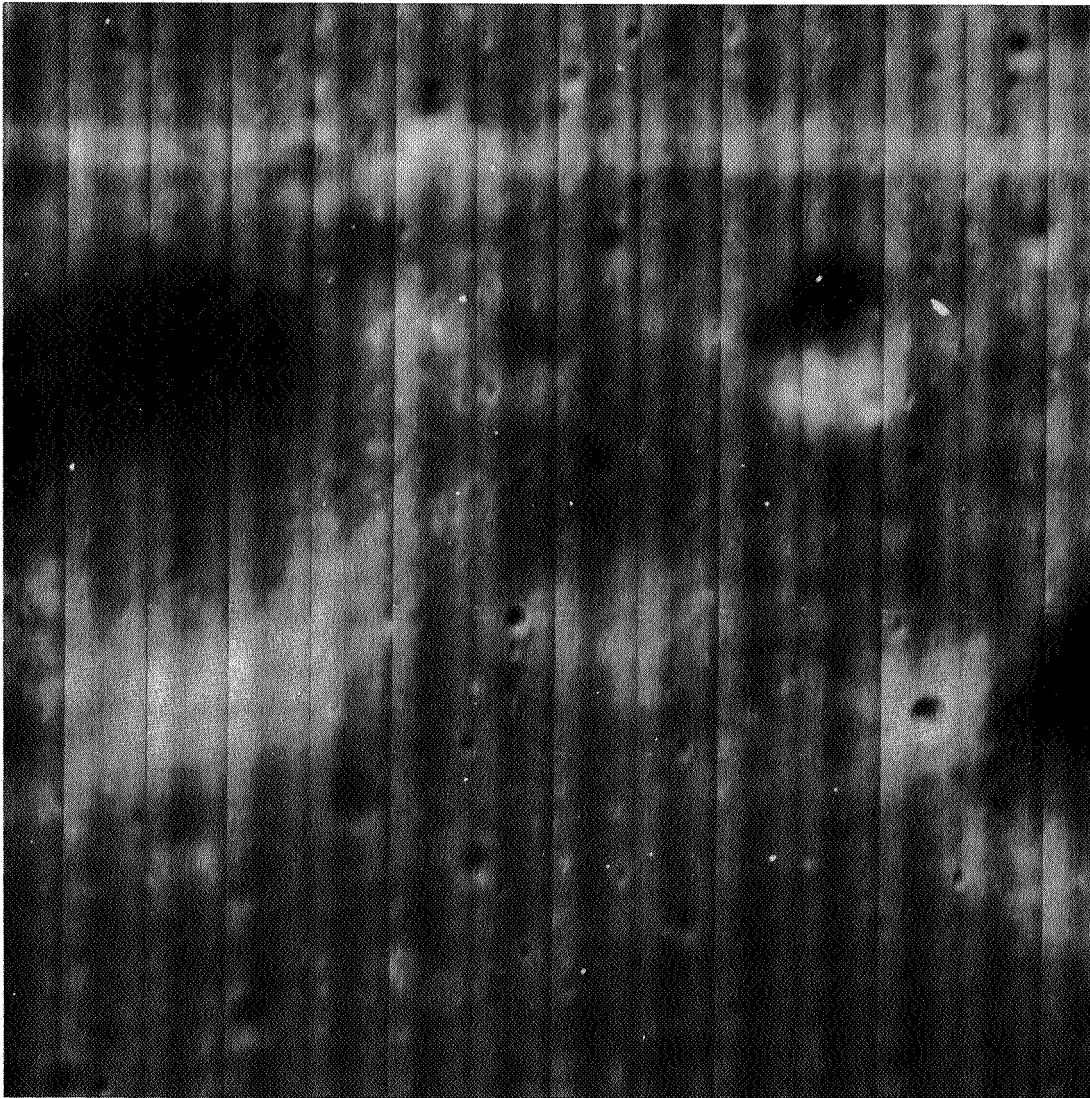
Site 1-6 (Figure 2.2-15) lies in the upland area south of Sinus Medii, and includes the area from Mösting A, the southern part of the old flooded crater Flammarion, and the uplands north of Herschel. The photographs show the area to be smooth, with gradual slopes and contours rather than a sharply delineated and rugged terrain as might be expected from the location.

As for Site 1-4, a sequence of eight frames was exposed in the slow mode, which resulted in more extensive coverage than planned prior to flight.

The combination of high albedo (0.125) and small phase angle (54 degrees) resulted in a very high surface luminance. A shutter speed of 0.01 second was used but the moderateresolution frames were overexposed. It should be noted that 0.01 second is the fastest available on the

Lunar Orbiter camera. Ideally, an exposure of 0.005 second should have been used to prevent the image density limitation being exceeded. Earlier mission plans, based upon then-available data, called for an exposure of 0.02 second, which would have resulted in disastrously overexposed photographs. This was changed to 0.01 second as a result of revised USGS albedo information available just prior to launch.

The short exposure reduced the image smear of the 610-mm-lens photographs and considerable terrain detail can be seen. An example of the high-resolution photography of Site 1-6 is shown in Figure 2.2-16. Detail such as shown provides qualitative information to supplement interpretation of the 80-mm photographs. The smaller IMC smear makes it possible to estimate the size of objects smaller than apparent on the moderateresolution photographs.



**Figure 2.2-16 Site I-6 Photographs - -
Example of 610-mm and
80-mm Photography**

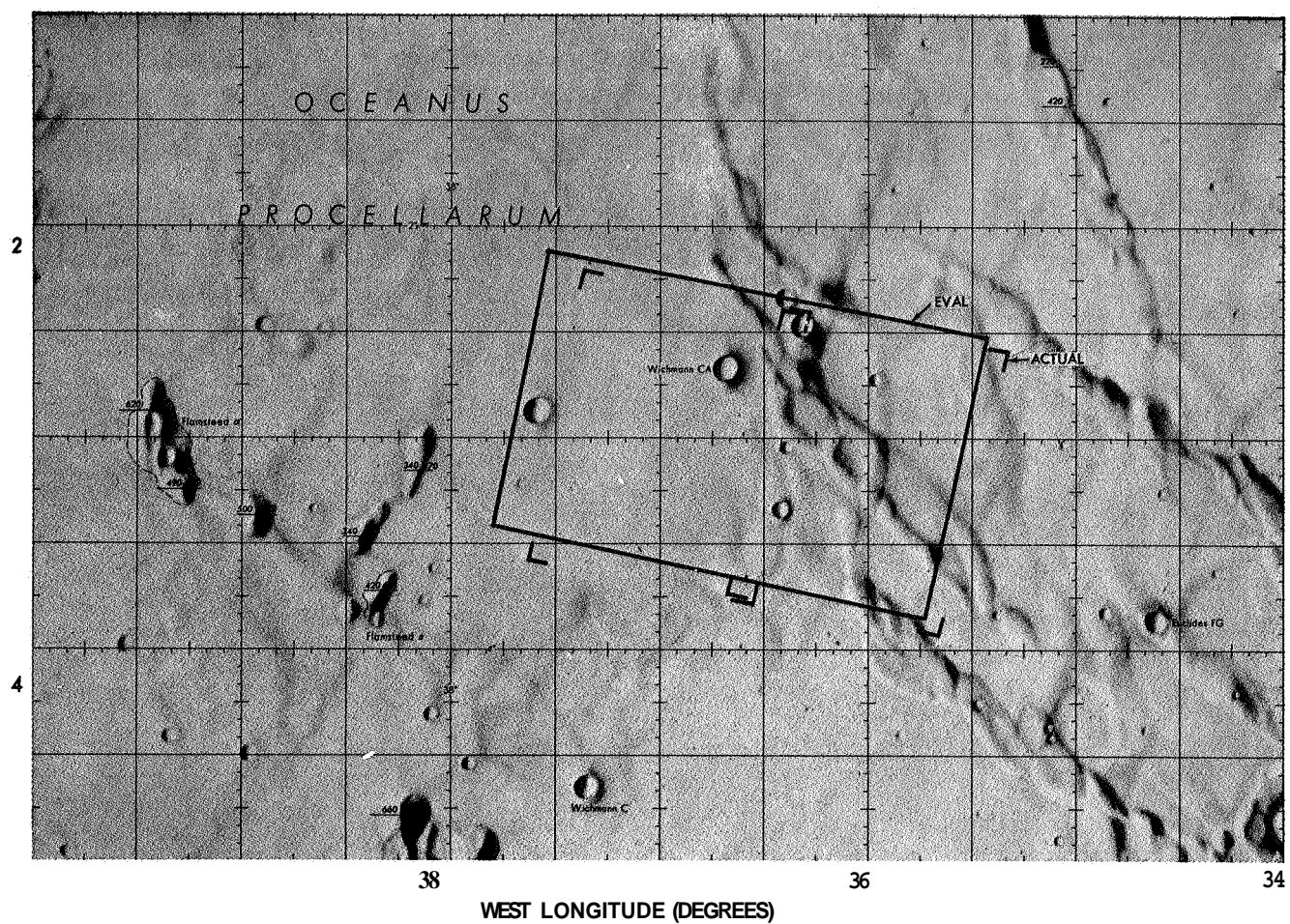


Figure 2.2-18: Site 1-8.1 Coverage

Site 1-8.1 (Figure 2.2-18) is also a flat mare area with no major topographic features. The larger phase angle resulted in greater contrasts than obtained in the previous two sites and more satisfactory exposure of the moderate resolution frames.

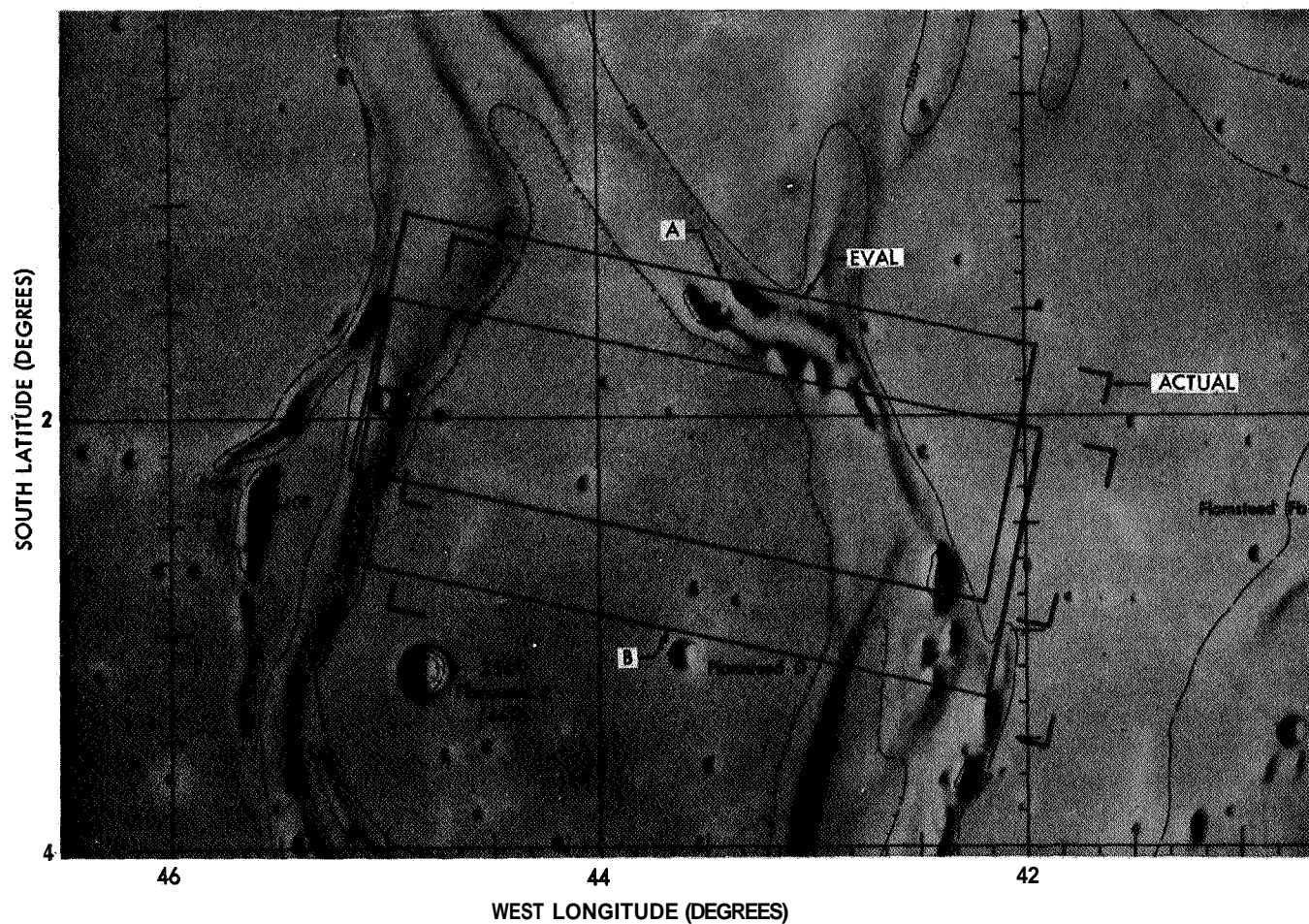


Figure 2.2-19: Site 1-9.2 Coverage

Site 1-9.2 (Figure 22-19), which includes the Surveyor I landing position, is a flat mare with only the ring-rills of the ghost crater Flamsteed P. Sequences of 16 exposures each were taken on each of two successive orbits. This resulted in a side-overlap of 68.6% as well as 88%

forward overlap of the photographs. The moderate-resolution photographs are of excellent quality with respect to exposure, resolution, and appearance. Detection of Surveyor I could not be confirmed.

2.2.1.3 OTHER PHOTOGRAPHS

A total of 55 dual-frame, were used to satisfy photographic subsystem operating constraints and to obtain special test data. Of these, 45 frames were used to obtain photographs of great interest not only to the Apollo program but also to the scientific community. The remaining ten were expended in camera operations for test or operational reasons. Four were made with the thermal door closed and are, therefore, blank. Except for the farside photographs, the spacecraft attitude was not changed for the exposure, but remained in Sun-Canopus orientation or pitched off Sunline.

Nearside Photographs

Fifteen dual-frames were used to photograph areas considered as prospective target sites. The photographs are intended as a guide to design of the following mission. All of these photographs were taken as single exposures, except for Site B-11 where four frames were used. Twenty-two additional frames were used to obtain supplementary photographs of the equatorial region.

In some instances, the photographs were exposed without the V/H sensor operating. In two of these cases both high-and moderate-resolution photographs are excellent. Smear due to spacecraft velocity is slight and requires magnification of the reassembled photographs to be apparent.

Because of their number and variety, individual photographs will not be described. It should be mentioned, however, that photographs of the evening terminator were successfully obtained.

Farside Photographs

Eleven frames were used to obtain photographs of the Moon's farside. These photographs were all taken at altitudes ranging between 1295 and 1453 km. and thus provide extensive coverage. A total of over 3 million square kilometers was photographed, much of the area being included on more than one frame. Resolution on the photographs taken with the 80-mm lens is about 240 meters, while that on the 610-mm photographs was 30 meters. All photographs were taken at an exposure of 0.02 second. Because of the altitude, each photograph covers a wide range of longitude and thus of illumination. The coverage of these photographs overlaps that of Site I-0 and extends around to 100° W. longitude. The western limb region could not be photographed because this area was not illuminated during the photographic phase of the mission.

The photographs are of excellent quality and provide the first such detailed photographs of the farside.

Earth Photographs

During the second ellipse, two frames were used to obtain photographs of the Earth's terminator with V/H commanded "OFF." The first photograph was taken on August 23, 1966, at 16:35:07.50 GMT with an exposure time of 0.01 second. This photograph, Frame 102, includes the Earth and a portion of the eastern limb of the Moon as viewed from the farside. The photograph shows Earth with slightly less than half of its nearside illuminated by the Sun. Cloud cover over the illuminated area of the Earth is very extensive. Continental land

masses are not apparent because of the extensive cloud cover. Positions of the continents, shown in Figures 2.5-2 and 2.5-7, were determined from the relative positions of the Earth and spacecraft at the times of exposure.

The oblique view of the limb of the Moon included in the photograph is very detailed and depicts this farside lunar area from a spacecraft altitude of approximately 1197 km. These photographs were of major importance from the standpoint of demonstrating the value of oblique photography for interpretation of lunar topography. The success of these photographs resulted in planning of additional oblique photographs for following missions.

The second Earth photograph, Frame 117, was taken on August 25 at 07:15:00.70 GMT with an exposure time of 0.02 second. This is a quarter-Earth photo with approximately 25% of the nearside of the Earth illuminated.

A third Earth photograph was obtained inadvertently by the 610-mm lens on Frame 103. This high-resolution photograph, which is smeared, was exposed shortly after Frame 102 (Orbit 16) when the 610-mm-lens shutter was apparently activated by noise or electromagnetic interference. However, the moderate-resolution portion of Frame 103 correctly records a planned photograph of Site B-5 taken on Orbit 18 of the second ellipse.

Special Test

Five frames scheduled to satisfy film-set constraints were used to perform special tests. These exposures were made with the camera thermal door closed. As an example of a test sequence, the following operations were commanded

- 1) Thermal door opened;
- 2) V/H turned on;
- 3) V/H turned off;
- 4) Thermal door closed;
- 5) Shutter operated.

This test was conducted to determine if V/H operation caused a transient pulse or noise that would trigger focal-plane shutter operation. If so, an exposure would appear on the 610-mm-lens format, but not on the 80-mm format. The results of these tests are discussed in Section 2.5.

2.2.2 RECONSTRUCTED RECORD

At the DSIF site or site, receiving the transmission from the spacecraft, the video signal is demodulated and converted into the reconstructed photographic image. This operation is accomplished by the ground reconstruction electronics (GRE) and the associated equipment of the ground reconstruction system (GRS). Users of the 35-mm reconstructed record film should note the following:

- 1) The direction of scanning across the spacecraft film is reversed for successive framelets. Scanning of the spacecraft film begins at the edge having the pre-exposed edge data and traverses the film. The direction of travel is then reversed, and scanning is carried out again, but the direction of scan across the framelet is not changed. (The framelets derived are designated A or B, dependent on the direction of scan). Edge data on B framelets appears reversed when viewed

with the film emulsion down or through the back of the film. The edge data occurs on the edge of the nearside photographs corresponding to the trailing edge with respect to the direction of travel over the lunar surface.

- 2) No distinction is made between framelets of photographs taken with the 80- or 610-mm lens. This must be determined from the data index.
- 3) The GRE reconstructed framelets of the 610-mm-lens photographs are mirror images and must be reversed with respect to the edge data for proper representation and comparison with the 80-mm lens photographs. The image reversal is produced by the folding mirror interposed in the optical train of the 610-mm camera.

During readout, the video signal was reconstructed on two operating GRE's and recorded on video tape at the DSIF site in view. When two sites were in view, four GRE records were produced. The 35-mm reconstructed record film was processed at the recording site prior to shipment to Eastman Kodak for reassembly and copying. The video tape recordings were shipped to NASA Langley Research Center, where additional reconstructions were prepared for evaluation and interpretation of the photographs.

2.2.2.1 PRIORITY READOUT

Following photography of Site I-0, processing time and camera operations were scheduled to permit readout of selected photographs or portions of photographs. The principal objectives of this procedure were to provide information for operational evaluation, control, and verification. The procedure also provided photographs for preliminary examination of the target areas. Prior to completion of photography and start of final readout, 106 individual photographs or portions of photographs, including film-set frames and those of the Mission I target sites, were read out. Before transfer from the first to second ellipse, seven complete and three partial moderate-resolution photographs and six complete and four partial high-resolution photographs of Site I-0 were read out.

Due to the high-resolution smear problem discussed previously, and requirements for evaluation of the shutter malfunction, premission planned scheduling and film budget were revised. The priority readout accomplished during the mission is diagrammed in Figure 2.2-20. Photos read out in the priority mode were again read out in final readout.

2.2.2.2 FINAL READOUT

The Bimat was successfully cut August 30 (Day 242) at 1814 GMT during Orbit 65. Final readout began during the next orbit at 2046 GMT with readout of the Site I-9.2 photographs. Final readout of all frames, including the Goldstone test image on the film leader, was accomplished without serious difficulty or malfunction. No degradation in quality of readout attributed to the subsystem was apparent through completion of final readout.

2.2.2.3 VIDEO TAPE

During both priority and final readout, the video signal

from the spacecraft was recorded on video tape by Ampex FR-900 recorders. Since the recording tapes had insufficient capacity to record a complete final readout period, tape reels had to be changed during each sequence with some loss of data. During final readout the time lost due to reel change had been reduced to about 1 minute.

The video tapes were shipped daily from each recording site to Langley Research Center, Hampton, Virginia. These tapes were used to prepare additional reconstructed records using a GRE installation at this location (Refer to Paragraph 2.6). These reconstructed records were equivalent to the reconstructed records prepared at each site from the received video signal.

2.2.3 REASSEMBLED NEGATIVES

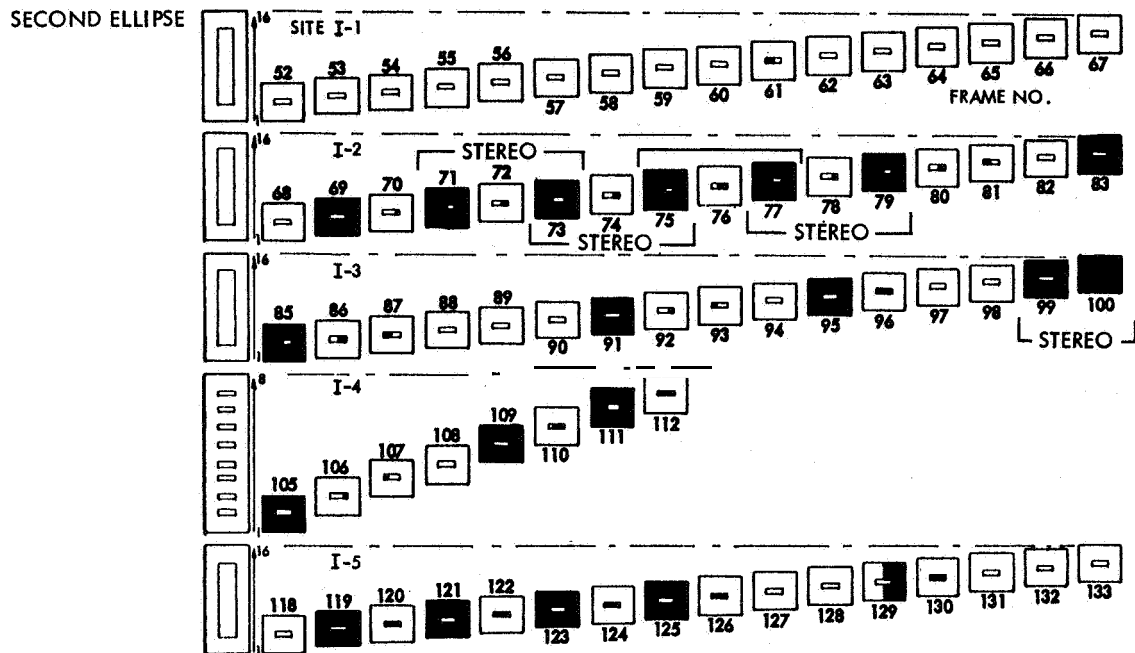
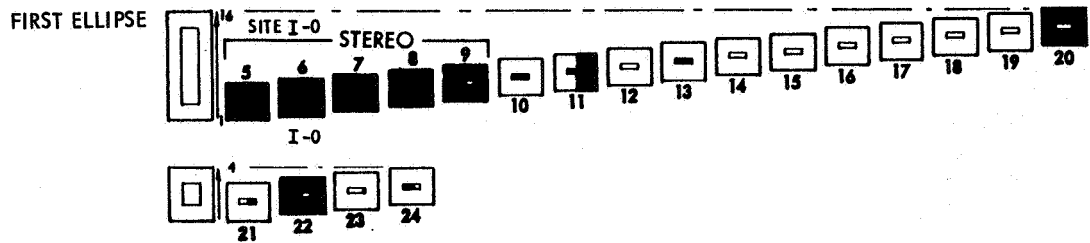
The 35-mm reconstructed record film, which had been processed at each recording site, was shipped to Eastman Kodak, Rochester, New York, for reassembly into 14-framelet subframes. The reassembly method and control is discussed in Paragraph 2.5.5.

During the first part of the reassembly operation, some difficulty was experienced in obtaining proper control of reassembly negative density. These problems were corrected and uniformity was improved. The nonuniformity of density between subframes appears most prominent in the frames from priority readout

During reassembly the 7.2-times enlargement of the reconstructed record over the spacecraft film is reduced to 6.5 times. Reassembly also results in an image reversal. Prior to the mission, the reassembly printer was set up to compensate for the reversal of the high-resolution photographs caused by the folding mirror in the optical train of the 610-mm camera on the spacecraft. The moderate-resolution photographs therefore are reassembled as mirror images. Data included in the title block of each subframe is exposed on the film in the reassembly printer. High-resolution photographs are in proper orientation when the title block appears normal. For moderate-resolution photographs, the data block appears as a mirror image. (The edge data appears reversed on high-resolution subframes and normal on moderate resolution.) A diagram of the reassembly process is shown in Figure 2.2-21.

In the reassembly process, each subframe was given a subframe number that is the serial number of the subframe reassembly as carried out by Eastman Kodak. It does not correlate with the target site or photographic frame number. Reassembly was carried out in readout sequence as received from the DSIF site. Due to the difference in shipping transit times, reassembly was not necessarily in the same order as the readout sequence.

Hand reassembly of the 35-mm reconstructed record produced by a GRE operating from the Ampex FR-900 video tape has been carried out for two purposes. Initially, hand reassembled photographs were planned for use by mission advisors in evaluating mission photography and photo-subsystem operations, and to provide a limited number of early photographs to the press. Subsequently, the technique was adopted to provide high-quality positive transparencies for interpretation and evaluation, principally at Langley Research Center, Photo Data Assessment Facility, ACIC, and the USGS.



SHADED AREAS
INDICATE
PORTIONS
OF FRAMES
READOUT.

Figure 2.2-20 Priority Readout Diagram

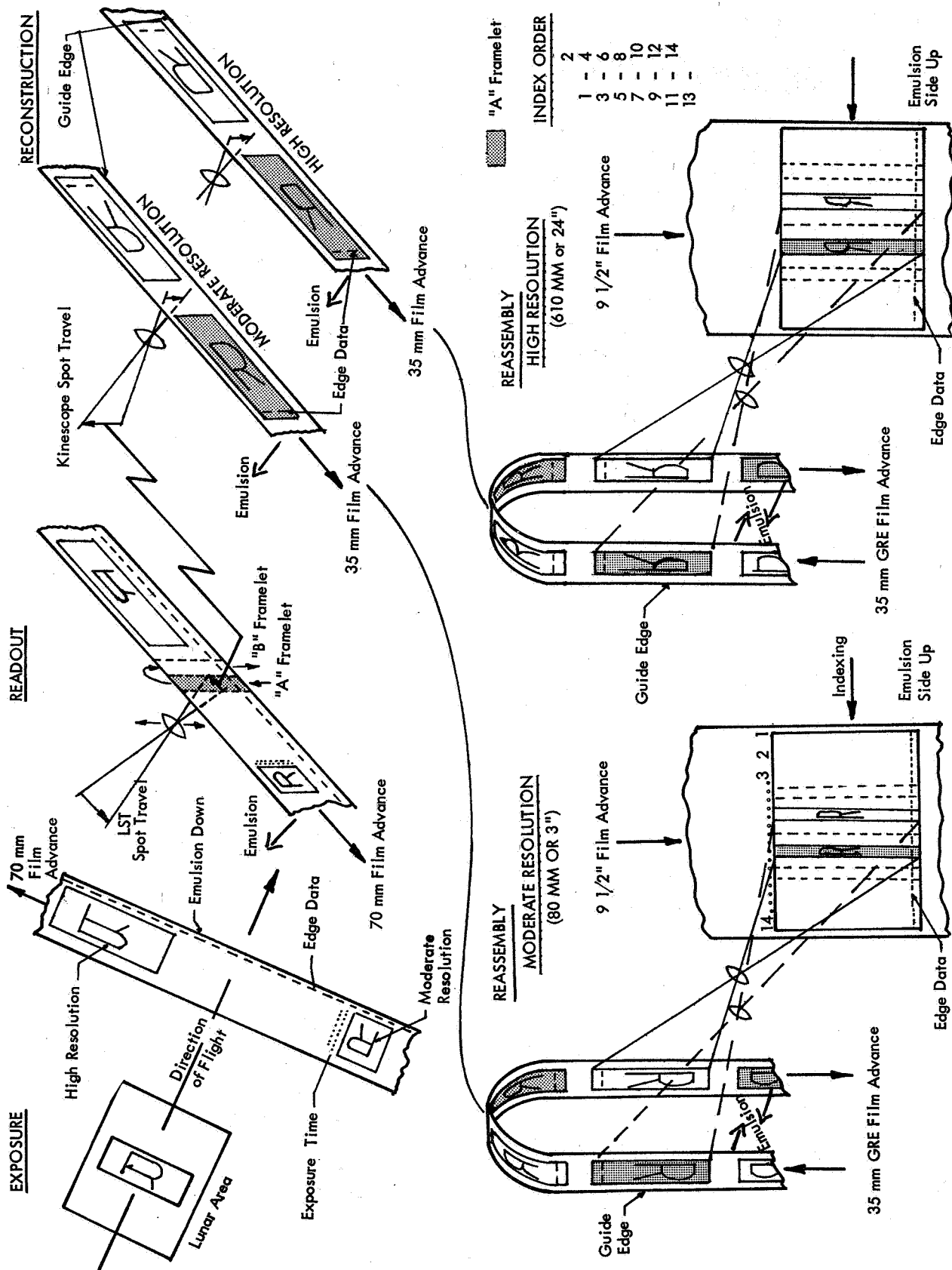


Figure 2.2-21: Reassembly Process Diagram

2.2.4 STEREO COVERAGE

The moderateresolution, wide-coverage photographs obtained at each site provide overlap in the flight direction and can be used for stereo observation of all but a small area at the beginning and end of the coverage. No forward overlap exists for 13% of the first and last exposure of the sequence.

Sequencing of exposures at all sites except 1-4 and 1-6 was in the fast mode to provide contiguous high-resolution coverage. Fast sequencing results nominally in 87% overlap of successive moderateresolution formats but **only** 5% of the high resolution. The slow mode nominally results in 50% overlap of moderateresolution photos. Sequencing is controlled by the V/H sensor, which adjusts timing to correct for variation in spacecraft altitude. The 5% nominal overlap of the high-resolution coverage was provided to ensure that contiguous coverage would be obtained; there was no intent to provide appreciable high-resolution stereo coverage in these photographs.

Priority readout provided stereo coverage with certain photos obtained in both the initial and final ellipses. Four stereo pairs included in the 20 frames exposed in the first ellipse were read out prior to transfer to the second ellipse. Stereo pairs read out during priority readout are indicated in Figure 2.2-20.

Forward overlap of moderateresolution photographs of each site was measured as the linear distance of image displacement in the direction of flight in successive frames, and then computed as a percent. No correction was made for crab angle, attitude, or surface curvature. A precise determination was not attempted. The overlap so determined is listed below in Table 2.2-1.

Site	Overlap (%)
I-0	88.1
I-1	88.1
I-2	87.8
I-3	88.1
14	53.8*
I-5	88.5
I-6	52.2*
I-7	87.8
I-8.1	88.0
I-9.2a	88.1
I-9.2b	88.1

*Slow mode sequencing

Table 2.2-1: Percent Forward Overlap

The side overlap between Sites I-9.2a and I-9.2b was 68.6%.

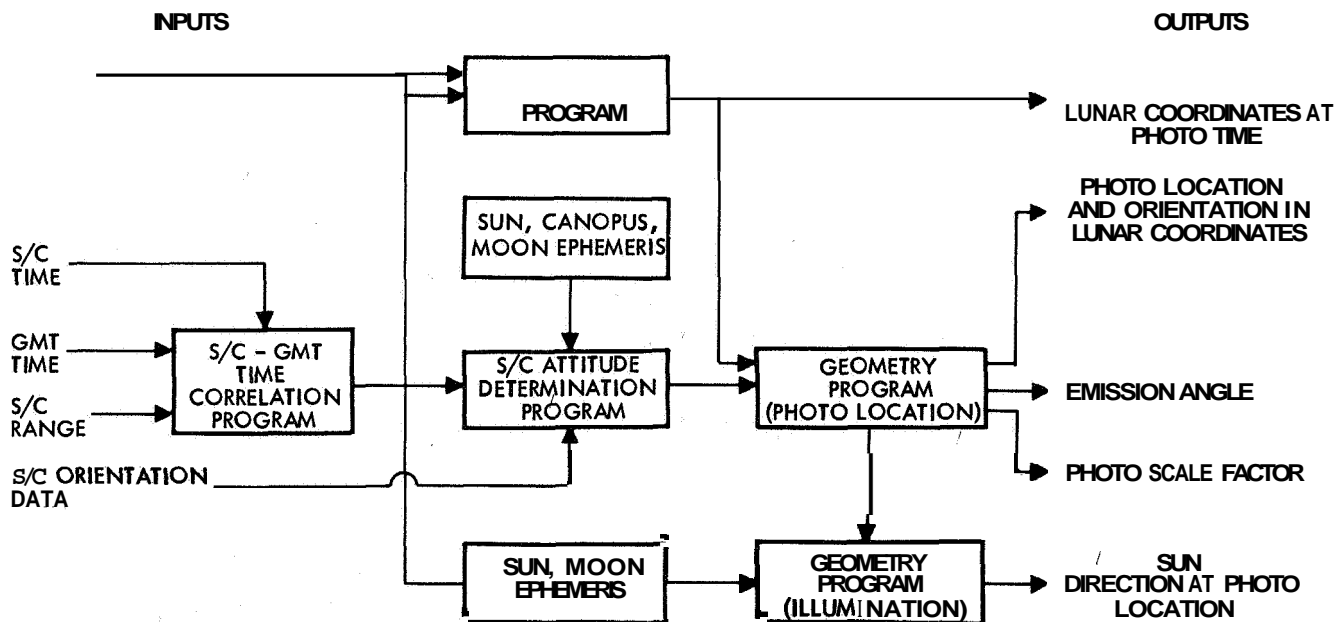


Figure 2.3-1: Photo Supporting - Data Flow

A cursory stereo examination has been made of a few pairs of the moderate resolution photographs from several sites, but no quantitative evaluation was attempted.

The forward overlap was suitable for stereo examination at all sites except for a portion of the first and last frames of the sequences. The nonlinearity of the space craft optical-mechanical scanner, with some contribution by the GRE, has caused stereo distortion. This distortion is frequently severe between adjacent framelets and may introduce an apparent slope within a framelet extending over an appreciable portion of its length. Since no Reseau grid or reference marks are included in the photographs, precise correction of the distortion will be difficult. Stereo examination will, however, enable relative slopes over limited distances to be approximated, and low-relief topography to be detected and interpreted more readily.

2.3 PHOTOGRAPHIC SUPPORTING DATA

Interpretation and evaluation of the lunar photographs requires specific information regarding spacecraft position, attitude, altitude and velocity at the time each picture was taken. Computer programs (photo and evaluation) were developed that combined prediction requirements for photo mission control, with postmission data requirements. Figure 2.3-1 illustrates the relationship between trajectory and spacecraft performance parameters required to compute the supporting data.

Pre-mission planning required that postmission photo data computations be made at the SFOF shortly after completion of the photo mission. Postmission factors negated these plans and required that the backup capability at Boeing, Seattle, be used to provide this data based upon the orbit determination program made at the SFOF to support the mission operational phase.

2.3.1 INPUT DATA SUMMARY

Input data were obtained primarily from postflight analysis of the doppler tracking data using the FPAC computer program ODPL, postmission evaluation of the spacecraft attitude, and time of exposure as read from the GRE film.

2.3.1.1 SPACECRAFT POSITION AND VELOCITY

Postflight orbit determination defined spacecraft position and velocity just prior to the first commanded camera-on time of the sequence for all the Site "I" photos. In all cases, data from at least two orbits prior to the site orbit and at least one orbit after the site orbit were used in these calculations. Whenever a "B" photographic site could be included in the data arc, this was done. With the exception of Site I-0, all site determinations were obtained by solving only for the state vector (X, Y, Z, \dot{X} , \dot{Y} , \dot{Z}) and using the values of the LRC lunar harmonic coefficients specified in Appendix B. ODPL Solution 4138 harmonics were used for Site I-0.

Following is a list of the postflight orbit determination solutions and their relation to photo sites. Under "OD solution" are serial numbers assigned by the orbit determination (OD) group; these state vectors for the specific photo sites listed and the amount of tracking data processes to obtain them are given in Appendix B tables.

State Vector for	O.P. Solution	Frame Number	Target
AO	90AO	5-24 25-27	I-0 Film Set
B3	90A1A2	50 51	B-3 Film Set
A1	90A1A2	52-67	I-1
A2	90A1A2	68-83	I-2
90A3	90A3	84	Film Set
A3	90A3	85-100	I-3
B5	90A4B5B7	103	B-5
A4	90A4B5B7	105-112	I-4
B-7	90A405B7	113-114 115-116	B-7 Film Set
A5	90A5	118-113	I-5
90A6	90A6	140	--
A6	90A6	141-148	I-6
B9A	90A6	149	B-9
B10	90A6	150	B-10
B9B	90A6	151	B-9
B11	90B11A7	153-156	B-11
A7	90B11A7	157-172	I-7
A7	90B11A7	173	I-7 Film Set
A7	90B11A7	174	Terminator
90A8A9	90A8A9	175	I-8.1 Film Set
A8.1	90A8A9	176-183	I-8.1
A9. 1a	90A8A9	184-199	I-9.2a
A9. 1b	90A8A9	200-215	I-9.2b

Appendix B Tables

All Tim-set sites were lower priority targets and hence were not supported by a postflight orbit determination except when it was convenient to include them in the "I" site data arcs. This remaining group of photos was analyzed using inflight orbit determination results as indicated in the following list

State Vector for	O.D. Solution	Frame Number	Target
4150	4150	28-42	--
Predicted Post-1st Transfer	5122	44-47 48-49	-- B-2
Predicted Port-2nd Transfer	5128	134-135 136-139	B-8 --

The photo supporting data resulting from the use of in-flight determinations is not as accurate as that generated using the "90-" series (posflight) OD data.

2.3.1.2 CAMERA-ON TIMES

Camera-on times were obtained by reading the digital time code exposed on the spacecraft film when the 80-mm shutter actuated. A computer routine (TIML) was developed and used to convert the spacecraft time, contained at the start of each telemetry frame, to the correct time and provide a tabulation of significant parameters at 10-minute intervals during any specified period. The digital format was converted to decimal values for entry into the TIML tabulations and the GMT time of exposure determined.

2.3.1.3 SPACECRAFT ATTITUDE

The roll, pitch, and yaw maneuver angles shown in Table 2.3-1 were used to describe the attitude of the spacecraft throughout each photograph sequence. Only the known roll offsets (from postmaneuver drift analysis) were added to the commanded roll angle. No attempt was made to incorporate the variations of pitch and yaw errors within the attitude-control limit cycle in the calculation. Note that all roll maneuvers were executed about the Sunline (H roll).

2.3.1.4 SITE EVALUATION

The following selenocentric site radii were provided by NASA and used in obtaining photo support data:

Site	Radius (km)
I-1	1739.5
I-2	1741.0
I-3	1738.5
I-4	1742.0
I-5	1741.0
I-6	1743.0
I-7	1740.5
I-8.1	1738.0
I-9.2	1739.5

All other sites were analyzed using 1738.09 km as site radius.

Frame No. or Site	Roll Deg.	Pitch Deg.	Yaw Deg.	Order
5-24 (I-0)	3.85	12.45	-8.1	ROLL, YAW, PITCH
25	-2.87	0	0	ROLL
27	0.38	0	0	ROLL
28	-179.65	0	0	ROLL
29	0.2	0	0	ROLL
30	-179.65	0	0	ROLL
31	0.5	0	0	ROLL
32	0.5	0	0	ROLL
33	0.5	0	0	ROLL
34	0.5	0	0	ROLL
35-40	180.0	0	0	ROLL
41	-0.8	0	0	ROLL
42	2.4	0	0	ROLL
44	1.3	0	0	ROLL
46, 47	-2.6	0	0	ROLL
48, 49	-0.9	0	0	ROLL
50, 51	-1.95	0	0	ROLL
52-67 (I-1)	5.43	12.46	9.60	ROLL, YAW, PITCH
68-83 (I-2)	5.43	12.48	4.98	ROLL, YAW, PITCH
84	-2.95	0	0	ROLL
85-100 (I-3)	5.95	12.6	1.6	ROLL, YAW, PITCH
102	188.8	25.6	0	ROLL, PITCH
103	-1.5	0	0	ROLL
105-112 (I-4)	5.94	12.5	-2.4	ROLL, YAW, PITCH
113, 114	-0.1	0	0	ROLL
115	0	0	0	ROLL
116	180.0	0	0	ROLL
117	187.2	45.4	0	ROLL, PITCH
118-133 (I-5)	6.5	12.6	-2.3	ROLL, YAW, PITCH
134	1.95	0	0	ROLL
135	-2.1	0	0	ROLL
136	181.9	0	0	ROLL
137	0.4	-35.7	1.5	ROLL, YAW, PITCH
138	-0.9	0	0	ROLL
139	-1.6	0	0	ROLL
140	-1.5	0	0	ROLL
141-148 (I-6)	7.18	12.9	-16.7	ROLL, YAW, PITCH
149	1.9	0	0	ROLL
150	1.3	0	0	ROLL
151	28.0	0	0	ROLL
153-156	14.0	0	0	ROLL
157-172 (I-7)	7.56	12.8	-12.9	ROLL, YAW, PITCH
173	-3.2	0	0	ROLL
174	-1.8	0	0	ROLL
175	-2.5	0	0	ROLL
176-183 (I-8.1)	8.49	12.81	-11.33	ROLL, YAW, PITCH
184-199 (I-9.2)	8.13	12.81	6.86	ROLL, YAW, PITCH
200-215 (I-9.2)	8.15	12.8	8.3	ROLL, YAW, PITCH

Note: Frames not listed were taken without maneuvers.

Table 2.3-1: Photographic Maneuver Angles

2.3.2 ACCURACY OF CALCULATIONS

The accuracy of data presented in the photo supporting data tabulation was estimated by performing a simplified error analysis using typical photo and orbital parameters, and the best estimates of errors in the flight hardware. The study scope was confined to an investigation of uncertainties in photo location and spacecraft altitude for the prime photo sites. A brief summary of the estimated 1-s errors is given below:

	Standard Deviations		
	Longitude	Latitude	Altitude
Photo Centers	0.0053 deg.	0.0092 deg.	0.315 km
Arc Distance	0.161 km	0.279 km	
Photo Corners			
High Resolution	0.0056 deg.	0.0108 deg.	---
Arc Distance	0.170 km	0.327 km	
Medium Resolution	0.0143 deg.	0.0147 deg.	---
Arc Distance	0.430 km	0.435 km	

2.3.2.1 ERROR SOURCES

For each primary input to the photoevaluation program (attitude maneuvers, time of photos, and state vector), there is some uncertainty of the exact value; each contributes something to the total uncertainty or error in the photo parameters. The following discussion identifies the various factors and their relationship to the uncertainty in longitude and latitude of photo centers and corners, and in photo altitude.

Timing Errors

After the time-code data is corrected for spacecraft clock errors, a timing uncertainty of 0.05 second still exists, which is due to roundoff, since the time given is correct only to the nearest 0.1 second. Distribution of the error is uniform, but relies on the definition of one standard deviation - that number which encompasses 68% of the possible cases, the standard deviation of the timing error being 0.034 second. A typical value for horizontal velocity at the time of photography is 1.9 kilometers per second; hence, the distance traveled downrange is:

$$1.9 \text{ km/s} \times 0.034 \text{ sec.} = 0.065 \text{ km}$$

Using an altitude of 50 kilometers as representative of those for the prime sites and an inclination figure of 12 degrees, the distance traveled downrange can be converted into degrees of longitude and latitude on the lunar surface:

$$\Delta\lambda = 0.0020 \text{ degree (longitude)}$$

$$\Delta\mu = 0.00045 \text{ degree (latitude)}$$

Uncertainty of exact photo time also contributes a small uncertainty of photo altitude. A typical value of mean altitude rate is 0.5 km/s, thus,

$$\Delta h = 0.05 \text{ km/s} \times 0.034 \text{ sec} = 0.002 \text{ km}$$

Attitude Maneuver Errors

Spacecraft attitude, and thus the camera pointing direction, is not precisely known. The dominant error source in the attitude control system is limit cycle error, which is inherent in system design. When all other sources (gyro drift, resolution error, V/H converter error) are included, the resultant error after a photo maneuver is about 0.12 degree in all axes. Using this figure as camera pointing error, and dividing the error equally in longitude and latitude,

$$\Delta\lambda, \Delta\mu = 0.00246 \text{ degree}$$

Uncertainty in State Vectors

Accuracy of the state vectors must be considered with the uncertainties in actual photo location. Typical uncertainties for a state vector at a photo site would be:

$$\sigma_x = 76 \text{ m} \quad \sigma_{\dot{x}} = 0.14 \text{ m/s}$$

$$\sigma_y = 130 \text{ m} \quad \sigma_{\dot{y}} = 0.33 \text{ m/s}$$

$$\sigma_z = 275 \text{ m} \quad \sigma_{\dot{z}} = 0.50 \text{ m/s}$$

The contribution in total error due to velocity component uncertainty is negligible, but the uncertainty in position is to be determined. Assuming a spacecraft attitude of 50 km,

$$\sigma_\lambda = 0.0042 \text{ degree}$$

$$\sigma_\mu = 0.0088 \text{ degree}$$

The uncertainty in position at the time of the photo is

$$\sigma_r = (\sigma_x^2 + \sigma_y^2 + \sigma_z^2)^{1/2}$$

$$\sigma_r = 0.314 \text{ km}$$

2.3.2.2 UNCERTAINTY IN SITE EVALUATION

Evaluation of prime photo sites above or below the mean radius of the Moon is known (1a basis) only to within about 1 km. Since the camera axis intersect is only very slightly different from the nadir (prime sites only), site evaluation uncertainty has no noticeable effect on location of the photo centers. However, location of the photo corners is directly dependent on site evaluation, and this relationship is to be investigated. Also, because the high- and medium-resolution lenses have different fields of view, the effects must be studied separately.

High Resolution

The high-resolution field of view is 20.36 degrees in the crossrange direction and 5.17 degrees in the downrange direction. An orbit inclination of 12 degrees and spacecraft altitude of 50 km are assumed. The longitude and latitude components in the crossrange direction were determined,

$$\Delta\lambda_c = 0.0012 \text{ degree}$$

$$\Delta\mu_c = 0.0058 \text{ degree}$$

Uncertainty due to the 5.17 degrees field of view downrange is similarly calculated

$$\Delta\lambda_d = 0.00147 \text{ degree}$$

$$\Delta\mu_d = 0.0031 \text{ degree}$$

Having found the downrange and crossrange components of uncertainty, it is necessary to sum these to complete the estimate of uncertainty in photo corner location due to site elevation,

$$\Delta\lambda = (\Delta\lambda_c^2 + \Delta\lambda_d^2)^{1/2} = 0.0019 \text{ degree (high-resolution longitude)}$$

$$\Delta\mu = (\Delta\mu_c^2 + \Delta\mu_d^2)^{1/2} = 0.0058 \text{ degree (high-resolution latitude)}$$

Medium Resolution

The medium-resolution-lens field of view is 44.24 degrees crossrange by 37.92 degrees downrange. Proceeding in identically the same manner,

$$\Delta \lambda c = 0.0027 \text{ degree}$$

$$\Delta \mu c = 0.0131 \text{ degree}$$

$$\Delta \mu d = 0.0112 \text{ degree}$$

$$\Delta \lambda d = 0.0023 \text{ degree}$$

Summing the downrange and crossrange components,

$$\Delta \lambda = 0.0133 \text{ degree}$$

$$\Delta p = 0.0115 \text{ degree}$$

2.3.2.3 SUMMATION OF ERRORS

Sources that are known to contribute uncertainty to photo locations and altitude and that have been investigated here are independent; hence, they can be lumped together by the root-sum-square method.

For the photo corner locations, effects due to uncertainty in site elevation must be added to the below figures for uncertainty in photo center location. This is done for both the high- and medium-resolution cases below.

It is repeated that the frames evaluated by use of in-flight orbit determination are not as accurate as those for which postflight OD was done using improved data. Where conflict with actual photos is observed to exist, the EVAL data must be adjusted to obtain meaningful

values. For instance, an error in longitude of frame locations requires approximately a one-to-one correction to the incidence angle printed (+ if away from Sun, - if toward Sun).

2.3.3 PHOTOGRAPH FRAME COORDINATION

Preliminary attempts were made to correlate the lunar topographic features in Mission I photographs with existing 1:500,000 and 1:1,000,000 scale Mercator charts. It was immediately apparent that such a correlation could only be approximate. In most cases, features larger than several kilometers could be identified on both charts and photographs. However, discrepancies amounting to several kilometers were frequently found between relative positions of these features. In other cases, features over two or three kilometers, seen in the photographs, could not be found on the charts or features depicted on the charts could not be identified on the photographs. The limitations that have been imposed by Earth-based observation in preparing current lunar charts, in some instances make their use for precisely locating the position of Lunar Orbiter photographs difficult. In plotting locations of photograph corners on the charts by the above method, deviations of as much as an order of magnitude greater than the errors shown in Paragraph 2.3.2.3 from the computed positions were noted. These deviations are shown graphically in the site coverage plots in Paragraph 2.2. This effort confirmed that an extensive study will be required to transfer the topographic information from the unrectified, non-orthographic projection photographs to lunar chart form.

Photo Centers

Source	$\sigma \lambda$	$\sigma \mu$	$\sigma \nu$
Photo Timing	0.0020 degree	0.0005 degree	0.002 km
Camera Pointing	0.0025 degree	0.0025 degree	--
Position	0.0042 degree	0.0088 degree	0.314 km
RSS Total	0.0053 degree	0.0092 degree	0.315 km
Arc distance on lunar surface	0.161 km	0.279 km	

Photo Corners

High Resolution

Source	$\sigma \lambda$	$\sigma \mu$
Site Elevation	0.0019 degree	0.0058 degree
Total of others above	0.0053 degree	0.0092 degree
RSS Total	0.0056 degree	0.0108 degree
Arc Distance	0.170 km	0.327 km

Medium Resolution

Source	$\sigma \lambda$	$\sigma \mu$
Site Elevation	0.0133 degree	0.0115 degree
Total of others above	0.0053 degree	0.0092 degree
RSS Total	0.0143 degree	0.0147 degree
Arc Distance	0.430 km	0.435 km

Furthermore, the currently available "actual" postmission EVAL data for frame coordinates have limited value in this application because of the assumptions made in the EVAL computer program. In this program the Moon was assumed to be a sphere, with each Mission I site assigned a given fixed selenographic radius. Consequently, elevation differences over a given site were not considered. Also, spacecraft dynamics were simplified and did not include pitch and yaw errors in the "actual" EVAL computation of frame corner coordinates. Further complications were introduced by uncertainties in timing, as well as by the different fields of view of the medium- and high-resolution cameras. To establish corner coordinates, and to properly correlate them to existing lunar charts, a full photogrammetric space resection should be performed. Each usable frame must be analyzed with respect to spacecraft position, altitude, velocity, and attitude prevailing at the moment a given target area was photographed. In turn, these factors must be related to camera geometry and the lunar surface. Because of their complexity, these studies cannot be completed to support this report. Further uncertainties in positional accuracy are inherent in the Lunar Orbiter photographic system.

- 1) The Schneider Xenotar lens used for the moderate-resolution photographs is not a photogrammetric lens and as such introduces some distortion. However, this lens was calibrated to provide corrections.
- 2) Processing of the film aboard the spacecraft and the subsequent reconstructed record introduces distortion of the film image. These distortions are sensitive to temperature and relative humidity of each film or copy generation.
- 3) A random error in the mechanical scan direction of the optical-mechanical scanner introduces one of the major errors in the spacecraft camera system. There are no means for measuring and correcting this error in Mission I photographs.
- 4) The optical-mechanical scanner may also introduce a small error in the film-advance direction.
- 5) Slight errors in both the longitudinal and transverse direction with respect to the spacecraft film may be introduced by the reassembly process.

Addition of Reseau marks pre-exposed on the spacecraft film has been implemented for subsequent missions because of the importance of metrical measurements on the photographs and because the above noted error sources are not fully controlled.

Although the primary objective of the Lunar Orbiter mission was to secure topographic data regarding the lunar surface, there was no specific requirement established for photogrammetric accuracy (to produce accurate maps

having topographic detail). The detailed error analysis, as discussed above and necessary for this type of photograph utilization, was not made and has not been incorporated into the photo data reduction as tabulated in Table 2.3-3.

2.3.3.1 PHOTO IMAGE DISTORTION

The final photo image in the spacecraft camera is distorted by an aggregate of internal camera phenomena. These can be conveniently lumped into two areas: (1) uncalibrated lens distortion; and (2) thermal-chemical emulsion distortions.

Lens Distortions

The Lunar Orbiter I mission was predominantly reconnaissance rather than cartographic. The 80-mm Xenotar lens used was chosen for its excellent resolution rather than metric fidelity. A typical 80-mm focal-length Xenotar can have as much as 340μ maximum distortion and still qualify as a suitable reconnaissance lens. This can be contrasted with a selected, 76-mm focal-length mapping Biogon that has a maximum distortion of 30μ radially and 10μ tangentially.

Because of the desirability of metrical measurements, the 80-mm lens was calibrated to provide data on radial and tangential distortions as described in Paragraph 2.4.1.1. The data from these measurements have been provided to NASA. This type of calibration of the 610-mm lens was not a requirement.

Thermal-Chemical Emulsion Changes

The Lunar Orbiter I mission used Type SO-243 film for the photography because of its high-resolution characteristics. Since SO-243 uses a triacetate base, it does not have the extreme dimensional stability characteristic of ester (mylar) base films used for cartographic photography.

Photographic film changes under the following primary influences:

- 1) Changes of temperature and humidity;
- 2) Aging, long term and short term;
- 3) Processing.

Second-order parameters influencing dimension changes do not contribute significantly. The unpredicted image distortion expected in Lunar Orbiter I photography from the cited internal camera influences is summarized in Table 2.3-2. It is emphasized that this table is by no means exhaustive, and is presented to show orders of magnitude of the problem rather than to determine a cartographic error budget for the film.

PARAMETER	RANGE	ILLUSTRATIVE VALUE	PARAMETRIC CHANGE	% FILM DIMENSION
% DIMENSION PER % RELATIVE HUMIDITY	0.008 - 0.010	0.009	10% RH	0.09
% DIMENSION PER DEGREE FAHRENHEIT	0.003 - 0.004	0.004	10° F	0.04
PROCESSING DIMENSION CHANGE	0.08 - 0.10	0.09	--	0.09
FILM AGING PAST PROCESSING	0.15 - 0.25	0.15	--	0.15
RSS = 0.20%				

ASSUMING 60-MM IMAGE AREA WIDTH, RANDOM DIMENSION UNCERTAINTY = 120μ

MAXIMUM METRIC LENS DISTORTION FOR TYPICAL 80-MM FL. XENOTAR = 340μ

AT 40-KM VEHICLE ALTITUDE, 1μ FILM EQUALS 0.5 METER ON SURFACE OF MOON. THEREFORE, THE INTERNAL THERMO-CHEMICAL PLUS LENS DISTORTIONS CAN ACCOUNT FOR UP TO 1/2 KM OF IMAGE DISTORTION IN LUNAR ORBITER I PHOTOGRAPHY.

Table 2.3-2: Sources of Image Distortion

 PHOTO FRAME NUMBER 5 OF 16

YEAR	MONTH	DAY	HOUR	MINUTE	SECOND
66	8	22	15	23	8.199
GMT 66					
LONGITUDE OF NADIR POINT = 41.4039001 DEG					
LONG OF CAMERA AXIS INTERSECT = 41.3765254 DEG					
SPACECRAFT RADIUS = 1792.4769135 KM					
MEAN ALTITUDE RATE = 0.0160402 KM/SEC					
HORIZONTAL VELOCITY = 1.9104250 KM/SEC					
SCALE FACTOR (HIGH) = 0.0 15144 M/KM					
SCALE FACTOR (LOW) = 0.0015101 M/KM					
IMAGE MOTION COMPENSATION (V/H) = 0.0360615 RAD/SEC					
EMISSION ANGLE = 0.0 39279 DEG					
PHASE ANGLE = 60.9241252 DEG					
TILT ANGLE = 0.9450705 DEG					
SUN ANGLE AT NADIR = 287.9833984 DEG					
SUN ANGLE AT NADIR = 61.8110108 DEG					
LONGITUDE DISTANCE TO TARGET = -0.9291000 DEG					
LONGITUDE ARC LENGTH TO TARGET = -28.2074792 KM					
FORWARD OVERLAP RATIO = 4.4297278 PCT					
TIME BETWEEN PHOTOS = 2.4004698 SEC					

	X	Y	Z	MAGNITUDE (KM)
DIRECTION COSINES TO TARGET	-0.9187260	-0.23316804	-0.03311074	60.28008604
CAMERA AXIS	-0.73947811	-0.67293753	0.01808885	52.98434448
C1	-0.77858521	-0.60073670	0.18144004	53.88946533
C2	-0.73437962	-0.65860177	-0.16410451	53.85446641
C3	-0.67565926	-0.72264478	-0.14586695	53.93672180
C4	-0.71985886	-0.66477972	0.19967759	53.97186279

	X	Y	Z	X DOT	Y DOT	Z DOT

	LATI	LONG	LATI	LONG
	-0.1655 DEG	-1.5517 DEG	41.5181 DEG	41.3892 DEG
	43.00822 KM	19.02404 KM	-0.4455 DEG	-1.0587 DEG

	LOW RESOLUTION	HIGH RESOLUTION	FRAME 5A
	36.54398 KH	4.78 99 KM	78500 KM

	LOW RESOLUTION	HIGH RESOLUTION
	43.51497 KM	1005312 KH

	LONG	LATI	LONG	LATI
	40.9306 DEG	40.6365 DEG	41.3638 DEG	41.2348 DEG
	0.0907 DEG	-1.3122 DEG	-0.4126 DEG	-1.0267 DEG

Figure 2.3-2: EVAL Program Tabulation (sample)

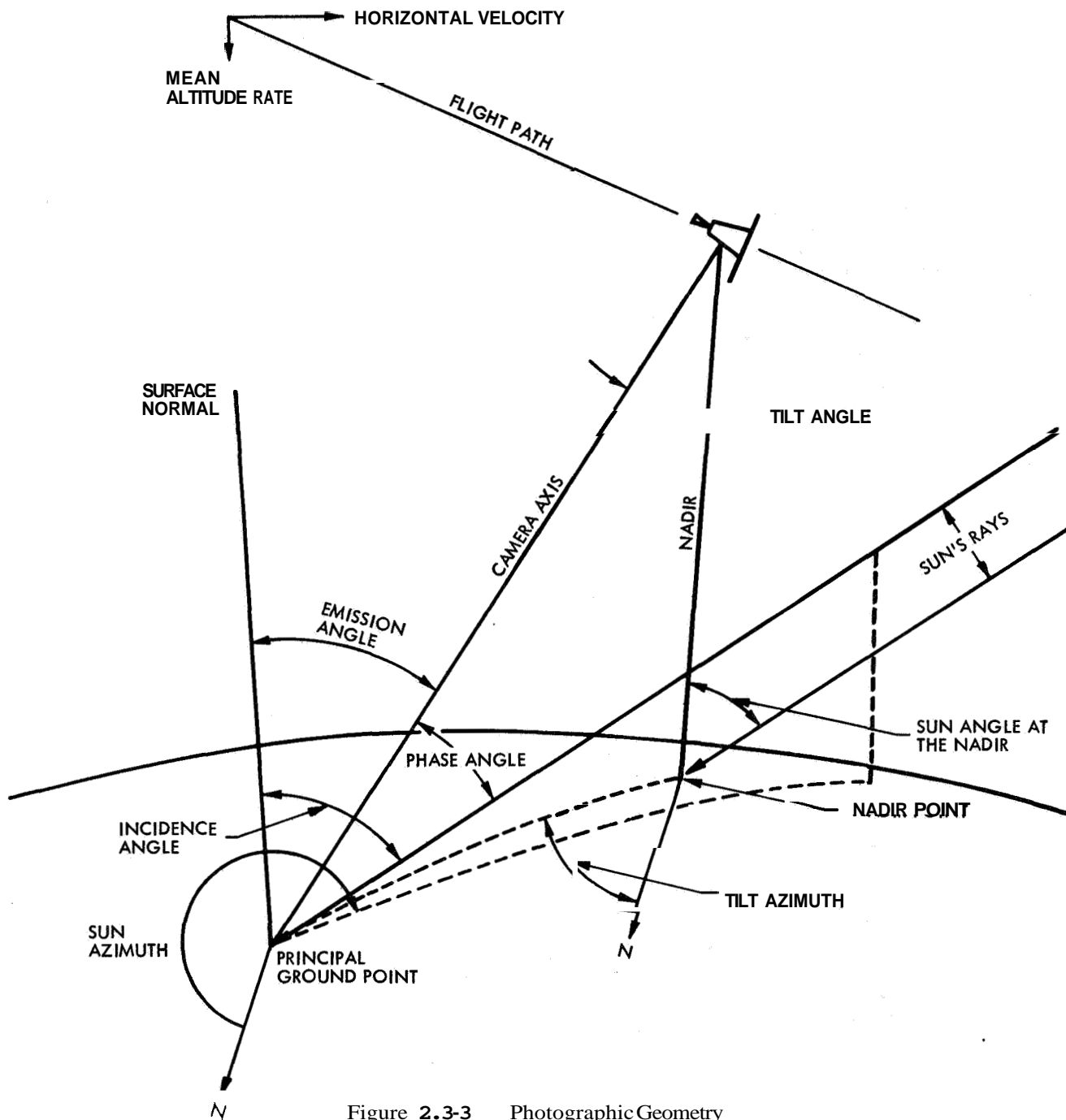


Figure 2.3-3 Photographic Geometry

2.3.4 PHOTOGRAPHIC SUPPORTING DATA TABLES

The information presented in the supporting data tables has been extracted from the computer program **EVAL** tabulated output. Figure 2.3-2 is a sample of **EVAL** program tabulations. The **EVAL** program was developed to satisfy the operational requirement of predicting photo coverage and determining spacecraft maneuvers required

to obtain the desired coverage for each photo sequence.

The following is a definition of terms used in the **EVAL** program and, with one exception, are the same terms and definitions used in the supporting-data tables. The single difference is that the term "camera axis magnitude" in the **EVAL** tabulation is identified as "slant distance" in the supporting-data table. Figure 2.3-3 is a diagram of the geometry of these parameters.

Definition of Terms

Camera Axis (Slant Distance): Direction cosines and magnitude (selenographic of date) of camera axis at time of photo.

C1, C2, C3, C4: Direction cosines and magnitude (selenographic of date) of the vectors from spacecraft to photo corners.

Direction Cosines to Target: The direction cosines and magnitude (selenographic of date) of the vector from the spacecraft to the point targets.

Emission Angle: Angle between surface normal and the camera axis. Also, the angle between the photo image plane and the subject plane.

Forward Overlap Ratio: Ratio of amount of overlap to frame dimension along the direction of the flight path.

Horizontal Velocity: That component of spacecraft velocity perpendicular to a radial line through the spacecraft and in the direction of the flight path.

Image Motion Compensation (V/H): The IMC rate is the instantaneous rate of movement of the image across the focal plane and is a function of spacecraft velocity and its height above the surface (V/H ratio), and the lens focal length.

Incidence Angle: The angle between surface normal and the Sun's rays.

Longitude (latitude) Arc Length to Target: Arc distance measured on lunar surface between the meridian (parallel) through the spacecraft nadir and the meridian (parallel) through the target. (+ is east longitude or north latitude).

Longitude (latitude) of Camera Axis Intersect: The selenographic longitude (latitude) of the point on Moon surface intersected by the camera axis. (+ is east longitude or north latitude).

Longitude (latitude) Distance to Target: Angular distance in longitude (latitude) between camera axis intersect and point target.

Longitude (latitude) of Nadir Point: The selenographic longitude (latitude) of the point on the Moon's surface directly below the spacecraft.

Mean Altitude Rate: Rate of change of altitude with respect to time.

North Deviation Angle: Deviation of north from the cross frame (cross) film axis (**Y-axis**) measured clockwise.

Phase Angle: The angle between the camera axis and the Sun's rays.

Principal Ground Point: Intersection of camera axis with the lunar surface

Resolution Constant: The theoretical ground resolution of the high-resolution photographs. Moderate resolution is larger by a factor of 8. The constant is equal to actual altitude in km divided by 46 (the nominal altitude giving 1-meter resolution on the high-resolution photographs).

Resolution Factor: The resolution constant to relate the resolution on the spacecraft film to resolution on the lunar surface. Given for both high and 80-mm resolution.

Side View Ratio: Ratio of amount of overlap to frame dimension perpendicular to flight path. (e.g. on adjacent orbits)

Spacecraft Height: Distance from spacecraft to lunar surface.

Spacecraft Radius: Distance from spacecraft to Moon center.

State Vector: Spacecraft position and velocity components in selenographic (of date) coordinates of the time of photo.

Sun Angle to Nadir: Angle between the spacecraft line and the Sun's rays.

Sun Arc to Nadir: Arc length from the nadir point to the intersection on lunar surface of a line from center to Sun center line.

Sun Azimuth at Principal Ground Point: Azimuth of Sun's rays at the principal ground point, measured clockwise from north.

Surface Normal: A line normal to the surface at the point of camera axis intersection.

Swing Angle: Angle between cross axis of film frame (labeled Y) and a line from center of the frame to the image of the nadir point. Measured positive clockwise from the positive Y-axis.

Tilt Angle: Angle between the camera axis and the spacecraft/nadir line.

Tilt Azimuth: Azimuth of principle point from spacecraft nadir.

Tilt Distance: Distance from the image of the camera axis intersect to the image of the nadir point measured on the spacecraft film. Given for both high-and low-resolution frames.

Time between Photos: Predicted time between exposure of current frame and succeeding frame taken in a film sequence based on the V/H at the time of current frame.

Time from Periapsis: Time in seconds before (minus) or after (plus) periapsis passage.

True Anomaly: The angle in the orbital plane measured from periapsis to the spacecraft in the direction of motion.

Direction of Motion: The arrow that appears on the printout illustrates the general direction of spacecraft motion for determination of the photo footprint orientation.

Photo Footprint: Numbered asterisks that appear on the printout which represent the four corners of the photo frames as projected on the lunar surfaces. Adjacent to each of the asterisks are the longitude and latitude of that corner of the footprint; between the asterisks is the surface distance in kilometers between those corners.

Information required to support the photo analysis function was coordinated with NASA and the user agencies during the program design period. These requirements were implemented in the form of the double page tables of supporting data, Table 2.3-3.

All of the spacecraft position and attitude data is listed on the left-hand page. The data tabulations on the right-hand page are grouped to support the high- and moderate-resolution photographs. The predicted corner positions are based on normal operation of each camera. Each line in the table presents all of the supporting data for that dual exposure. Spacecraft exposures 102 and 117 (Earth-Moon photographs) are not included in the table because of their unique conditions. These two photographs are discussed in detail in Paragraph 2.5.1.2.

Abnormal operation of the high-resolution-camera focal-plane shutter caused these photos to be taken at different times than commanded. Although many of these photos contained smeared lunar features, it was possible to identify the coverage within the corresponding moderate-resolution photo by lunar features. This matching study was initiated but, due to capacity limitations of the re-assembly printer delaying the delivery schedule of re-assembled photographs, it was not completed prior to the deadline of this report. Therefore, data for correction of the predicted corners of the high-resolution photographs is not included in this report.

The supporting data in Table 2.3-3 has been arranged by order of exposure for each primary site. This is then followed by the photo subsystem constraint photographs arranged by order of exposure for farside, Mission II sites, nearside areas of interest, and special test sequences.

The theoretical on-axis ground resolution of the photographs is given by:

High resolution

$$R = \frac{H}{46}$$

Moderate resolution

$$R = \frac{H}{5.75}$$

where R = ground resolution in meters,

and H = actual altitude, in kilometers, of the spacecraft at the time of exposure. (Column 5, Table 2.3-3)

System resolution = 3 scan lines (0.09) on GRE record.

The convention for presenting the coordinates of the four corners is illustrated in Figure 2.3-4.

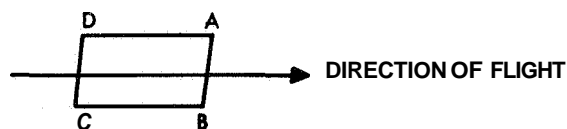


Figure 2.3-4:

Corner Coordinate Designation Convention

PHOTO		TIME OF EXPOSURE		SPACECRAFT				GROUND POINT		LAN'	SUN	EMIS-	PHASE	INCI-	TILT	TILT	SWING	NORTH
S	E	S/C	GMT	ALT	ALT RT	UT	LONG	LAT	LONG	DIST	AZIM	SION	ANGLE	DENCE	ANGL	AZIM	ANGLE	DEVIA
N	N	SECONDS	HR:MIN:SEC	KM	KM/SEC	DEG	DEG	DEG	DEG	KM	DEG	DEG	DEG	DEG	DEG	DEG	DEG	DEG
O.	O.	ESTIMATED	ERROR	1.03	1.1	0.001	0.01	0.006	0.01	0.006	1.1	0.01	0.12	0.12	0.01	0.12	0.01	0.1
1.0	5	45244.2	Day 230 14:42:49.9	216	-.081	1.66	84.61	1.90	83.99	217	89.07	6.0	62.9	68.42	5.3	291.60	99.21	347.7
	6	45254.1	14:42:59.8	216	-.077	1.55	85.11	1.78	84.56	216	89.04	5.4	62.9	67.85	4.8	291.64	100.2	347.7
	7	45264.0	14:43:9.7	215	-.073	1.44	85.62	1.65	85.14	215	89.00	4.8	62.9	67.27	4.3	293.93	101.5	347.6
	8	45273.8	14:43:19.5	214	-.069	1.33	86.13	1.53	85.71	215	88.96	4.2	62.9	66.71	3.8	295.55	103.1	347.6
	9	45583.5	14:43:29.2	213	-.066	1.22	86.63	1.41	86.27	214	88.92	3.7	62.9	66.14	3.3	297.64	105.2	347.6
	10	45393.5	14:43:39.2	213	-.062	1.11	87.15	1.28	85.85	213	88.88	3.1	62.9	65.56	2.8	300.56	108.1	347.6
	11	45333.4	14:43:49.0	212	-.058	1.00	87.65	1.16	87.42	212	88.83	2.6	62.9	65.00	2.3	304.68	112.2	347.6
	12	45313.2	14:43:58.9	212	-.055	0.89	88.16	1.04	88.00	212	88.78	2.0	62.9	64.42	1.8	311.02	118.6	347.6
	13	45323.0	14:44:8.7	211	-.051	0.78	88.67	0.91	88.56	211	88.73	1.6	62.9	63.86	1.4	321.43	129.0	347.6
	14	45332.8	14:44:18.5	211	-.047	0.67	89.18	0.79	89.13	211	88.67	1.2	62.9	63.29	1.0	339.87	147.5	347.6
	15	45342.7	14:44:28.4	210	-.043	0.56	89.69	0.67	89.71	210	88.62	1.0	62.9	62.73	0.9	10.19	177.7	347.6
	16	45353.9	14:44:38.1	210	-.040	0.45	90.19	0.55	90.27	210	88.56	1.1	62.9	62.15	1.0	41.02	208.6	347.6
	17	45362.2	14:44:47.9	209	-.036	0.34	90.69	0.42	90.84	209	88.50	1.0	62.9	61.58	0.9	60.98	228.5	347.5
	18	45372.0	14:44:57.7	209	-.030	0.23	91.21	0.30	91.41	209	88.43	0.9	62.9	61.01	0.8	72.21	239.8	347.5
	19	45381.7	14:45:7.4	209	-.029	0.13	91.71	0.18	91.97	239	88.37	2.5	62.9	60.44	2.2	78.65	245.4	347.5
	20	45391.5	14:45:17.2	209	-.024	0.05	92.21	0.05	92.54	209	88.30	3.0	62.9	59.89	2.7	83.22	250.8	347.5
	21	45477.0	14:46:42.7	208	-.008	-.094	96.65	-1.02	97.51	210	87.56	8.0	62.9	54.95	7.2	95.07	262.7	347.7
	22	45637.1	14:46:52.8	208	-.012	-1.05	97.17	-1.14	98.10	210	87.46	8.6	62.9	54.37	7.7	95.55	253.2	347.7
	23	45497.3	14:47:3.0	208	-.016	-1.17	97.70	-1.27	98.69	210	87.36	9.2	62.9	53.78	8.2	95.97	253.6	347.7
	24	45507.4	14:47:13.1	208	-.020	-1.28	98.23	-1.40	99.29	211	87.24	9.8	62.9	53.20	8.8	96.33	254.0	347.7
1.1	52	78580.2	Day 234 15:22:58.6	53	-.011	-0.62	40.83	-0.61	40.79	53	87.98	1.6	60.9	62.44	1.5	265.65	98.8	348.1
	53	78582.6	15:23:1.0	53	-.012	-0.65	40.97	-0.64	40.93	53	87.95	1.4	60.9	61.96	1.4	265.05	94.2	348.1
	54	78585.0	15:23:3.4	53	-.014	-0.68	41.12	-0.67	41.08	53	87.94	1.3	60.9	61.48	1.3	265.54	94.7	348.1
	55	72687.4	15:23:5.8	53	-.015	-0.71	41.26	-0.70	41.23	53	87.92	1.1	60.9	61.00	1.1	267.17	95.3	348.1
	56	78689.8	15:23:8.2	53	-.016	-0.74	41.40	-0.74	41.38	53	87.90	1.0	60.9	60.52	1.0	287.95	96.1	348.1
	57	78592.3	15:23:10.7	53	-.017	-0.78	41.55	-0.77	41.53	53	87.88	0.8	60.9	60.04	0.8	289.16	97.3	348.1
	58	78694.7	15:23:13.1	53	-.019	-0.81	41.70	-0.80	41.68	53	87.86	0.7	60.9	59.56	0.6	290.81	98.9	348.1
	59	78697.1	15:23:15.5	53	-.020	-0.84	41.84	-0.83	41.82	53	87.84	0.5	60.9	59.08	0.5	293.38	101.5	348.1
	60	78599.6	15:23:18.0	53	-.021	-0.87	41.99	-0.86	41.98	53	87.81	0.4	60.9	58.60	0.4	298.29	106.4	348.2
	61	78702.0	15:23:20.4	53	-.022	-0.90	42.13	-0.89	42.13	53	87.79	0.2	60.9	58.12	0.2	309.18	117.3	348.2
	62	78704.5	15:23:22.9	53	-.024	-0.93	42.28	-0.93	42.28	53	87.77	0.1	60.9	57.64	0.1	349.15	157.3	348.2
	63	78706.9	15:23:25.3	53	-.025	-0.95	42.42	-0.96	42.42	53	87.74	0.2	60.9	57.16	0.2	57.91	226.1	348.2
	64	78709.4	15:23:27.8	53	-.026	-0.99	42.57	-1.00	42.57	53	87.72	0.3	60.9	56.68	0.3	80.48	248.6	348.2
	65	78711.8	15:23:30.2	53	-.027	-1.02	42.72	-1.03	42.72	53	87.70	0.4	60.9	56.20	0.4	87.85	256.0	348.2
	66	78714.3	15:23:32.7	54	-.029	-1.05	42.86	-1.06	42.86	54	87.68	0.6	60.9	55.72	0.6	91.59	259.8	348.2
	67	78716.8	15:23:35.2	54	-.030	-1.08	43.01	-1.09	43.01	54	87.65	0.7	60.9	55.24	0.7	93.77	261.9	348.2
1.2	68	91146.9	Day 234 18:50:45.2	52	-.028	0.30	34.45	0.29	34.45	52	85.50	1.7	65.4	65.44	1.6	283.61	91.7	348.1
	69	91149.3	18:50:47.6	52	-.026	0.27	34.60	0.26	34.60	52	85.48	1.5	65.4	64.96	1.4	283.78	91.7	348.1
	70	91151.7	18:50:50.0	52	-.025	0.24	34.74	0.23	34.74	52	85.47	1.4	65.4	64.48	1.3	284.00	92.1	348.1
	71	91154.1	18:50:52.4	52	-.024	0.21	34.88	0.20	34.88	52	85.46	1.2	65.4	64.00	1.2	284.25	92.3	348.1
	72	91156.5	18:50:54.8	52	-.023	0.18	35.02	0.17	35.02	52	85.44	1.1	65.4	63.52	1.1	284.50	92.7	348.1
	73	91158.9	18:50:57.2	51	-.021	0.15	35.17	0.14	35.17	51	85.43	0.9	65.4	63.04	0.9	285.04	93.1	348.1
	74	91161.3	18:50:59.6	51	-.020	0.12	35.31	0.11	35.31	51	85.41	0.8	65.4	62.56	0.8	285.67	93.8	348.1
	75	91163.7	18:51:2.0	51	-.019	0.09	35.45	0.08	35.45	51	85.40	0.6	65.4	62.08	0.6	286.62	94.7	348.1
	76	91166.1	18:51:4.4	51	-.018	0.06	35.60	0.05	35.60	51	85.38	0.5	65.4	61.60	0.5	288.19	96.3	348.1
	77	91168.5	18:51:6.8	51	-.017	0.03	35.74	0.02	35.74	51	85.37	0.3	65.4	61.12	0.3	291.33	99.4	348.1
	78	91170.9	18:51:9.2	51	-.015	0.00	35.88	-0.01	35.88	51	85.35	0.1	65.4	60.64	0.1	300.50	108.6	348.1
	79	91173.3	18:51:11.6	51	-.014	-0.03	36.03	-0.04	36.03	51	85.34	0.1	65.4	60.16	0.1	16.35	184.4	348.1
	80	91175.7	18:51:14.0	51	-.013	0.06	36.17	0.05	36.17	51	85.32	0.2	65.4	59.68	0.2	84.17	252.3	348.1
	81	91178.1	18:51:16.4	51	-.012	0.09	36.31	0.08	36.31	51	85.30	0.3	65.4	59.20	0.3	92.70	260.8	348.1
	82	91180.5	18:51:18.8	51	-.010	0.12	36.46	0.11	36.46	51	85.28	0.5	65.4	58.72	0.5	95.71	263.8	348.1
	83	91162.9	18:51:21.2	51	-.009	0.15	36.60	0.14	36.60	51	85.27	0.6	65.4	58.24	0.6	97.24	265.3	348.1

Table 2.3-3 Photo Supporting Data

EXP NO.	TILT DIST	SCALE FACTOR	HIGH RESOLUTION								MODERATE RESOLUTION									
			PHOTO CORNER COORDINATES								TILT DIST	SCALE FACTOR	PHOTO CORNER COORDINATES							
			A		B		C		D				A		B		C		D	
			LAT	LONG	LAT	LONG	UT	LONG	LAT	LONG			LAT	LONG	LAT	LONG	LAT	LONG	LAT	LONG
			MM	X10 ⁻³	DEG	DEG	DEG	DEG	DEG	DEG	DEG	DEG	MM	X10 ⁻³	DEG	DEG	DEG	DEG	DEG	DEG

Table 2.3-3 (cont'd)

Table 2.3-3 (cont'd)

EXP N.O.	TILT DIST	SCALE FACTOR	HIGH RESOLUTION								TILT DIR	SCALE FACTOR	MODERATE RESOLUTION							
			PHOTO CORNER COORDINATES										PHOTO CORNER COORDINATES							
			A		B		C		D				A		B		C		D	
			LAT	LONG	LAT	LONG	LAT	LONG	LAT	LONG			LAT	LONG	LAT	LONG	LAT	LONG		
			DEG	DEG	DEG	DEG	DEG	DEG	DEG	DEG			DEG	DEG	DEG	DEG	DEG	DEG	DEG	
MM	X10 ⁻³	DEG	DEG	DEG	DEG	DEG	DEG	DEG	DEG	MM	X10 ⁻³	DEG	DEG	DEG	DEG	DEG	DEG	DEG	DEG	
2%	2%									2%	2%									
35	8.3	11.3	1.08	25.17	0.45	25.04	0.48	24.89	1.11	25.01	1.1	1.48	25.78	0.05	25.48	0.19	24.29	1.62	24.57	
36	8.0	11.3	1.05	25.32	0.42	25.20	0.45	25.05	1.08	25.17	1.1	1.49	25.93	0.08	25.64	0.16	24.44	1.59	24.72	
37	8.0	11.4	1.02	25.47	0.39	25.35	0.42	25.19	1.05	25.31	1.1	1.49	26.08	0.11	25.78	0.13	24.59	1.55	24.87	
38	8.4	11.4	0.99	25.62	0.36	25.50	0.39	25.34	1.02	25.47	1.1	1.49	26.23	0.14	25.94	0.11	24.75	1.52	25.03	
39	9.0	11.4	0.95	25.77	0.33	25.65	0.36	25.49	0.99	25.62	1.2	1.49	26.38	0.16	26.09	0.08	24.90	1.49	25.17	
40	9.8	11.4	0.92	25.93	0.30	25.80	0.33	25.65	0.95	25.77	1.3	1.50	26.53	0.19	26.24	0.05	25.05	1.45	25.33	
41	10.8	11.4	0.89	26.07	0.27	25.95	0.30	25.79	0.92	25.92	1.4	1.50	26.68	0.22	26.39	0.02	25.20	1.42	25.48	
42	11.9	11.5	0.86	26.23	0.24	26.10	0.27	25.95	0.89	26.07	1.6	1.50	26.83	0.25	26.54	-0.01	25.36	1.39	25.63	
43	13.1	11.5	0.83	26.37	0.21	26.25	0.25	26.10	0.86	26.22	1.7	1.51	26.98	-0.28	26.69	-0.04	25.51	1.36	25.78	
44	14.5	11.5	0.80	26.53	0.18	26.40	0.21	26.25	0.83	26.37	1.9	1.51	27.13	-0.31	26.84	-0.07	25.67	1.32	25.94	
45	15.8	11.5	0.77	26.68	0.15	26.55	0.19	26.40	0.80	26.52	2.1	1.51	27.28	-0.34	26.99	-0.10	25.81	1.29	25.69	
46	17.1	11.5	0.74	26.82	0.12	26.70	0.16	26.55	0.77	26.67	2.2	1.51	27.43	-0.37	27.14	-0.12	25.96	1.26	26.24	
47	18.6	11.5	0.71	26.98	0.09	26.85	0.13	26.70	0.74	26.82	2.4	1.51	27.58	-0.40	27.29	-0.15	26.12	1.23	26.39	
48	20.0	11.6	0.68	27.13	0.06	27.00	0.10	26.85	0.71	26.9	2.6	1.52	27.73	-0.43	27.44	-0.18	26.27	1.20	26.54	
49	21.5	11.6	0.65	27.27	0.03	27.15	0.07	27.00	0.68	27.12	2.8	1.52	27.87	-0.46	27.59	-0.21	26.42	1.16	26.69	
50	23.0	11.6	0.62	27.43	0.00	27.30	0.04	27.15	0.65	27.27	3.0	1.52	28.03	-0.49	27.74	-0.24	26.57	1.13	26.84	
51	26.4	12.5	0.70	11.69	0.14	11.56	0.17	11.42	0.74	U.54	2.7	1.63	0.95	12.23	-0.32	11.94	-0.09	10.85	1.21	11.15
52	14.3	12.6	0.57	12.25	0.01	12.13	0.04	11.99	0.60	12.11	1.9	1.65	0.82	12.80	-0.44	12.51	-0.21	11.43	1.07	11.72
53	8.3	12.7	0.44	12.82	-0.11	12.69	-0.08	12.55	0.47	12.68	1.1	1.66	0.69	13.35	-0.57	13.07	-0.33	12.00	0.93	12.29
54	24	12.8	0.31	13.37	-0.24	13.25	-0.21	13.11	0.34	13.23	0.3	1.67	0.56	13.91	-0.69	13.63	-0.45	12.57	0.80	12.85
55	3.6	12.8	0.19	13.93	-0.36	13.80	-0.33	13.67	0.22	13.79	0.5	1.68	0.43	14.46	-0.82	14.18	-0.58	13.13	0.67	13.41
56	9.4	12.9	0.06	14.48	-0.49	14.35	-0.46	14.22	0.09	14.34	1.2	1.69	0.30	15.01	-0.94	14.73	-0.70	13.69	0.53	14.00
57	15.3	13.0	-0.07	15.03	-0.61	14.91	-0.58	14.77	-0.04	14.89	2.0	1.70	0.18	15.56	-1.06	15.28	-0.82	14.24	0.40	14.52
58	21.2	13.0	-0.19	15.58	-0.74	15.46	-0.70	15.33	-0.16	15.45	2.8	1.71	0.05	16.12	-1.19	15.84	-0.94	14.81	0.27	15.08
59	19.2	12.5	0.53	-2.43	-0.03	-2.55	-0.00	-2.69	0.56	-2.57	2.5	1.64	0.78	-1.89	-0.49	-2.16	-0.27	-3.25	1.03	-2.97
60	17.8	12.5	0.50	-2.29	-0.06	-2.42	-0.03	-2.56	0.53	-2.44	2.3	1.64	0.75	-1.75	-0.51	-2.03	-0.29	-3.11	1.00	-2.83
61	16.3	12.5	0.47	-2.15	-0.09	-2.27	-0.06	-2.42	0.50	-2.29	2.1	1.65	0.72	-1.61	-0.54	-1.89	-0.32	-2.97	1.00	-2.69
62	14.8	12.6	0.44	-2.01	-0.12	-2.13	-0.09	-2.27	0.47	-2.15	1.9	1.65	0.69	-1.47	-0.57	-1.75	-0.35	-2.82	0.93	-2.55
63	13.3	12.6	0.41	-1.87	-0.15	-1.99	-0.12	-2.13	0.44	-2.01	1.7	1.65	0.66	-1.33	-0.60	-1.60	-0.38	-2.68	0.90	-2.41
64	9.9	12.6	0.38	-1.74	-0.18	-1.86	-0.15	-2.00	0.41	-1.88	1.6	1.65	0.63	-1.20	-0.63	-1.47	-0.41	-2.54	0.87	-2.27
65	10.4	12.6	0.35	-1.60	-0.21	-1.72	-0.18	-1.86	0.38	-1.74	1.4	1.66	0.60	-1.06	-0.66	-1.33	-0.44	-2.40	0.84	-2.13
66	9.0	12.7	0.32	-1.46	-0.24	-1.58	-0.21	-1.72	0.35	-1.60	1.2	1.66	0.57	-0.92	-0.69	-1.19	-0.47	-2.26	0.81	-1.99
67	7.5	12.7	0.29	-1.32	-0.27	-1.44	-0.24	-1.58	0.32	-1.46	1.0	1.66	0.54	-0.78	-0.72	-1.05	-0.50	-2.12	0.77	-1.85
68	6.1	12.7	0.26	-1.18	-0.30	-1.30	-0.27	-1.44	0.29	-1.32	0.8	1.67	0.51	-0.64	-0.75	-0.91	-0.52	-2.00	0.74	-1.71
69	4.7	12.7	0.23	-1.04	-0.33	-1.16	-0.30	-1.30	0.26	-1.18	0.6	1.67	0.48	-0.51	-0.78	-0.78	-0.55	-1.84	0.71	-1.57
70	3.3	12.7	0.20	-0.90	-0.36	-1.02	-0.33	-1.16	0.23	-1.04	0.4	1.67	0.45	-0.37	-0.81	-0.64	-0.58	-1.70	0.68	-1.43
71	2.2	12.8	0.17	-0.77	-0.39	-0.89	-0.36	-1.03	0.20	-0.91	0.3	1.67	0.42	-0.23	-0.84	-0.50	-0.61	-1.56	0.65	-1.29
72	1.7	12.8	0.14	-0.63	-0.42	-0.75	-0.39	-0.89	0.17	-0.77	0.2	1.68	0.39	-0.10	-0.86	-0.37	-0.64	-1.42	0.62	-1.16
73	2.3	12.8	0.11	-0.49	-0.45	-0.61	-0.42	-0.75	0.14	-0.63	0.3	1.68	0.36	0.05	-0.89	-0.23	-0.67	-1.28	0.58	-1.01
74	3.3	12.8	0.08	-0.36	-0.47	-0.48	-0.44	-0.62	0.11	-0.50	0.4	1.68	0.33	0.17	-0.92	-0.10	-0.69	-1.15	0.56	-0.88
75	4.4	13.8	-3.26	-4.01	-3.78	-4.10	-3.75	-4.23	-3.24	-4.13	0.6	1.81	-3.02	-3.51	-4.19	-3.74	-4.00	-4.73	-2.83	-4.50
76	2.0	13.5	-3.36	-3.47	-3.89	-3.57	-3.86	-3.70	-3.34	-3.60	0.3	1.78	-3.11	-2.97	-4.30	-3.19	-4.11	-4.20	-2.92	-3.97
77	7.3	13.3	-3.46	-2.92	-4.00	-3.03	-3.97	-3.16	-3.44	-3.06	1.0	1.74	-3.21	-2.41	-4.42	-2.64	-4.22	-3.67	-3.02	-3.44
78	13.0	13.0	-3.56	-2.38	-4.11	-2.48	-4.08	-2.62	-3.54	-2.51	1.7	1.71	-3.30	-1.85	-4.54	-2.09	-4.33	-3.13	-3.11	-2.90
79	18.9	12.8	-3.66	-1.81	-4.22	-1.92	-4.19	-2.06	-3.64	-1.95	2.5	1.68	-3.40	-1.27	-4.67	-1.52	-4.45	-2.58	-3.28	-2.34
80			-3.77	-1.24	-4.33	-1.34	-4.31	-1.49	-3.74	-1.38	3.3	1.64	-3.49	-0.68	-4.80	-0.93	-4.57	-2.02	-1.78	-3.30
81			-3.88	-0.63	-4.46	-0.74	-4.43	-0.89	-3.85	-0.78	4.1	1.61	-3.59	-0.09	-4.93	-0.32	-4.69	-1.43	-3.40	-1.19
82			-3.98	-0.03	-4.58	-0.15	-4.55	-0.29	-4.00	-0.18	4.9	1.57	-3.69	-0.55	-5.06	-0.29	-4.82	-0.85	-3.50	-0.60

Table 2.3-3 (cont'd)

PHOTO		TIME OF EXPOSURE		SPACECRAFT				PRINCIPAL GROUND POINT		SLANT	SUN	EMIS-	PHASE	INCI -	TILT	TILT	SWING	NORTH
S	E	S/C	GMT	ALT	ALT RT	LAT	LONG	LAT	LONG	DIST	AZIM	SION	ANGLE	DENCE	ANGLE	AZIM	ANGLE	DEVIA
N	N	SECONDS	HR:MIN:SEC	KM	KM/SEC	DEG	DEG	DEG	DEG	KM	DEG	DEG	DEG	DEG	DEG	DEG	DEG	DEG
O.	O.	ESTIMATED	ERROR	0.03	1.1	0.001	0.01	0.006	0.01	0.006	1.1	0.01	0.12	0.12	0.01	0.12	0.01	0.1
I-7	157	40712.3	DAY 240	46	0.066	-3.25	-23.20	-3.29	-23.18	46	86.19	1.8	58.3	57.87	1.8	162.43	329.8	347.4
	158	40712.3	06:28:18.3	46	0.067	-3.27	-23.06	-3.32	-23.05	46	86.12	1.9	58.3	57.74	1.8	158.8	326.2	347.4
	159	40716.7	06:28:20.5	46	0.068	-3.30	-22.93	-3.35	-22.91	46	86.09	2.0	58.3	57.60	1.9	155.35	322.8	347.4
	160	40718.8	06:28:22.7	46	0.069	-3.32	-22.80	-3.37	-22.78	46	86.07	2.1	58.3	57.48	2.0	152.35	319.8	347.4
	161	40721.0	06:28:24.8	47	0.070	-3.35	-22.67	-3.40	-22.64	47	86.04	2.1	58.3	57.34	2.1	149.46	316.9	347.4
	162	40723.2	06:28:27.0	47	0.071	-3.38	-22.54	-3.42	-22.51	47	86.01	2.2	58.3	57.21	2.2	146.81	314.2	347.5
	163	40725.5	06:28:29.2	47	0.072	-3.40	-22.40	-3.45	-22.37	47	85.97	2.3	58.3	57.07	2.3	144.27	311.7	347.5
	164	40727.7	06:28:31.5	47	0.074	-3.43	-22.27	-3.48	-22.23	47	85.94	2.4	58.3	56.94	2.4	142.04	309.5	347.5
	165	40729.9	06:28:33.7	47	0.075	-3.46	-22.14	-3.51	-22.10	47	85.91	2.5	58.3	56.80	2.5	140.00	307.5	347.5
	166	40732.1	06:28:35.9	47	0.076	-3.48	-22.01	-3.53	-21.96	47	85.88	2.7	58.3	56.67	2.6	138.12	305.6	347.5
	167	40734.4	06:28:38.1	48	0.077	-3.51	-21.87	-3.56	-21.82	48	85.85	2.8	58.3	56.53	2.7	136.32	303.8	347.5
	168	40736.6	06:28:40.4	48	0.078	-3.53	-21.74	-3.59	-21.68	48	85.82	2.9	58.3	56.40	2.8	134.73	302.2	347.5
	169	40738.9	06:28:42.6	48	0.079	-3.56	-21.60	-3.62	-21.54	48	85.78	3.0	58.3	56.26	2.9	133.20	300.7	347.5
	170	40741.2	06:28:44.9	48	0.080	-3.59	-21.46	-3.64	-21.40	48	85.75	3.1	58.3	56.12	3.1	131.79	299.3	347.5
	171	40743.5	06:28:47.2	48	0.082	-3.62	-21.32	-3.67	-21.26	48	85.72	3.3	58.3	55.98	3.2	130.49	298.0	347.5
	172	40745.8	06:28:49.5	48	0.083	-3.64	-21.19	-3.70	-21.11	49	85.68	3.4	58.3	55.84	3.3	129.28	296.8	347.5
I-8.1	176	22475.5	DAY 241	50	0.059	-2.88	-37.12	-2.88	-37.12	50	86.53	0.4	59.3	59.4	3.3	328.30	119.0	348.8
	177	22477.7	06:31:59.1	50	0.060	-2.91	-36.98	-2.91	-36.99	50	86.50	0.3	59.3	59.3	3.3	357.24	118.6	348.8
	178	22480.0	06:32:01.3	50	0.061	-2.94	-36.84	-2.94	-36.84	50	86.47	0.2	59.3	59.56	0.4	166.1	166.1	348.8
	179	22482.2	06:32:03.6	50	0.062	-2.97	-36.71	-2.96	-36.71	50	86.45	0.2	59.3	59.44	0.2	39.04	207.9	348.9
	180	22484.5	06:32:05.8	50	0.063	-3.00	-36.57	-2.99	-36.57	50	86.42	0.3	59.3	59.02	0.3	646	233.5	348.9
	181	22486.7	06:32:08.1	50	0.064	-3.02	-36.44	-3.02	-36.43	50	86.39	0.4	59.3	58.83	0.4	76.20	243.1	348.9
	182	22489.0	06:32:10.3	50	0.065	-3.05	-36.31	-3.05	-36.29	50	86.36	0.6	59.3	58.74	0.6	251.6	251.6	348.9
	183	22491.3	06:32:12.6	50	0.067	-3.08	-36.17	-3.08	-36.15	50	86.33	0.7	59.3	58.60	0.7	86.58	254.6	348.9
	184	34760.3	06:32:14.9	50	0.067	-3.08	-36.17	-3.08	-36.15	50	86.33	0.7	59.3	58.60	0.7	86.58	254.6	348.9
	185	34762.4	09:56:43.8	45	0.012	-1.75	-44.49	-1.75	-44.53	45	87.51	1.6	63.6	65.17	1.5	275.92	84.3	348.4
I-9a	186	34764.5	09:56:45.9	45	0.013	-1.78	-44.36	-1.78	-44.40	45	87.49	1.4	63.6	65.04	1.4	275.36	83.8	348.4
	187	34766.6	09:56:48.0	45	0.014	-1.81	-44.24	-1.81	-44.27	45	87.47	1.3	63.6	64.91	1.3	274.70	83.1	348.4
	188	34768.7	09:56:50.1	45	0.015	-1.83	-44.11	-1.83	-44.14	45	87.45	1.2	63.6	64.78	1.1	273.88	82.3	348.4
	189	34770.8	09:56:52.2	45	0.016	-1.86	-43.98	-1.86	-44.01	45	87.43	1.0	63.6	64.65	1.0	272.86	81.3	348.4
	190	34772.9	09:56:54.3	45	0.017	-1.89	-43.86	-1.89	-43.88	45	87.41	0.9	63.6	64.53	0.9	271.54	80.0	348.4
	191	34775.0	09:56:56.4	45	0.018	-1.91	-43.73	-1.91	-43.75	45	87.39	0.8	63.6	64.40	0.8	269.78	78.2	348.4
	192	34777.1	09:56:58.5	45	0.019	-1.94	-43.61	-1.94	-43.62	45	87.37	0.6	63.6	64.27	0.6	267.33	75.8	348.5
	193	34779.2	09:57:00.6	45	0.020	-1.97	-43.48	-1.97	-43.49	45	87.35	0.5	63.6	64.14	0.5	263.66	72.1	348.5
	194	34781.3	09:57:02.7	45	0.021	-1.99	-43.35	-1.99	-43.36	45	87.33	0.4	63.6	64.01	0.4	257.69	66.2	348.5
	195	34783.4	09:57:04.8	45	0.022	-2.02	-43.23	-2.02	-43.24	45	87.31	0.3	63.6	63.89	0.3	246.60	55.1	348.5
	196	34785.5	09:57:06.9	45	0.023	-2.05	-43.10	-2.05	-43.11	45	87.29	0.2	63.6	63.76	0.2	222.88	31.4	348.5
	197	34787.6	09:57:09.0	45	0.024	-2.07	-42.98	-2.08	-42.98	45	87.27	0.2	63.6	63.63	0.2	179.88	348.4	348.5
	198	34789.8	09:57:11.1	45	0.025	-2.10	-42.85	-2.10	-42.85	45	87.25	0.2	63.6	63.50	0.2	146.13	314.6	348.5
	199	34791.9	09:57:13.3	46	0.027	-2.13	-42.72	-2.13	-42.71	46	87.23	0.3	63.6	63.37	0.3	129.89	298.4	348.5
			09:57:15.4	46	0.028	-2.15	-42.59	-2.16	-42.58	46	87.21	0.5	63.6	63.24	0.5	122.23	290.7	348.5

Table 2.3-3 (cont'd)

EXP N.O.	HIGH RESOLUTION										MODERATE RESOLUTION										
	TILT DIST	SCALE FACTOR	PHOTO CORNER COORDINATES								TILT DIST	SCALE FACTOR	PHOTO CORNER COORDINATES								
			A		B		C		D				A		B		C		D		
			LAT	LONG	LAT	LONG	LAT	LONG	LAT	LONG			LAT	LONG	LAT	LONG	LAT	LONG	LAT	LONG	
			MM	X10 ³	DEG	DEG	DEG	DEG	DEG	DEG			DEG	DEG	MM	X10 ³	DEG	DEG	DEG	DEG	DEG
		2%	2%								2%	2%									
157	18.9	13.3	-3.04	-23.06	-3.57	-23.17	-3.55	-23.30	-3.01	-23.20	2.5	1.74	-2.79	-22.55	-4.01	-22.78	-3.80	-23.82	-2.60	-23.57	
158	19.7	13.2	-3.07	-22.93	-3.60	-23.03	-3.57	-23.17	-3.04	-23.06	26	1.74	-2.82	-22.41	-4.04	-22.64	-3.83	-23.68	-2.62	-23.43	
159	20.5	13.2	-3.09	-22.79	-3.63	-22.90	-3.60	-23.03	-3.07	-22.92	2.7	1.73	-2.84	-22.28	-4.07	-22.51	-3.86	-23.55	-2.65	-23.30	
160	21.3	13.2	-3.12	-22.66	-3.66	-22.77	-3.63	-22.90	-3.09	-22.79	2.8	1.73	-2.86	-22.14	-4.10	-22.38	-3.88	-23.42	-2.67	-23.17	
161	22.2	13.1	-3.14	-22.52	-3.68	-22.63	-3.66	-22.77	-3.12	-22.66	2.9	1.72	-2.89	-22.01	-4.13	-22.24	-3.91	-23.29	-2.70	-23.08	
162	23.2	13.1	-3.17	-22.39	-3.71	-22.49	-3.68	-22.63	-3.14	-22.52	3.0	1.71	-2.91	-21.87	-4.16	-22.10	-3.94	-23.15	-2.72	-22.90	
163	24.3	13.0	-3.20	-22.25	-3.74	-22.35	-3.71	-22.49	-3.17	-22.38	3.2	1.71	-2.94	-21.72	-4.19	-21.96	-3.97	-23.01	-2.75	-22.76	
164	25.3	13.0	-3.22	-22.11	-3.77	-22.22	-3.74	-22.35	-3.20	-22.25	3.3	1.70	-2.96	-21.58	-4.22	-21.82	-4.00	-22.88	-2.77	-22.63	
165	26.4	12.9	-3.25	-21.97	-3.80	-22.08	-3.77	-22.22	-3.22	-22.11	35	1.70	-2.99	-21.45	-4.25	-21.68	-4.03	-22.75	-2.80	-22.49	
166	27.6	12.9	-3.27	-21.84	-3.82	-21.94	-3.80	-22.08	-3.25	-21.97	3.6	1.69	-3.01	-21.31	-4.28	-21.54	-4.05	-22.61	-2.82	-22.36	
167	28.8	12.8	-3.30	-21.69	-3.85	-21.80	-3.82	-21.94	-3.27	-21.83	39	1.68	-3.04	-21.16	-4.31	-21.40	-4.08	-22.47	-2.85	-22.22	
168	30.0	12.8	-3.33	-21.56	-3.88	-21.67	-3.85	-21.81	-3.30	-21.70	37	1.68	-3.06	-21.02	-4.34	-21.26	-4.11	-22.34	-2.87	-22.08	
169	31.2	12.7	-3.35	-21.42	-3.91	-21.52	-3.88	-21.67	-3.33	-21.56	41	1.67	-3.09	-20.88	-4.37	-21.12	-4.14	-22.20	-2.90	-21.94	
170	32.5	12.7	-3.38	-21.27	-3.94	-21.38	-3.91	-21.52	-3.35	-21.41	43	1.67	-3.11	-20.73	-4.41	-20.97	-4.17	-22.06	-2.92	-21.80	
171	33.5	12.6	-3.41	-21.13	-3.97	-21.24	-3.94	-21.38	-3.38	-21.27	44	1.66	-3.14	-20.59	-4.44	-20.83	-4.20	-21.92	-2.95	-21.66	
172	35.1	12.6	-3.43	-20.99	-4.00	-21.10	-3.97	-21.24	-3.41	-21.13	46	1.65	-3.16	-20.44	-4.47	-20.68	-4.23	-21.78	-2.98	-21.52	
176	3.9	12.3	-2.61	-36.99	-3.18	-37.11	-3.15	-37.25	-2.58	-37.13	0.5	1.62	-2.34	-36.44	-3.64	-36.71	-3.42	-37.81	-2.11	-37.54	
177	2.7	12.3	-2.63	-36.85	-3.21	-36.97	-3.18	-37.12	-2.60	-37.00	0.4	1.61	-2.37	-36.30	-3.67	-36.57	-3.45	-37.68	-2.14	-37.41	
178	1.9	12.3	-2.66	-36.71	-3.24	-36.83	-3.21	-36.98	-2.63	-36.86	0.3	1.61	-2.39	-36.15	-3.70	-36.43	-3.48	-37.53	-2.16	-37.26	
179	2.1	12.2	-2.69	-36.58	-3.27	-36.70	-3.24	-36.84	-2.66	-36.72	0.3	1.60	-2.42	-36.02	-3.73	-36.29	-3.51	-37.40	-2.19	-37.13	
180	3.1	12.2	-2.72	-36.43	-3.30	-36.55	-3.27	-36.70	-2.68	-36.58	0.4	1.60	-2.45	-35.87	-3.77	-36.14	-3.54	-37.26	-2.22	-36.99	
181	4.3	12.2	-2.74	-36.30	-3.33	-36.42	-3.30	-36.57	-2.71	-36.45	0.6	1.59	-2.47	-35.73	-3.80	-36.01	-3.56	-37.13	-2.24	-36.85	
182	5.7	12.1	-2.77	-36.16	-3.36	-36.28	-3.33	-36.42	-2.74	-36.30	0.7	1.59	-2.50	-35.59	-3.83	-35.86	-3.59	-36.99	-2.27	-36.71	
183	7.1	12.1	-2.80	-36.01	-3.39	-36.14	-3.36	-36.28	-2.77	-36.16	0.9	1.58	-2.53	-35.44	-3.86	-35.72	-3.63	-36.85	-2.30	-36.57	
184	16.2	13.6	-1.50	-44.41	-2.02	-44.52	-2.00	-44.65	-1.47	-44.54	21	1.78	-1.27	-43.91	-2.44	-44.15	-2.24	-45.16	-1.05	-44.91	
185	14.8	13.6	-1.53	-44.28	-2.05	-44.39	-2.02	-44.52	-1.50	-44.41	1.9	1.78	-1.29	-43.78	-2.47	-44.03	-2.27	-45.03	-1.07	-44.78	
186	13.5	13.5	-1.56	-44.15	-2.08	-44.26	-2.05	-44.39	-1.53	-44.28	1.8	1.78	-1.32	-43.65	-2.50	-43.90	-2.29	-44.90	-1.10	-44.65	
187	12.1	13.5	-1.58	-44.02	-2.11	-44.13	-2.08	-44.26	-1.56	-44.15	1.6	1.78	-1.35	-43.52	-2.53	-43.77	-2.32	-44.77	-1.13	-44.52	
188	10.8	13.5	-1.61	-43.89	-2.13	-44.00	-2.11	-44.13	-1.58	-44.02	1.4	1.77	-1.37	-43.39	-2.55	-43.64	-2.35	-44.64	-1.16	-44.39	
189	9.4	13.5	-1.64	-43.76	-2.16	-43.87	-2.13	-44.00	-1.61	-43.89	1.2	1.77	-1.40	-43.26	-2.58	-43.51	-2.38	-44.51	-1.18	-44.26	
190	8.1	13.5	-1.67	-43.63	-2.19	-43.74	-2.16	-43.87	-1.64	-43.76	1.1	1.77	-1.43	-43.13	-2.61	-43.38	-2.40	-44.38	-1.21	-44.13	
191	6.7	13.5	-1.69	-43.50	-2.22	-43.61	-2.19	-43.74	-1.66	-43.63	0.9	1.77	-1.45	-43.00	-2.64	-43.25	-2.43	-44.25	-1.24	-44.00	
192	5.4	13.5	-1.72	-43.37	-2.24	-43.48	-2.22	-43.62	-1.69	-43.50	0.7	1.77	-1.48	-42.87	-2.67	-43.12	-2.46	-44.13	-1.27	-43.87	
193	4.1	13.5	-1.75	-43.24	-2.27	-43.35	-2.24	-43.49	-1.72	-43.38	0.5	1.77	-1.51	-42.74	-2.69	-42.99	-2.49	-44.00	-1.29	-43.74	
194	2.9	13.5	-1.77	-43.11	-2.30	-43.22	-2.27	-43.36	-1.75	-43.25	0.4	1.77	-1.53	-42.61	-2.72	-42.86	-2.51	-43.87	-1.32	-43.61	
195	2.0	13.4	-1.80	-42.99	-2.33	-43.10	-2.30	-43.23	-1.77	-43.12	0.3	1.76	-1.56	-42.48	-2.75	-42.73	-2.54	-43.74	-1.35	-43.49	
196	1.7	13.4	-1.83	-42.86	-2.35	-42.97	-2.33	-43.10	-1.80	-42.99	0.2	1.76	-1.58	-42.35	-2.78	-42.60	-2.57	-43.61	-1.37	-43.36	
197	2.4	13.4	-1.85	-42.73	-2.38	-42.84	-2.35	-42.97	-1.83	-42.86	0.3	1.76	-1.61	-42.22	-2.81	-42.47	-2.60	-43.48	-1.40	-43.23	
198	3.6	13.4	-1.88	-42.59	-2.41	-42.70	-2.38	-42.83	-1.85	-42.72	0.5	1.76	-1.64	-42.08	-2.84	-42.33	-2.62	-43.34	-1.43	-43.09	
199	4.8	13.4	-1.91	-42.46	-2.44	-42.57	-2.41	-42.71	-1.88	-42.59	0.6	1.75	-1.66	-41.95	-2.87	-42.20	-2.65	-43.22	-1.46	-42.96	

Table 2.3-3 (cont'd)

PHOTO		TIME OF EXPOSURE			SPACECRAFT			PRINCIPAL GROUND POINT		SLANT DIST	SUN AZIM	EMIS- SION ANGL	'HASE NGU	NCI - JENCE ANGLE	TILT ANGLE	TILT AZIM	SWING ANGLE	NORTH DEVIATION															
SITE NO.	EXP NO.	S/C	GMT	ALT	ALT RT	LAT	LONG	LAT	LONG																								
																			SECONDS	HR:MIN:SEC	KM	CM/SEC	DEG	DEG	DEG	DLG	KM	DEG	DEG	DEG	DEG	DEG	DEG
ESTIMATED	ERROR	0.03	1.1	0.001	0.01	0.006	0.01	0.006	0.01	0.12	0.01	0.12	0.01	0.12	0.01	0.1	0.1																
MY 241																																	
-1	200	47167.0	13:23:30.5	46	0.027	-2.15	-44.55	-2.15	-44.58	46	87.22	1.3	52.2	63.49	1.2	271.50	80.0	398.5															
	201	47169.1	13:23:32.6	46	0.028	-2.18	-44.42	-2.18	-44.45	46	87.20	1.1	52.2	63.36	1.1	270.30	78.8	348.5															
	202	47171.2	13:23:34.7	46	0.029	-2.21	-44.29	-2.21	-44.32	46	87.18	1.0	52.2	63.23	1.0	268.80	77.3	348.5															
	203	47173.3	13:23:36.8	46	0.030	-2.23	-44.17	-2.23	-44.19	46	87.15	0.9	52.2	63.11	0.9	266.85	75.3	348.5															
	204	47175.5	13:23:39.0	46	0.031	-2.26	-44.04	-2.26	-44.06	46	87.13	0.7	52.2	62.97	0.7	264.10	72.6	348.5															
	205	47177.7	13:23:41.2	46	0.032	-2.29	-43.91	-2.29	-43.92	46	87.11	0.6	52.2	62.84	0.6	260.19	68.7	34235															
	206	47179.8	13:23:43.3	46	0.033	-2.32	-43.78	-2.32	-43.79	46	87.09	0.5	52.2	62.71	0.5	254.56	63.1	348.5															
	207	47182.0	13:23:45.5	46	0.034	-2.34	-43.65	-2.35	-43.66	46	87.06	0.4	62.2	62.58	0.4	244.94	53.5	348.5															
	208	47184.2	13:23:47.7	46	0.035	-2.37	-43.52	-2.38	-43.52	46	87.04	0.3	52.2	62.44	0.3	227.77	36.3	348.5															
	209	47186.3	13:23:49.8	46	0.036	-2.40	-43.39	-2.40	-43.39	46	87.02	0.2	52.2	62.31	0.2	200.05	8.58	348.5															
	210	47188.5	13:23:52.0	46	0.038	-2.42	-43.26	-2.43	-43.26	46	86.99	0.3	52.2	62.18	0.2	166.96	335.5	348.5															
	211	47190.6	13:23:54.1	47	0.039	-2.45	-43.13	-2.46	-43.13	47	86.97	0.3	52.2	62.05	0.3	145.59	314.1	348.5															
-2	222	47192.8	13:23:56.3	47	0.040	-2.48	-43.00	-2.49	-42.9	47	86.95	0.4	62.2	61.92	0.4	132.99	301.5	348.5															
	213	47194.9	13:23:58.4	47	0.041	-2.50	-42.87	-2.51	-42.86	47	86.92	0.6	52.2	61.79	0.5	125.92	294.5	348.5															
	214	47197.1	13:24:00.6	47	0.042	-2.53	-42.74	-2.54	-42.73	47	86.90	0.7	62.2	61.66	0.7	121.18	289.7	348.6															
	215	47199.3	13:24:02.8	47	0.043	-2.56	-42.61	-2.57	-42.59	47	86.88	0.8	62.2	61.52	0.8	117.95	286.5	348.6															
	MS ION B PHOTON SITES																																
-2	48	28272.5	01:22:50.9	80	-0.152	3.40	29.08	3.05	28.57	82	89.01	13.8	70.3	86.68	13.2	235.40	54.2	358.1															
	49	28285.6	01:23:04.0	78	-0.146	3.24	29.84	2.89	29.38	80	89.03	13.3	70.3	80.87	12.7	232.95	51.7	358.0															
-4	84	UU0.4	01:44:26.3	78	-0.158	3.49	15.13	3.05	14.56	81	88.93	16.4	70.3	83.28	15.7	232.35	50.8	357.5															
	DAY 235																																
-5	103	86441.0	22:39:56.8	66	-0.123	2.47	8.44	2.12	8.11	67	88.95	13.1	70.3	79.11	12.6	222.51	40.7	357.5															
	DAY 236																																
-7	113	44229.6	16:04:03.1	75	-0.155	3.21	-4.78	2.88	-5.35	78	88.86	15.5	70.3	83.70	14.8	239.77	58.9	358.3															
	114	44236.3	16:04:09.8	74	0.152	3.12	-4.39	2.79	-4.93	77	88.87	15.2	70.3	83.28	14.5	238.74	57.8	358.3															
-8	134	39629.9	19:55:00.8	57	-0.132	2.03	-15.19	1.81	-15.49	59	88.84	11.7	70.3	79.71	11.4	233.08	52.2	358.5															
	135	52027.9	23:21:38.8	55	-0.124	1.79	-16.01	1.44	-16.28	57	88.82	14.1	70.3	78.75	13.7	217.10	35.0	357.1															
	DAY 237																																
-9	149	46288.7	02:53:37.1	47	-0.069	0.14	-24.27	-0.10	-24.34	47	88.45	9.5	70.3	72.86	9.3	195.63	13.9	358.1															
	151	71116.5	09:47:24.9	43	-0.032	-0.79	-23.63	-0.42	-23.62	45	88.05	14.9	70.3	68.65	14.6	157	188.7	7.1															
	DAY 239																																
B-10	150	58589.8	06:18:38.3	54	-0.107	1.04	-30.67	0.77	-30.89	55	88.67	11.6	70.3	77.66	11.2	219.47	38.0	358.0															
B-11	DAY 239																																
	153	15668.7	23:30:54.7	50	-0.081	0.34	-36.89	0.41	-37.03	50	88.51	5.5	70.3	75.07	5.4	297.86	119.9	22.1															
	154	15678.7	23:31:04.7	49	-0.076	0.22	-36.29	0.29	-36.41	50	87.48	4.9	70.3	74.46	4.8	299.90	122.0	2.2															
	155	15688.6	23:31:14.6	49	-0.071	0.10	-35.70	0.16	-35.80	49	88.44	4.3	70.3	73.85	4.2	302.48	124.6	2.2															
	156	15698.6	23:31:24.6	48	-0.066	-0.03	-35.10	0.03	-35.19	48	88.40	3.7	70.3	73.23	3.6	305.91	128.0	2.2															

Table 2.33 (cont'd)

EXP NO.	HIGH RESOLUTION										MODERATE RESOLUTION									
	TILT DIST	SCALE FACTOR	PHOTO CORNER COORDINATES								TILT DIST	SCALE FACTOR	PHOTO CORNER COORDINATES							
			A		B		C		D				A		B		C		D	
			LAT	LONG	LAT	LONG	LAT	LONG	LAT	LONG			LAT	LONG	LAT	LONG	LAT	LONG	LAT	LONG
			MM	X10 ⁻³	DEG	DEG	DEG	DEG	DEG	DEG			DEG	DEG	MM	X10 ⁻³	DEG	DEG	DEG	DEG
1%	2%									1%	2%									
00	13.2	13.3	-1.90	-44.46	-2.43	-44.57	-2.41	-44.70	-1.87	-44.59	1.7	1.75	-1.66	-43.95	-2.86	-44.20	-2.65	-45.22	-1.44	-44.96
01	11.8	13.3	-1.93	-44.33	-2.46	-44.44	-2.43	-44.57	-1.90	-44.46	1.5	1.75	-1.69	-43.82	-2.89	-44.07	-2.68	-45.09	-1.47	-44.84
02	10.5	13.3	-1.96	-44.20	-2.49	-44.31	-2.46	-44.44	-1.93	-44.33	1.4	1.74	-1.71	-43.69	-2.91	-43.94	-2.71	-44.96	-1.49	-44.71
03	9.1	13.3	-1.98	-44.07	-2.51	-44.18	-2.49	-44.31	-1.95	-44.20	1.2	1.74	-1.74	-43.56	-2.94	-43.81	-2.94	-44.83	-1.52	-44.58
04	7.8	13.3	-2.01	-43.93	-2.54	-44.05	-2.52	-44.18	-1.98	-44.07	1.0	1.74	-1.77	-43.42	-2.97	-43.67	-2.76	-44.70	-1.55	-44.44
05	6.4	13.2	-2.04	-43.80	-2.57	-43.91	-2.54	-44.04	-2.01	-43.93	0.8	1.74	-1.80	-43.29	-3.00	-43.54	-2.79	-44.56	-1.58	-44.31
06	5.2	13.2	-2.07	-43.67	-2.60	-43.78	-2.57	-43.92	-2.04	-43.80	0.7	1.73	-1.82	-43.15	-3.03	-43.41	-2.82	-44.44	-1.60	-44.18
07	3.9	13.2	-2.09	-43.53	-2.63	-43.65	-2.60	-43.78	-2.07	-43.67	0.5	1.73	-1.85	-43.02	-3.06	-43.27	-2.85	-44.30	-1.63	-44.04
08	2.9	13.2	-2.12	-43.40	-2.66	-43.51	-2.63	-43.64	-2.09	-43.53	0.4	1.73	-1.88	-42.88	-3.09	-43.13	-2.88	-44.17	-1.66	-43.91
09	2.4	13.2	-2.15	-43.27	-2.69	-43.38	-2.66	-43.52	-2.12	-43.40	0.3	1.73	-1.90	-42.75	-3.12	-43.00	-2.91	-44.04	-1.69	-43.78
10	2.6	13.1	-2.18	-43.13	-2.71	-43.24	-2.69	-43.38	-2.15	-43.27	0.3	1.72	-1.93	-42.61	-3.15	-42.87	-2.93	-43.90	-1.71	-43.64
11	3.4	13.1	-2.20	-43.00	-2.74	-43.12	-2.71	-43.25	-2.17	-43.14	0.4	1.72	-1.95	-42.48	-3.18	-42.74	-2.96	-43.77	-1.74	-43.52
12	4.6	13.1	-2.23	-42.87	-2.77	-42.98	-2.74	-43.12	-2.20	-43.00	0.6	1.72	-1.98	-42.34	-3.21	-42.60	-2.99	-43.64	-1.77	-43.38
33	5.8	13.1	-2.26	-42.74	-2.80	-42.85	-2.77	-42.99	-2.23	-42.87	0.8	1.72	-2.01	-42.21	-3.24	-42.47	-3.02	-43.51	-1.79	-43.25
14	7.1	13.0	-2.28	-42.60	-2.83	-42.72	-2.80	-42.85	-2.26	-42.74	0.9	1.71	-2.03	-42.08	-3.27	-42.33	-3.05	-43.38	-1.82	-43.12
35	8.5	13.0	-2.31	-42.47	-2.86	-42.58	-2.83	-42.72	-2.28	-42.60	1.1	1.71	-2.06	-41.94	-3.30	-42.20	-3.08	-43.24	-1.85	-42.98
48	43.1	7.66	3.49	28.78	2.53	28.59	2.57	28.34	3.54	28.54	18.8	1.00	3.87	29.59	1.77	29.28	1.96	27.22	4.29	27.86
49	37.2	7.85	3.33	29.58	2.39	29.40	2.43	29.15	3.37	29.36	18.0	1.03	3.70	30.38	1.64	30.07	1.85	28.08	4.10	28.70
84	71.2	7.80	3.49	14.76	2.53	14.59	2.56	14.33	3.53	14.53	22.5	1.02	3.88	15.55	1.77	15.29	1.89	13.18	4.26	13.84
03	36.4	9.28	2.48	8.29	1.68	8.12	1.72	7.91	2.52	8.10	17.9	1.22	2.79	8.96	1.01	8.69	1.25	7.01	3.13	7.57
13	61.3	8.13	3.30	-5.14	2.39	-5.33	2.42	-5.58	3.35	-5.37	21.2	1.07	3.64	-4.38	1.67	-4.69	1.84	-6.67	4.07	-6.01
14	58.0	8.25	3.21	-4.73	2.31	-4.92	2.35	-5.16	3.25	-4.95	20.7	1.08	3.55	-3.97	1.60	-4.29	1.78	-6.23	3.97	-5.58
34	22.6	10.6	2.12	-15.34	1.44	-15.48	1.47	-15.66	2.16	-15.50	16.1	1.39	2.39	-14.75	0.88	-14.99	1.06	-16.42	2.70	-15.98
35	48.3	11.0	1.75	-16.13	1.07	-16.27	1.10	-16.44	1.78	-16.29	19.5	1.45	2.01	-15.57	0.50	-15.77	0.69	-17.21	2.28	-16.73
149	99.7	13.1	0.15	-24.21	-0.41	-24.32	-0.38	-24.47	0.18	-24.35	13.1	1.72	0.39	-23.73	-0.89	-23.91	-0.67	-25.04	0.59	-24.71
151	58.9	14.1	-0.15	-23.49	-0.69	-23.60	-0.66	-23.73	-0.12	-23.63	20.8	1.84	0.14	-22.93	-1.06	-23.28	-0.88	-24.19	0.40	-24.04
50	20.9	11.4	1.07	-30.75	0.42	-30.87	0.45	-31.04	1.10	-30.90	15.9	1.49	1.33	-30.20	-0.11	-30.41	0.08	-31.74	1.58	-31.34
53	57.3	12.2	0.69	-36.90	0.11	-37.02	0.14	-37.16	0.73	-37.04	7.5	1.59	0.95	-36.34	-0.33	-36.62	-0.14	-37.75	1.24	-37.48
154	51.1	12.3	0.56	-36.28	-0.01	-36.40	0.01	-36.54	0.59	-36.43	6.7	1.62	0.82	-35.74	-0.45	-36.01	-0.26	-37.11	1.08	-36.85
155	44.9		0.43	-35.67	-0.14	-35.79	-0.11	-35.93	0.46	-35.82	5.5	1.64	0.68	-35.13	-0.57	-35.40	-0.38	-36.49	0.95	-36.23
156	38.9	12.7	0.30	-35.06	-0.26	-35.17	-0.23	-35.31	0.33	-35.20	5.1	1.67	0.55	-34.53	-0.69	-34.79	-0.49	-35.86	0.80	-35.61

Table 2.3-3 (cont'd)

PHOTO		TIME OF EXPOSURE		SPACECRAFT				PRINCIPAL GROUND POINT		SLANT	SUN	EMIS-	PHASE	INCI-	TILT	TILT	WING	NORTH
S	E			ALT	ALT RT	LAT	LONG	LAT	LONG	DIST	AZIM	SION	ANGLE	DENCE	ANGLE	AZIM	ANGLE	DEVIA
N	P	SECONDS	HR:MIN:SEC	KM	KM/SEC	DEG	DEG	DEG	DEG	KM	DEG	ANGLE	DEG	DEG	DEG	DEG	DEG	TION
O.	N.	ESTIMATED	ERROR	0.03	1.1	0.001	0.01	0.006	0.01	0.006	1.1	0.01	0.12	0.12	0.01	0.12	0.01	0.1
FARSIDE PHOTO SITES																		
	20	35337.7	DAY 231 17:05:21.0	1	0.338	-9.45	-153.0	-10	-154.3	1303	275.36	3.8	70.3	67.39	2.2	33.77	228.7	174.9
	30	87517.6	DAY 232 07:35:00.8	1295	0.340	-9.45	-161.3	-10	-163.3	1298	275.54	5.1	70.3	65.86	2.9	45.98	240.7	174.7
	35	08880.2	14:52:01.0	1336	0.329	-9.06	-162.6	-9.4	-162.8	1336	274.93	0.8	70.3	69.87	0.5	12.11	207.1	175.0
	36	08893.4	14:52:14.2	1340	0.328	-9.02	-162.3	-9.3	-162.3	1340	274.86	0.5	70.3	70.36	0.4	77.67	172.7	175.0
	37	09009.1	14:54:09.9	1377	0.317	-8.67	-159.9	-8.7	-158.0	1379	274.31	4.3	70.3	74.60	2.4	0.38	85.8	175.4
	38	09022.3	14:54:23.1	1381	0.316	-8.62	-159.7	-8.6	-157.5	1384	274.25	4.8	70.3	75.09	2.7	9.43	84.9	175.4
	39	09240.3	14:58:01.1	1448	0.294	-7.94	-155.2	-7.3	-149.2	1469	273.35	13.1	70.3	83.17	7.1	3.79	79.8	176.0
	40	09448.7	14:58:09.5	1450	0.293	-7.91	-155.1	-7.2	-148.9	1472	273.32	13.4	70.3	83.48	7.3	3.69	79.8	176.0
	115		DAY 237 00:05:55.0	1379	0.346	-8.43	144.15	-7.6	144.24	1379	274.67	1.8	70.3	70.31	1.0	.93	0.6	174.7
	116	73367.5	00:09:40.9	1454	0.319	-7.66	148.55	-6.1	152.33	1463	273.71	8.9	70.3	78.27	4.8	7.89	63.3	175.3
	1136	68044.8	DAY 238 03:48:35.7	1321	0.355	-7.92	129.27	-8.0	128.64	1321	274.63	1.4	70.3	68.84	0.8	67.04	262.2	175.2
MISCELLANEOUS PHOTO SITES																		
	25	71259.3	DAY 230 21:56:25.0	225	-0.111	2.52	76.41	1.27	76.12	228	89.2	11.0	70.3	72.6	9.8	192.8	10.1	357.1
	26	97350.5	DAY 231 05:11:16.2	226	-0.114	2.55	72.10	1.65	71.75	228	89.2	8.3	70.3	73.3	7.4	201.3	19.6	358.1
	27	05541.4	08:48:44.6	226	-0.114	2.53	70.09	1.68	69.72	228	89.2	8.1	70.3	73.5	7.1	203.4	21.8	358.2
	29	57728.5	23:18:31.8	227	-0.118	2.66	61.57	1.77	61.05	230	89.2	8.8	70.3	74.7	7.8	210.5	28.9	358.2
	31	04978.5	DAY 232 13:46:59.3	233	-0.151	3.55	48.96	2.76	47.68	244	89.15	12.3	70.3	80.7	10.8	238.0	57.1	358.6
	32	05012.4	13:47:33.2	233	-0.140	3.20	50.67	2.38	49.66	238	89.17	10.9	70.3	78.7	9.6	230.9	49.8	358.5
	33	05131.0	13:49:31.8	220	-0.097	1.92	56.72	1.00	56.54	222	89.07	8.4	70.3	n.9	7.4	191.1	9.3	358.1
	34	05156.3	13:49:57.0	218	-0.088	1.64	58.01	0.69	57.99	220	89.00	8.5	70.3	70.4	7.5	181.1	359.2	358.0
	41	30996.0	21:00:36.9	252	-0.180	4.36	40.84	3.42	38.82	262	88.97	17.1	70.3	85.9	14.9	245.0	64.4	358.6
	42	57040.0	DAY 233 04:14:40.8	263	-0.199	4.89	34.06	4.43	31.45	276	88.77	19.5	70.3	89.51	16.8	260.1	80.6	0.1
	43		TEST DOOR CLOSED															
	44	83039.5	11:28:00.3	68	-0.102	2.24	42.59	1.99	42.41	68	89.06	8.1	70.3	74.94	7.8	215.1	33.8	358.4
	46	03084.3	18:23:02.7	96	-0.193	4.50	27.55	4.04	26.64	101	88.80	18.8	70.3	87.13	17.8	242.5	62.2	358.2
	47	03091.2	18:23:09.6	95	-0.190	4.42	27.95	3.96	27.07	99	88.82	18.5	70.3	86.70	17.5	242.1	61.4	358.1
	50	53554.8	DAY 234 08:24:13.1	55	-0.010	-0.06	42.11	-0.4	42.29	56	88.32	13.5	70.3	64.47	13.1	155.3	331.9	357.1
	51	53561.5	08:24:19.8	55	-0.006	-0.14	42.51	-0.5	42.70	56	88.27	13.8	70.3	64.1	13.3	154.6	330.5	357.1
	101		DAY 235 TEST DOOR CLOSED															
	102	64627.8	16:36:23.6	EARTH AND LIMB OF MOON														
	104		TEST DOOR CLOSED															
	117	98887.5	DAY 237 13:02:05.0	EARTH AND LIMB OF MOON														
	137	76800.0	DAY 238 06:14:30.9	54	-0.119	1.61	-19.07	1.37	-20.81	77	88.79	45.7	34.6	79.79	43.9	262.2	76.1	351.7
	138	89225.0	09:41:35.9	50	-0.097	1.03	-18.28	0.72	-18.43	51	88.70	12.2	70.3	75.67	11.8	206.5	24.32	357.3
	139	09150.5	16:34:39.0	48	-0.086	0.70	-20.67	0.37	-20.78	49	88.62	12.7	70.3	74.54	12.4	199.5	17.4	357.0
	140	21543.0	20:01:11.5	46	-0.064	0.09	-20.08	-0.24	-20.13	47	88.43	12.6	70.3	72.16	12.3	189.6	6.2	357.0
	173	65532.6	DAY 240 13:21:58.6	54	0.099	-4.07	-22.92	-4.68	-22.4	60	85.17	25.0	70.3	53.72	24.2	139.6	313.8	357.4
	174	89714.8	20:06:00.8	70	-0.158	2.10	-57.18	1.64	-57.8	74	88.66	18.8	70.3	85.34	18.1	232.7	51.4	357.3
	175	10092.3	DAY 241 03:05:35.9	49	0.056	-2.78	-35.64	-3.26	-35.3	52	86.61	19.9	70.3	59.55	19.3	148.6	323.5	357.0

Table 2.3-3 (cont'd)

HIGH RESOLUTION											MODERATE RESOLUTION										
EXP N.O.	TILT DIST	SCALE FACTOR	PHOTO CORNER COORDINATES								TILT DIST	SCALE FACTOR	PHOTO CORNER COORDINATES								
			A		B		C		D				A		B		C		D		
			LAT	LONG	LAT	LONG	LAT	LONG	LAT	LONG			LAT	LONG	LAT	LONG	LAT	LONG	LAT	LONG	
			MM	X10 ⁻³	DEG	DEG	DEG	DEG	DEG	DEG			DEG	DEG	MM	X10 ⁻³	DEG	DEG	DEG	DEG	DEG
	2%	2%									2%	2%									
28	23.4	0.469	-2.47	-153.42	-17.97	-151.2	-18.56	-155.4	-2.93	-157.31	3.1	0.061	11.2	-140.7	-27.8	-132.46	-34.3	-173.4	8.19	-174.99	
30	31.0	0.471	-2.41	-162.37	-17.8	-160.2	-18.42	-164.3	-2.85	-166.26	4.1	0.062	11.0	-149.9	-27.3	-142.18	-34.35	-177.13	8.64	-175.50	
35	53	0.457	-1.17	-161.94	-17.1	-159.5	-18	-163.7	-1.72	-165.92	0.7	0.060	14.1	-148.1	-27.1	-139.47	-33.0	-179.51	9.41	-176.25	
36	40	0.455	-1.06	-161.44	-17.0	-159.0	-18	-163.2	-1.63	-165.44	0.5	0.060	14.4	-147.4	-27.1	-138.64	-32.9	-179.8	9.44	-176.80	
37	25.8	0.443	-0.13	-157.11	-16.6	-154.4	-17	-158.7	-0.82	-161.23	34	0.058	17.5	-141.1	-27.7	-130.76	-32.3	-174.4	9.78	-178.53	
38	28.7	0.442	-0.02	-156.62	-16.5	-153.9	-17	-158.2	-0.73	-160.75	3.8	0.058	17.9	-140.3	-27.7	-129.77	-32.2	-173.8	9.83	-178.02	
39	75.9	0.421	1.98	-148.37	-15.7	-145.1	-16	-149.8	1.00	-152.82	100	0.055	29.4	-120.8	-30.1	-107.12	-31.2	-10.9	-169.79		
40	77.7	0.421	2.06	-148.04	-15.6	-144.7	-16	-149.5	1.07	-152.52	102	0.055	30.8	-118.8	-30.5	-104.63	-31.2	-163.9	10.9	-169.48	
115	11.0	0.443	1.00	144.91	15.4	147.79	-16	143.55	0.30	140.78	1.4	0.058	18.7	159.97	-24.9	168.30	-31.4	127.68	12.0	121.32	
116	51.5	0.420	3.16	153.03	14.3	156.39	-15	151.85	2.18	148.62	6.8	0.055	28.3	175.53	-25.7	175.64	-30.3	137.36	13.0	129.99	
136	8.7	0.462	0.21	129.35	15.5	131.95	-16	127.87	-0.39	125.40	1.1	0.061	15.5	142.79	-24.8	150.97	-31.4	111.80	10.6	107.06	
25	105.0	2.71	2.51	76.72	-0.21	76.17	- .06	75.48	2.64	76.07	13.8	0.356	3.62	79.11	-2.75	78.21	-1.57	72.57	4.63	74.33	
26	78.7	2.70	2.88	72.35	0.21	71.80	0.35	71.12	3.02	71.70	10.3	0.354	4.01	74.77	-2.19	73.78	-1.11	68.27	5.07	69.91	
27	76.2	2.70	2.91	70.32	0.24	69.77	0.38	69.09	3.05	69.67	100	0.354	4.09	72.74	-2.14	71.74	-1.08	66.24	5.11	67.87	
29	83.4	2.68	3.02	61.65	0.32	61.10	0.45	60.41	3.15	60.99	109	0.352	4.14	64.06	-2.06	63.08	-1.06	57.49	5.24	59.16	
31	115.9	2.55	4.08	48.32	1.22	47.75	1.34	47.00	4.23	47.62	152.0	0.335	5.23	50.80	-1.11	49.79	-0.45	43.66	6.54	45.53	
32	102.8	2.61	3.66	50.28	0.88	49.72	1.00	48.99	3.81	49.60	13.5	0.342	4.80	52.72	-1.46	51.72	-0.68	45.82	6.03	47.62	
33	79.3	2.77	2.20	57.12	-0.4	56.58	-0.3	55.92	2.33	56.49	104	0.364	3.30	59.50	-2.80	58.53	-1.66	53.17	4.30	54.77	
34	80.8	2.80	1.88	58.57	-0.7	58.04	-0.6	57.38	2.01	57.95	106	0.367	2.98	60.96	-3.12	59.99	-1.89	54.70	3.95	56.26	
41	162.2	2.42	4.84	39.51	1.77	38.90	1.86	38.07	5.00	38.74	21.3	0.317	6.05	42.09	-0.63	41.10	-0.36	34.11	7.53	36.35	
42	184.5	2.32	5.93	32.17	2.73	31.55	2.82	30.66	6.11	31.34	242	0.305	7.17	44.91	0.41	33.81	0.48	26.36	9.01	28.55	
43			TEST DOOR CLOSED																		
44	83.6	9.03	2.36	42.59	1.56	42.43	1.60	42.22	2.40	42.40	11.0	1.18	2.69	43.30	0.89	43.01	1.17	41.38	3.01	41.86	
46	196.0	6.36	4.59	26.90	3.40	26.68	3.43	26.35	4.64	26.61	25.71	0.834	5.05	27.88	2.51	27.54	2.57	24.85	5.59	25.71	
47	192.4	6.45	4.50	27.33	3.33	27.11	3.36	26.79	4.56	27.04	252	0.846	5.00	28.29	2.45	27.95	2.52	25.32	5.48	26.16	
50	142.0	11.2	0.14	42.44	-0.8	42.30	-0.8	42.13	-0.1	42.28	18.6	1.46	0.15	43.06	-1.5	42.83	-1.1	41.48	0.36	41.87	
51	144.7	11.2	0.22	42.85	-0.9	42.71	-0.8	42.55	-0.19	42.69	19.0	1.46	0.06	43.47	-1.6	43.25	-1.15	41.89	0.27	42.29	
101			TEST DOOR CLOSED																		
102			EARTH AND LIMB OF MOON																		
104			TEST DOOR CLOSED																		
117			EARTH AND LIMB OF MOON																		
137	587.2	11.2	1.79	-20.57	0.9	-20.75	0.9	-21.10	1.84	-20.87	77.0	1.47	2.06	-19.81	0.49	-20.01	-0.52	-23.67	2.82	-22.17	
138	127.7	12.2	0.99	-18.30	0.4	-18.42	0.4	-18.58	1.02	-18.44	16.8	1.61	1.23	-17.78	0.14	-18.00	0.08	-19.23	1.47	-18.83	
139	133.6	12.7	0.64	-20.66	0.05	-20.77	0.08	-20.92	0.67	-20.79	17.5	1.66	0.87	-20.16	-0.5	-20.34	-0.25	-21.56	1.09	-21.16	
140	132.9	13.4	0.02	-20.02	-0.5	-20.12	-0.51	-20.26	0.04	-20.15	17.4	1.75	0.24	-19.54	-1.06	-19.70	-0.82	-20.85	0.43	-20.49	
173	274.2	11.3	-4.4	-22.24	-5.09	-22.37	-5.0	-22.56	-4.3	-22.41	36.0	1.48	-4.05	21.52	-6.04	-21.66	-5.29	-23.23	-3.9	-22.83	
174	198.9	8.67	2.04	-57.59	1.16	-57.76	1.2	-58.00	2.08	-57.80	26.1	1.14	2.38	-56.88	0.47	-57.12	0.55	-59.10	2.75	-58.42	
175	213.8	12.5	-2.98	-35.20	-3.7	-35.32	-3.6	-35.48	-2.95	-35.35	28.0	1.64	-2.73	-34.61	-4.3	-34.78	-3.82	-36.08	-2.5	-35.71	

Table 2.3-3(cont'd)

2.4 PHOTOGRAPHIC SUBSYSTEM CALIBRATION

Calibration of the photographic subsystem was accomplished to satisfy two requirements. (1) establish that the system met the specifications required to meet mission objectives, and (2) provide data necessary for proper interpretation and analysis of the photographs. Calibration measurements were made on certain components of only one of the photographic subsystems produced for the Lunar Orbiter project as indicated in Table 2.4-1. Certain of these measurements, required for only one photo subsystem or component, were not completed prior to Mission I because of scheduling requirements. Those tests delayed

did not compromise probability of operational success.

The following discussion is limited to a description of calibration techniques and to some nominal values. In all cases, the actual calibration values fell within design limits. Measurement data, including the actual test film, applicable to the specific subsystem (Serial Number 4) for Mission I has been delivered to NASA.

Tests and calibrations performed are summarized in Table 2.41.

Item	610-MM COMP. LEVEL	80-MM COMP. LEVEL	CAMERA LEVEL	PS LEVEL	COMPONENT DATA PACKAGE OF TEST REPORTS	PS DATA PACKAGE	SPACECRAFT LEVEL	READOUT AT ETR	READOUT IN FLIGHT	SPACECRAFT DATA PACKAGE	DELIVERED TO NASA
2.4.3.1 SINE WAVE RESPONSE MTF OF READOUT DENSITY VARIATIONS LENS TRANSMISSION MTF OF LENS SPECTRAL TRANSMISSION LENS DISTORTION SYSTEM VEILING GLARE	X X	<div>1</div> <div>2</div> X	X X	X <div>3</div>		X X X	X X	X X	X X	X X	X X X X
2.4.3.2 SHUTTER SPEED SHUTTER LINEARITY PRE-EXPOSED EDGE DATA	X X			<div>3</div> <div>3</div>	X		X	X	X	X	X
2.4.3.3 PLATEN FORMAT PLATEN MOTION	X	X		<div>X</div> <div>4</div>		X X					X
2.4.3.4 BORESIGHTING				<div>5</div>		X					X
2.4.3.5 TIME CODE DATA SHUTTER TIMING	X	X	X	X X	X	X	X			X	X
2.4.3.6 READOUT				X		X	X	X	X	X	


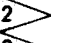



-  DATA AVAILABLE BASED ON SIMILAR UNIT
-  DATA TO BE OBTAINED ON ONE FLIGHT LENS ONLY (NOT AVAILABLE)
-  DATA TO BE OBTAINED ON ONE PS AT A LATER DATE
-  DATA AVAILABLE ON BOTH PLATENS AT THREE SHUTTER SPEEDS AND TWO V/H RATIOS
-  DATA ACCOMPLISHED WITH

Table 2.41: Photographic Subsystem Tests and Calibrations

2.4.1 SPACECRAFT PHOTOGRAPHIC SUBSYSTEM

The Lunar Orbiter photo subsystem was designed primarily for photo reconnaissance, and as such did not employ optics, film, or Reseau control required for photogram-

metry. Limitations of the photo subsystem and ground reconstruction of photographs constrain use of photographs for this purpose. Because the importance of metrical measurements was later realized, calibrations were performed on the camera system to permit at least partial corrections

for known distortions. The following paragraphs describe the tests performed. Specific calibration data are not included here as the measurement data has been submitted to NASA for evaluation.

2.4.1.1 LENS - FILM CHARACTERISTICS

Sine-Wave Response

The capability of a camera system to resolve image detail under ideal conditions is a function of its optical system and the characteristics of the photographic film recording the image. Therefore, both lens and film must be considered together. The sine-wave response or modulation transfer function (MTF) provides a measure of this capability. Further, the MTF provides a technique for following the *effect* on the image of each operation lens to the photograph being examined by the analyst. The MTF is a function that relates image modulation to target modulation as a function of spatial frequency. The lens-film system is used to photograph a target, similar to a bar pattern, on which the intensity varies as a sine function of constant amplitude and with an increasing frequency of variation per unit length (i.e., cycles per mm). Test targets provide for measurement of radial and tangential MTF as a function of field angle and density. Exposures are made both at the camera level and at the subsystem level where the film is processed so that the film-Bimat function is included. Pertinent processing and environmental parameters are included in the calibration data. A typical MTF curve for the on-axis position of the 80-mm camera is shown in Figure 2.41.

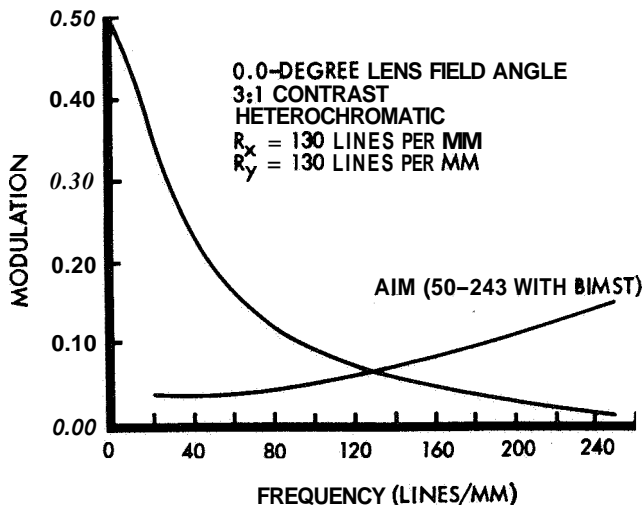


Figure 2.41: Modulation Transfer Function-80-mm Lens

Lens Transmission

Lens transmission varies as a function of wavelength. However, this factor largely can be neglected for the Lunar Orbiter camera, since only black-and-white photography is used and also because of the apparent absence of appreciable color contrasts on the lunar surface. Of considerably more importance is the variation in transmission with off-axis line-of-sight and the difference in transmission characteristics between the 610- and 80-mm lenses.

Lens transmission is determined on-axis and off-axis at 5-degree intervals along the diagonal of the field of view. An accuracy of $\pm 2\%$ in the measurement is obtained. Typical lens transmission for both the 610- and 80-mm lens is shown in Figure 2.42. The difference in transmission characteristics should be noted because of the direct bearing on relative exposure of the photographs taken with the respective lenses.

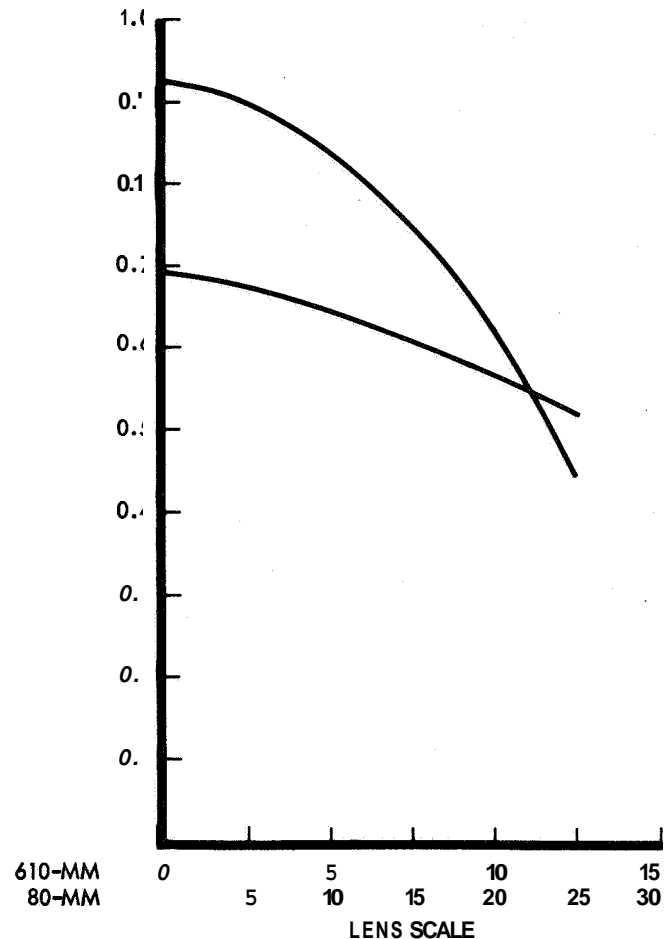


Figure 2.42 Lens Transmission - 80-mm and 610-mm Lenses

Transmission data of the specific 80-mm lens used on Mission I was not obtained because of a replacement that was made in the camera system prior to acceptance.

Distortion

Both radial and tangential distortion of the 80-mm lens is determined. These measurements are made on each flight lens to an accuracy of 10 microns at the film plane, and are performed at camera level. Tests are conducted using the collimator method as defined in Mil-Standard 150A, Photographic Lenses. Equivalent focal length - - the focal length for best camera definition - - as well as the calibrated focal length are determined. The calibrated focal length is the adjusted focal length to distribute the effects of lens distortion over the entire field.

If y is the radial distance of the object point from the optical axis, y_0' the ideal distance of the corresponding image point, and α the off-axis angle, freedom from distortion is defined by

$$y_0' = f \tan \alpha$$

where f is the lens focal length. In the presence of distortion, the actual position of the image point, y' , differs from y_0' . Then the radial linear distortion, D , is given by

$$D = y' - y_0'$$

Tangential distortion is caused by imperfect centering of lens elements. It results in displacement of the image point and is measured in the direction perpendicular to the radial lines.

Both radial and tangential distortion of the 80-mm Schneider Xenotar lens is plotted in Figure 2.43.

Flare and Glare

Veiling glare is determined at both system and lens levels. Each of the lenses is measured for veiling glare to an accuracy of 2% to ensure that the lens meets requirements. One camera system will be subjected to a veiling glare test using Method 34 of the Mil-Standard 150A methods. The test is performed for both camera and film with the film processed in the photo subsystem. The camera-level test is made to ensure that no light reflections from any internal camera surfaces or from the platen occur. In comparison to the veiling glare originating in the lens itself, reflections within the camera are negligible.

2.4.1.2 EXPOSURE CALIBRATION AND CONTROL

Shutter Speeds

The speed of the 80-mm-lens shutter is measured in accordance with Paragraph 6.3 of Eastman Kodak Company Procedure QC-B-310, In Process Test Procedure for 80-mm Shutter. The shutter is placed between a light source and a photocell. The output of the photocell,

Nominal	Actual
1/25 sec	30-50 milliseconds
1/50 sec	15-25 milliseconds
1/100 sec	7.5 - 12.5 milliseconds

uniform calibrated light source as the shutter is operated. The exposed film is processed by standard methods and the resulting density is scanned, in the direction of curtain travel, at 5-mm intervals by a precision densitometer. Requirements for shutter speed linearity are:

Nominal Speed	Tolerance
1/25	8%
1/50	10%
1/100	12%

Edge Data

Edge data consistency is determined. The data processing checks - consisting of measured densities and the flash lamp record - have been supplied to NASA,

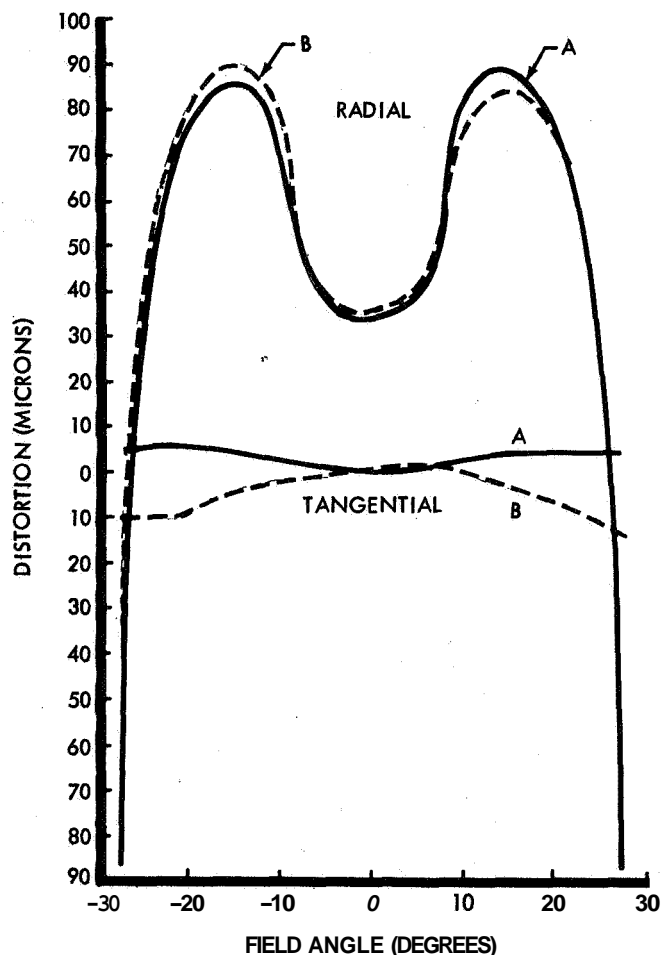


Figure 2.43 Radial and Tangential Distortion - 80-mm Lens

2.4.1.3 IMAGE MOTION COMPENSATION

V/H Sensor

The V/H sensor is tested, at the photo subsystem level, according to Paragraph 6.3.8 of Eastman Kodak Procedure 1231-107, Acceptance Test Procedure for Photographic Subsystem, by means of the V/H test set. Standardized V/H ratios and crab angle errors, generated by the test set, are optically sensed by the **sensor**. **Sensor** outputs obtained from the V/H ratio test point are then compared with the known values supplied by the test set. Response times of the sensor to change in the value of the V/H ratio and crab angle error are also determined during calibration.

The V/H ratios are used in the calibration range between 0.0066 and 0.045 radian per second and the crab angle errors between ± 3 degrees. The sensor output error should be within 1% of the V/H ratio. The response time should be less than 2 seconds for a 1% step change of 50%. The crab angle error should track within 0.0225 degree per second.

Platen Motion

A determination of the motion of the 80-mm platen was made with respect to its rest position during an exposure of 0.04 second and at a nominal image motion compensation (IMC) rate of 0.010 and 0.0375 radian per second. Shutter timing is established to **occur** at the center of the linear portion of the IMC platen motion.

2.4.1.4 TIMING

Time Code

The time code exposed on each dual frame is generated

by a combination of signals from both the photo subsystem and the spacecraft. The time interval between the start of a camera cycle and the request for time by the photo subsystem from the spacecraft is determined in accordance with Paragraph 6.2, Section 3 of Boeing Document D2-100457-1, Photo Subsystem Procedures-Lunar Orbiter. The 20-bit time code is generated within 70 +50, -65 milliseconds following photo subsystem request.

Exposure

The time difference between the start of 610-mm focal-plane shutter and the 80-mm shutter is determined in accordance with Paragraph 6.7 of Eastman Kodak Procedure QC-B-319, In Process Test Procedure for Camera Assembly. A light source is positioned in front of the 610-mm lens and a photocell behind it. The time interval between the signal actuating the 80-mm shutter and the photocell response is measured on an oscilloscope. The time difference required is between 30 and 50 milliseconds.

2.4.1.5 IN-FLIGHT CHECKS

Measurements of the in-flight readout of flight **film** leader targets were made and correlated to a sample of **film** removed prior to flight. The data was also correlated to the measurements made, during prelaunch readout, on the GRE film.

2.4.2 GROUND EQUIPMENT

Standardization and control procedures used to maintain proper operation of the ground reconstruction system are discussed in Section 2.5.5.

2.5 PHOTOGRAPHIC MISSION ANALYSIS

This section considers premission planning, flight operations, ground reconstruction, and production of the photographs with respect to the photographic results of the mission. Problems and real-time solutions are analyzed and discussed in detail.

Premission studies (Boeing Document **D2-100293-1**, January 7, 1965, Picture Data Systems Analysis; and Boeing Document **D2-100628-1**, March 18, 1966, Effects of Illumination on Signal-to-Noise Ratio for the P-5 Mission Photography) had indicated that, to meet the surface-feature detection criteria, the on-axis phase angle must be within the range of 50 to 75 degrees. Prediction of effective illumination or reflection of the lunar surface was subject to appreciable uncertainty because of inadequate information on the normal albedo and the photometric function. The estimated uncertainty was as much as 40%. Direct measurements of normal albedo, by definition, are impossible to obtain by Earth-based observation. Values must be derived by extrapolation of data taken when lunar reflectance changes rapidly with change in phase and based on a limited range of observational geometry.

Albedo values used in early premission studies were based on an albedo chart prepared from unpublished data by Shorthill and Saari referenced to values reported by Sytinskaya (Sytinskaya, N.N. (USSR), *Svondnyy katalog absol'yutnykh znacheniy visual'noy otrazhatel'noy sposobnosti 104 lunnykh ob'yektov*, *Astronomicheskii Zhurnal* **30295** (1953)). Corrections to this data were made on the basis of further studies. Just prior to launch, revised albedos based on USGS measurements were supplied by NASA.

Limitations on acceptable phase angle were a major constraint on mission design since it was necessary to have the spacecraft pass over each target position, in turn, at a time when illumination was within the specified limits. Because of target locations and orbital parameters, site photography was accomplished during the descending node and with morning illumination.

2.5.1 PHOTOGRAPHIC ANALYSIS

A mission designed months before the actual launch of Lunar Orbiter I demonstrated that the spacecraft could meet the requirements of a typical lunar photographic mission within limitations of the hardware design. Testing defined hardware capabilities and identified potential problems that had to be recognized in mission design. The design was repeatedly improved to take advantage of the new data. The resulting "nominal mission plan" served as the guide line for the actual mission. This plan not only satisfied all known hardware limitations, but scheduled processing and readout periods within these constraints to provide "priority readout" of selected frames prior to the complete final readout. Priority readout of all or parts of 51 high-resolution frames and 50 moderate resolution frames was planned. Particular frames were selected for operational evaluation and control as well as to provide stereo samples of each primary photographic site in case final readout could not be completed.

The starting point for readout following a processing period is determined by position of frames at the end of that processing period. In accordance with this operation,

film management was carefully planned to position the particular frames selected for priority readout at the proper location at the time when readout could be accomplished. This had to be done within the following constraints:

- 1) To avoid Bimat stick, process at least two dual frames every 15 hours.
- 2) To avoid Bimat dryout and accompanying processing degradation, process at least two dual frames every 4 hours.
- 3) The camera storage loop capacity is 20 dual frames.
- 4) The camera storage loop should always contain a minimum of two dual frames, and can accept a maximum total of 20.

At least two frames are required in the camera storage loop to enable Bimat cutting at any time should film advancement through the camera become impossible. This capability was not provided early in the mission as it would have either used one additional frame of film and Bimat or would have lengthened the time the splice was under tension. To read out more than four continuous frames of data, film must pass backward through the processor-dryer. This is physically impossible as long as film and Bimat are in mutual contact. To cut and clear Bimat requires the processor to be running with at least two frames available to expel the Bimat after it is cut. Thus, these two frames must be available in the camera storage loop if the camera became inoperable.

For a complete list of existing constraints refer to Boeing Document **D2-100617-2**, Spacecraft Mission Event Sequence and Time Line Analysis, P-5B Mission-Lunar Orbiter; Boeing Document **D2-100617-3**, October 1, 1966, Spacecraft Mission Event Sequence and Time Line Analysis, P-5C Mission-Lunar Orbiter; and Boeing Document **D2-100106**, Revision A, Spacecraft/SFO Systems Specification-Lunar Orbiter. Boeing Document **D2-100617-3** also gives a complete description of the planned mission and the associated photo subsystem management techniques.

In the actual mission, photography was begun according to the plan by advancing 11 frames to move active film into the camera. This was followed immediately by processing 11 frame lengths. Until this time the taped splice connecting the spacecraft film to the leader was safely on the supply reel under several wraps of leader. Camera activity was timed to complete processing just before Sunset of the orbit planned for Site I-0 photography. A sequence of 16 frames were taken of Site I-0, followed immediately by a sequence of four frames. This filled the camera storage loop to capacity. All 20 frames were immediately processed, moving the taped splice completely through the system onto the takeup reel. The splice was then no longer in tension or in danger of separating. This began a period in which the Bimat stick constraint was satisfied by processing at least two frames every four orbits. However, the Bimat dryout constraint was ignored because only processing degradation in some less important frames was expected.

At this point, approximately three frame lengths of exposed processed film was in position to be read out on Orbits 27, 28, and 29. As this film was read out, it was stored in the readout looper until Orbit 30 when two frames of film were processed. This processing emptied the readout looper and advanced two more frame lengths past the optical-mechanical scanner for subsequent readout on Orbits 31 and 32.

It was in this early readout that problems were detected in the high-resolution system. However, the first frame of Site I-0 appeared to be sharp. Because of this it was desired to look at the first high-resolution photograph of the sequence of four that followed Site I-0 to see if it, too, were sharp. Early readout of this frame was not planned previously and was not possible without exposing and processing additional frames to advance it to readout position. Ten exposures were made on Orbit 39 and 8.4 frame lengths were processed. Processing this exact amount positioned the film so that one frame length of readout would include a portion of each of the first two high-resolution frames of the sequence of four. Inspection revealed faulty shutter timing on each. Further analysis of the first high-resolution photo of Site I-0 that appeared sharp revealed that it was a double exposure, and that one of the images was smeared.

At this time one of the photo analysts reported possible evidence of Bimat stick. Processing then was increased to at least two frame lengths every other orbit, until photographing Site I-1. This also required exposing additional frames not previously planned.

The higher V/H values obtained by transferring into the second ellipse did not correct the problem as anticipated. Various test exposures were proposed and carried out to diagnose the problem. Of course, for these exposures to be helpful, processing had to be scheduled to enable their being read out. Also included in the test were other special photographs, such as the first Earth photo, which was taken on Orbit 16 of the second ellipse. Early readout of this frame, during Orbit 31, was also scheduled. Camera testing was not allowed to interfere with photography of Sites I-1, I-2, and I-3, which were photographed with 16 frames each as originally planned. However, by the time Site I-4 was reached, 14 additional exposures had been made for testing or other purposes, and there was not enough film to complete the mission as previously planned. Coverage of Sites I-4, I-6, and I-8.1 was therefore reduced from 16 to eight frames each. The eight frames of Sites I-4 and I-6 were taken at the slow rate but the eight frames of I-8.1 were taken at the fast rate. This appears to have saved 24 frames, when only 14 were needed. However, to avoid Bimat dryout it was still necessary to process two frames every orbit. To satisfy this processing requirement and, because of the number of orbits between photo sites, it was necessary to take additional frames.

Other changes to the film management plan were found necessary when the number of orbits between photo sites was increased from that planned. This sometimes required exposure of an additional film-set frame and processing of additional frames. Satisfying these requirements used the rest of the 24 frames saved at Sites I-4, I-6, and I-8.1.

The landing point of Surveyor I was called Site I-9.1 in the planning mission. The coordinates of this point were changed shortly before photography. This new location was given the designation I-9.2.

It was not originally planned to read out in the priority mode any of the photos taken of the Surveyor I landing site. Because of the importance of these photos, however, the decision was made to delay cutting the Bimat until after some of them were read out. Aplan was devised and implemented in which three consecutive exposures of each of the two 16-frame passes of the Surveyor I site were read out. A sequence for cutting the Bimat and advancing the last exposure to the readout position was successfully carried out on Orbit 65, enabling final complete readout to commence on Orbit 66.

2.5.1.1 SITE PHOTOGRAPHY

Exposure

Shutter settings during the early part of the mission were based upon the predicted albedo for each site. The original values were revised twice before the mission was flown. These values are listed in Table 2.5-1. The maximum acceptable phase angles were desirable to obtain increased contrasts and optimum compromise of signal-to-noise ratios at all sites. Planning was based upon minimum albedo within the planned target area.

SITE	INITIAL PLANNING MINIMUM	CORRECTED MINIMUM	USGS VALUE USED
I-0	--	0.065	0.065
I-1	0.065	0.060	0.081
I-2	0.097	0.090	0.118
I-3	0.070	0.065	0.075
I-4	0.108	0.108	0.135
I-5	0.075	0.070	0.076
I-6	0.100	0.095	0.125
I-7	0.065	0.060	0.076
I-8.1	0.055	0.055	0.069
19.2	0.055	0.055	0.068

Table 2.5-1: Predicted Site Albedoes

Mission trajectory and orbit design were based on patched conic computations using Clarke's model of the Moon without Earth effects. With a Site I-3 maximum phase limitation of 70 degrees, the phase at each site was determined. The phase angles that were predicted and the actual phase angle obtained at each site are tabulated in Table 2.5-2. In each case, the phase shown is for the on-axis line of sight.

Variations in the obtained phase from planned values are due to deviations of the actually attained orbit and orbit parameters from the premission prediction and lunar model used. The exposures predicted for each site and those actually used are shown in Table 2.5-2.

Selection of proper shutter speed required consideration of image density, signal-to-noise ratio, contrast, image smear, differential lens characteristics, and possible deviation of the system from nominal. During photography of the first few sites, exposure was weighted more toward characteristics of the 610-mm lens but later biased more toward those of the 80-mm lens.

SITE	PHASE ANGLES		SHUTTER SPEED	
	PREDICTED	ACTUAL	PREDICTED	USED
I-0	--	62.9	--	0.02
I-1	61.8	60.9	0.02	0.02
I-2	66.3	65.4	0.02	0.02
I-3	68.7	69.2	0.04	0.04
I-4	68.3	68.5	0.02	0.02
I-5	68.4	68.6	0.04	0.02
I-6	54.0	54.1	0.02	0.01
I-7	56.3	58.3	0.02	0.02
I-8.1	61.2	59.3	0.04	0.02
I-9.2a	66.3	63.6	0.04	0.02
I-9.2b	64.5	62.2	0.04	0.02

Table 2.5-2 Primary Site Phase Angles and Shutter Speeds

The brightness range of the lunar surface exceeded system limitations and resulted in underexposure and overexposure within limited areas because of topography and variation in surface character. This occurs in areas of rugged terrain, or those including both upland and mare areas of widely differing albedo, or where bright rayed craters occur in maria. It commonly occurs within craters where both hard shadows and the very bright opposite slopes are found.

The general overexposure of the 80-mm-lens photographs is due principally to higher lens transmission and uncertainties in photometric data rather than to system malfunction or to improper operational control. Selection of a shutter speed was based upon a lunar luminance predicted on the basis of the best information available. Where post-mission analysis of photographs indicated that the shutter speed used was too fast or too slow, the error is attributed to the difference between the predicted and the actual luminance of the area photographed.

Coverage

Target site coverage expected from the nominal altitude of 46 km was 37.8 by 90.6 km in moderate resolution and 16.5 by 63.0 km in high-resolution. This is based on a 16-frame sequence exposed in the fast mode to provide 87% overlap of moderate resolution and 5% in the high-resolution.

Actual coverage of the target areas was very close to that planned at all sites except I-4, I-6, and I-8. At Sites I-4 and I-6 where eight frames were exposed in the slow mode, areal coverage by the 80-mm lens was increased by 60% because of the decreased overlap. The fast sequencing mode was used at Site I-8.1 and therefore the 80-mm lens coverage was decreased to 64% of that planned. The actual area included in the moderate resolution photographs compared with premission planned is shown for each primary site in Figures 2.2-8 through 2.2-19. The coverage of the photographs was determined from the computed locations of the photograph corners and by comparison of the features included in the photographs with the representation on the A.C.I.C. LAC and AIC series of lunar charts. The coverage of some sites appears slightly distorted from the planned coverage. This is caused by a slight tilt of the camera

axis from nadir and by change in altitude of the spacecraft during the sequence.

Resolution

The moderate resolution lens produced photographs consistently having resolution better than the specified requirement on axis, where exposure was correct. Features of the minimum required size were detected and usually identified at all sites. Detection of limiting size detail became difficult only where scene contrast was low due to surface character or where exposure was excessive. Routine evaluation of resolution was based upon examination of a second-generation copy of the 35-mm reconstructed record. The requirement criterion was detection of surface detail spanning four or less scan lines, since this measure of system performance is independent of spacecraft altitude.

No attempt was made to establish a measure of resolution for 610-mm site photographs because of image smear. It has been pointed out in Section 2.2 that detection of the presence of detail smaller than that resolved by the 80-mm lens frequently was possible by the characteristics of the streaked image.

2.5.1.2 OTHER PHOTOGRAPHY

Film budgeted to satisfy film-set or Bimat dryout constraints was used to photograph other locations selected during the mission and presented problems of spacecraft operation and control that were unprecedented. Prior to this mission, operation of unmanned spacecraft was accomplished by commanding execution of certain programmed sequences; thus little flexibility was allowed in conduct of a mission. The Lunar Orbiter design included provisions for changing the mission and inserting real-time commands to increase the accuracy and versatility of mission photography.

Nearside Photography

Most of the nearside camera operations required to satisfy film-set and Bimat dryout constraints were used to provide a preliminary assessment of potential target areas for Mission B, to obtain photographs of scientific value, or to supplement photography of some Mission I sites. The spacecraft was in Sun-Canopus orientation or pitched off Sunline; therefore, the camera axis did not coincide with the vehicle nadir, and the photographs are to some extent oblique. The amount of obliqueness is a function of spacecraft position in its orbit at the time of exposure and its attitude. Coordinates of the corners of each photograph, data defining the spacecraft attitude, the illumination, and other photographic parameters will be found in the tabulation of photo data, Section 2.3.

In most cases, a particular feature, location, or illumination condition was selected prior to camera operation. The time constraint was flexible enough to permit variation of position in the orbit for the exposure. This flexibility allowed the proper true anomaly and time of exposure to be computed for each operation to obtain a photograph of the selected area. Where the spacecraft was not in a particular area of special interest for a constraint operation, the exposure time was selected to occur at or near perilune. Preliminary photographs of potential Mission B sites were given first priority. However, passage of the spacecraft over these locations did not always occur when the film-set operations were scheduled. Photographs at or near

seven of the 11 proposed Mission B sites were obtained. Although scheduling of the constraint operations was predetermined in mission planning, the photography of unplanned specific targets required computation and spacecraft control essentially in real time since each target presented a unique problem.

Farside Photography

Photography of the Moon's farside was discussed during mission planning and was considered to be desirable from the standpoint of scientific interest and of value to the Apollo mission for information on possible landmarks. However, the coverage was not planned for the mission because of the increased hazard of additional maneuver sequences and the anticipated problems of guidance and control.

Based on the excellent operation and control of the spacecraft at Site I-0, it was apparent that unplanned operations were feasible in real time. The decision to attempt farside photography using some of the film budgeted for the constraint camera operations was made. In one case, a series of camera operations for tests associated with malfunction of the focal-plane shutter was used for farside photography. Eleven frames of the farside were exposed, eight of which were taken while the spacecraft was in the first ellipse. In all cases, these photographs required reorientation of the camera axis which pointed away from the Moon while in cruise mode (Sun-Canopus orientation) over the farside. Reorientation was accomplished by a roll maneuver of approximately 180 degrees but without a change in pitch or yaw. This photography occurred during Earth occultation; thus, the necessary commands were placed in memory for execution on the basis of programmed spacecraft times.

The nature of the orbit resulted in all farside photographs being taken from relatively high altitudes. The resulting extended coverage, particularly by the 80-mm lens, spanned a wide range of surface illumination. The illumination and average slope due to curvature of the Moon was expected to result in a brightness range possibly exceeding the latitude capabilities of the system. Therefore, a shutter speed of 0.02 second was selected as a logical compromise for all farside photographs.

Most farside photographs were exposed during tests made to diagnose the malfunction of the focal-plane shutter. All moderate resolution and seven high-resolution photos were of high quality; they provided information of outstanding value. Over three million square kilometers of the farside was photographed. Because of the high altitude, approximately 80% of the farside photography is overlapping coverage.

Earth Photos

These paragraphs describe the nonstandard photos of the combined Earth and Moon's limb that were taken in Orbits 16 and 27 of the second ellipse during Mission I. Included is a summary of the evolution and execution of these photos as well as technical data relating to the designed photos.

Origin of Photos

The initial idea of taking a photo of Earth from lunar orbit probably dated back at least as far as the proposal

stage. Discussion of the idea of taking such a photo with and without the inclusion of the Moon's limb had occurred within the flight operation team during the 6 to 12 months before the mission. Such discussions were of a preliminary nature for there was no direction to include such a photo in the mission. During the mission, however, the first serious thought of taking such a photo was expressed by NASA personnel on Day 234 at about 05:00 GMT. This discussion convinced the mission director that FPAC had the procedures and software available to design this photo mission. Formal direction to proceed with the design of this photo for Orbit 16 was given, and the design was completed.

After the Orbit 16 photo was taken, FPAC was informed that the spacecraft might have "set" (with respect to Earth) about 1 minute earlier than the "set" time used for design. If this were true, the Moon's limb would have occulted most of the Earth, and the resulting photo would not have included the illuminated portion of the Earth. Because of this uncertainty, the FPAC team suggested that one more such photo be taken, the new photo to be designed with greater spacing from Earth to Moon limb. The mission director provided formal direction to design the photo for the film-set frame on Orbit 27.

Orbit 16 Photo (Frame 102)

The first design of this photograph was completed using a three-axis attitude maneuver. The commands were:

Photo time:	Day 235 16356.3 GMT
HRoll:	6.97 degrees
Yaw:	14.73 degrees
Pitch:	-165.77 degrees

A constraint—new to FPAG—was reported. The photo sub system was not designed to operate properly due to a voltage level constraint if the solar panel orientation exceeded 45 degrees from the Sunline. (On the basis of later information, it is not known how far the panels can be from the Sun for one frame. Thus, single-frame photos may, in the future, not be limited by this constraint.) A two-axis maneuver that did not violate this constraint was computed and the photo time was adjusted based on improved tracking data. The final commands were:

Photo time:	Day 235 163623.0 GMT
HRoll:	188.69 degrees
Pitch:	25.56 degrees

The equivalent first roll maneuver (360 degrees-188.69 degrees=171.31 degrees) caused the Canopus tracker to intercept the bright Moon while the 188.69-degree roll resulted in the low-gain antenna passing through the edge of a null region. The latter maneuver was adopted as being less risky.

The choice of photo time is based on the predicted DSS-61 Earthset time of 16:37:38.0.

It is expected that the actual photo coverage will be affected more by errors in the photo time than attitude pointing errors. Generally, attitude errors are about 0.1 degree,

TIME OF PHOTO: 23 AUGUST, 1966 (DAY 235)

16:36:23.0 (GMT) OR 09:36:23.0 (PDT)

STATE VECTOR, SELENOCENTRIC MEAN 1950.0 COORDINATES

$X = -2498.7714 \text{ km,}$	$Y = -1128.8056 \text{ km,}$	$Z = -1046.2494 \text{ km}$
$\dot{X} = 0.21174442 \text{ km/sec,}$	$\dot{Y} = 1.1521353 \text{ km/sec,}$	$\dot{Z} = -0.38538441 \text{ km/sec}$

REFERENCE TRAJECTORY RUN : TRJL, 8-23-66, TAPE 8533, ITEM 2424

SPACECRAFT ORBIT, SELENOGRAPHIC COORDINATES

PERILUNE ALTITUDE	51.8	km
APOLUNE ALTITUDE	1858.7	km
INCLINATION TO LUNAR EQUATOR	11.97	DEGREES
ARGUMENT OF PERILUNE	183.4	DEGREES
LONGITUDE OF ASCENDING NODE	203.0	DEGREES
TIME OF LAST PERILUNE	23 AUG., 1966	15 : 45 : 52.6 GMT

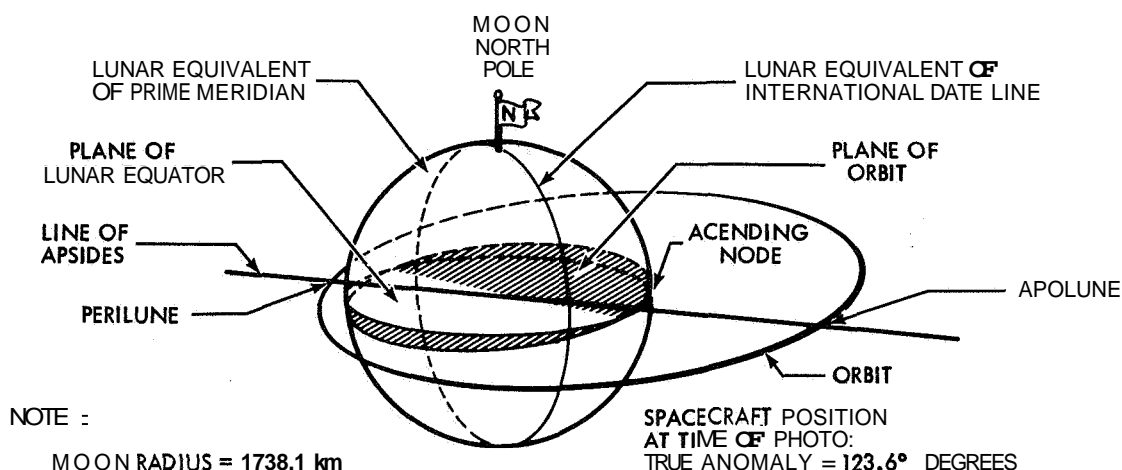


Figure 2.5-1: Design of Earth-Moon Photograph: Orbit 16

while trajectory timing errors are about 10.0 seconds. Since the Moon is entering the camera field of view at about 0.023 deg/sec, Moon inaccuracy of about 0.23 degree results. Technical data for the photo design is summarized in Figures 2.5-1 through 2.5-8.

Orbit 26 Photo (Frame 117)

On Day 236 at 0900, a direction to design the second Earth photo for Orbit 27 was given. This design was completed and commands released at 1430

Photo Time: Day 237 07150.0 GMT

HRoll: -173.00 degrees

Pitch: 45.40 degrees

A more conservative approach was adopted for this photo by spacing the Earth disk and Moon limb 1.0 degree apart. Thus, large timing errors—as indicated by the apparent early DSS-61 “set” of the Orbit 16 photo—would not cause occultation of any part of the Earth, but if these errors did not really exist, less of the Moon would be seen.

The predicted Earthsets in this orbit were:

DSS 41: Day 237 07:17:58.0 GMT

DSS 12: Day 237 07:16:29.0 GMT

See Figures 2.5-1 through -8 for detail summary of this photo.

EARTH - MOON GEOMETRY

	IN EARTH FIXED (GEOGRAPHIC) COORDINATES	IN MOON FIXED (SELENOGRAPHIC) COORDINATES
SPACECRAFT LATITUDE	-22.97 DEGREES	-9.54 DEGREES
SPACECRAFT LONGITUDE	24.02 DEGREES	150.52 DEGREES
SPACECRAFT ALTITUDE	379,720. KM	1196.7 KM
SUN LATITUDE	11.52 DEGREES	1.50 DEGREES
SUN LONGITUDE	291.35 DEGREES	90.34 DEGREES
EARTH LATITUDE		1.96 DEGREES
EARTH LONGITUDE		7.36 DEGREES
MOON LATITUDE	-22.91 DEGREES	
MOON LONGITUDE	24.06 DEGREES	

OTHER IMPORTANT PARAMETERS ARE

- AS SEEN BY SPACECRAFT:

ANGULAR SEMIDIAMETER OF MOON: 36.31 DEGREES

ANGULAR SEMIDIAMETER OF EARTH: 0.947 DEGREE

ANGLE FROM CENTER OF EARTH TO CENTER OF MOON: 37.13 DEGREES

ANGLE FROM CENTER OF EARTH TO NEAR LIMB OF MOON: 0.82 DEGREE

- ON THE EARTH

ANGLE FROM SUBSPACECRAFT POINT TO TERMINATOR: 6.7 DEGREES

ANGLE FROM TERMINATOR TO POLE: 11.5 DEGREES

ROUGH SKETCH OF EARTH
AT TIME OF PHOTO

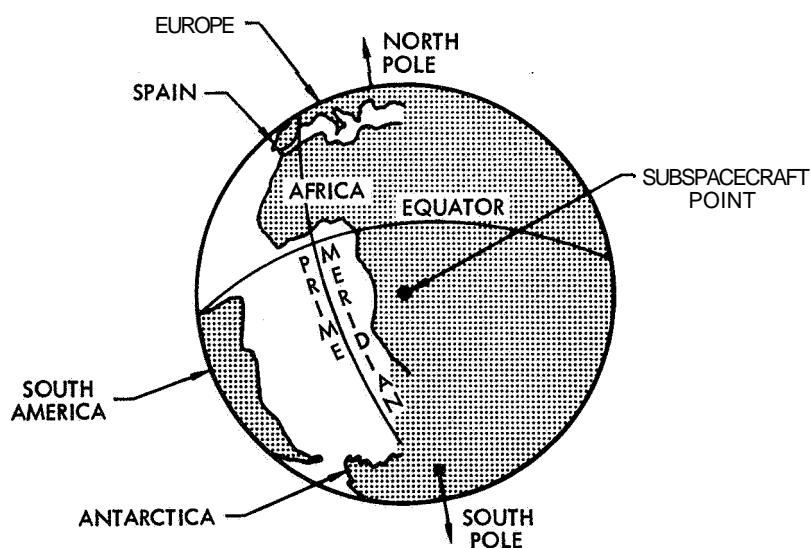


Figure 2.5-2: Earth-Moon Geometry

SKETCH OF EARTH-MOON-SPACECRAFT
GEOMETRY AT TIME OF PHOTOGRAPH

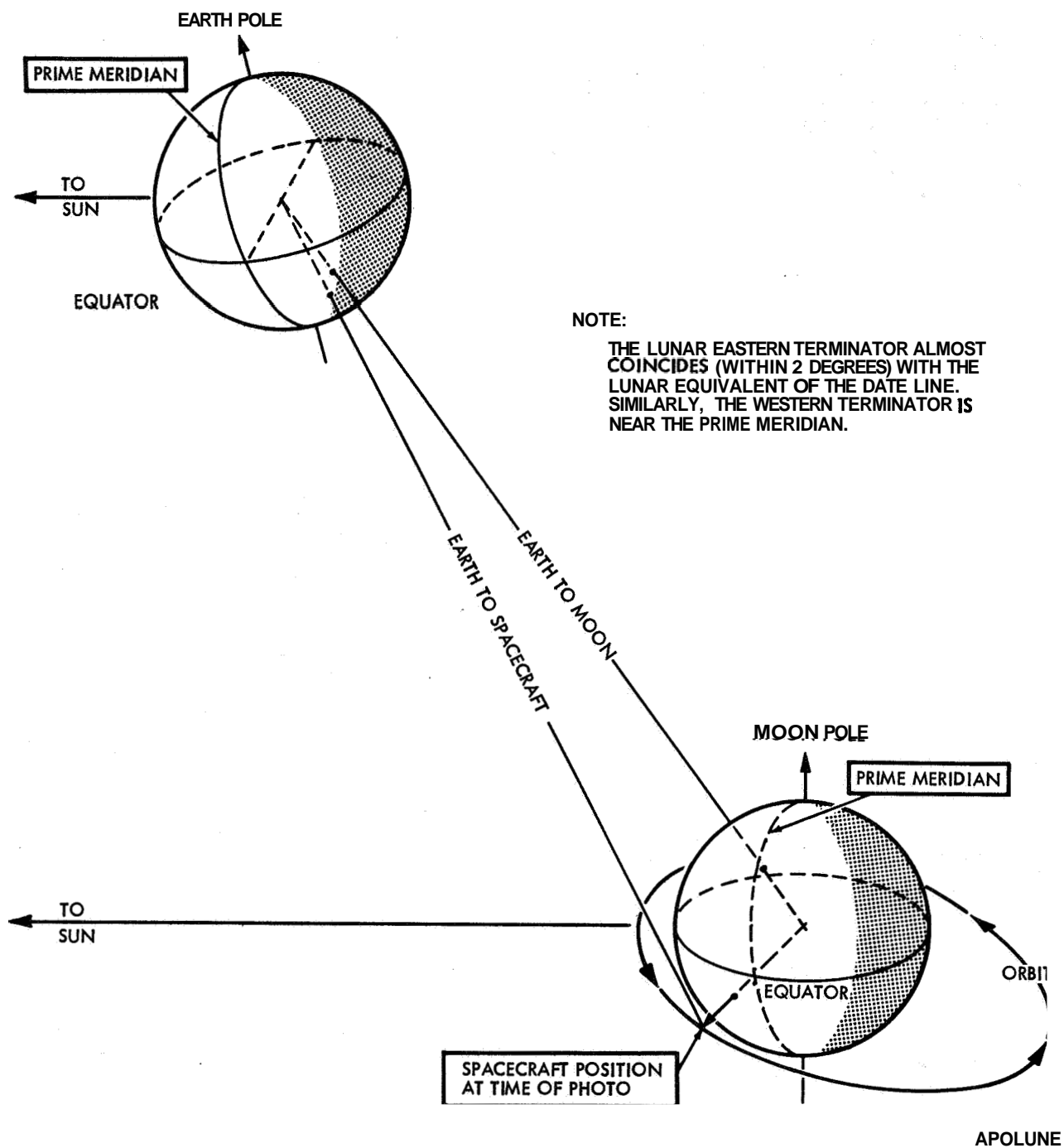
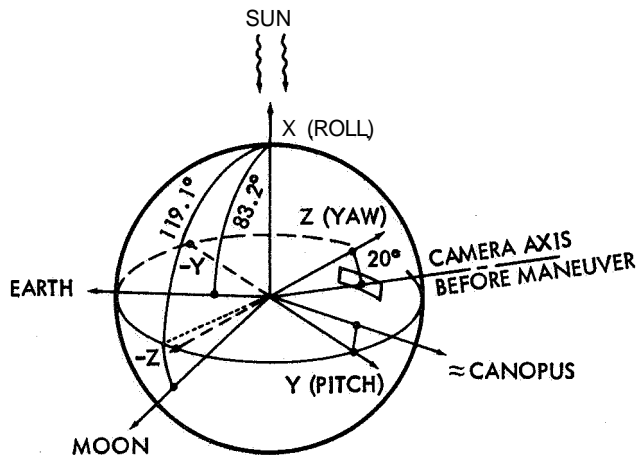


Figure 2.53 Earth-Moon-Spacecraft Geometry at Time of Photograph

CAMERA AXIS POSITIONING

IN SPACECRAFT IRU COORDINATES (PRIOR TO ANY MANEUVERS)

EARTH CONE ANGLE: 83.2 DEGREES
 EARTH CLOCK ANGLE: 278.6 DEGREES
 MOON CONE ANGLE: 119.1 DEGREES
 MOON CLOCK ANGLE: 268.7 DEGREES



IN THIS FIGURE AN APPROXIMATE TWO-AXIS MANEUVER IS EASILY VISUALIZED:

+ROLL BY \approx EARTH CLOCK -90 DEGREES
 \approx 188.6 DEGREES

+PITCH BY \approx 20° + (90° - EARTH CONE)
 \approx 26.8 DEGREES

HOWEVER, POSITIONING AIM POINT 1.0 DEGREE FROM CENTER OF EARTH, AND COMPUTING MANEUVERS IN FAIL PROGRAM, GIVES THE FINAL ATTITUDE COMMANDS:

H-ROLL: 188.7 DEGREES
 PITCH: 25.6 DEGREES

NOTE: MOON LIMB EXTENDS ABOUT 0.16 DEGREE OVER AIM POINT. HENCE, THIS MUCH OF EARTH DISK (DARK SIDE) IS OCCULTED BY MOON.

FIELD OF VIEW: HIGH-RESOLUTION CAMERA

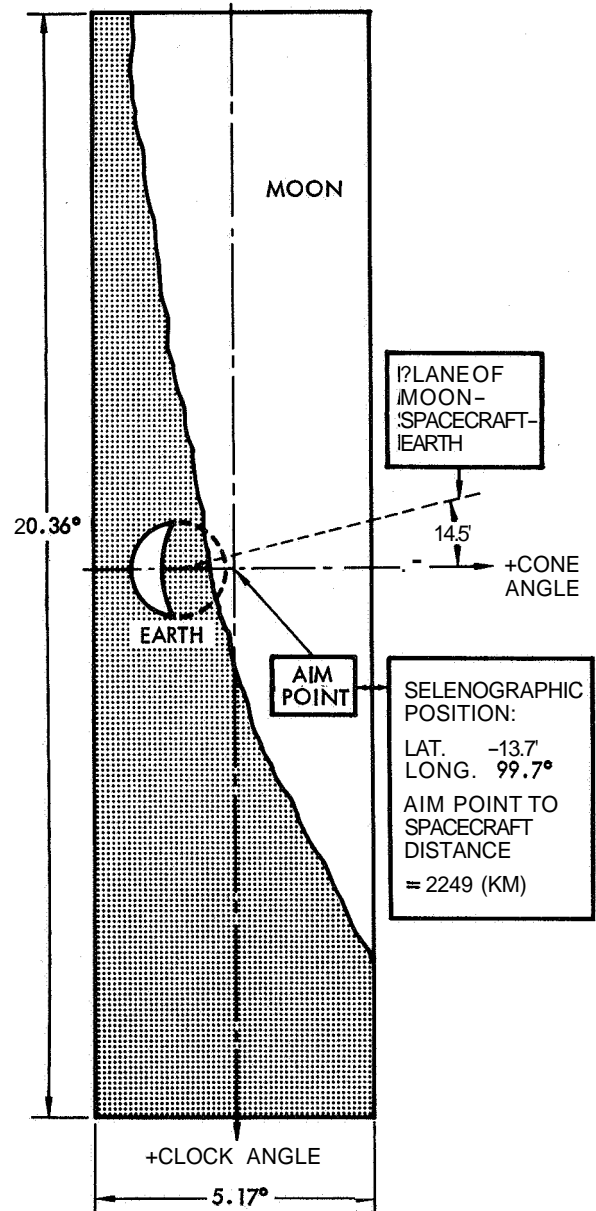


Figure 2.54 Camera Axis Positioning

SPACECRAFT MANEUVERS

H-ROLL: 188.7 DEGREES

PITCH: 25.6 DEGREES

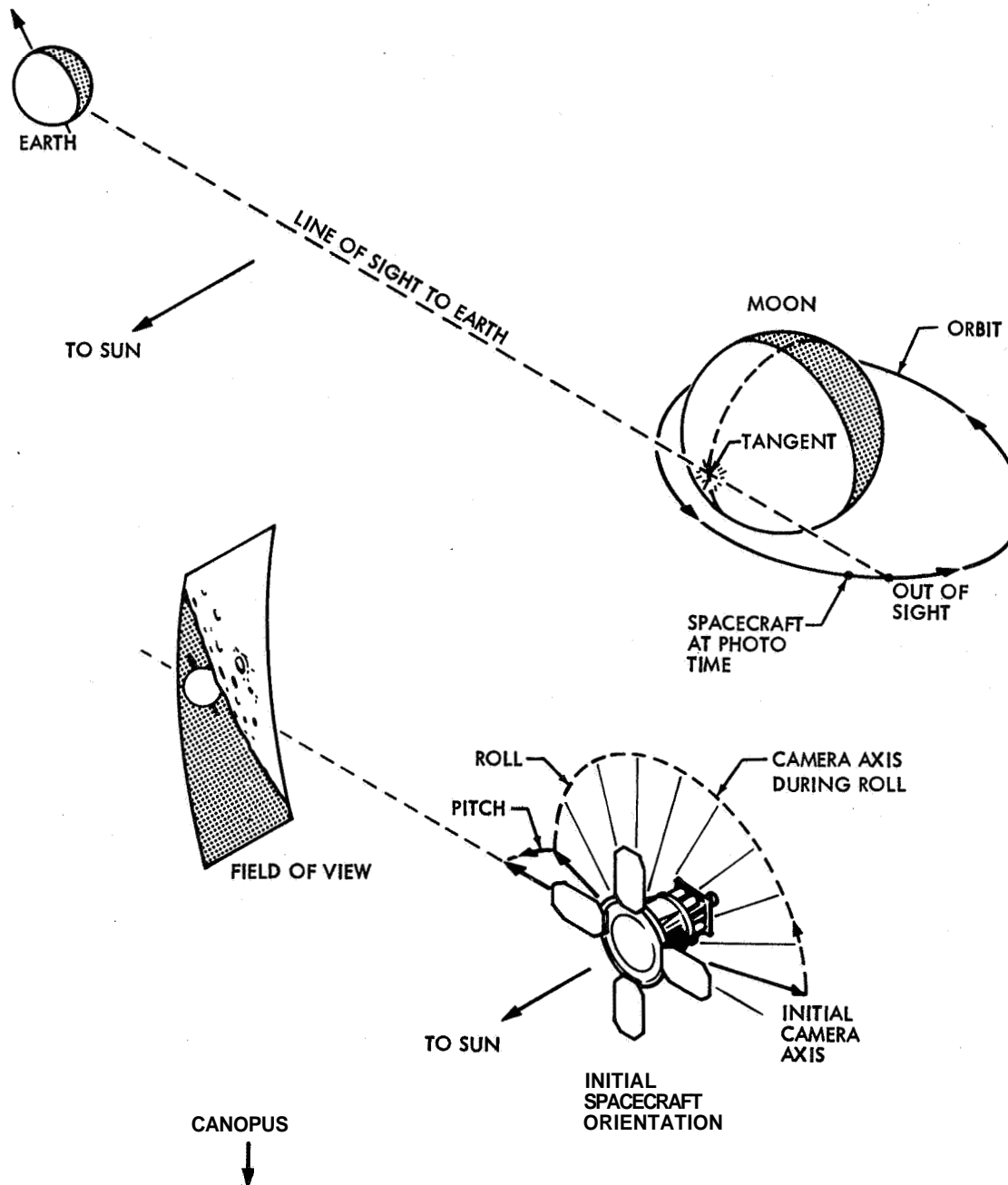


Figure 2.5-5: Spacecraft Maneuvers

Time of Photo: 25 August 1966 (Day 237)
07:15:00 GMT or 00:15:00 PDT

State Vector, Solenocentric Mean 1950.0 Coordinates

$\dot{X} = -1939.3018$ $\dot{Y} = -2332.1688$ $\dot{Z} = -1353.4807$
 $\dot{X} = 0.64839479$ $\dot{Y} = -0.83005038$ $\dot{Z} = -0.14950476$

Reference Trajectory Run: TRJL 8-23-66, Tape 8893, Item 2554

Spacecraft Orbit, Solenographic Coordinates

Perilune altitude 49.1 km
Apolune altitude 1861.1 km
Inclination to Lunar equator 12.08 degrees
Argument of perilune 185.7 degrees
Longitude of ascending node 180.2 degrees
Time of last perilune 25 August 1966, 06:05:18.8 GMT

Earth-Moon Geometry

	In Earth Fixed (Geographic) Coordinates	In Moon Fixed (Solenographic) Coordinator
Spacecraft latitude	-26.53 degrees	-5.57 degrees
Spacecraft longitude	185.29 degrees	153.34 degrees
Spacecraft altitude	388,040.0 km	1583.4 km
Sun latitude	10.97 degrees	1.51 degrees
Sun longitude	71.59 degrees	70.69 degrees
Earth latitude	---	4.06 degrees
Earth longitude	---	6.80 degrees
Moon latitude	-26.51 degrees	---
Moon longitude	185.33 degrees	---

Other important parameters are:

- As seen by spacecraft ...
- Angular semidiameter of Moon: 31.55 degrees
- Angular semidiameter of Earth: 0.927 degrees
- Angle from center of Earth to center of Moon: 33.11 deg.
- Angle from center of Earth to near limb of Moon: 1.56 deg.

Figure 2.5-6 Design of Earth-Moon Photograph Orbit 27

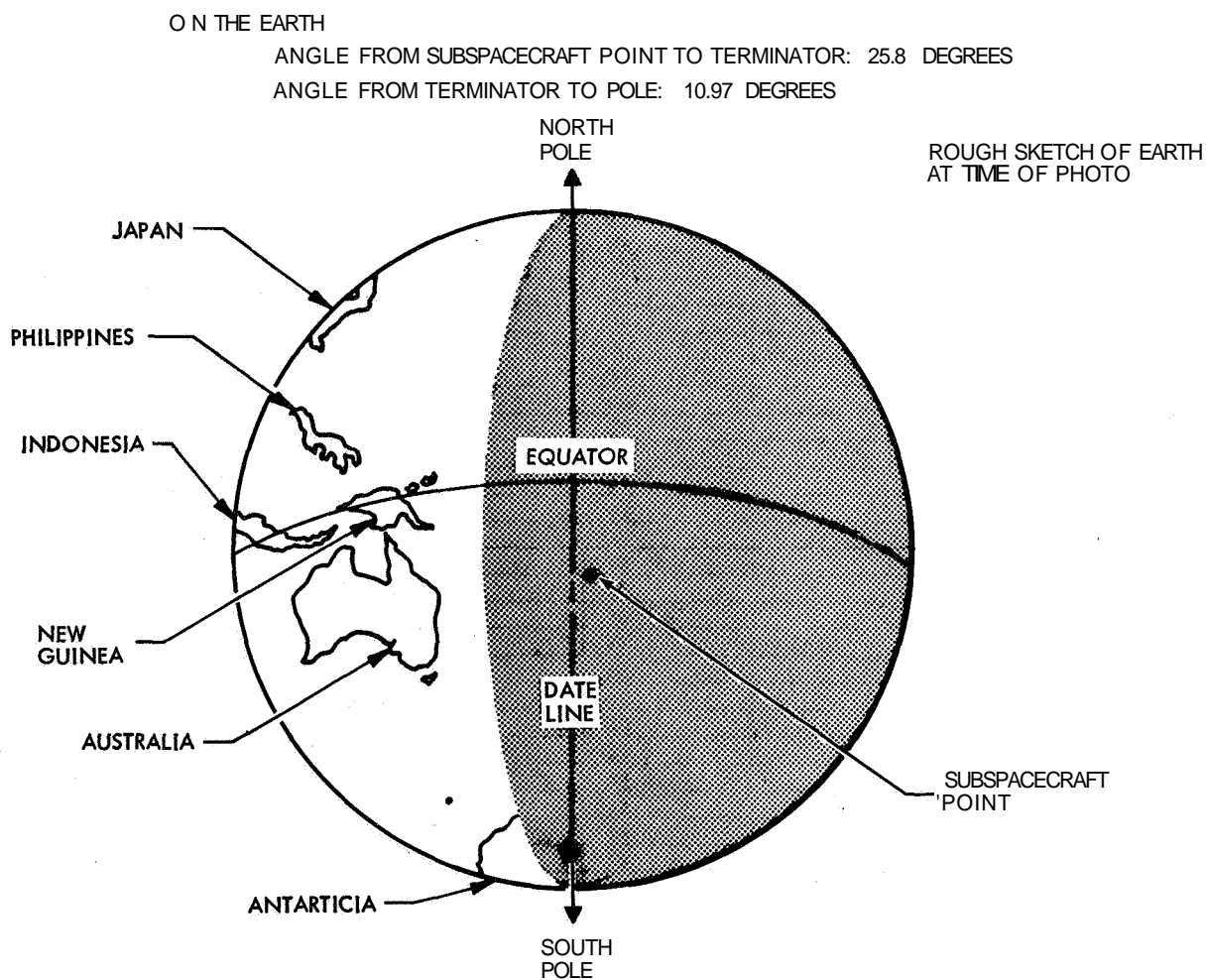
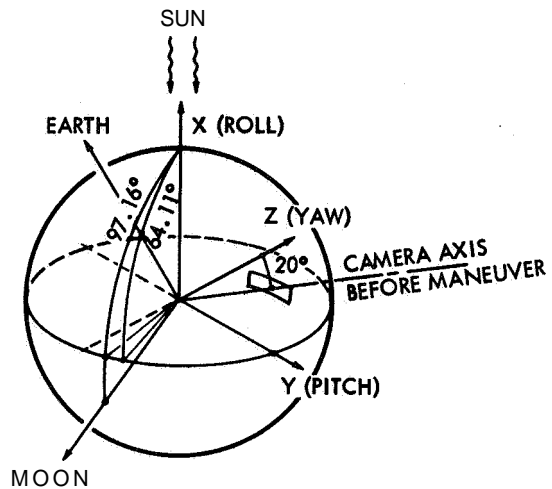


Figure 2.5-7: Representation of Earth in Orbit 27 Photograph

CAMERA AXIS POSITIONING

IN SPACECRAFT IRU COORDINATES (PRIOR TO ANY MANEUVERS)

EARTH CONE ANGLE:	64.11	DEGREES
EARTH CLOCK ANGLE:	277.01	DEGREES
MOON CONE ANGLE:	97.16	DEGREES
MOON CLOCK ANGLE:	275.00	DEGREES



IN THIS FIGURE AN APPROXIMATE TWO-AXIS MANEUVER IS EASILY VISUALIZED:

- ① +ROLL BY \approx EARTH CLOCK -90.00 DEGREES
 $= 187.00$ DEGREES
- ② +PITCH BY $\sim 20^\circ + (90^\circ - \text{EARTH CONE})$
 $= 46.00$ DEGREES

HOWEVER, POSITIONING AIM POINT 1.0! DEGREE FROM CENTER OF EARTH, AND COMPUTING MANEUVERS IN FAIL GIVES THE FINAL ATTITUDE COMMANDS:

- ① H-ROLL: -173.00 DEGREES
- ② PITCH: 45.40 DEGREES

FIELD OF VIEW: HIGH-RESOLUTION CAMERA

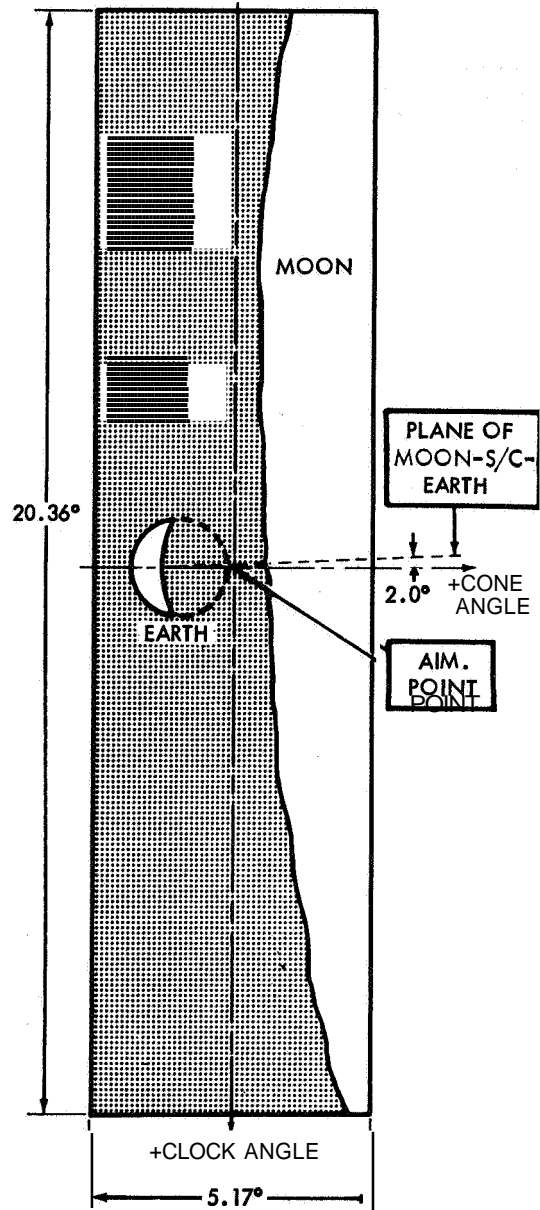


Figure 2.58: Camera Axis Positioning

2.6.1.3 EVALUATION OF NASA TARGET FILMS

The special NASA target films, which consisted of the reassembly negative and three following generations of reproduction, were evaluated. The quality parameters that were measured were those of resolution and tone reproduction.

The designation used for the generations of reproduction are as follows:

IN reassembled negative copy of original GRE film
 2F? transparent positive of IN
 3N. negative copy of 2P
 4P: paper print of 3N

Resolution readings were taken using the edge data bar charts. These bar charts provided resolution values in the electrical scan direction (bars perpendicular to electrical scan direction), mechanical scan direction (perpendicular to mechanical scan direction), and diagonal bars at 45 degrees to the other two patterns. Resolution readings were made on 36 sets of bars for each generation of film. The data from these readings are plotted in Figure 2.5-9. The results are typical of other test data read out through the Lunar Orbiter system, with the resolution values for the diagonal bars being the highest and those for the mechanical bars being the lowest. The steps in the resolution bar patterns are rather coarse. The resolution steps in terms of spacecraft film scale are 160, 126, 100, 80, 63, 50, 40, and 32 lines per millimeter. As the data shows, only about a 7% loss in resolution takes place in going from IN to the 3N generation. Approximately another 15% is lost in resolution when going to the paper prints. This

is not considered a problem in line with the original philosophy of using the paper prints only for gross screening and file records and using the transpositives for detail analysis.

Figure 2.59 indicates that the resolution loss between the first and third-generation negatives is 7%. Table 2.5-3 indicates that the standard deviation is slightly over nine resolution units for IN and 3N. Considering a Sigma value as being typical for engineering accuracies, this would compare favorably with the spacing of the resolution elements. A Sigma value of 30 lines per millimeter is typically a reasonable amount for a resolution chart interval of 20 lines per millimeter. This means that the 7% loss of resolution is well within the experimental error capability of this experiment. It is reasonable to conclude that the loss of resolution is less than the 7%. It is most probable that the experiment would give a 12% loss of resolution as indicated by the standard deviation.

The MTF for the film shows a very slight dropoff at 10 lines per millimeter, which corresponds roughly with 80 lines per millimeter on the spacecraft film. The small amount of deviation as shown in the IN and 3N columns could quite possibly be due to slight variations in film characteristics. This can be concluded because a loss of correlation from reading to reading is evidenced by an IN reading of 80 and a 3N reading of 100, which is theoretically impossible. The conclusion from the test should be that the degradation of the 3N negative is negligible. Further, if we wish to establish an exact degradation number, it would require extensive experimentation using resolution charts which are separated by only a few lines per millimeter in the region of 100 to 60 lines per millimeter. This second action does not seem warranted in light of the small loss in resolution.

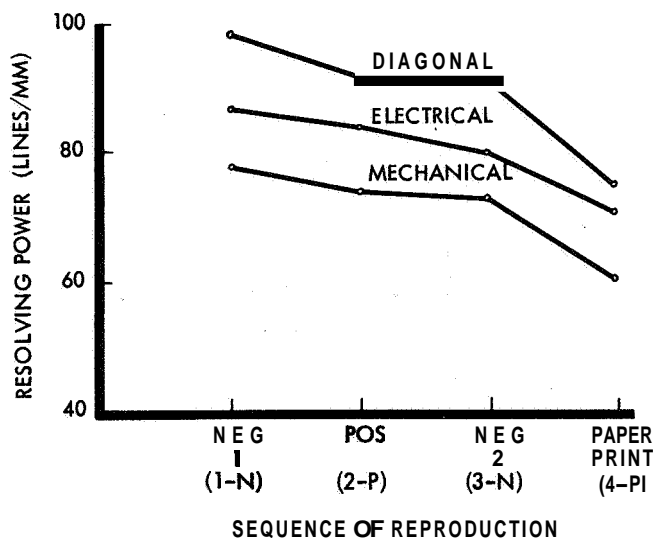


Figure 2.59 Reduction of Resolving Power Due to Multiple Reproduction

IN	3N
12 = 100 LINES PER MM	5 = 63 LINES PER MM
24 = 80 LINES PER MM	27 = 80 LINES PER MM
N = 36	4 = 100 LINES PER MM
$\bar{X} = 86.7$ LINES PER MM	N = 36
$\delta = 9.55$ LINES PER MM	$\bar{X} = 79.9$ LINES PER MM
	$\delta = 9.34$ LINES PER MM

WHERE	$\bar{X} = \frac{1}{N} \sum x_i$
AND	$\delta = \left[\frac{1}{N-1} \sum (x_i - \bar{X})^2 \right]^{1/2}$

Table 2.5-3: Computation of Standard Deviation of Resolution Measurements

The tone reproduction analysis was made using the nine step gray scale in the edge data. An Ansco Model 4 scanning microdensitometer was used to scan 12 gray scales from each film generation. A sensitometric strip exposed on each generation was scanned to calibrate the microdensitometer readout in units of ASA diffuse density. This data is plotted in Figure 2.5-10. As can be seen from this plot, the tone reproduction was maintained with good fidelity. Figures 2.5-11 and 2.5-12 illustrate the linear density transfer characteristic from 1-N to 3-N to 2-P.

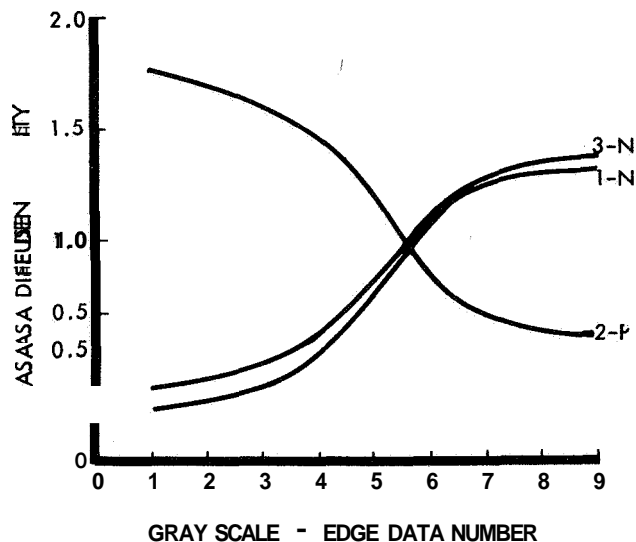


Figure 2.5-10: Tone Reproduction

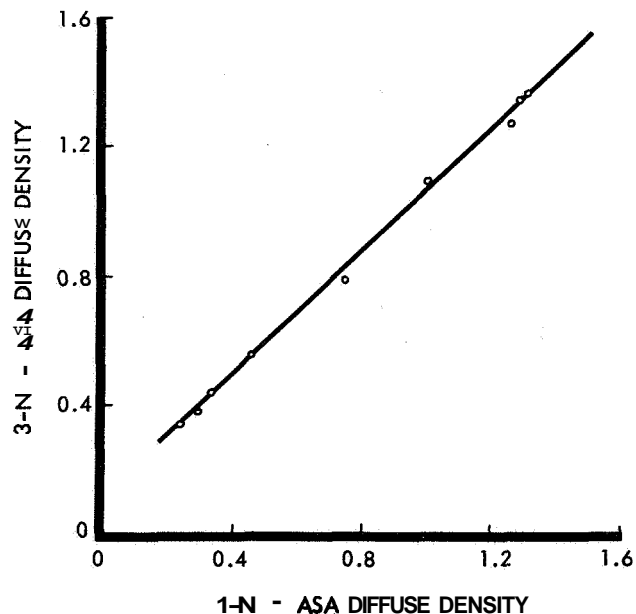


Figure 2.5-11: 1-N to 3-N Tone Reproduction

2.5.2 SPACE FLIGHT OPERATION FACILITY

The Control Point at the SFOF provided the means for the flight planning of the mission. Changes in the planned photographic mission dictated by particular circumstances were executed in the direction of the mission director and the SFOD.

Throughout the mission, prime photo objectives were of first concern to mission control decisions in the SFOF. Midcourse correction, injection into the first ellipse, and transfer to the second ellipse were each evaluated to ensure placing the spacecraft in the proper position for photography. Each of these maneuvers was executed and nominal conditions defined for the mission were obtained. Although the second ellipse was close to nominal, a transfer to a third ellipse was executed to provide a higher V/H ratio in an attempt to improve photography by reducing the photographic altitude. This decision was based partly on the precision and reliability that had been demonstrated in previous maneuvers and partly on the growing knowledge of the Moon's effects on the spacecraft orbit.

In addition, evaluation of photo subsystem performance indicated the desirability of other deviations from mission design to optimize spacecraft performance and photography. These deviations are considered in the following paragraphs.

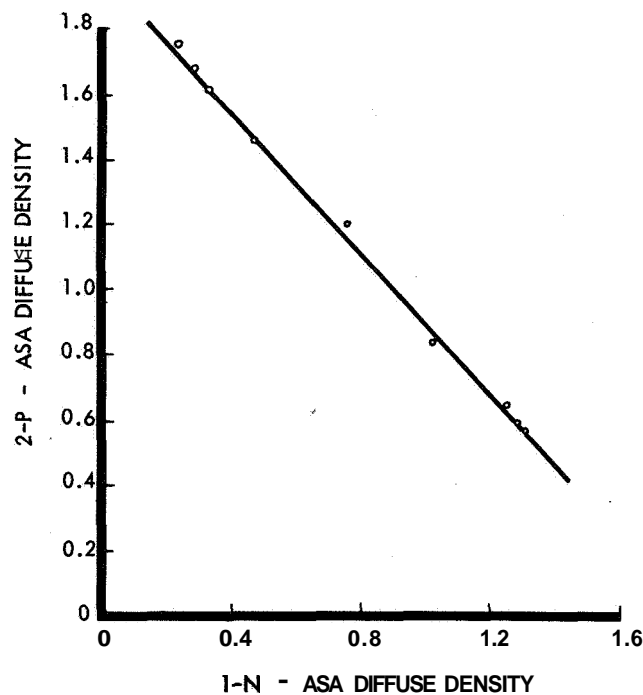


Figure 2.5-12: 1-N to 2-P Reproduction

2.5.2.1 SITE I-0

After photography of Site I-0, priority readout of selected photographs indicated that a problem existed with the high-resolution camera. The focal-plane shutter appeared to be operating at an incorrect time. The V/H sensor apparently was triggering the shutter prematurely. It was later established to be the film-damp and vacuum-draw motor. Refer to Section 2.7. The first high-resolution picture is a double exposure, one of which was taken earlier than intended. Several tests were proposed in an attempt to substantiate the hypotheses proposed to explain the difficulties. One test required taking 10 additional pictures for the purpose of advancing Frame 26 (the first picture of the four-frame sequence of Site I-0) into position for readout to determine if that frame might also be a double exposure. No double exposure was found upon readout of that frame. Additional frames that were taken to provide the readout were used for two diagnostic tests. One test involved different cycling rates, with and without the V/H sensor turned on. A second experiment to determine if the V/H sensor was causing the shutter to trip was accomplished, as discussed in Paragraph 2.2.1.3.

In accordance with plans previously developed, mission revision had been expected if the V/H sensor was degrading the high-resolution photographs. The revision dictated that the spacecraft remain in the initial ellipse and continue to take pictures from the higher altitude which would produce photographs with approximately the same resolution but with greater coverage. Since the image smear would be about equal, the same ground resolution could be obtained from the high altitude without the V/H sensor, and a large lunar surface area could be covered. However, it was theorized at the time that proper V/H and high-resolution camera operation might be obtained with the lower altitude and a higher V/H ratio in the second ellipse. It was believed that the problem would be corrected if the V/H ratio were higher than 37 milliradians per second. Therefore, it was decided to make the transfer to the lower altitude for mission photo sites as originally planned.

Prior to transfer, a readout of one of the early frames was reported by the GRE operator to have evidence of Bimat stick. Although the film handling constraint that relates to Bimat stick had been exceeded during the mission, there was some concern that the constraint possibly was too liberal. This constraint, stating that the Bimat must be moved to place fresh Bimat on the processor drum at least every 15 hours, was being observed by processing at least two frames every fourth orbit. This placed completely fresh Bimat on the processor drum every 14 hours. Because of the report from the GRE operator, the decision was made, one orbit before transfer, to use the additional eight frames required for processing every other orbit, or every 7 hours. The decision to take these additional frames came after computations for this time period were completed and commands were in the spacecraft. Advancement of the film at this time could not be used for photography of the lunar surface without jeopardizing the remainder of the program memory.

Thus, the first two of these additional photographs were not exposed. The camera thermal door was not opened.

2.5.2.2 SITES I-1 AND I-2

Priority readout of Site I-1 frames, after photography of Sites I-1 and I-2, indicated that the focal-plane shutter

was still operating erratically and further diagnosis was desired. The Eastman Kodak representative referred this problem to Rochester and tests of another photo subsystem were made there. These tests indicated that the V/H sensor could cause the focal-plane shutter to trip prematurely. Eastman Kodak recommended that the V/H ratio should be increased to at least 37.5 milliradians per second. It was anticipated that Sites I-4 and I-5 would obtain such a V/H ratio; however, after having taken Site I-3, it appeared that spacecraft altitude was greater than had been anticipated. After confirming this from Site I-4 priority readout, a transfer to the third ellipse was planned for execution immediately after photography of Site I-5. The third ellipse was planned to obtain V/H ratios of 37.5 milliradians per second or greater. A V/H ratio of 50 milliradians per second was considered the maximum rate permitted.

2.5.2.3 SITE I-5

Priority readout of a Site I-3 frame confirmed that the V/H sensor was still causing the focal-plane shutter to operate at incorrect times. Eastman Kodak confirmed that proper operation might be obtained with a higher V/H ratio. The Site I-6 altitude was anticipated to be such as to produce an "acceptable" V/H ratio after transfer to the third ellipse.

2.5.2.4 SITE I-6

After photography of Site I-6, telemetry data indicated that the V/H ratio was not as high as had been anticipated and the "magic number" of 37.5 milliradians per second had not been obtained. On the basis of that telemetry data, photography of Site I-7 was rescheduled to occur one orbit earlier than had been planned for the site. Photography on the earlier orbit would be closer to perilune, therefore a higher V/H ratio would be anticipated. If the camera were to operate correctly at all, the lower altitude should provide good high-resolution coverage. The original coordinates of Site I-7 would not, however, be covered by the redirected photography.

2.5.2.5 SITE I-7

Prior to redirection, the trajectory computations indicated that photography of Site I-7 would have to occur on Orbit 49. The mission design planned Site I-7 photography on Orbit 47. Film-set and Bimat dryout constraints required using an additional four frames of film on Orbits 47 and 48 to be assured of having two frames to process each orbit, and at least two frames in the camera storage loop at all times so that Bimat cut could be commanded and executed if necessary. These additional four frames were commanded and the operations executed through the programmer. After the decision was made to reschedule the photography of Site I-7 from Orbit 49 to Orbit 48, it was not necessary to take two of the four frames. Again because the program to take four additional frames was already loaded into the spacecraft, it would be dangerous to try to change that program. Therefore, it was decided to continue with the plan as programmed (i.e., take four frames on Orbit 47, process two frames on Orbit 47, and photograph Site I-7 on Orbit 48).

2.5.2.6 SITES I-4, I-6, AND I-8

There was an insufficient number of frames available to complete the mission as planned because of using extra

frames in the first ellipse for photographic diagnostic purposes and those required by the operational constraints. At the direction of the mission director, photography of Sites **1-4**, **1-6**, and **1-8** were reduced from 16 to **8** frames per photo pass.

2.5.2.7 SITE I-9.2

After completion of photography, priority readout of the center three frames from each of the **two** photo passes of Site I-9.2 was directed. Surveyor would most likely occur in one of those **six** frames, and priority readout at **this** time permitted the quick evaluation of the frames that would most probably include Surveyor.

2 5 PHOTOGRAPHIC SUBSYSTEM OPERATIONAL ANALYSIS

The photo subsystem operation was analyzed on the basis of:

- 1) Evaluation of real-time telemetry during the mission;
- 2) Analysis of photography after priority and final readout.

A major photo subsystem deviation from specification cannot invariably be detected by analysis of mission telemetry.

Telemetry channels must be limited to a number consistent with communications system capabilities and requirements for an acceptable data sampling rate. This does not allow a comprehensive analysis, by telemetry, of all spacecraft operational functions during flight. Lunar Orbiter is not unique in this limitation. Because of this factor, performance telemetry did not reveal all operational malfunctions at the time of occurrence. Analysis of the photographs from priority readouts, however, showed certain problems; most important was evidence of shutter malfunction in the 610-mm camera. The major problems present within the system were:

- 1) There was a malfunction in the 610-mm-camera focal-plane shutter.
- 2) Bimat appeared to be sticking to the spacecraft film. The amount of sticking increased as the Bimat aged.
- 3) The photo subsystem temperature increased above 70°F limit due to the overall spacecraft heating problem. (This was determined from telemetry.)
- 4) There are scratches on the spacecraft film attributed to mechanical handling problems.
- 5) There are uneven processing bands on the film attributed to differential roller pressures.
- 6) There is evidence of deterioration of the OMS CRT anode during the mission life.
- 7) The V/H sensor appeared to be reading 8% low. (This was determined from telemetry.)

2.5.3.1 CAMERA SYSTEM OPERATION SUMMARY

Analysis of the photography from priority readout showed smear in three directions in the 610-mm-camera photography. The 80-mm-camera photographic quality was within specification, with the exception of a part of Site I-0 where photos were degraded by the focal-plane-shutter malfunction and of some instances of overexposure

Smear in 610-mm Camera

The three basic modes of smear apparent in the 610-mm camera are:

- 1) Smear in image-motion compensation (IMC) direction;
- 2) Smear in film-advance direction;
- 3) Smear having components of both IMC and film advance

Since the camera was not recovered, no final diagnosis of the failure can be made from equipment examination.

Extensive study of the problem by both Eastman Kodak and Boeing personnel commenced once the photo evidence showed smear. Circuit analysis plus special laboratory testing showed that the 610-mm-camera shutter control circuitry was susceptible to radio frequency interference/electromagnetic interference (RFI/EMI). It was hypothesized that the electronic control logic interpreted electronic transients (attributed to motor starting) as command pulses. Thus, the 610-mm-camera focal-plane shutter fired at incorrect times within the film handling cycle. The following incorrect shutter firing modes were observed

Shutter Operation During IMC Reset

This smear occurs parallel to the short dimension of a high-resolution frame. The platen motion for image-motion compensation is cyclic and must be reset after each exposure. Normally, the focal-plane shutter is capped (closed) during IMC reset; however, considerable evidence points to accidental shutter operation during this cycle. The fact that the IMC reset cycle contains some nonlinear motion should be considered while analyzing the smear. Typical photographic example of IMC smear alone is shown in Figures 2.2-5 and 2.2-6.

Smear During Film Advance

This smear occurs parallel to the long dimension of a high-resolution frame. Film is advanced between exposure cycles and the focal-plane shutter is normally capped during this film handling. The film-advance cycle contains many nonlinear events involving film acceleration and deceleration. Any measurement on the imagery obtained during film advance should include consideration of this fact.

Combined IMC Cycle and Film Advance Smear

Certain photo frames from the 610-mm camera show smear having both IMC and film-advance components. The direction of this smear is the vector sum of the two motions. Since nonlinear motions exist in both the IMC and film-advance cycles, the direction of smear is not fixed and can vary within a single photo frame. This smear is attributed to accidental shutter actuation at either:

- 1) The end of IMC reset cycle and the beginning of film advance;
- 2) The end of film advance and the beginning of the IMC cycle

This effect is readily seen in Frames 86 and 120.

No Smear in High-Resolution Frame

Some high-resolution frames did not contain smear. These frames were, in general:

- 1) Single constraint frames using no IMC;
- 2) The first high-resolution shot taken (Frame 5);
- 3) The photos of Earth over the lunar horizon.

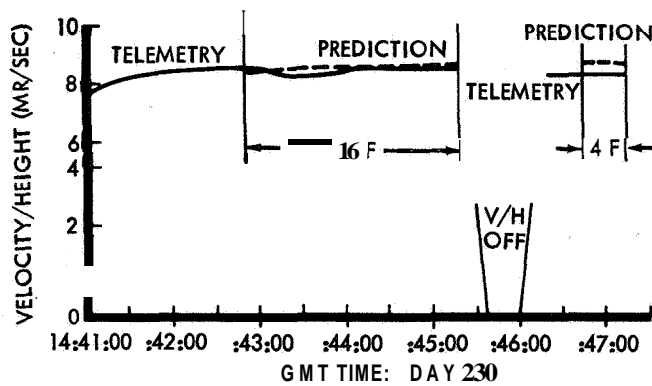


Figure 2.5-13 V/H Ratio Site I-0

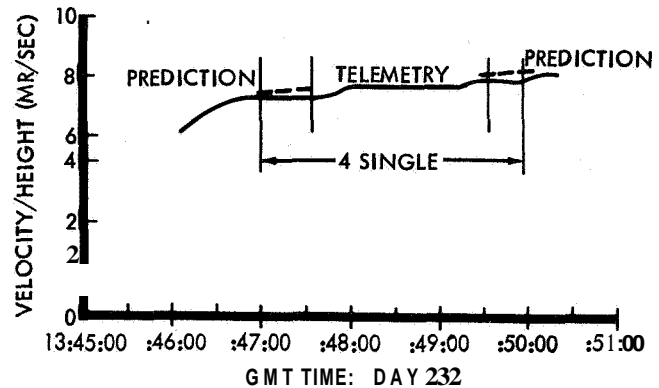


Figure 2.5-14: V/H Ratio Test Site

In all cases except Frame 5, the absence of IMC cycling indicated that the shutter may have actuated at the proper time in the IMC cycle or, in absence of IMC, improper operation of the shutter would not be detected except during film advance.

Several unusual diagnostic camera cycles were attempted once priority readout photos revealed a malfunction. Specifically:

- 1) The first test was a "V/H On" sequence involving four frames (31, 32, 33, and 34) with individual programmed camera-on times (i.e., a series of single photos with IMC).

Frame	Camera-On Times (Seconds)
31	
32	33.9
33	118.6
34	25.2

- 2) The second test was effected without V/H or IMC.

Frame	Camera-On Times (Seconds)
35	
36	13.2
37	115.7
38	13.2
39	218.0
40	8.4

The purpose of these tests was to gather photos at different cycling rates with and without IMC. It was hoped to determine and measure **any** minimum time between non-interference of the IMC and the focal-plane shutter. The test was inconclusive; however, photos of the farside of the Moon were a system first.

- 3) A more conclusive test was effected in Frame 104. This exposure was run to study the electronic interference concept as the focal-plane shutter trouble source. The test consisted of:

- a) Camera door open
 - b) V/H On
 - c) V/H Off
 - d) Camera door closed
 - e) Camera on for one frame
- IMC functioning

The frame was exposed in the 610-mm camera and blank in the 80-mm camera. This indicates that the focal-plane shutter was fired before the Camera-On command was given. The 80-mm camera shutter operated at the specified command after the door was closed. The event sequence seems to support the EMI/RFI theory since the focal-plane shutter was fired during a time when RFI/EMI could be present in the camera logic circuitry.

2.5.3.2 V/H SENSOR PERFORMANCE

The V/H sensor telemetry output has been compared to the best available predicted values. The discrepancies are negligible in the initial orbit but average -8.1% (relative to the predicted values) at second- and third-ellipse altitudes. Known sources of error are insufficient to account for the discrepancies. Therefore, either the V/H sensor was operating improperly or the prediction was in error. Because the moderate-resolution photographs were not affected by this quantity of smear, photographic verification is not possible.

Data

V/H ratio, as indicated by the PR01 telemetry channel, was plotted for each period of sensor operation (Figures 2.5-13 to -24). A faired curve was drawn through all data points to allow interpolation to actual photo times. In most cases, an extrapolation to the V/H off time (last frame) was required. V/H ratio is plotted against GMT, corrected to the actual spacecraft times at which the ratio was sampled. Correction during the photo mission was

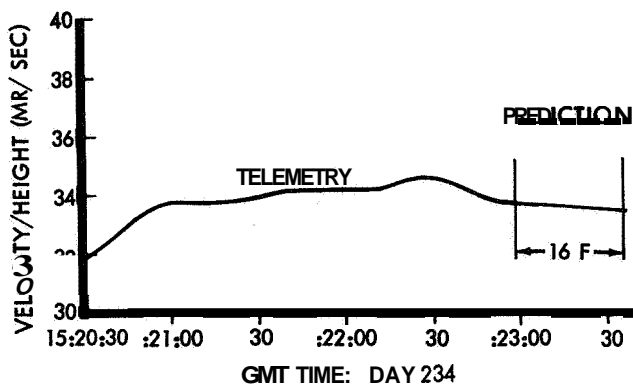


Figure 2.515: V/H Ratio Site I-1

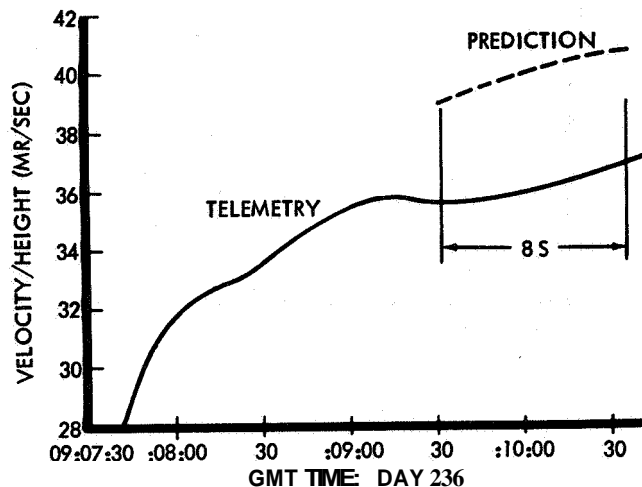


Figure 2.5-18 V/H Ratio Site 1-4

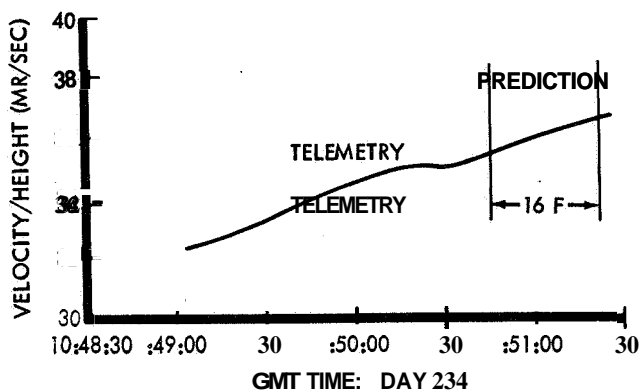


Figure 2.5-16: V/H Ratio Site I-2

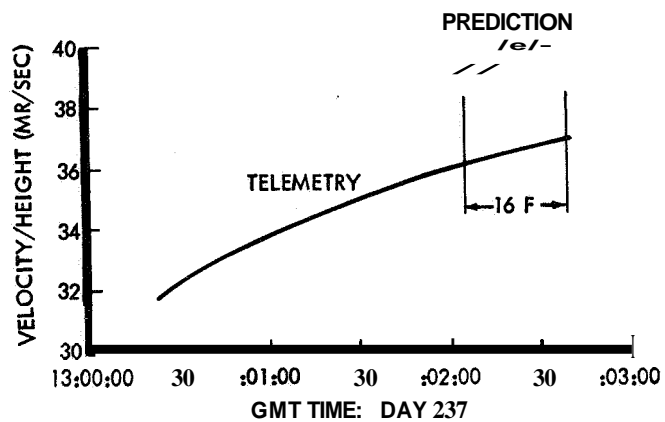


Figure 2.5-19 V/H Ratio Site 1-5

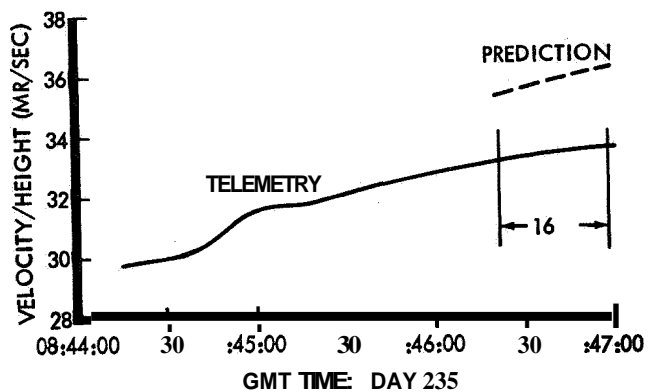


Figure 2.517: V/H Ratio Site 1-3

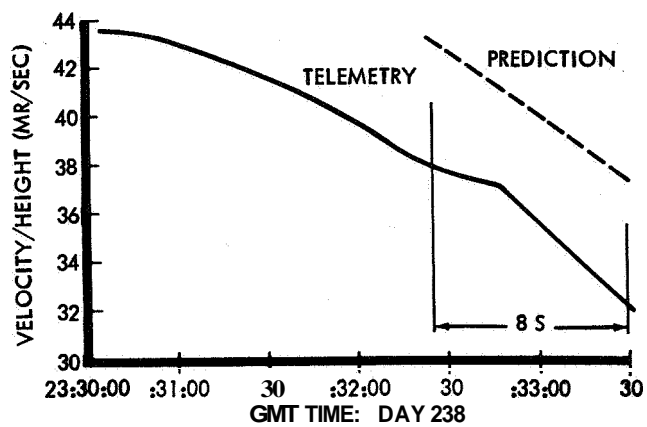


Figure 2.5-20 V/H Ratio Site 1-6

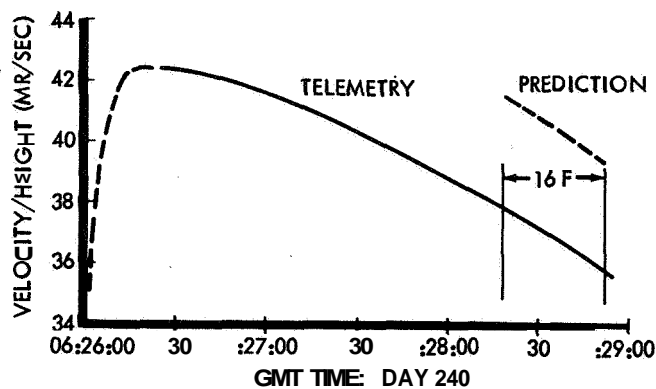


Figure 2.521: V/H Ratio Site I-7

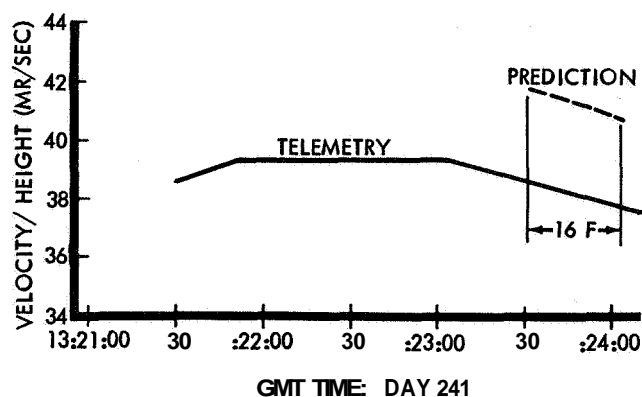


Figure 2.5-24: V/H Ratio Site I-9.2b

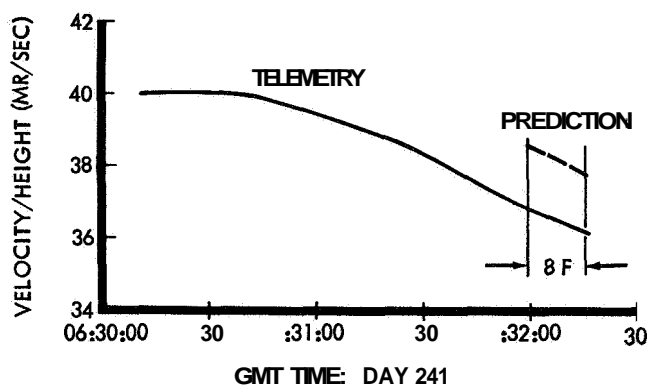


Figure 2.5-22 V/H Ratio Site I-8.1

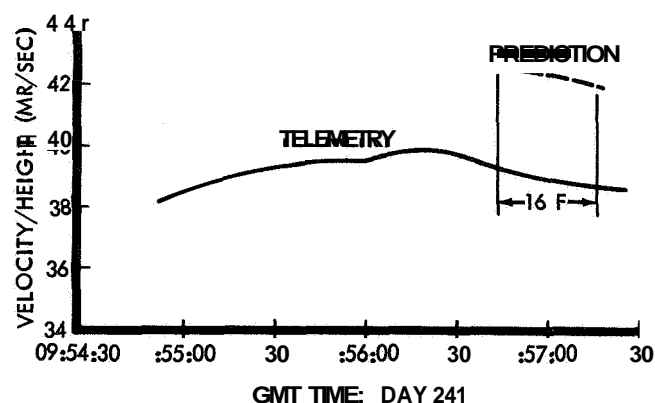


Figure 2.523: V/H Ratio Site I-9.2a

-4.4 seconds relative to the GMT tag of the telemetry frame, and includes transmission time and the time position of PR01 within the frame. The nominal accuracy of this data is 2 to 4% of full scale or 1 to 2 milliradians per second (Photographic Subsystem Reference Handbook for the Lunar Orbiter, Eastman Kodak, L-018357-RU, March 15, 1966). This figure includes nominal sensor accuracy. The observed V/H ratio can be verified by comparison with total platform operations over several telemetry frames, as discussed below.

Predicted V/H ratios are also shown in Figures 2.5-13 to -24 for each photo. These values are taken from post-mission EVAL analysis of all photo sites and are part of the final description of photo geometry and lighting. The maximum expected error in the V/H predictions is 2%, due mainly to possible altitude errors.

Analysis

In the initial ellipse—Site I-0, 210-km altitude and Day 232 test site, 239-km altitude—the V/H ratio fell to the 7 to 9 mr per sec. range. The measured values were a maximum of 0.4 mr per sec. lower than that predicted (4% of predicted), but this shift is not significant compared to the nominal system errors.

In the final ellipses, five observations are in order:

- 1) Sites I-1, I-5, I-7, I-9.2a, and I-9.2b. Altitudes: 46 to 53 km. For these sites, departures from predicted values ranged between -2.4 and -4.7 mr per sec., or between -6.6 and -9.1% of the predictions. The slopes of both curves were essentially the same, and no significant difference in curvature is indicated by the data.
- 2) Sites I-2, I-3, and I-4. Altitudes: 47 to 54 km. Here the measured ratios were between -2.2 and -3.8 mr per sec. These shifts are equivalent to -6.2 and -9.3% of the predicted ratios. The I-2 and I-3 curves exhibit marked differences in slope, while the I-4 curves differ in curvature.
- 3) Site I-6. Altitudes: 44 to 51 km. The measured ratios were 5.1 to 5.2 mr per sec lower than predicted, or 12 to 14% lower: the largest observed deviation. The overall predicted and observed slopes are the same, but the observed data shows definite peaking trend near the fourth photograph. This site also has the greatest relative altitude change.
- 4) Site I-8.1. Altitude: 50 km. This site is exceptional for its small deviation from the predicted behavior. The measured V/H ratio was a maximum of 1.7 mr per sec below the prediction (4.4% of the predicted value).

- 5) General. The average final ellipse V/H deviation from prediction is -3.2 mr per sec or 6.4% of full scale. The value is equivalent to -8.1% of the predicted V/H ratios.

The effect of the observed V/H deviation was calculated for Sites 1-3 and 1-5. The predicted smear for the 80-mm lens would be 5 and 9 microns respectively. Since these values are smaller than resolution of the 80-mm camera, no observation of smear caused by these deviations can be expected. A spot check of Sites 1-3 and 1-5 revealed no observable smear. The predicted 40-to 70-micron smear in the 610-mm camera was not observable due to the improper shutter operation.

Over a period of V/H operation, the PR01 (V/H ratio) telemetry channel can be verified by comparison with platen operations (PB05). Total platen operations, based on the observed V/H ratio, were computed by averaging PR01 over 2- to 3-minute periods. Average V/H was converted to platen cycle rate by applying the relation: 12.16 cycles/second = 1 radian/second. The resultant rate was multiplied by the elapsed time to obtain platen cycles for comparison with total platen counts during the same period. In 9 out of 10 cases, the two values agreed within one count, or about 2% of the observed total count.

The V/H sensor-on time per use cycle is limited by two constraints:

- 1) 130°F maximum V/H temperature;
- 2) 6.6-minute maximum on time per site (approximately).

The second of these constraints is of thermal origin and is the estimated time to heat the V/H sensor from the camera system normal temperature (70°F) to the 130°F V/H electronics maximum temperature limit.

This thermal constraint was not violated during the mission. The maximum V/H temperature observed during a photo pass was 72.3°F.

The 6.6-minute time maximum was exceeded, with NASA cognizance, during Site I-0 photography. Twenty frames of photography were exposed by programming a burst of 16 fast followed by four fast. The V/H sensor automatically turned off at the end of the 16-fast burst. The sensor was programmed back on after a 57-second pause.

Table 2.5-4 cites V/H sensor-on time plus accumulated time.

Conclusions

The 8% V/H anomaly contributed no significant smear to the moderate-resolution photographs. Had the high-resolution camera operated properly, it would have been possible to establish whether the anomaly was prediction accuracy or V/H malfunction. Because the average deviation (3.2 mr/sec.) is larger than the combined telemetry, sensor, and prediction tolerances by at least a factor of 2, the discrepancy must be considered as real. The most reasonable remaining explanations for the effect are a V/H telemetry malfunction, a V/H sensor malfunction or a large unknown in the prediction. The slope and form deviations observed for Sites 1-2, 1-3, 1-4, and 1-6 are not necessarily anomalous since they may be due to real terrain variations. A detailed analysis of site topography would be required to verify this point.

2.5.3.3 FILM TRANSPORT MECHANISM

Indexing of film within the photo subsystem is accom-

	TIME ON		TOTAL ON TIME (ACCUMULATED)	
	MIN.	SEC.	MIN.	SEC.
SITE I-0				
16 FAST	4	30	4	30
4 FAST	2	00	6	30
SPECIAL TEST	4	14	10	44
SITE I-1	4	37	15	21
SITE I-2	3	04	18	25
SITE I-3	3	27	21	52
SPECIAL TEST	3	00	24	52
SITE I-4	3	51	28	43
SITE I-5	2	19	31	02
SITE I-6	3	50	34	52
SITE I-7	4	14	39	06
SITE I-8.1	3	27	42	33
SITE I-9.2a	3	50	46	23
SITE I-9.2b	4	22	50	45
AVERAGE ON TIME	3	37		
TOTAL USE TIME	50	45		

Table 2.5-4 V/H sensor Duty Cycle

plished, initially, on the basis of preflight measurements and tests. As the mission progresses, reference points become available and characteristics of the subsystem known. This makes indexing of the film for priority readout more certain. Following exposure, forward movement of the film is governed by the processing rate. The actual processing rate is determined by noting the amount of film processed during the processing periods. The position of the film in the readout gate can then be established. Bookkeeping of framelet numbers read out, together with processing time, loop contents, and takeup reel contents enables indexing of film to within one inch. Timing of frame edges, time codes, and processor-stop lines by the video engineer during readout enabled accuracy of indexing to be improved slightly more during the latter portion of the mission as operational history was developed.

Camera Film Advance

Film advance was nominal throughout the mission as evidenced by the constant 11.7-inch dimension between time codes. Some time codes appeared within the high-resolution format but that was attributable to the 610-mm-camera shutter failure.

Processing Rate

Processing rate calculated from telemetry was well within the 2.4 ± 0.1 inches-per-minute specification. Orbits in which 10 or more frames were processed were used for analysis to minimize any telemetry error. Range was 2.46 to 2.37 inches per minute.

Readout Film Advance Rate

Readout film advance rates calculated from telemetry were within the 0.272 inch-per-minute nominal rate ± 0.005 telemetry accuracy. Range was 0.277 to 0.270 inch per minute.

Vacuum Channels

On the high-resolution platen, the channels appear to have made a faint impression on the spacecraft film. It is known that mechanical flexure of photographic film prior to or during exposure can change the film's light sensitivity. Possible bending of the film into the vacuum channels may have caused this effect.

Processor-Dryer Coast

The processor-dryer coasts after shutoff; however, this action could not be observed within the 23 seconds per telemetry frame.

Scratches Parallel to Spacecraft Film Edge

Such scratches were present on most of the film. The scratches are attributable to the film handling system, but are not severe enough to detract from the information contained on the photo.

Time Codes

No time code is issued to the photo subsystem when the programmer is in a Compare Time mode, as occurred several times during the mission. No system problem was created by this effect.

2.5.3.4 PROCESSOR-DRYER

Operation of the processor-dryer was within specifications. There were, however, some problems associated with processing and blemishings described in Paragraph 2.2.1.1. The primary film processing problems appear to be

- 1) Some Bimat sticks to the processed film. The amount increases with Bimat age, and is attributed to Bimat deterioration.
- 2) Banding of uneven processing along the film travel direction, which is attributed to uneven roller pressures or metering-roller pressure.
- 3) Bimat stick and dryout zones are present and cause some loss of image detail.
- 4) Miscellaneous unexplained spots may be positions of bad Bimat-film contact.

The time between processor acutations is of interest because of Bimat dryout film-stick constraints. These times are tabulated by orbit in Table 2.5-5. The frequency plot of Figure 2.5-25 shows that 175 to 200 minutes is the most probable "time between processing." The four times shown in excess of 500 minutes occurred during initial ellipse while the Bimat dryout constraint was waived.

2.5.3.5 PHOTO-VIDEO CHAIN

This section includes a discussion of readout to support analysis of mission photography.

Readout Sequence, Data Collection, and Interpretation

Priority readout was limited to periods having a duration not exceeding 43 minutes (one frame). During final readout, the original constraint of 86 minutes (two frames)

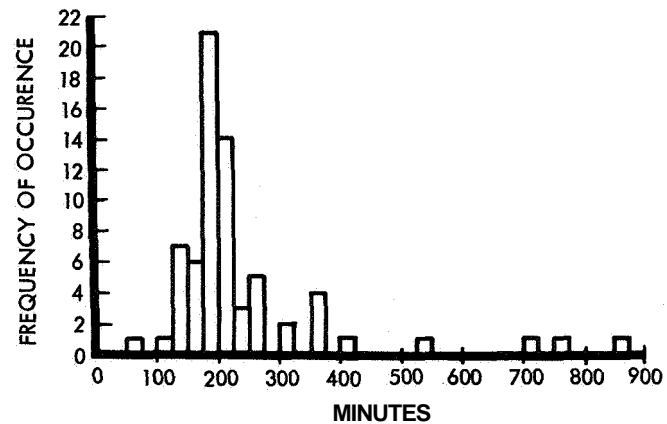


Figure 2.5-25: Frequency Plot: Processor-off Duration

was exceeded purposely. However, violation of thermal limits was avoided by careful monitoring telemetry data, particularly Readout Thermal Fin Plate Temperature. The longer readouts tended to increase the spacecraft temperature to a level that required cancelling a readout occasionally to permit cooling.

Processor stop lines and the adjacent 3 or 4 inches of film that had dried out or remained in contact with the film for extended periods caused some problems in PVC optimization. It was noticed that the video white level increased in the 3 to 4 inches of film just before the stop line. Correspondingly, it decreased in the 3 to 4 inches beyond the stop line. PVC optimization performed in this area of the spacecraft film was improper for those frames processed normally. Optimization in these areas must be avoided.

Bimat dryout on the edge of the spacecraft film rarely reached such proportions as to obscure the edge data. To evaluate the effect of overall dryout would require more data than available. Edge data would have to be correlated with the section of Bimat used to process it. The edge data around the processor stop lines has the same trend exhibited by the video signal. The densities before the stop line tend to increase, while those after it tend to decrease.

GRE Film Control

It was necessary to switch emulsions for the GRE film twice during the mission. Limited readout was performed using SO-349508-3. Just prior to final readout, a switch was made to SO-349-525-4. It was necessary to switch again to SO-394-525-36 prior to the end of readout. This latter film is the same emulsion (525) as the previous one but uses a different coating.

Upon switching to a new emulsion, the process control charts for the GRE film show very large excursions. This is due to differences in emulsion sensitivity. No adjustments were made in the processor operation. The only required change was in the GRE exposure calibrations. These were changed to adjust to obtain the 0.50 and 2.00 densities. The control chart parameters were shifted to new mean values after sufficient data was obtained to establish them. The ± 2 and ± 3 sigma values were not changed but only shifted to follow the new mean values.

ORBIT	At MIN.	PROC. START	INDEX STOP
INITIAL			
26	START	-3.00	16.80
30	767	16.80	18.80
33	705	18.56*	21.03
37	859	21.03	23.04
39	364	23.04	25.04
39	72	25.04	31.36
41	318	31.54*	33.52
43	534	33.52	35.58
FINAL			
1	416	35.58	37.58
3	304	37.58	39.34
5	352	39.34	41.38
7	352	41.38	43.41
SITE	I-1		
9	355	43.41	58.40
10	135	58.40	68.41
11	155	68.41	70.41
12	201	70.41	72.38
13	234	72.38	75.40
14	194	75.40	80.30
15	186	80.30	82.30
16	217	82.30	84.33
17	189	84.33	86.36
18	198	86.36	88.36
19	201	88.36	90.36
20	198	90.36	92.51
21	205	92.51	94.51
22	192	94.51	96.51
23	204	96.51	90.51
24	203	98.51	100.51
25	179	100.51	102.37
26	225	102.37	104.23
27	141	104.23	106.23
28	262	106.23	108.23
29	204	108.23	110.23
30	199	110.23	112.22"
31	202	112.22	114.23
32	203	114.23	116.21

ORBIT	At MIN.	PROC. START	INDEX STOP
33	151	116.21	118.19
34	252	118.19	120.17
35	180	120.17	121.59
36	191	121.59	123.55
37	187	123.55	125.53
38	209	125.53	128.20
39	197	128.20	130.18
40	202	130.18	132.17
41	174	132.17	134.16
42	202	134.16	136.23*
43	194	136.23	138.22
44	197	138.22	140.21
45	218	140.21	142.20
46	133	140.20	143.46*
47	256	143.46	145.44
48	226	145.44	147.43
49	186	147.43	154.40
50	156	154.40	156.38
51	197	156.38	159.35
52	124	159.35	161.33
53	258	161.33	163.31
54	144	163.31	165.28
55	201	165.28	171.26
56	176	171.26	187.20
57	190	187.20	195.26
58	165	195.26	197.26
59	135	197.26	199.26
60	193	199.26	201.26
61	262	201.26	203.26
62	135	203.26	213.26
63	152	213.26	215.26
64	199	215.26	217.26
65	265	217.26	220.84
65	21	BIMAT	CLEAR

At = TIME SINCE LAST PROCESS
* = CORRECTION

Table 2.5-5: Processing Record

Readout Analysis Log

- Refer to Boeing Document D2-100376-1, Volume I, Spacecraft Performance Analysis and Command (SPAC) Operating Procedure, a description of the data to be entered on the R/O analysis log. Below, exceptions or conventions that deviate from the previously documented descriptions are listed by item number.

Item 1: S/C Number—Either a “4” or a “1” is logged here. The “4” resulted from Boeing’s convention of numbering the spacecraft built by Boeing. A NASA letter, after Mission I had begun, directed that the spacecraft number be a “1.” The “4” convention appears on the logs up to Sequence 033. Refer to Item 6 for the spacecraft number change effect on the recording camera run reference number.

Item 2: Date—The usual convention is GMT day followed by a slash and the last two digits of the current year. In some isolated cases, DSIF local day is reported.

Item 6: Recording Camera R Reference Number

XX/ GRE Number	XX/ S/C Number	XXX/ R/O Sequence Number	X/ Test Number
DSS-12: 03 OR 04	At mission beginning: 04, otherwise 01 (represent the same spacecraft)	001 through 141	An “0” represents S/C readouts. Other than “0” represents tests between S/C readouts.
DSS-41: 05 OR 06			

Item 7: Footage Counter—7a Start: Usually not logged; a zero is understood.

Item 8: GRE Film Roll Number

Example: 0-349-508-40

- 0 = Special Order
- 349 = Film Type SO-349
- 508 = Emulsion batch number
- 40 = 40th Coating

NOTE: This number is different from the GRE roll number used for readout identification and appearing on the Photo Identification Log and on the reassembled negative subframe title block.

Item 9c: Frame Number—Either the R/O index number or the actual frames read out were reported. The letter “M” or “H” following the frame number represents either a medium-or-high-resolution subframe.

As the time code appears at about 0.74 of the frame, a readout index number greater than XX.74 means the readout begins in a medium-resolution subframe. Sometimes the R/O indices at the beginning and at the end of readout were logged.

The following items were not reported for final readouts except by DSS-41: 1b, 11c, 11d, 13a-h, 14, 15, 16, 17.

Items 11e & 15e: Fiducial Line Length—DSS-41 reported the length of one cycle. DSS-12 and -61 reported the length of the line (approximately one-half the period).

Items 13c & 17c: Direction of Smear—(See also Item 22) Flight direction smear was described with such terms as: flight, toward edge data, IMC, perpendicular to edge data. Film advancement direction smear was described with such terms as parallel to edge data, film advancement.

Item 19: Optimization Stew—The absolute focus or gain step number was reported by DSS-41 and -61. DSS-12 reported the number of optimization commands sent just prior to the readout.

Item 20a: Tie Code Lamps Lit—The template supplied to the video engineers to read out the time code lamps reads them out in reversed order. DSS-61 video engineer corrected this template. The time code lamps lit as reported by the DSS-41 and DSS-12 video engineers are usually logged in reversed order. The conventions on reporting the lamps were taken into consideration in converting the binary to decimal spacecraft time.

When more than one time code has been logged, the check or mark opposite the lamp designation in the first vertical column corresponds to the top number or numbers logged in item 20b.

Post-Readout Period

The spacecraft clock time at the moment of exposure was recorded on the spacecraft film with a timing light. The twenty lamps formed a binary code with true bits being lit. These lamps were recorded on the GRE during readout. The video engineer used a numbered template to determine the lamps that were lit. There was confusion regarding use of the template, with DSS-61 reporting the lamps in proper sequence and DSS-41 and -12 reporting them in reverse sequence. This information was transmitted verbally to the Photo Data Analyst (PDA) and the time codes were recorded in the logs in both proper and reverse sequence.

The PDA converted the timing light code to spacecraft clock time in seconds by setting up the lights as a binary code and using a conversion table.

A computer program was used to convert spacecraft clock time to GMT. The computer converted spacecraft clock time from telemetry channel AB01 to GMT.

The telemetry from nearest the exposure time was used as a sample. Truncation errors were determined by observing frames on either side of the sample frame. Both the spacecraft time and the GMT were corrected for this error. Equipment and transmission delays were subtracted from the GMT, producing a correct GMT corresponding to the spacecraft clock time for the sample frame.

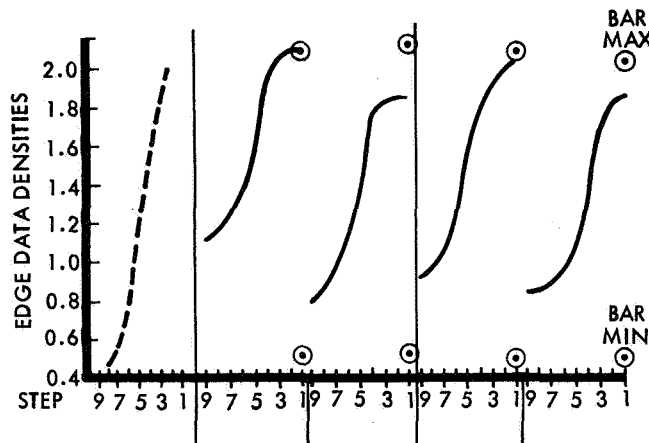


Figure 2.5-26: Simultaneous Recording During Priority Readout

The difference between exposure and sample frame times was added to the GMT sample time to give the correct exposure time in GMT. This procedure was normally used for only one frame of a sequence. All the corrections were constant during any one sequence so the time of other exposures in a sequence was determined by adding the difference between the uncorrected spacecraft clock time of the subject frame and the benchmark frame to the corrected GMT of the benchmark frame.

As exposure times were determined following preliminary readout, the information was transmitted verbally to the video engineer for inclusion in the photo identification form shipped with the film to Eastman Kodak.

Initial times were reconfirmed later when entire sequences could be compared. Any corrected times were noted and sent directly to Eastman Kodak.

Readout Problems Associated with Processing of Spacecraft Film

Throughout Mission I, edge data densities followed a significant pattern of higher than nominal value. Figure 2.5-26 shows the nominal range of density values and values obtained where the same readout was received at more than one DSIF. The cause of this higher than nominal value initially was attributed to:

- 1) Improper Bimat processing;
- 2) Improper edge data printing;
- 3) Improper GRS-site processor setup;
- 4) Improper video gain setting.

However, after several priority readouts and when data was available from all sites, all of these items were discounted. Subsequently the cause has been attributed to excessive glow or halo of the kinescope tube face due to higher than normal beam current. The priority readouts

were continued, and various tests between the sites were conducted. DSS-12 experimented with masks on the face of the GRE kinescope tubes and developed a possible work-around based on the assumption that secondary emission of the phosphor occurred and caused fogging of the edge data steps. The edge data densities on the spacecraft film are surrounded by a controlled density that corresponds to white level. Additional light would be strongest from secondary emission during scan of the background density and fog the edge data steps.

Step 9 corresponds to the control density and is most affected by this phenomenon as plotted in Figure 2.5-27. The plot is from one framelet in each readout. No attempt is made to account for different GRE's, different processing, different video-gain settings, Bimat dryout, emulsion differences, and other effects. The significant aspect of this plot is the drop in density from unmasked kinescopes to masked kinescopes at DSS-12 and -61. DSS-41 did not mask the kinescopes because it was felt that DSS-41 GRE's were not experiencing this problem. Masking at DSS-61 and -12 brought the GRE's relatively close in their reproduction of edge data densities.

Two sets of priority readout edge data densities are shown in Figure 2.5-28. The video gain in Sequence 027 was dropped from Step 10 to Step 8 to verify that a change in video gain did not increase the dynamic range of the edge data. This change brought the curve down approximately 0.1 in density in all steps but did not significantly alter the shape.

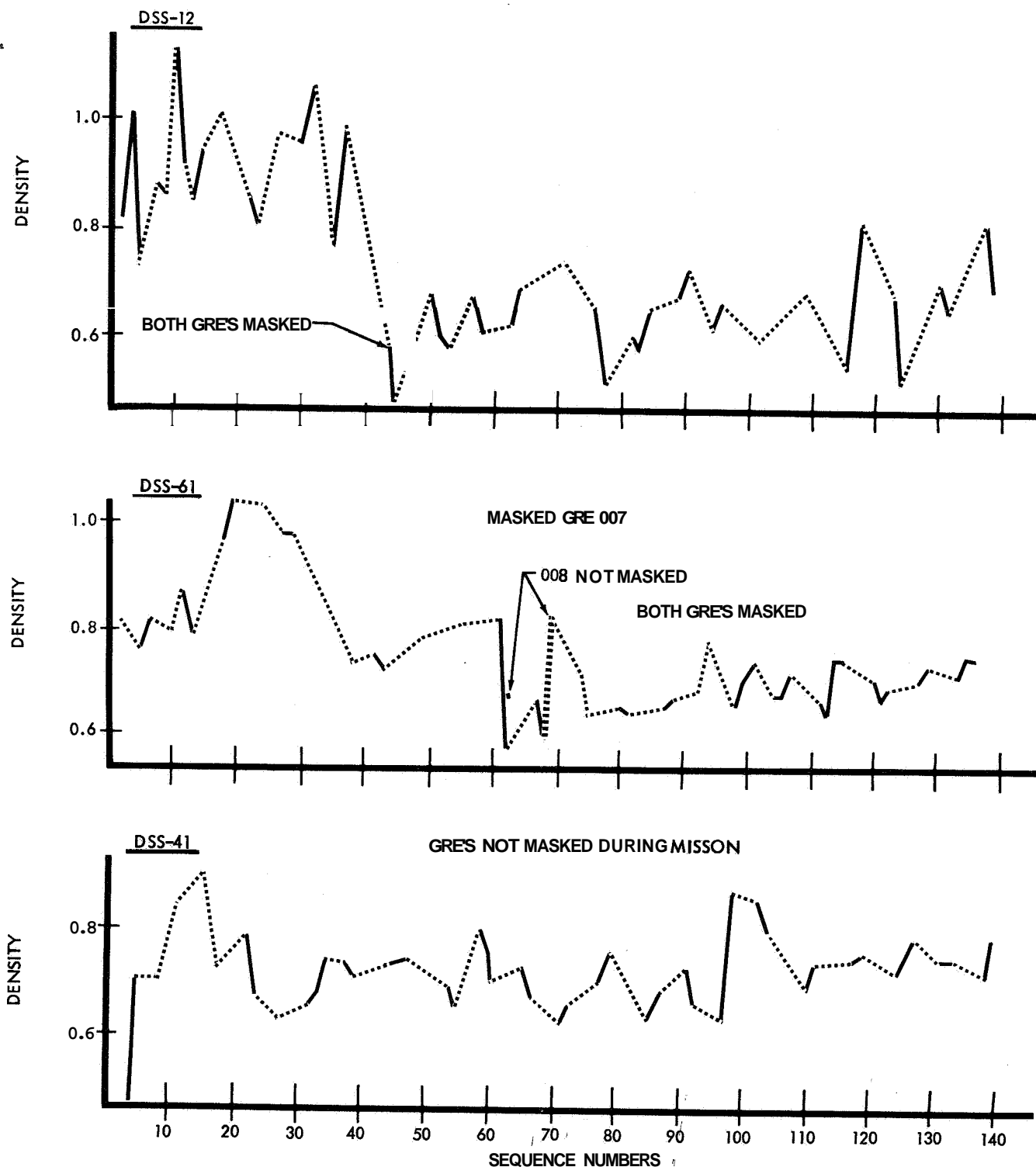
Two framelets from the same readout, Sequence 110, are shown in Figure 2.5-29. There is little difference between the curves from Framelet 723 of Sequence 110 and Gain Step 14 (from final readout) and Framelet 889 of Sequence 040 and Gain Step 11. This similarity indicates that the:

- 1) Video-gain increase during the mission was required to maintain the proper white level;
- 2) Reproduction of the edge data at DSS-41 throughout the mission was consistent.

The difference in the curve for Framelets 723 and 583 is due to Bimat dryout between processing periods. A processor stop line occurred in Framelet 680; Figure 2.5-30 shows the relationship of the stop line and the framelets. Framelet 583 was processed by Bimat that lay in the processor diffusion channel for one orbit and experienced partial dryout; the dryout shown in Figure 2.5-29 indicates acceptable degradation.

Figures 2.5-31 and -32 show the significant improvement of masking the GRE kinescopes at DSS-12 and -61. Sequences 031 and 029 were conducted before masking; Sequences 100 and 109 were conducted after masking. Masking occurred at DSS-12 for Sequence 044 and at DSS-61 for Sequence 061 for GRE 007.

Masking the kinescope requires recalibration of the GRE because significant changes in density occur. GRE 008 did not remain masked until Sequence 074 and on. Figure 2.5-33 shows the curves for masked and unmasked GRE kinescopes for Sequence 062.



1. SEQ. 1 & 141 WERE READOUT OF LEADER
2. STEP 9 IS NOMINALLY 0.42 TO 0.50 DENSITY WITH GRE SETUP OF
BAR MIN = 0.50 AND BAR MAX = 2.00

Figure 2.5-27: Edge-Data Step Nine Density - Mission I

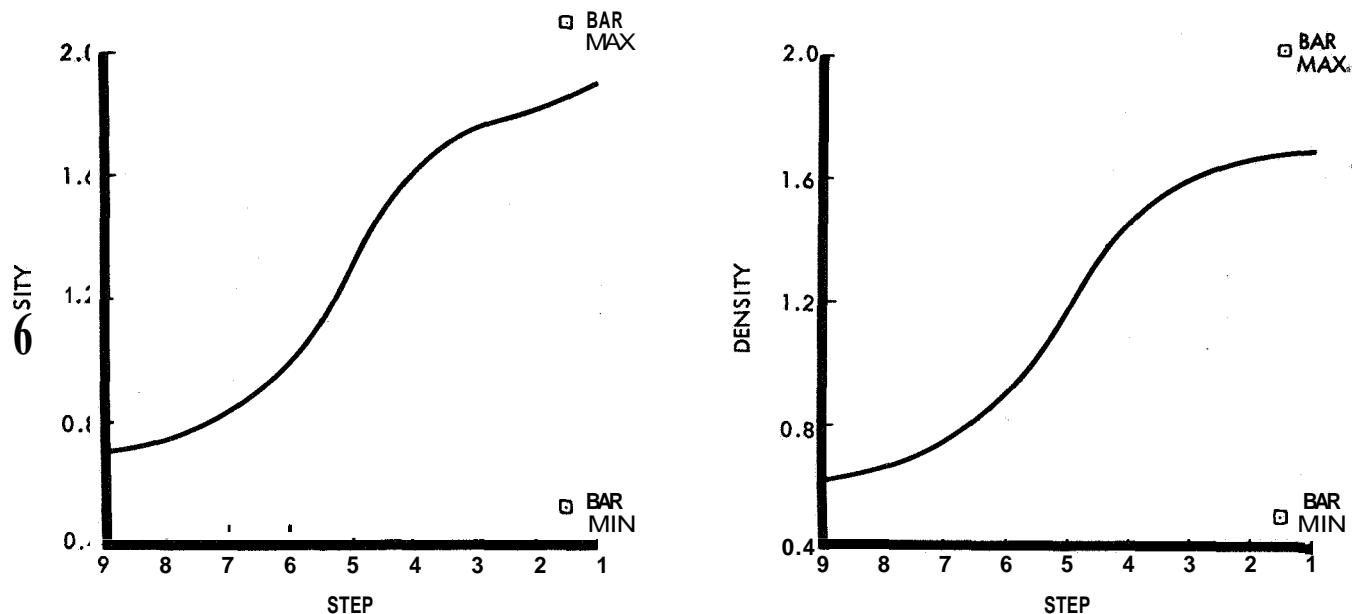


Figure 2.528 Edge Data Densities - Effect of Video Gain Change

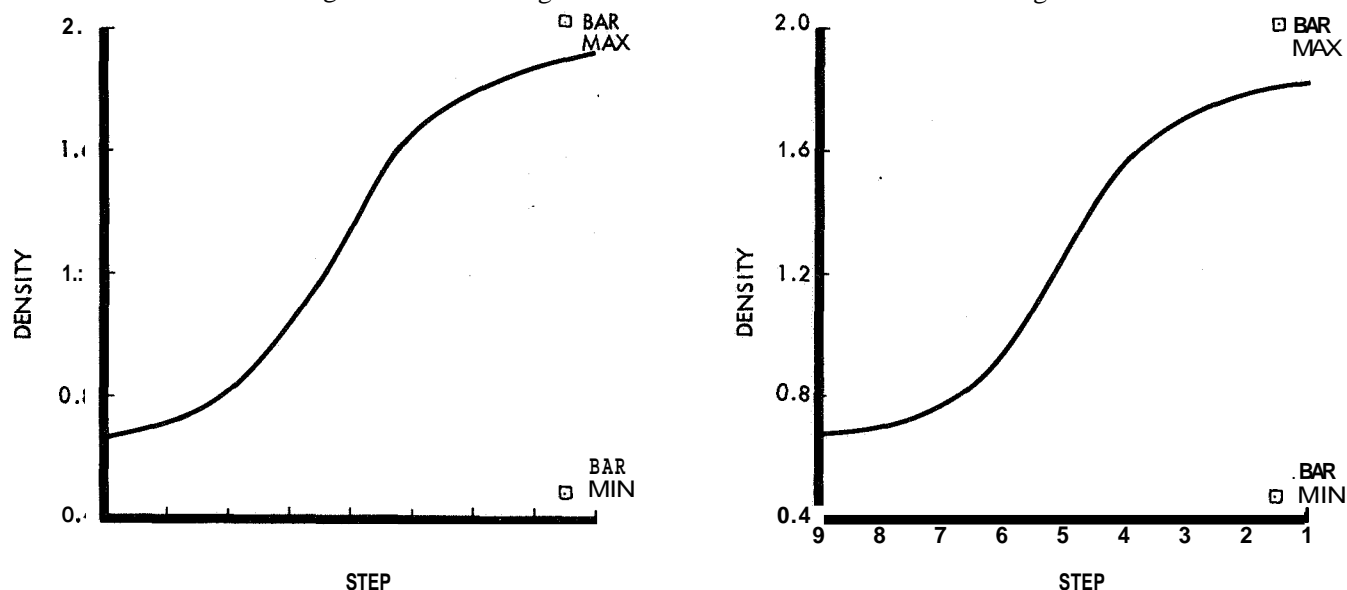


Figure 2.5-29: Edge Data Densities - Final Readout

Figure 2.5-34 is a plot of the nominal edge data densities. Comparison of Figure 2.534 with Figures 2.5-28 through -33 indicates that the masking was not entirely successful but did get the GRE's to track together and did significantly improve the edge data reproduction, which indicates a definite improvement in GRE reproduction quality of the spacecraft film. However, performance during Mission B should be improved to bring the edge data reproduction in line with the nominal values. Further experiment with the masking technique at all sites is required until a permanent solution is obtained.

Since no film is available for extensive checks of density variations, no correlation of densities and thread-up lengths are possible as recommended in the reference. How-

ever, some data is available from the readout analysis logs and limited measurements made at the DSS.

The data from Sequences 93 and 94 (final readout) is shown in Figure 2.5-35. The white level drops an average of 0.2 to 0.4 volt in the area processed by Bimat left in the diffusion channel between the Bimat supply and the processor; in Sequence 117, the white level dropped to 4.0 volts during readout of a similar area. This indicates excessive and unanticipated Bimat dryout. The frames that were read out in Sequences 93 and 94 were processed per Bimat dryout constraints. Conclusive data could be derived from density measurements on the GRE film.

The densities received in Sequence 121 are plotted in Figure 2.5-36. Both GRE's are masked.

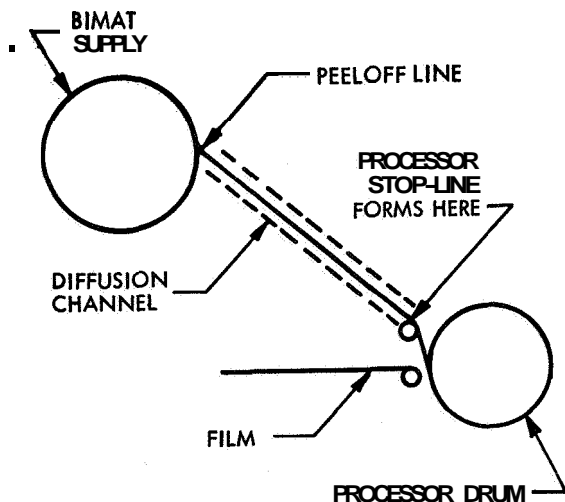


Figure 2.5-30 Position of Processor Lines

Active Readout Phase

The active readout phase is started by thesecond readout-drive on command. The video waveform is displayed on the GRE oscilloscopeto indicate what is being scanned by the optical-mechanical scanner; the telemetry and film records kept at the SFOF are handled by the photo data analyst. The video engineer detected the edges of frames and time codes for coordinating FR-900 videotape changing; the photo data analyst used them as a check on the film budget. FR-900 tape changing was originally planned to take place during the scanning of a medium-resolution frame. However, this was changed for final readout to occur during a high-resolution frame since those were degraded due to the shutter problem in the high-resolution camera. The video engineer periodically made a video status check of the waveform and reported these estimates to the photo data analyst; the check includedthe following parameters:

- 1) White level - The average video level while scanning through the film control density at focus stop.

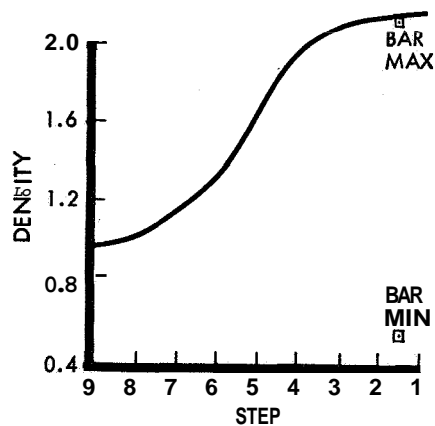


Figure 2.5-32: Edge Data Densities, DSS-61 Before Masking

- 2) Active scan time - The timebetweenfiducial marks.
- 3) Mechanical scan time - The time required by the optical-mechanical scanner to scan an A and a B framelet.
- 4) Sync pulse height - The amplitude of the sync pulse of the composite video signal.

The video engineer was also requested to report received signal strength with the video status report. This data was used by the communications analyst in SPAC to aid analysis of high-gain-antenna pointing.

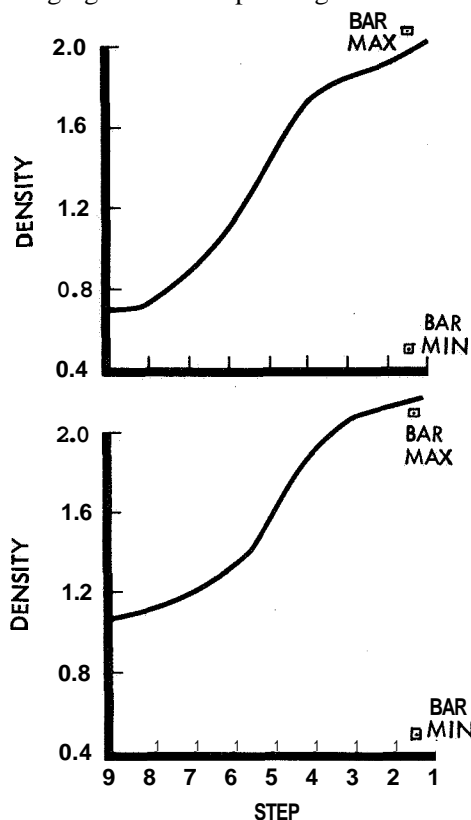
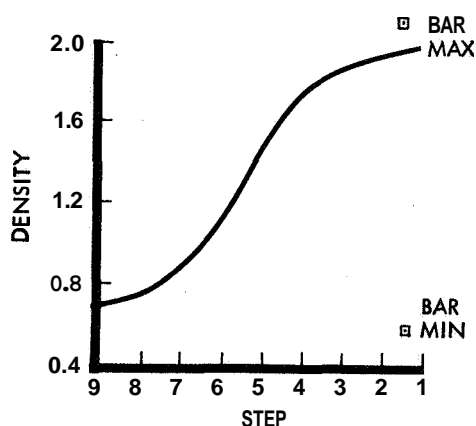


Figure 2.5-31: Edge Data Densities, DSS-12



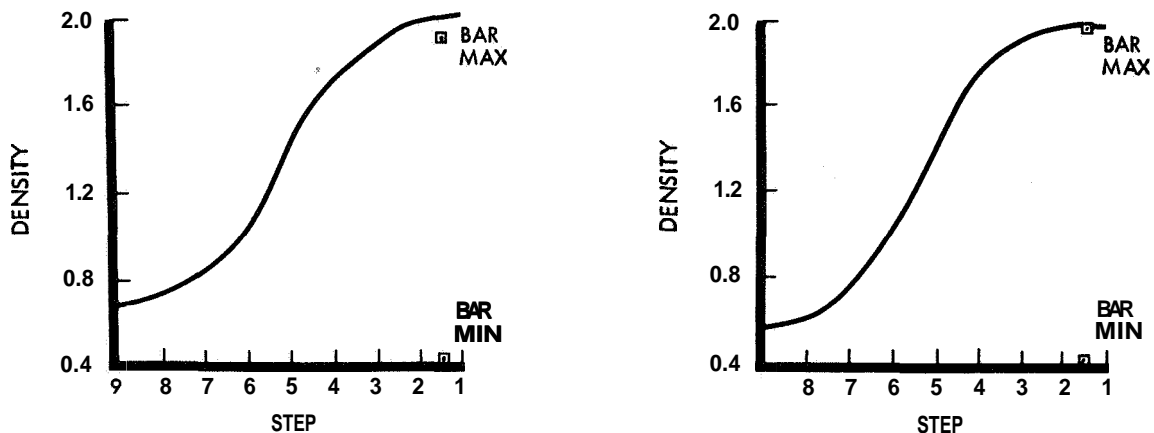


Figure 2.5-33: Edge Data Densities, DSS-61 After Masking

The white level varied approximately 0.5 volt during readout due to variations in density of the spacecraft film. Active scan time, mechanical scan time, and sync pulse height remained constant.

At the end of readout, video engineers noted any anomalies in the readout--these were mainly variations in white level. The video engineer reported the GMT's when the readout electronics were shut off and the video signal on the GRE was lost. The video engineer estimated the time required to prepare a preliminary analysis of the processed film, the time codes read out, and the first and last framelet numbers read out.

Twelve channels concerning the readout were plotted on a Milgo plotter in real time as shown in Figure 2.5-37 for Sequence 121 in Orbit 146. The PE01 reading (10 v.d.c.) remained at 9.93 volts until the spacecraft bus voltage dropped below 24 v.d.c. after a period of Sun occultation.

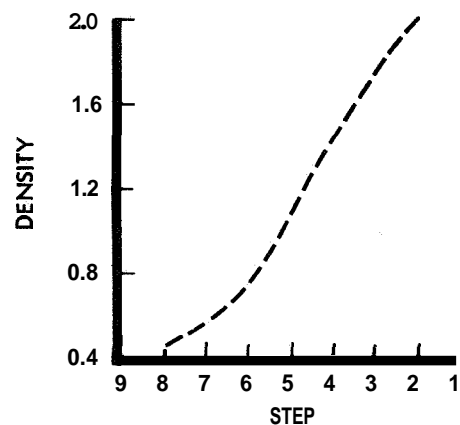


Figure 2.5-34: Nominal Edge Data Densities

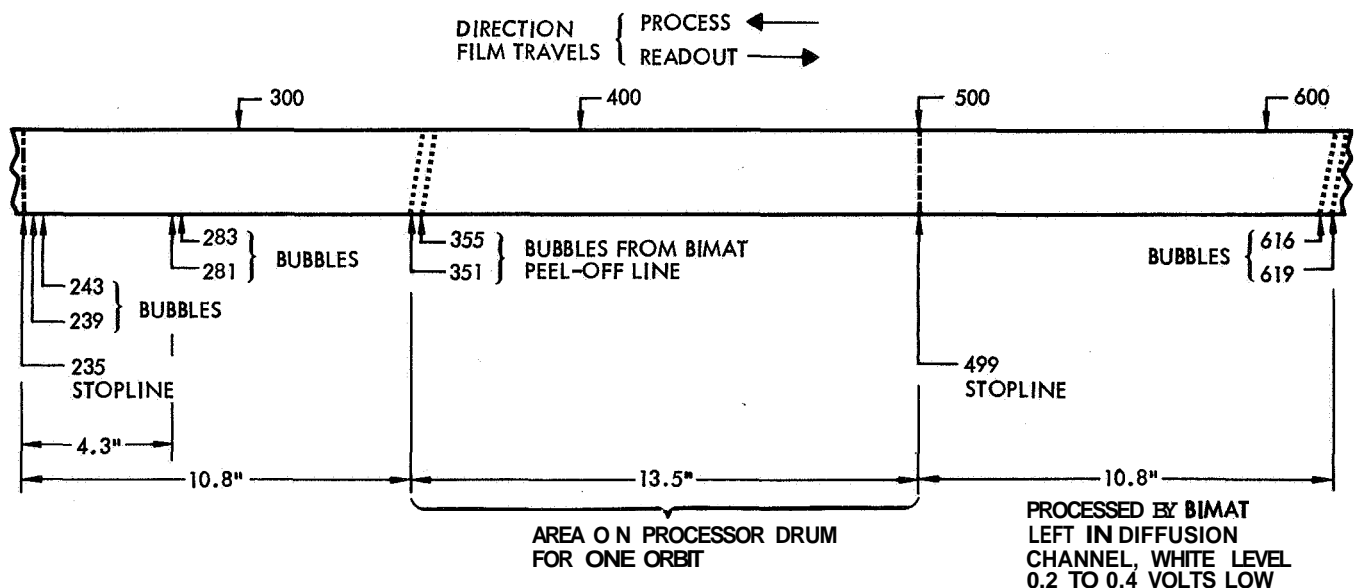


Figure 2.5-35: Effect of Bimat Dryout

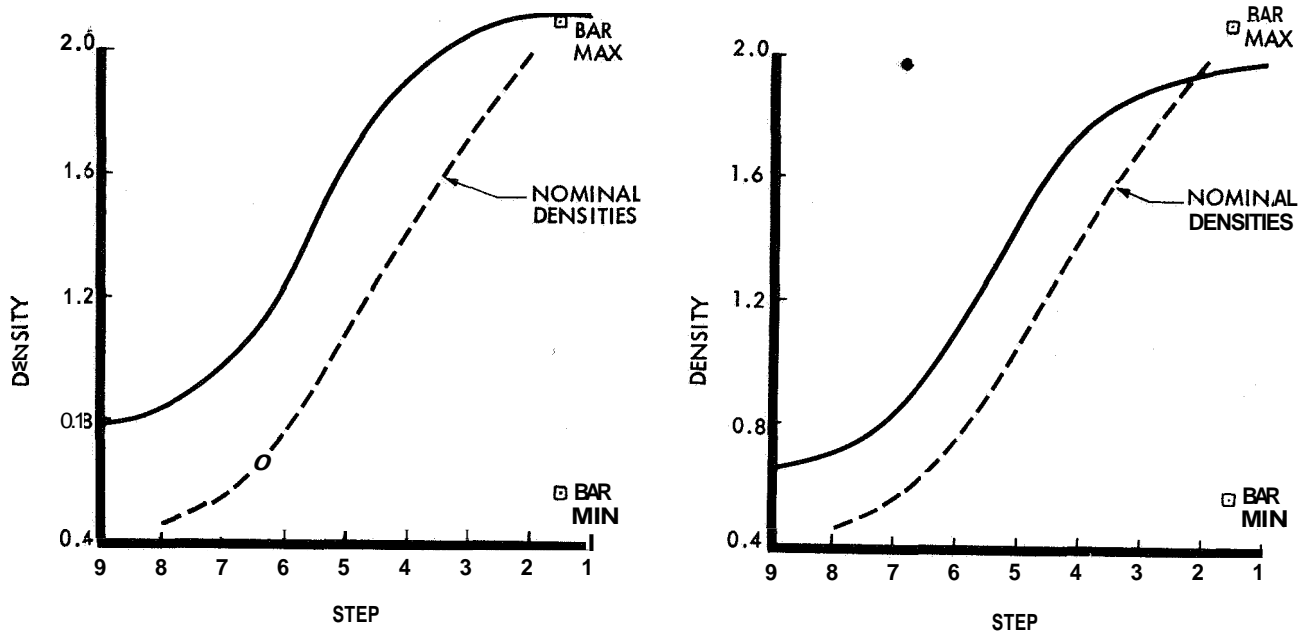


Figure 2.5-36: Edge Data Densities Readout Sequence 121

The photomultiplier voltage (PE06) increased slightly from -1836 to -1844 volts. PE06 is changed by video-gain commands by approximately 20 volts; this represents an increase of half a gain step. The high-voltage supply increased from 20.25 to 20.43 kvolts, not a significant change. The peak video voltage (PE04) has a 1- to 6-second time constant and a gain of 0.6 to 0.8. When the optical-mechanical scanner was in the focus-stop position (readout electronics on) and the first readout-drive on command executed, PE04 was 4.020 volts corresponding to the 5.0-volt white level as read on the DSS-61 oscilloscope. This is at Gain Step 15 and Focus Step 9. The beat of the 23-second telemetry sample rate with the 22-second framelet scan can be distinguished with the high white level of the framelets between frames as marked in the real-time plot. The line-scan-tube current (PE03) increased from 19.32 to 19.79 microamps, not a significant increase. The upper shell temperature (PT09), upper environment temperature (PT08), and upper PS humidity voltage (PH02) followed their normal pattern. The readout thermal fin plate temperature rose from 78.0 to 93.5°F and dropped after the Sun was occulted; this is well within operational constraints. The readout loop contents began rising from 3.07 inches following the second readout drive on command, and filled to 30.92 inches—2.40 frames. Two communications channels, TWTA temperature (CT01) and TWTA power out (CE02) were also plotted and show their normal pattern.

The spacecraft bus voltage was 27.68 v.d.c. when mechanical scan was initiated and rose above 28.0 v.d.c. shortly thereafter, but no degradation due to low bus voltage was experienced.

Beginning and End of Mission Readout Test

A readout of the Goldstone test target was performed at

the beginning and end of Mission I (Readouts 001 and 141). The purpose was to determine what degradation had occurred to the photo-video chain during the mission. The second readout was normalized to the first to eliminate the effects of variations in film processing and GRE exposure calibration.

Resolution values showed that focus did not change during the entire mission. Gain settings required to produce 5.0 volts in the focus-stop position indicate that considerable degradation occurred in the PVC. Comparison of readout density values from the edge data is obscured due to the halo effect of the GRE kinescope tubes noticed during early phases of limited readout.

Procedure. To determine the exact gain setting during the last readout (141), a series of gain commands were sent to the spacecraft. After two commands were executed, the readout electronics reset to the first step at a white level of 2.5 volts. Thirteen more gain commands were required for a white level of 5.0 volts in focus stop as viewed on the GRE monitor oscilloscope.

To eliminate processing variation, the sensitometric processing curves were drawn for each readout (Figures 2.5-38 and 2.5-39). The edge data step wedge densities for the last readout were located on the curve for that process, and their associated log exposure values found. The same log exposure values were located on the sensitometric curve for the first readout process. The densities corresponding to these values were read off that curve. This set of densities then represents what the edge data densities would have looked like had there been no differences between the two readouts due to the GRE film processing.

The other variable to be removed was the variations due to the GRE exposure calibrations. This was performed using the staircase function in the test signal signature.

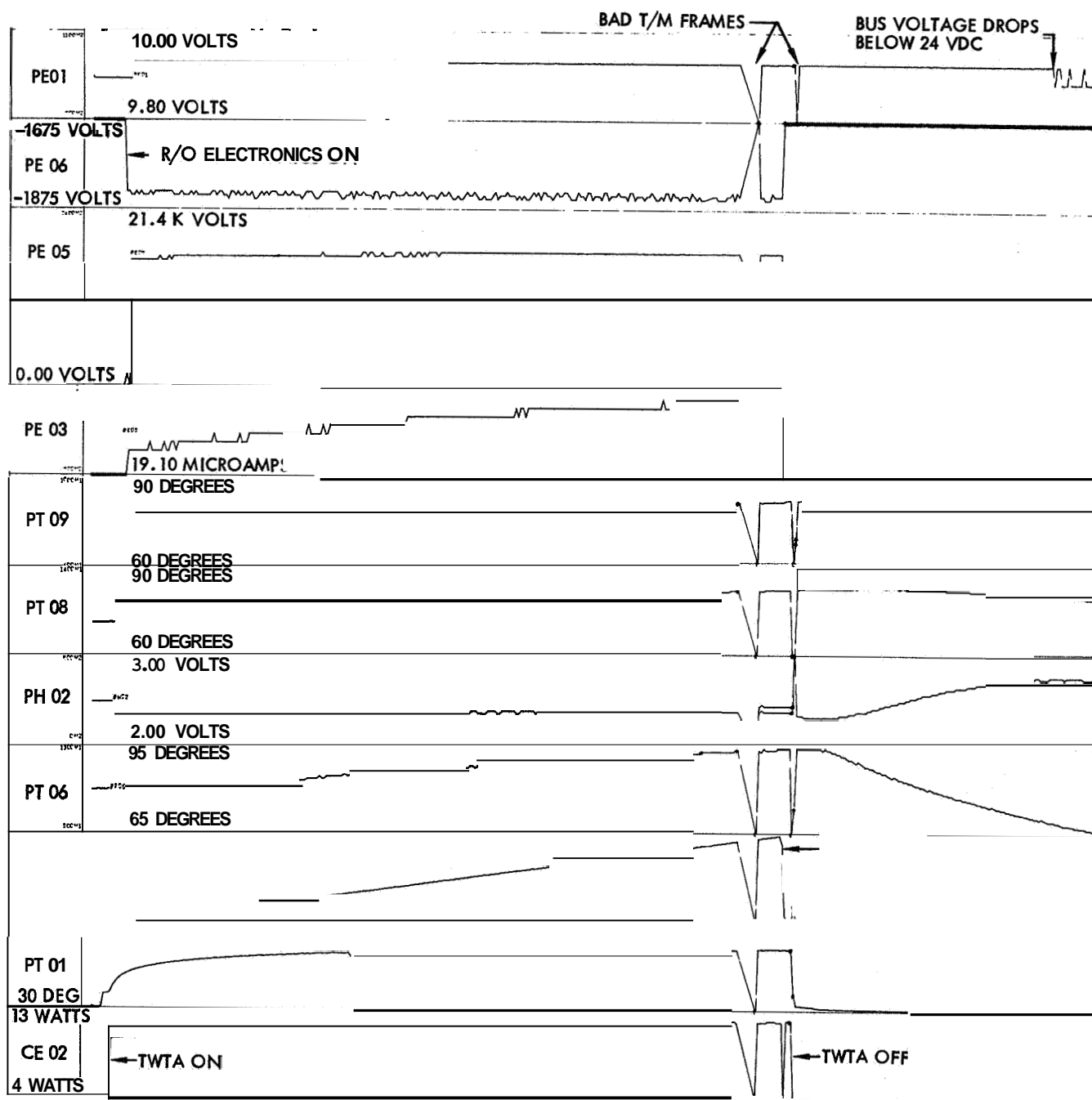


Figure 2.5-37: Milgo Plot of Telemetry During Readout

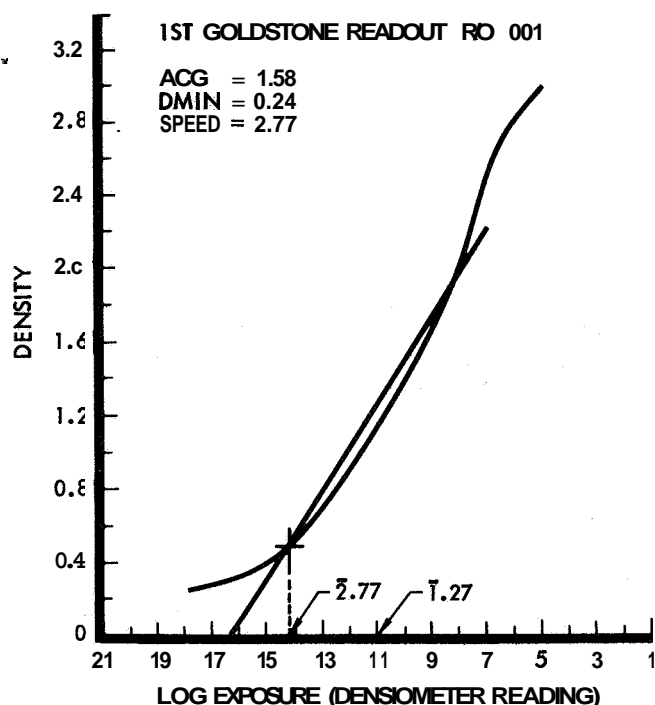


Figure 2.5-38:

GRE Sensitometric Processing Curve, Emulsion
SO-349-505-3

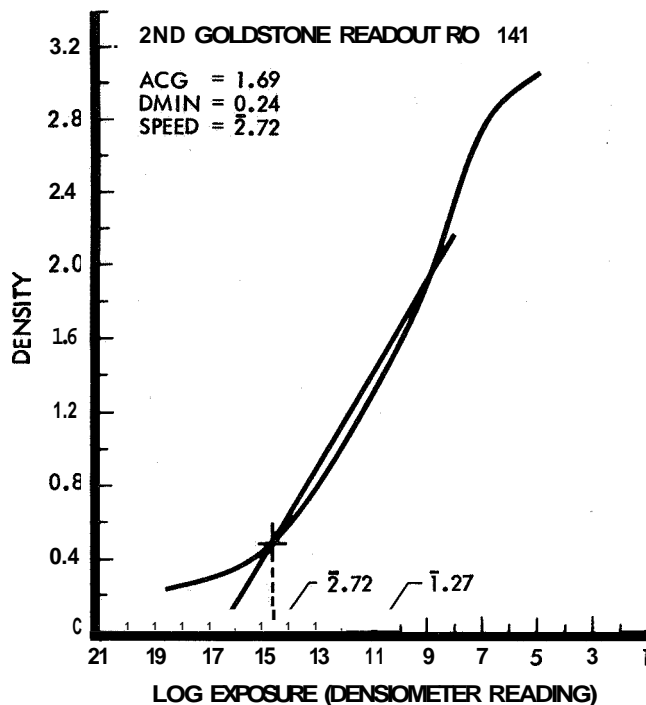


Figure 2.539

GRE Sensitometric Processing Curve, Emulsion
SO-349-525-36

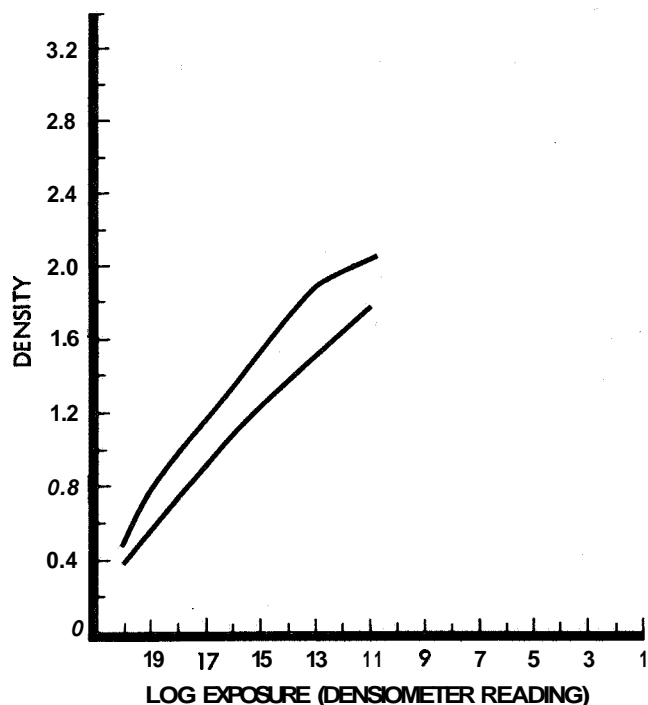


Figure 2.5-40:

Sensitometric Curve for Stairstep Function

The curves for the two stairstep functions were drawn (Figure 2.5-40). The same procedure was used in this step as was used to eliminate processing variation. The resulting set of edge data densities shows the variation due to degradation of the PVC. The values are shown in Table 2.5-6 for each step of the normalization procedure.

A third variable—commonly called “halo”—was present during the first readout but not operating in the last. It is characteristic of many kinescope tubes presently used in the GRE’s. It could not be removed from the first set of edge data densities as no accurate description of the effect exists.

Conclusions

The “halo” problem affecting the densities from the first readout (001) makes valid comparisons between the two readouts difficult. Additional unaccountable factors—primarily in the area of data collection technique—influence the data and make absolute comparison difficult.

No focus adjustments were required for the entire mission. Resolution values remained constant.

There was degradation in the PVC output as can be seen by the two different gain settings required to produce 5.0 volts in the focus-stop position. This degradation could be due to aging of the linescan tube anode or to the electronics associated with the photo multiplier.

SEQUENTIAL STEPS IN EDGE DATA DENSITY NORMALIZATION				ANALYSIS DATA READOUTS 001 AND 141			
1ST READOUT - 001		LAST READOUT - 141		READOUT 001 - GRE 4		READOUT 141 - GRE 3	
STEP NO.	DENSITY	STEP NO.	DENSITY	SENSITOMETRY		SENSITOMETRY	
1	1.06	1	0.57	5	3.00	5	3+ 6 2.93
2	1.06	2	0.58	7	2.49	7	2.75 8 2.36
3	1.06	3	0.63	9	1.70	9	1.92 10 1.60
4	1.10	4	0.75	11	1.19	11	1.30 12 1.06
5	1.18	5	1.04	13	0.75	13	0.81 14 0.60
6	1.39	6	1.48	15	0.44	15	0.46 16 0.35
7	1.66	7	1.83	17	0.30	17	0.29 18 0.26
8	1.95	8	2.06	ACG = 1.56		ACG = 1.69	
9	1.95	9	2.06	DMIN. = 0.24		DMIN. = 0.24	
1ST READOUT - 001		AST REA - 4 CORREC OR FILM E I C: VARIAI		*RESOLUTION - EDGE DATA		*RESOLUTION - EDGE DATA	
NO CHANGE		1	0.52	ELECTRICAL 80 L/MM		ELECTRICAL 80 L/MM	
		2	0.54	MECHANICAL 80 L/MM		MECHANICAL 80 L/MM	
		3	0.59	ANGULAR 100 L/MM		ANGULAR 100 L/MM	
		4	0.71	*RESOLUTION - TRI BAR TARGET		*RESOLUTION - TRI BAR TARGET	
		5	0.99	ELECTRICAL 85 L/MM		ELECTRICAL 85 L/MM	
		6	1.32	MECHANICAL 81 L/MM		MECHANICAL 81 L/MM	
		7	1.62	FIDUCIAL LINE LENGTH 0.017 INCH		FIDUCIAL LINE LENGTH 0.0175 INCH	
		8	1.83	EDGE DATA GRAY SCALE		EDGE DATA GRAY SCALE	
		9	1.83	1 1.06 2 1.06		1 0.57 2 0.58	
1ST READOUT - 001		LAST READOUT - 141. CORRECTED FOR FILM PROCESSING VARIATIONS AND GRE EXPOSURE VARIATIONS		3 1.06 4 1.10		3 0.63 4 0.75	
NO CHANGE		1	0.73	5 1.18 6 1.39		5 1.04 6 1.48	
		2	0.75	7 1.66 8 1.95		7 1.83 8 2.06	
		3	0.83	9 1.95		9 2.06	
		4	0.97	BAR DENSITIES		BAR DENSITIES	
		5	1.23	MIN. 0.53 MAX. 2.05		MIN. 0.44 MAX. 2.08	
		6	1.66	GAIN STEP 6		GAIN STEP 13	
		7	1.98	FOCUS STEP 9		WCUS STEP 9	
		8	2.07	*RESOLUTION TARGET CONTRAST IS 3:1			
		9	2.07				

Table 2.5-6: Normalization Procedures

Small specks noted in both readouts, apparently on the spacecraft film, are believed to be particles pulled from the Bimat or abraded for the SO-243. This may have contributed to the scratching of the SO-243 flight film noticed throughout the mission. Some scratches ran the entire length of the flight film and were probably due to particles caught in the readout gate or some other part of the film handling mechanism.

2.5.3.6 ENVIRONMENTAL CONTROL

The photo subsystem environmental control was nominal

for the mission.

The gradual spacecraft heating trend resulted in several orbits where the photo system interior approached 75°F for longer periods of time. The original goal was to keep the photo system temperature below 70°F due to Bimat lifetime and storage constraints. This temperature was clearly exceeded during the active Bimat lifetime. There is a possibility that Bimat processing effectiveness after Site 1-7 photography may have been slightly affected by this temperature. Long-term thermal trends are shown in the section on mission thermal history.

The photo system pressure during the mission was:

Start of mission	1.7 psia
End of readout	1.62 psia

No use of storage N₂ was observed.

The photo system humidities varied between 20 to 25°F above the dew point for the entire mission.

2.5.3.7 CAMERA SHUTTER CONTROL

Shutter Speed Selection

A photo quality prediction computer program (Boeing Document D2-100663-1, Request for Programming Photo Quality Prediction) (QUAL) was developed to assist in determining the desired shutter speed for given sites and conditions. To obtain a ground-resolution prediction, the program measures the signal-to-noise ratio (S/N) for each case by scanning a mathematical model of a densitometer across the cone and slope models reproduced at the GRE using the characteristics of the camera system, spacecraft film, photo-video chain, etc., along with the mission-dependent parameters. One or more iterations are required to obtain a specific S/N, but in practice no more than three are generally required.

The predicted ground resolution is obtained for the following criteria:

- 1) The diameter of a cone with a 4 to 1 base-to-height ratio obtained at a S/N of 3:1;
- 2) The slope angle of a 7-by 7-meter plane surface obtained at a S/N of 1:1;
- 3) The 3:1 contrast tri-bar resolution obtained at a S/N of 1:1. In addition, the output shows the expected film densities for both lenses at the three shutter speeds.

The mission-dependent parameters required to be inputted for each run include: albedo, phase angle, altitude, smear rate, smear angle, and radiation dose.

Option switches are used to select the desired output from:

- 1) Type target (cone, slope, or tri-bar);
- 2) Lens (80 mm or 610 mm);
- 3) Output point (Spacecraft film, GRE, or magnetic tape);
- 4) Shutter speed (1/25, 1/50, or 1/100 sec);
- 5) Type of display.

For Lunar Orbiter Mission I, a set of values based on the nominal mission plan were determined for the phase angle at each site. Expected albedos were also specified. These predictions, a 46-km altitude, and nominal smear, were used for a series of QUAL runs prior to the mission; the output was used as a guide. During the mission, QUAL was run using updated parameters as obtained from FPAC along with observed radiation doses.

Since the final orbit was very close to nominal, the early QUAL runs verified the predicted shutter speeds. Analysis of early priority readouts indicated that the film densities were generally high. This overexposure could be accounted for by: (1) actual albedos being slightly higher than those predicted or (2) the spacecraft film H & D curve differing slightly from the curve used in the QUAL program. This difference was established from priority readout before Site 1-5 photography. Subsequent shutter-speed determinations were made by assuming film densities 0.10 to 0.15 higher than those indicated in QUAL. At about this same time, it was established that the anomaly in the 610-mm system could not be corrected, so the selection of shutter speed for later sites was based primarily on the outputs for the 80-mm lens.

A summary of site parameters is shown in Table 2.5-6.

QUAL Runs for Exposure Control

Table 2.5-7 summarizes pertinent QUAL initial conditions.

During the mission, the exposure procedure was to pick a shutter time giving spacecraft film densities as close to 0.8 as possible. A typical choice is illustrated for Site 1-2, QUAL run.

DENSITIES

Shutter Speed	Slow (1/25 sec)	Medium (1/50 sec)	Fast (1/100 sec)
610-mm Camera	1.13	0.67	0.36
80-mm Camera	1.34	0.88	0.48

Clearly, the 1/50 sec (medium) shutter speed best achieves the 0.8 density goal.

Priority readout showed that the 0.8 density criterion resulted in some over-exposure. Based on this finding, the exposures were biased to the lower densities whenever possible.

Additionally, once malfunction of the 610-mm-camera shutter was confirmed, densities for the 80-mm focal-length camera were those examined for exposure control.

Site 1-5 gave the following choice for the 80-mm camera:

<u>Second</u>	<u>Density</u>	
1/25	0.99	
1/50	0.56	Exposure Used
1/100	0.30	

Subsequent readout showed excellent photo quality was obtained using 1/50 second. Based on this priority readout, "calibration for QUAL," subsequent exposures favored a lower density when possible.

SITE	ALBEDO			PHASE ANGLE (degrees)			ALTITUDE (km)			SHUTTER SPEED		RAD. DOSE	SMEAR (nominal)	
	BOEING	NASA	NASA PREFER'D	NOMINAL MISSION	PRED'TD	ACTUAL	NOMINAL MISSION	PRED'TD	ACTUAL	NOMINAL MISSION	ACTUAL		RADS	ANGLE
													*	**
1-1	0.075 (0.105)	0.081 - 0.121	0.081	61.8	60.9	60.9	46	54.3	53.1	1/50	1/50	1.25	125	60°
1-2	0.115 (0.075)	0.075 - 0.118	0.118	66.3	65.4	65.4	46	53.6	51.3	1/50	1/50	1.25	125	60°
1-3	0.075	0.075	0.075	68.7	68.8	69.2	46	54.0	53.2	1/25	1/25	1.50	125	60°
1-4	0.105	0.135	0.135	68.3	69.0	68.5	46	52.2	47.7	1/50	1/50	1.50	125	60°
1-5	0.080	0.076	0.076	68.4	69.0	68.6	46	50.4	48.1	1/25	1/50	1.50	125	60°
1-6	0.110	0.125	0.125	54.0	53.3	54.1	46	50.0	46.4	1/50	1/100	1.50	125	60°
1-7	0.070	0.076	0.076	56.3	57.4	58.3	46	50.0	47.1	1/50	1/50	1.50	125	60°
1-8.1	0.065	0.069	0.069	61.2	59.0	59.3	46	50.7	49.8	1/25	1/50	1.75	125	60°
1-9.2a				66.3	63.9	63.6	46	46.5	45.2	1/25	1/50	1.75	125	60°
	0.055	0.068	0.068											
1-9.2b				64.5	62.3	62.2	46	47.5	46.2	1/25	1/50	1.75	125	60°
* MICRONS PER SECOND														
** THIS ANGLE IS QUAL INPUT ANGLE AND REPRESENTS SMEAR 30° OFF FLIGHT DIRECTION														

It was determined after the mission that obsolete H and D (film density versus log exposure) curve data had been programmed into the QUAL common environment. The data resulted in density calculation being as much as 0.17 low.

The series of postmission QUAL runs that were made in Seattle is enclosed (Table 2.5-8) to illustrate the effect.

2.5.4 SPACECRAFT SUPPORTING FUNCTIONS

The primary-site photos required three-axis maneuvering from the normal Canopus-Sun reference to a reference that aligned the camera axis to a predetermined position computed by the photo subsystem group and FPAC. A roll, yaw, pitch rotation sequence was followed for primary-site photos ("I" series). Several possible sources of attitude error that could have affected successful photography were attitude maneuver angle error, holding error, and high attitude rates.

The attitude maneuver-angle error consisted primarily of the roll-angle deviation from Canopus prior to starting the maneuver sequence. This error would not normally have existed if proper operation had been possible with

the Canopus tracker. Tracker operation was hampered by a high glint problem due to Sunlight reflection off the spacecraft. The roll axis was, therefore, placed in an inertial hold mode that had an inherent drift rate of approximately +0.51 degree per hour. The attitude control analyst recommended a roll axis update during the Sunset period prior to each photographic site to provide accurate roll updates. Table 2.5-9 contains a list of attitude maneuver errors for each photo site. An accuracy tolerance of ± 0.2 degree was satisfied in all cases except for Site 1-7, which had an error of -1.75 degrees. Canopus reference had been lost during the previous orbit. However, a roll update maneuver was recommended after Canopus had been reacquired using the high-gain signal-strength map technique. A decision was made by the space flight operations director (SFOD) not to perform the update due to the close proximity of the photographic site maneuver. The roll error was within an acceptable tolerance for a successful photograph.

Attitude holding accuracy and attitude rates during the interval between shutter operations are listed in Table 2.5-8. Attitude positions and attitude rates were well within design tolerances of ± 0.2 degree and ± 0.01 degree per second respectively.

	QUAL. RUN (PASADENA)			POSTMISSION QUAL. (SEATTLE)			DIFFERENCE			MM		QUAL. RUN (PASADENA)			POSTMISSION QUAL. (SEATTLE)			DIFFERENCE			MM
	1/25	1/50	1/100	1/25	1/50	1/100	1/25	1/50	1/100			1/25	1/50	1/100	1/25	1/50	1/100	1/25	1/50	1/100	
SITE I-0					↓					610 80						↓					
SITE I-1	1.00 1.22	0.56 0.76	0.31 0.40	1.06 1.31	0.59 0.80	0.33 0.43	0.06 0.09	0.03 0.04	0.02 0.03	610 80	SITE I-6	1.45 1.67	1.00 1.22	0.57 0.76	1.60 1.83	1.10 1.34	0.64 0.84	0.15 0.16	0.10 0.12	0.07 0.08	610 80
SITE I-2	1.13 1.34	0.67 0.88	0.36 0.48	1.23 1.47	0.74 0.97	0.40 0.53	0.10 0.13	0.07 0.09	0.04 0.05	610 80	SITE I-7	1.08 1.30	0.63 0.84	0.34 0.45	1.14 1.38	0.66 0.88	0.36 0.47	0.06 0.08	0.03 0.04	0.02 0.02	610 80
SITE I-3	0.72 0.93	0.38 0.52	0.24 0.29	0.80 1.04	0.43 0.58	0.28 0.33	0.08 0.11	0.05 0.06	0.04 0.04	610 80	SITE I-8.1	0.95 1.17	0.54 0.72	0.29 0.38	1.05 1.28	0.59 0.79	0.33 0.42	0.10 0.11	0.05 0.07	0.04 0.04	610 80
SITE I-4	1.14 1.36	0.68 0.90	0.36 0.49	1.24 1.48	0.75 0.99	0.40 0.54	0.10 0.12	0.07 0.09	0.04 0.05	610 80	SITE I-9.2a	0.85 1.07	0.46 0.63	0.27 0.34	0.89 1.14	0.48 0.66	0.30 0.36	0.04 0.07	0.02 0.03	0.03 0.02	610 80
SITE I-5	0.77 0.99	0.41 0.56	0.25 0.30	0.83 1.07	0.44 0.61	0.28 0.33	0.06 0.08	0.03 0.05	0.03 0.03	610 80	SITE I-9.2b	0.80 1.02	0.43 0.59	0.26 0.31	0.95 1.19	0.52 0.70	0.30 0.38	0.15 0.17	0.09 0.11	0.06 0.07	610 80

Table 2.5-8: Postmission QUAL Computations of Image Densities

PHOTO SITE 6 FRAME	TIME (DAY - HR - MIN.)	ATTITUDE MANEUVER (DEG)				ATTITUDE ACCURACY DURING PHOTO TIME (DEG)				ATTITUDE RATE DURING PHOTO TIME (DEG/SEC)		
		ROLL	YAW	PITCH	ERROR	ROLL	YAW	PITCH	CRAB ANGLE	ROLL	YAW	PITCH
I-0 (5 - 24)	230 - 14 - 43	+3.6	+12.45	-8.10	(0.25	0.04 to 0.131	0 to 0.13	-0.13 to 0.14	0 to 0.9	+0.003	-0.0018	+0.0015
I-1 (52 - 67)	234 - 15 - 23	+5.36	+12.46	-9.60	(0.07							
I-2 (68 - 83)	234 - 18 - 51	6.43	+12.48	-4.98	0	-0.10 to -0.15	0.10 to 0.14	-0.06 to -0.12	0.2 to 0.5	+0.0083	-0.0035	+0.0015
I-3 (85 - 100)	235 - 08 - 46	6.70	+12.60	-1.60	+0.25	-0.06 to -0.12	0.05 to 0.10	-0.02 to 0.04	0.15 to 0.17	+0.0015	-0.0025	+0.0015
I-4 (105 - 112)	236 - 09 - 10	6.90	+12.50	-2.40	(0.04	4.07 to -0.11	0.05 to 0.14	-0.09 to 0.03	0.10 to 0.3	(0.0010	-0.0024	+0.0019
I-5 (118 - 133)	237 - 13 - 02	+6.50	+12.60	-2.30	0	4.06 to -0.10	0.16 to 0.11	-0.05 to -0.09	0.10 to 0.15	+0.0011	-0.0033	+0.0012
I-6 (141 - 148)	238 - 23 - 33	+6.90	+12.90	-16.70	+0.28	0.12 to 0.14	-0.03 to 0.07	0.06 to 0.12	0.10 to 0.20	-0.0020	-0.0017	+0.0020
I-7 (157 - 172)	240 - 06 - 28	+7.60	+12.80	-12.90	-1.75	0 to -0.06	0.01 to 0.23	0 to 0.09	1.00	(0.0013	-0.0018	+0.0020
I-8.1 (176 - 183)	241 - 06 - 32	+8.04	+12.81	-11.33	+0.45	0.02 to 0.15	+0.03 to -0.16	-0.06 to -0.15	0 to 0.15	+0.0021	+0.0024	+0.0008
I-9.2a (184 - 199)	241 - 09 - 57	+8.11	+12.81	-6.86	+0.02	0.12 to 0.14	0.05 to 0.06	-0.03 to 0.05	0.15	0	-0.0010	+0.0012
I-9.2b (200 - 215)	241 - 13 - 24	6.20	+12.80	-8.30	-0.05	0.07 to 0.13	0.16	0.05 to 0.15	0.15 to 0.50	(0.0017	0	+0.0022

Table 2.5-9: Spacecraft Attitude During Primary Site Photographs

FRAME	ATTITUDE ANGLE (DEG)		
	ROLL	PITCH	YAW
25	-2.87	0	0
26	+0.31	0	0
27	+0.38	0	0
28	-179.65	0	0
29	+0.8	0	0
30	-179.65	0	0
31	+0.5	0	0
32	+0.5	0	0
33	+0.5	0	0
34	+0.5	0	0
35	-180.0	0	0
36	-180.0	0	0
37	-180.9	0	0
38	-180.0	0	0
39	-180.0	0	0
40	-180.0	0	0
41	-0.8	0	0
42	+2.4	0	0
43	--	--	--
44	+1.3	0	0
45	--	--	--
46	-2.6	0	0
47	-2.6	0	0
48	-0.9	0	0
49	-0.9	0	0
50	-195.0	0	0
51	-195.0	0	0
84	-2.95	0	0
101	--	--	--

FRAME	ATTITUDE ANGLE (DEG)		
	ROLL	PITCH	YAW
102	+188.8	+25.6	0
103	-1.5	0	0
104	--	--	--
113	-0.1	0	0
114	-0.1	0	0
115	--	--	--
116	+180.0	0	0
117	+127.2	+45.4	0
134	+1.95	0	0
135	-2.1	0	0
136	+181.9	0	0
137	+0.4	-35.7	+1.5
138	-0.9	0	0
139	-1.6	0	0
140	-1.5	0	0
149	+1.9	0	0
150	+1.3	0	0
151	+29.0	0	0
152	--	--	--
153	+14.0	0	0
154	+14.0	0	0
155	+14.0	0	0
156	+14.0	0	0
173	-3.2	0	0
174	-1.8	0	0
175	-2.5	0	0
NOTE: A TOLERANCE OF ± 0.2 MUST BE ASSUMED ABOUT ALL AXES			

Table 2.5-10: Spacecraft Attitude During Film Set

Figures 2.5-41 through 2.5-51 contain gyro position, crab angle, and maneuver magnitude as a function of time for the primary-site photos. The attitude control system optional feature of crab angle control by V/H sensor measurement was not used on this mission. It should be noted that the crab angle was greater than ± 0.2 degree for the majority of the photographic sites. No correlation could be made between yaw angle and crab angle in terms of magnitude or sign. The discontinuities on gyro position in Figures 2.5-43 through 2.5-51 occur when the gyro switches from a rate mode to an inertial hold mode in the presence of an overshoot from the attitude maneuver. A certain amount of cross-coupling can also be noted in the roll axis whenever a pitch or yaw maneuver is performed.

An analysis of disturbance torques, including thermal door opening and closing, can be found in the attitude disturbance torque section, Paragraph 3.1.4.

Film-set photos generally did not require maneuvers and were taken merely by opening the camera door and shutter. Farside photographs were made by rotating the spacecraft about the roll axis. Only the two Earth photographs required two axis maneuvers.

Table 2.510 contains attitude angles at the time the shutter was open. Attitude accuracy and rates were within the tolerance of ± 0.2 degree and ± 0.01 degree per second, respectively.

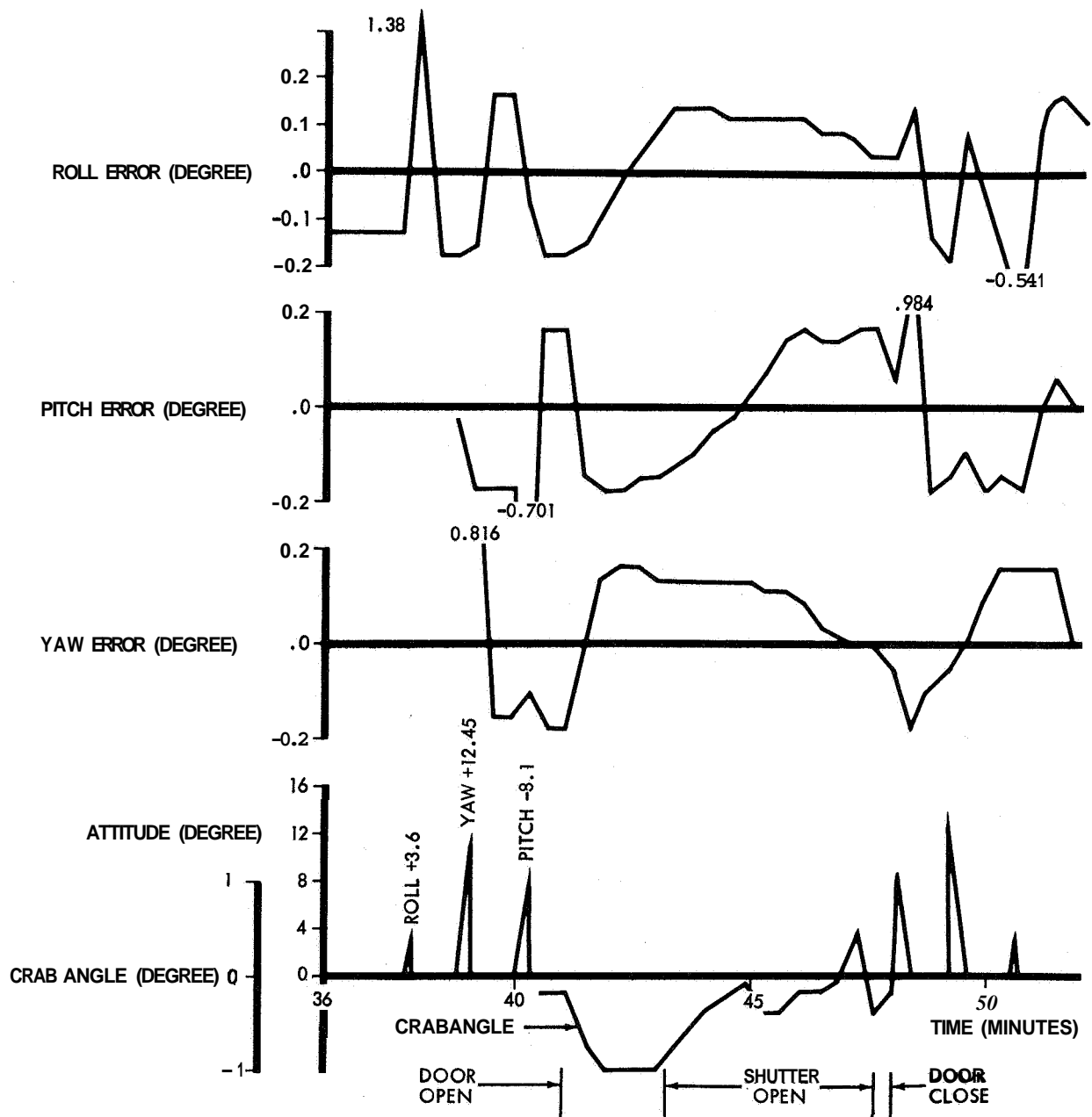


Figure 2.5-41: Gyro Position, Crab Angle, and Maneuver During Photography Site I-0

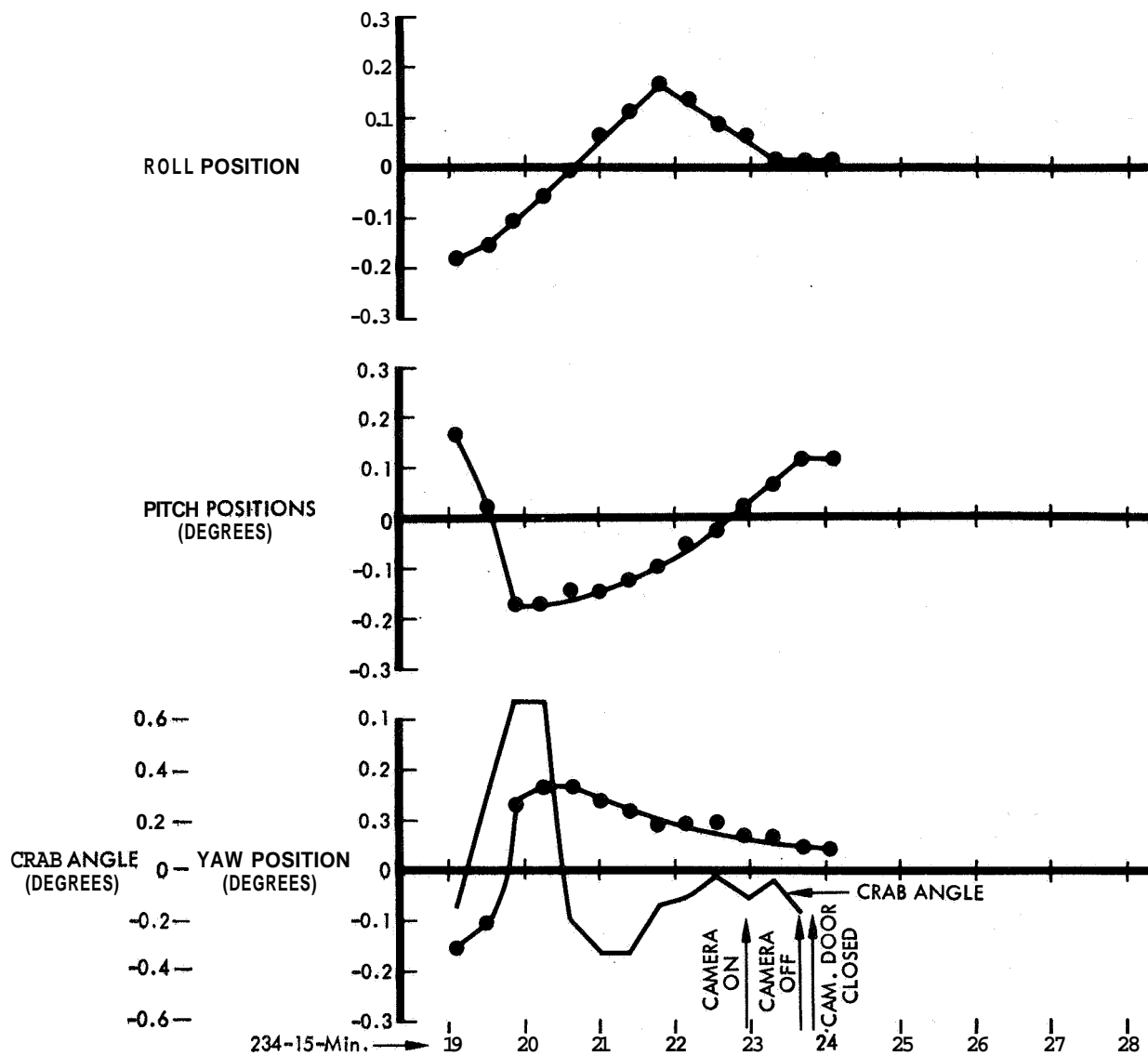


Figure 2.5-42 Gyro Position, Crab Angle, and Maneuver During Photography Site I-1

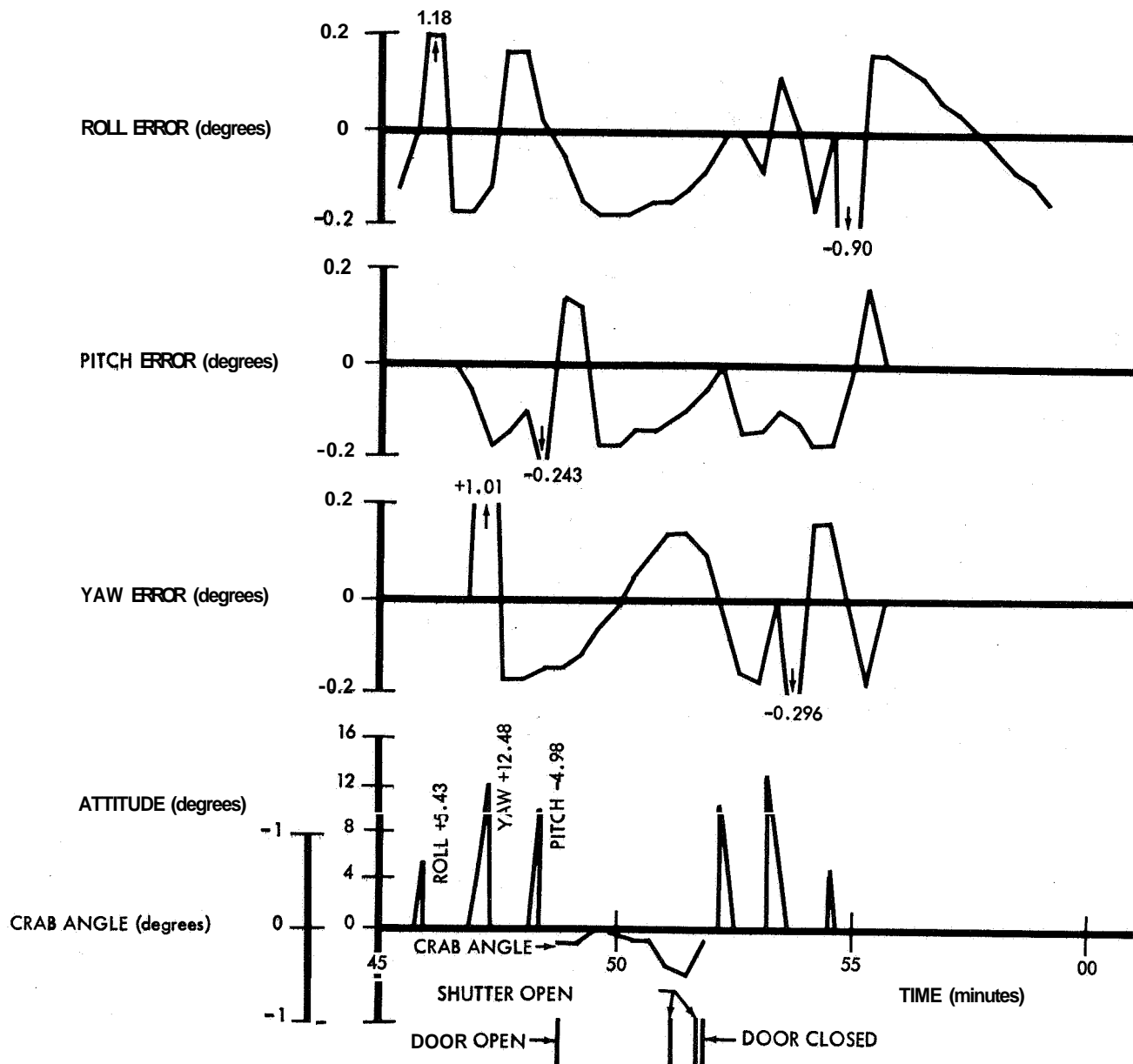


Figure 2.5-43: Gyro Position, Crab Angle, and Maneuver During Photography Site 1-2

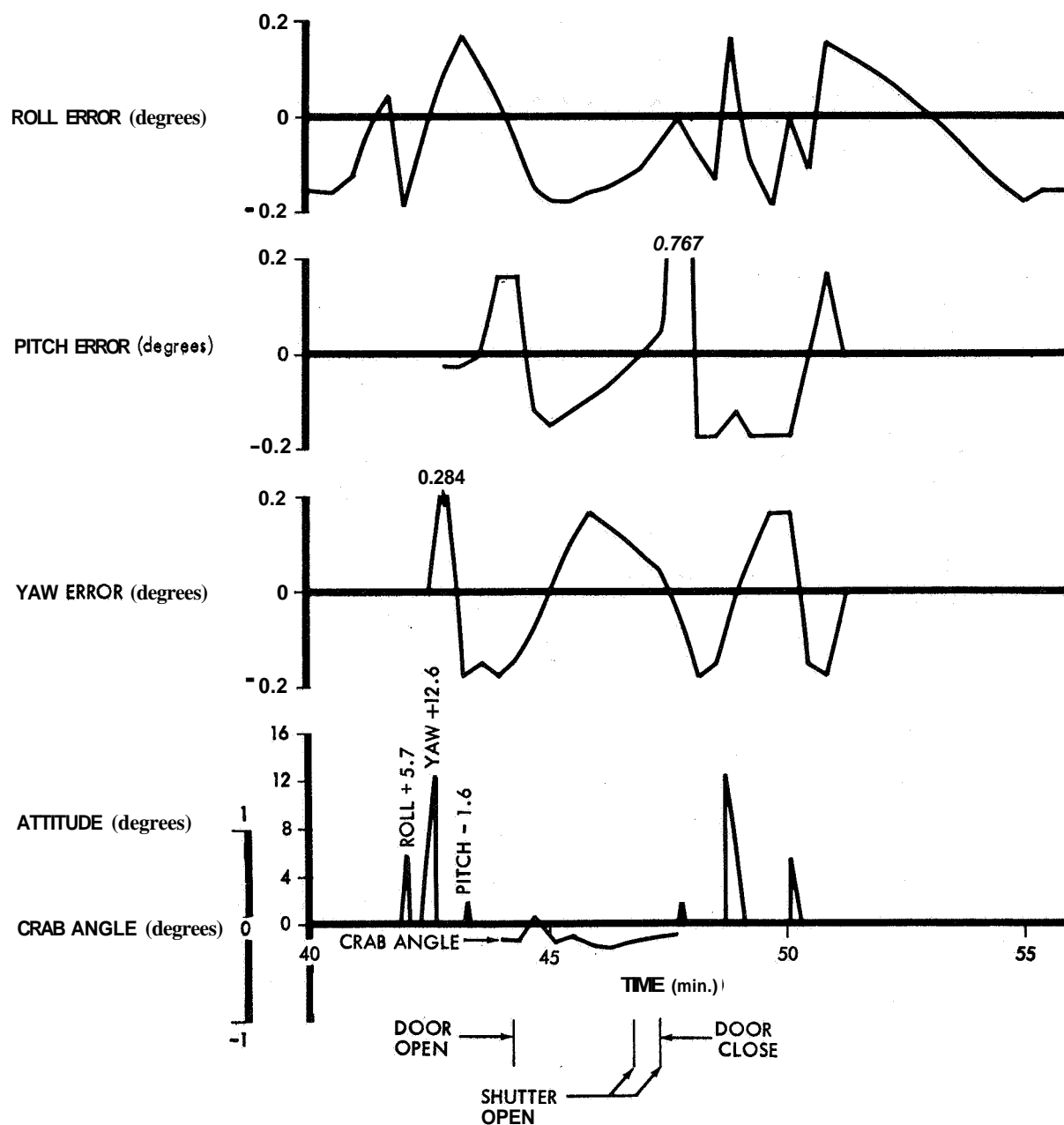


Figure 2.5-44: Gyro Position, Crab Angle, and Maneuver During Photography Site 1-3

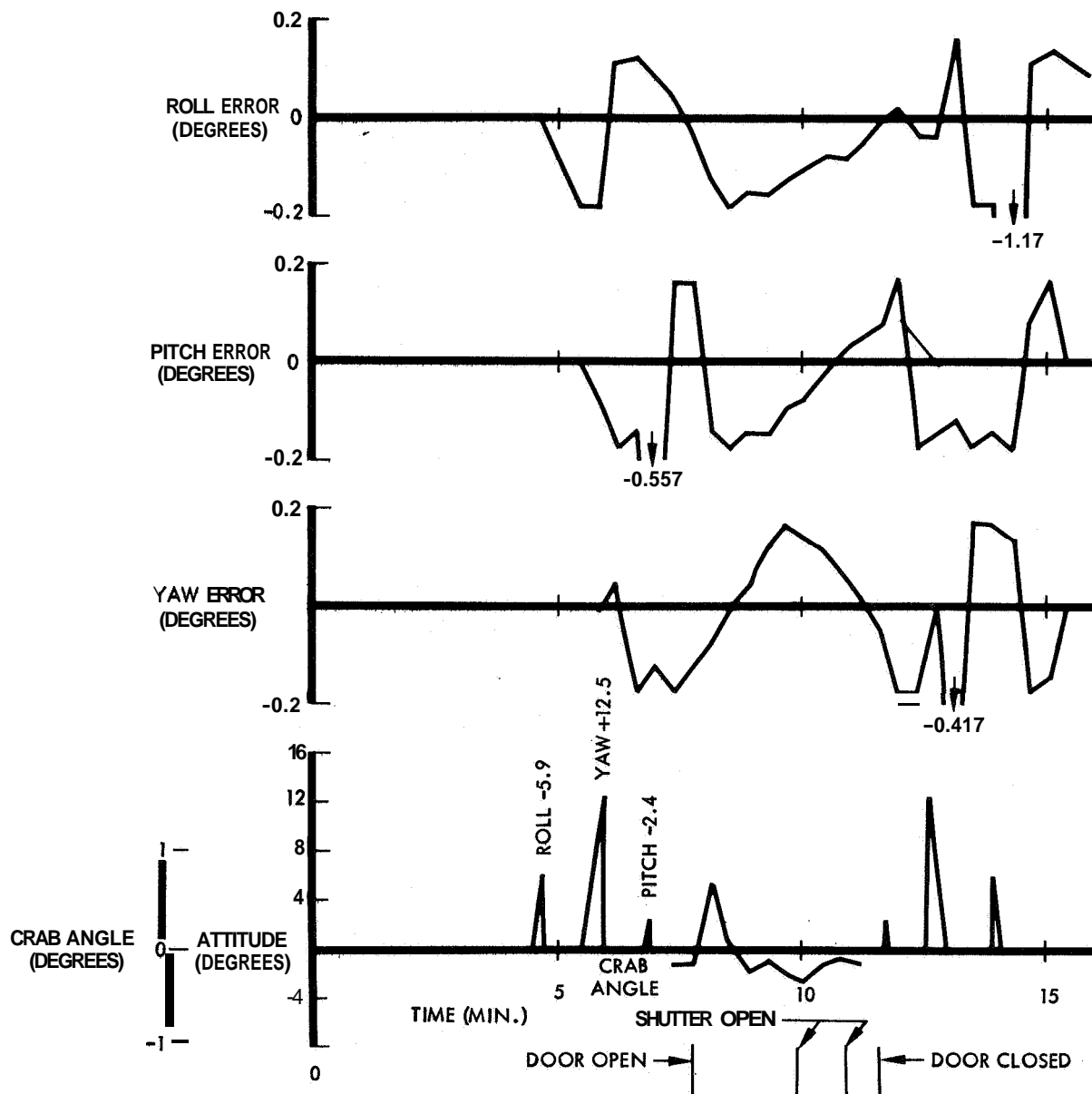


Figure 2.5-45: Gyro Position, Crab Angle, and Maneuver During Photography Site 1-4

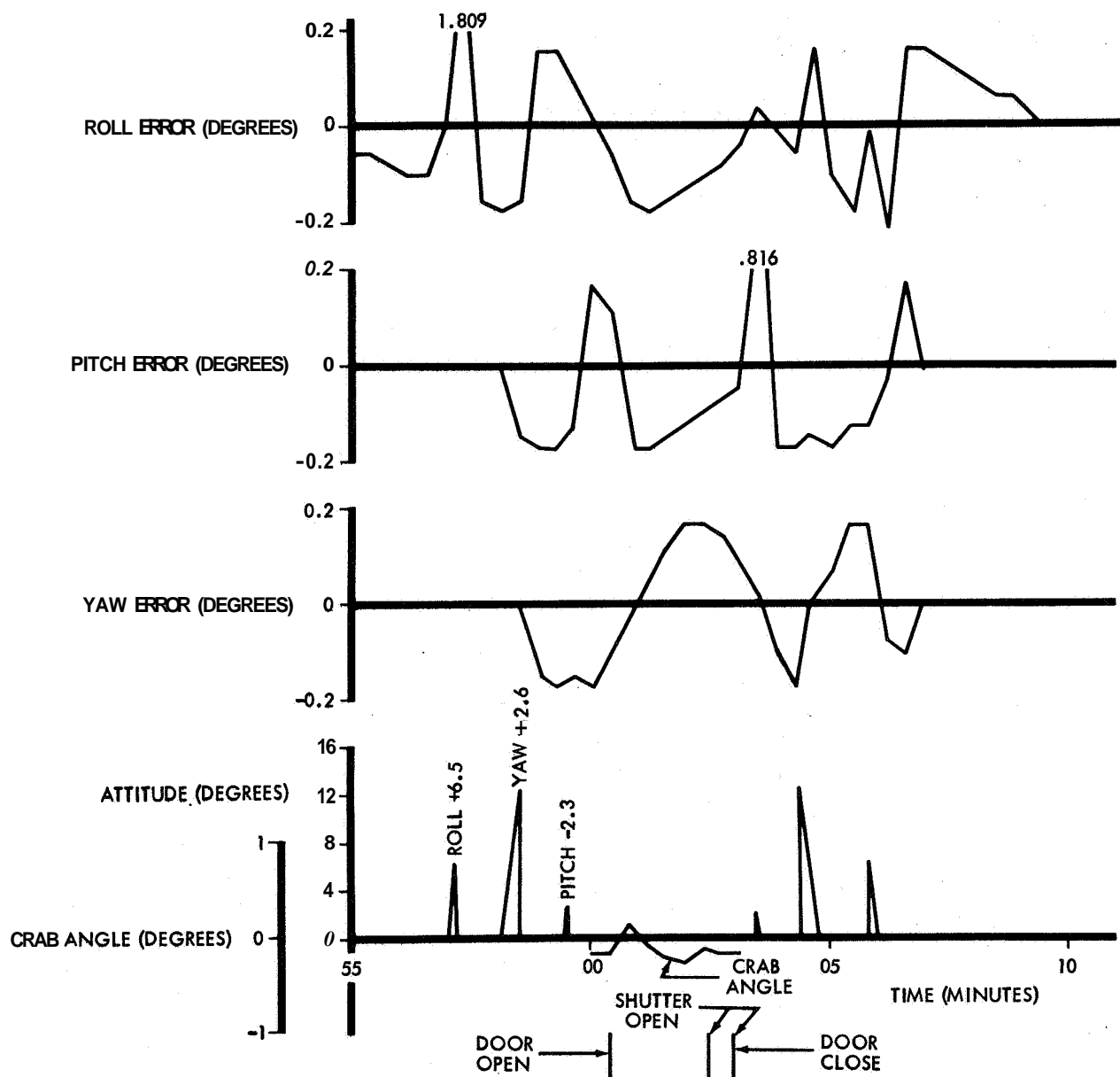


Figure 2.5-46: Gyro Position, Crab Angle, and Maneuver During Photography Site 1-5

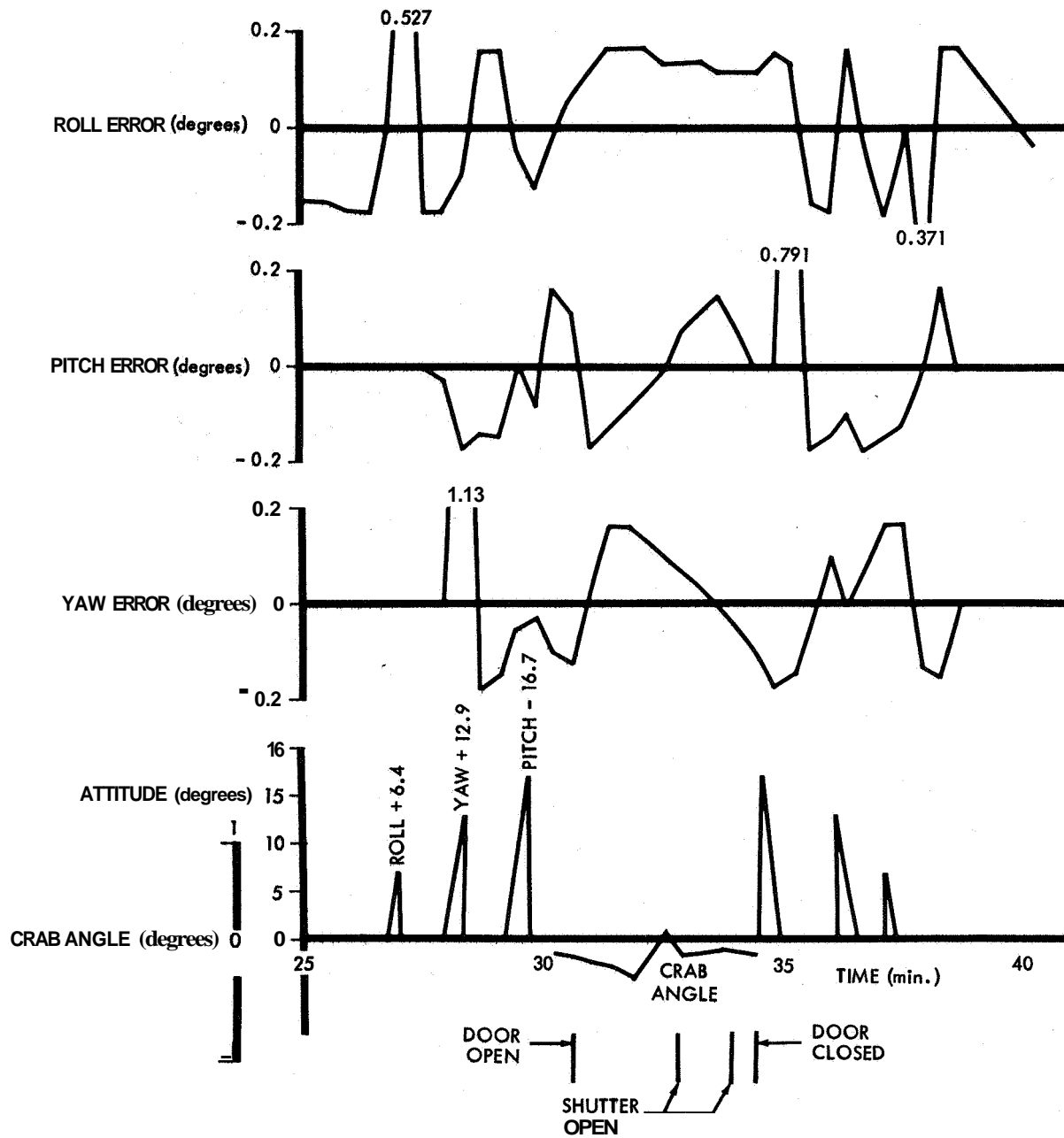


Figure 2.547: Gyro Position, Crab Angle, and Maneuver During Photography Site 1-6

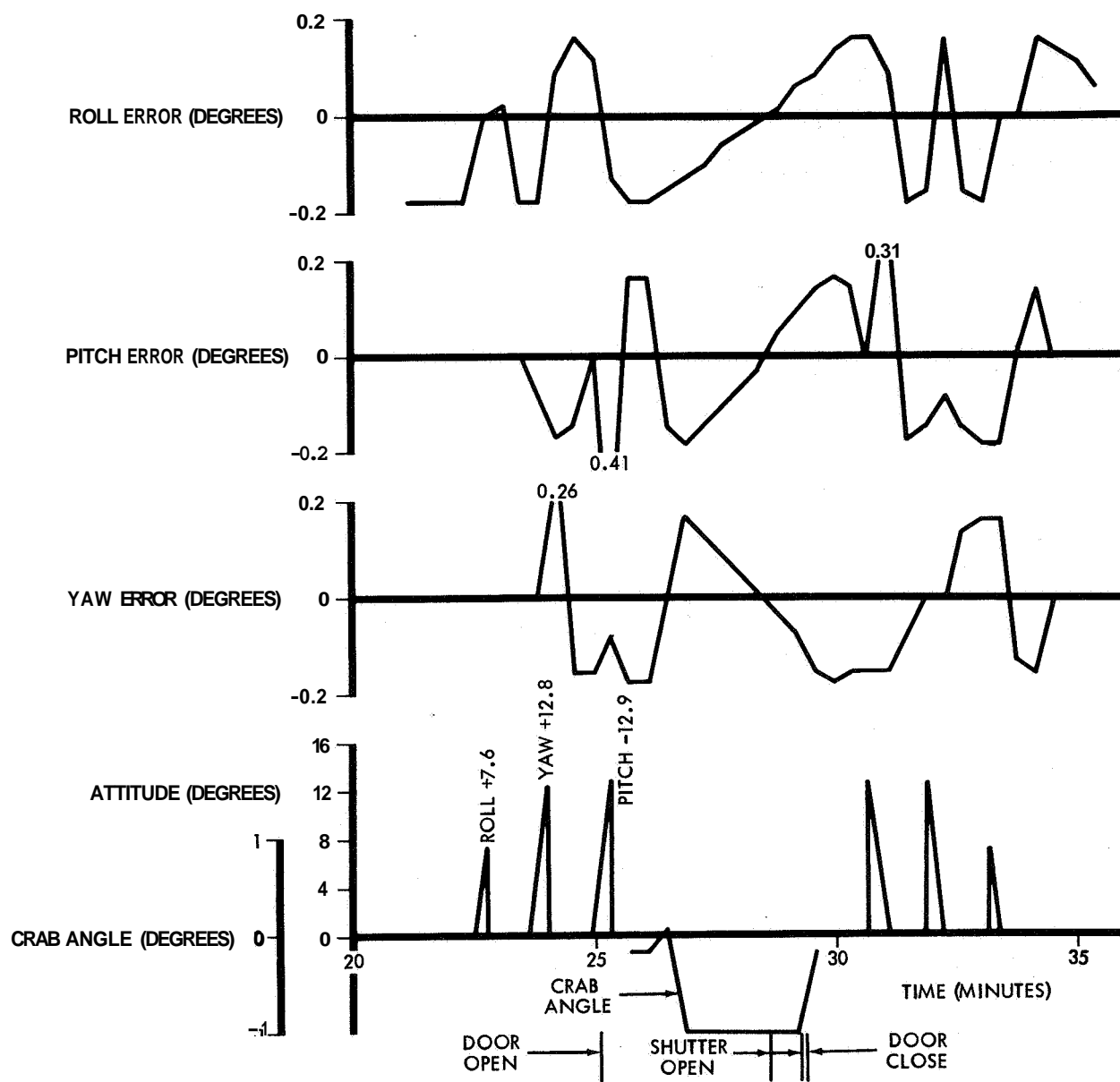


Figure 2.548: Gyro Position, Crab Angle, and Maneuver During Photography Site 1-7

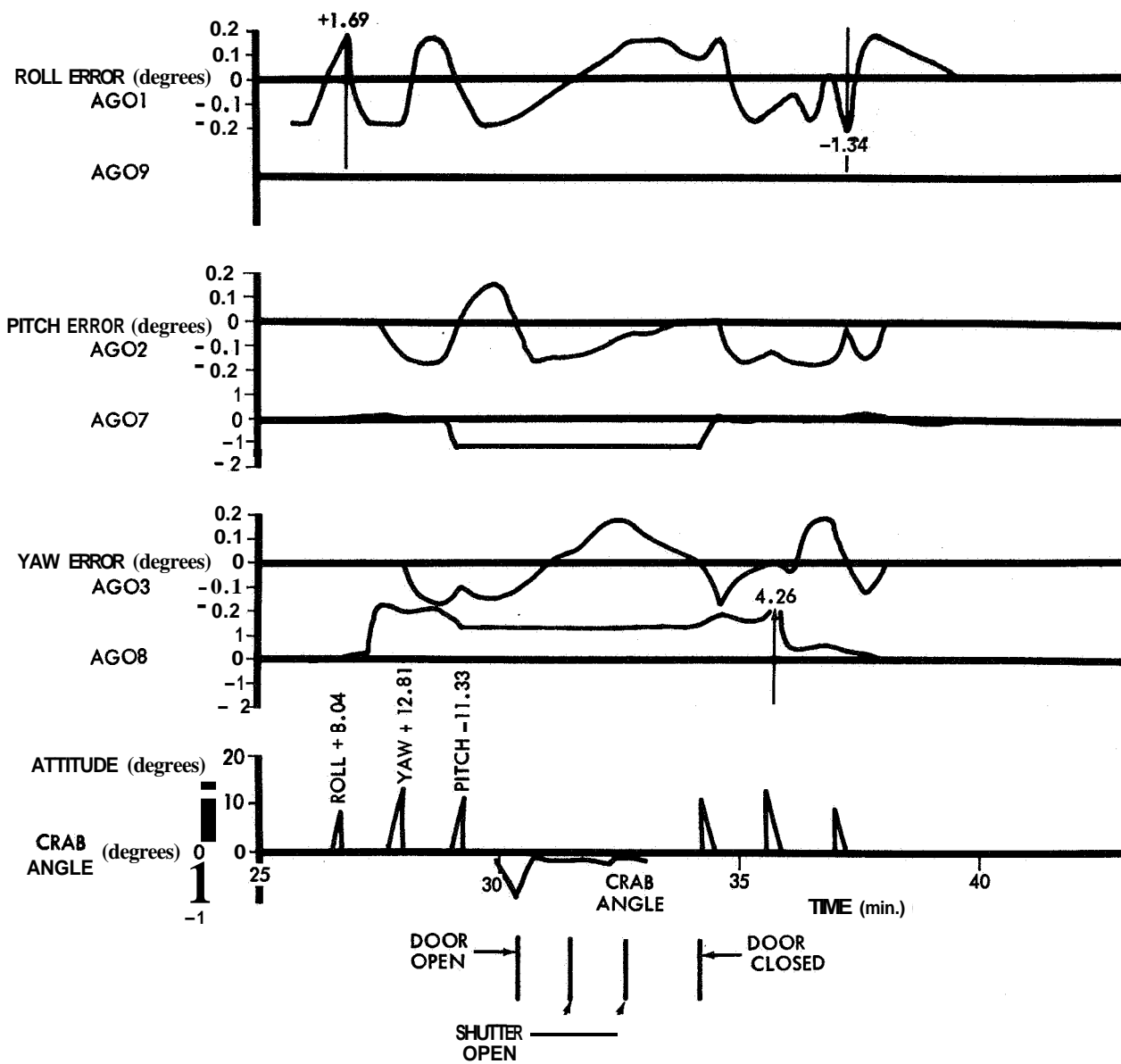


Figure 2.5-49 Gyro Position, Crab Angle, and Maneuver During Photography Site 1-8.1

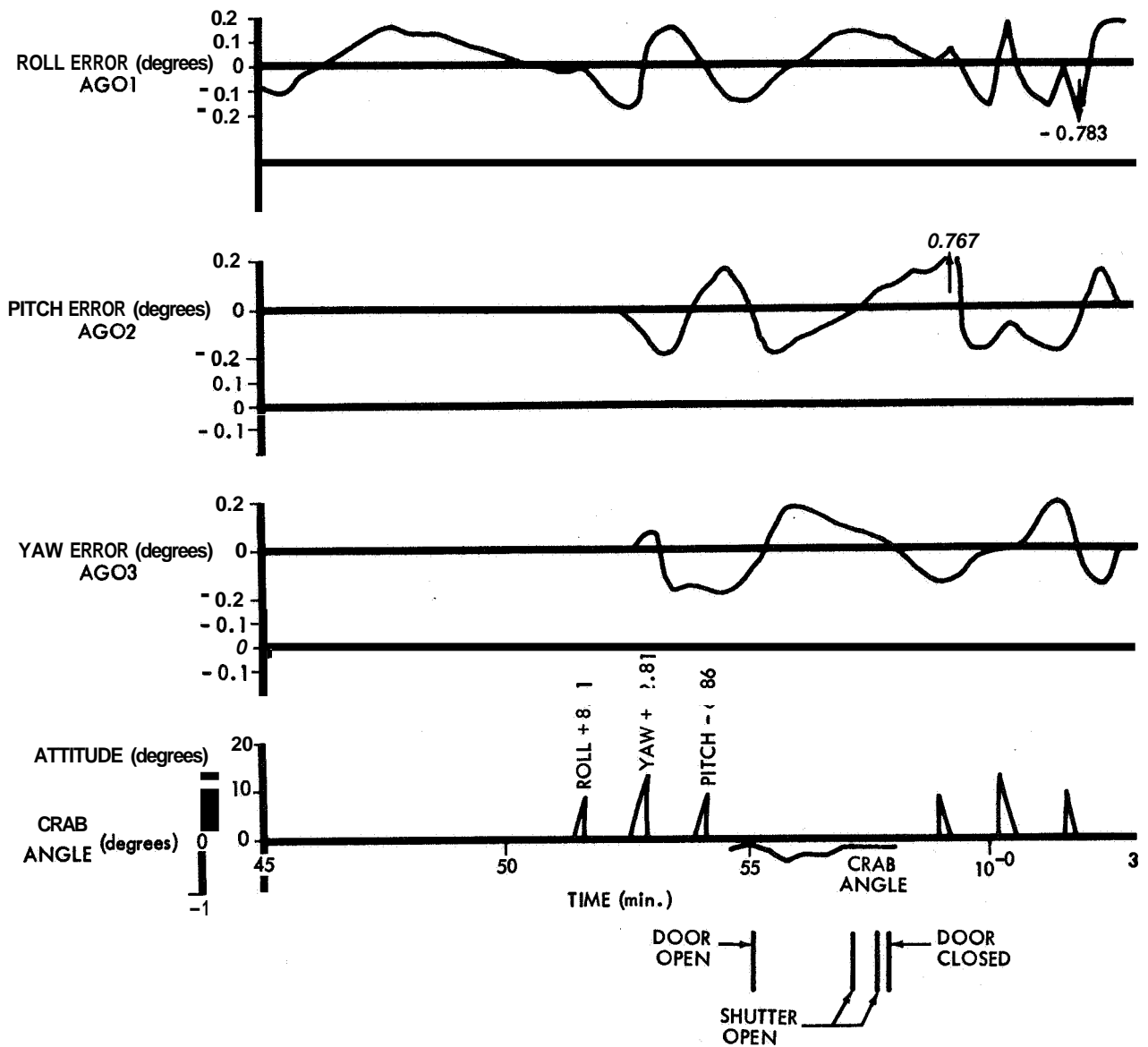


Figure 2.5-50: Gyro Position, Crab Angle, and Maneuver During Photography Site I-9.2a

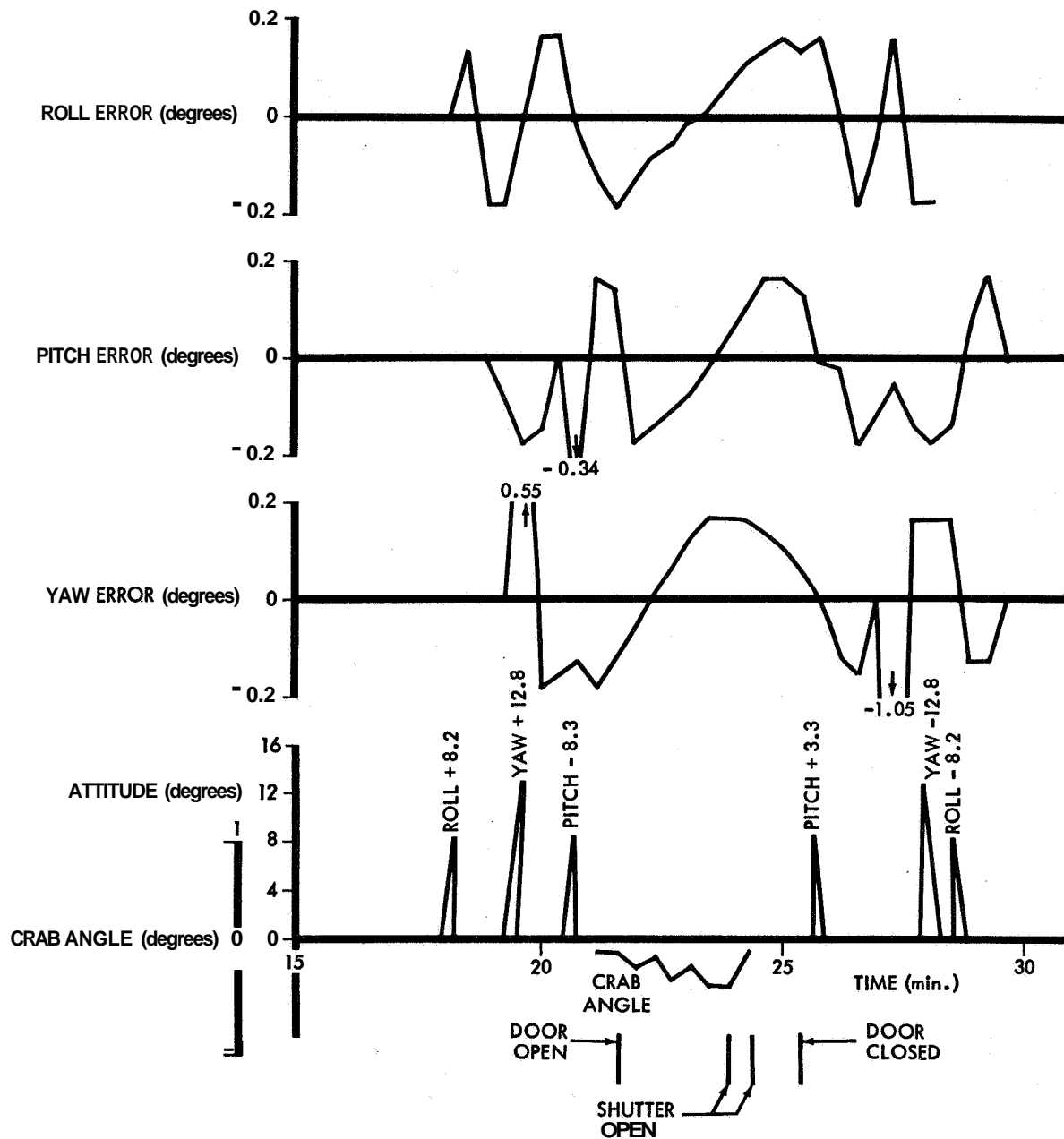


Figure 2.5-51: Gyro Position, Crab Angle, and Maneuver During Photography Site I-9.2b

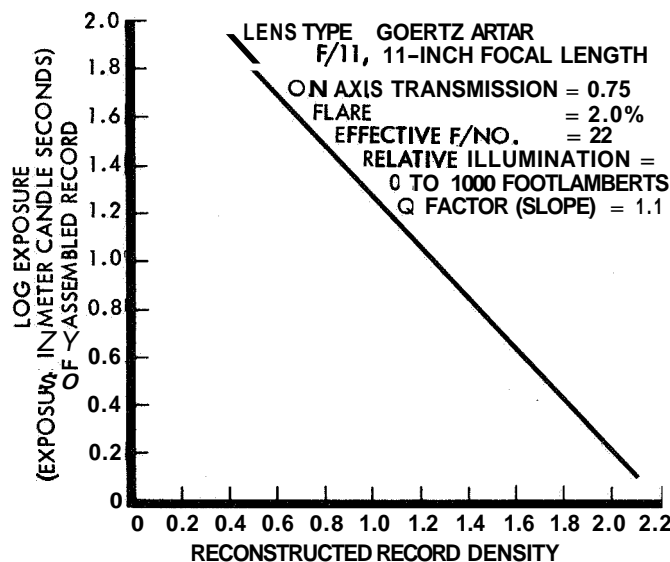


Figure 2.5-52: Reassembly Printer Transfer Characteristic

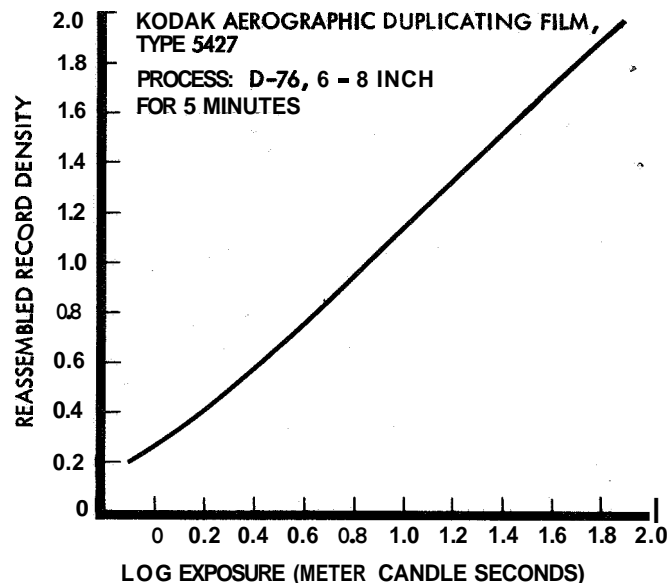


Figure 2.5-53: H & D Curve for Kodak Aerographic Duplicating Film, Type 5427

2.5.5 GROUND RECONSTRUCTION AND PRODUCTION

2.5.5.1 GROUND RECONSTRUCTION ELECTRONICS

Relative position of image points within the framelet is controlled by electrical scan linearity of the spacecraft scanner and GRE kine sweep circuits. Sweep should be linear within 4% in ground equipment. In practice, GRE linearity is checked by measuring the distance traveled by successive 50-Hz increments of a 400-kHz test signal across the image.

In the mechanical scan direction, the GRE camera drive moves the film 2.07 cm per second. The source frequency is 60 ± 0.0006 Hz, which drives a synchronous motor. A time track is written on the GRE film edge by a square wave derived from the 60-Hz drive; 120 cycles of this image are held to a dimension of 4.15 ± 0.00916 cm. In addition, scan nonlinearities in the mechanical scan drive of the optical-mechanical scanner will cause some error.

Reassemble Printing Characteristics

The transfer of reconstructed record density to reassembled record density is quite linear, as shown by the lens and film curves of Figures 2.5-52 and 2.5-53. Density points from these graphs are tabulated below.

Reconstructed Record (Positive)	Reassembled Record (Negative)
0.5	1.90
1.0	1.38
1.5	0.87
2.0	0.39

Signal Selector

In the GRE signal selector, the video signal is taken through the selector to one of two sync generators in the signal processing unit. (The selector also enables application of internally generated test signals to the GRE or

other communications equipment.) Some of the significant processing details include:

- 1) The sync pulse from the video signal, used to phase-lock on an internal oscillator, generates the master system timing pulse—appropriate blanking prevents locking to spurious signals. Noise spikes, etc., outside the desired video voltage range are suppressed by clamping the “back porch” of the sync and timing pulse waveform to the ground return and adding clipping circuits that compress (5:1) any video outside these levels. At a zero-signal (black reference) level, the kinetube spot intensity is maintained at a level that produces a 0.5 density on the recording camera film. The gain is adjusted so that a 5-volt (white reference) signal level gives a kinetube spot intensity that produces 2.0 film density. A typical waveform is shown in Figure 2.5-54.
- 2) Horizontal aperture equalization (HAE) provides up to 3:1 gain increase at 230 kHz (100 lines per millimeter). An amplitude-versus-frequency cosine function with linear phase characteristics (Figure 2.5-55) is obtained by comparing input and output gain characteristics of an unterminated half-wave delay line. The increased gain directly varies the contrast of high-frequency detail and substantially improves resolution (on the GRE film) in the direction of electrical scan. (There is little degradation of resolution in the mechanical scan direction.) Normal operation is with HAE set at 3:1 peaking.
- 3) A 2-MHz vertical spot wobble is introduced to compensate for the difference in thickness of the scan line in the spacecraft LST and the corresponding line on the GRE kinetube. Spot wobble increases the thickness of the kinetube scan line to expose more fully the area between successive traces and thereby decreases scan line modulation.

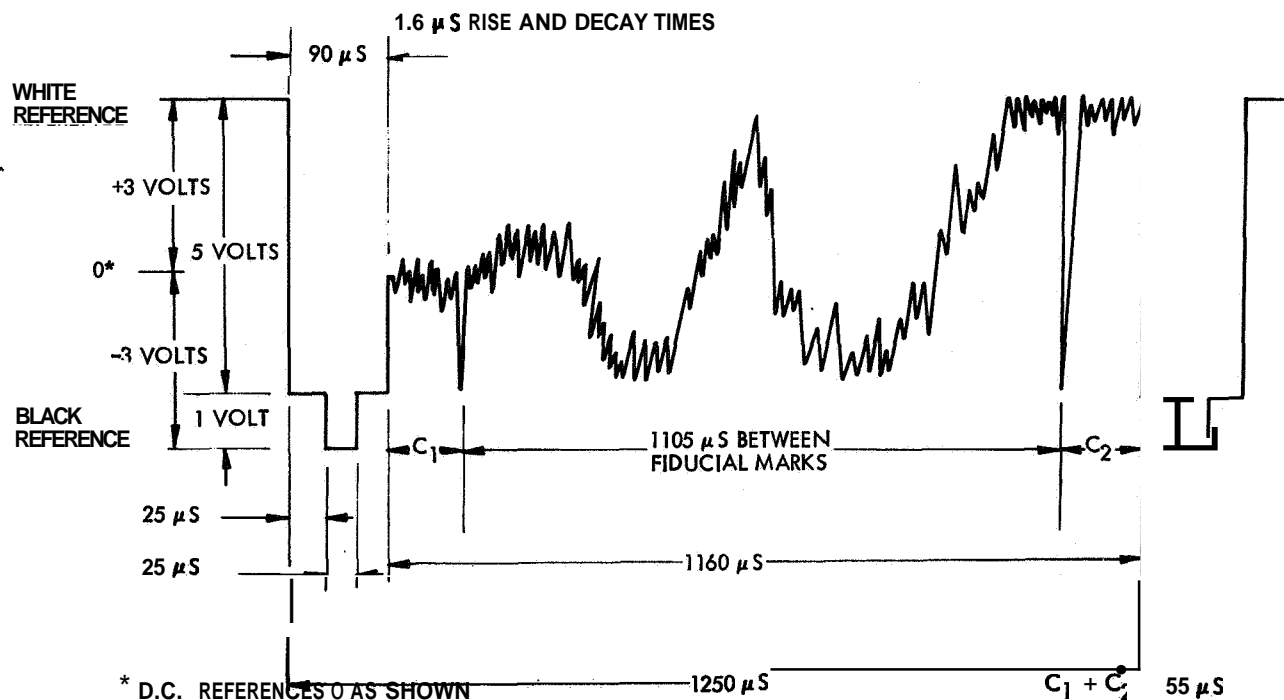


Figure 2.5-54: Video Output Waveform

Figure 2.5-56 shows microdensitometer scans with and without spot wobble; mechanical scan resolution is not significantly degraded with this amount of wobble.

Recording Camera

The recording camera records the horizontal line image, appearing on the kintube face on Type SO-349 television recording film. The geometry of the kintubeline image production is shown in Figure 2.5-57. The camera has a slowspeed drive of 2.07 cm per second. The drive sprocket and mechanical filtering rollers are shown in Figure 2.5-58. A roller on the front film edge (not shown) forces the film against the inside filtering roller flanges; thus, the film guides on one edge, forming an image positioning reference for photo reassembly. Possibility of error due to varying film widths is also decreased. In addition to the main image lens, there are two other sets of optics, one to record timing marks and one to record film identification numbers.

Timing and Identification

A squarewave output from a glow modulator tube is imaged through timing-channel optics onto the near edge of the film outside the sprocket holes to produce the 60-Hz time track indicated in Figure 2.5-57. The voltage source is the same precise 60-Hz source used for the camera motor; thus, variations in film speed can be measured.

An eight-digit code number is imaged through number-channel optics onto the far edge of the film outside the sprocket holes. Prior to recording, each readout sequence from the spacecraft is assigned a number that is manually set on a register in the camera base when the film is loaded. During operation, a flash-tube illuminates the register exposing the film at about 6-inch intervals for positive identification on all 35-mm GRE films.

2.5.5.4 FILM PROCESSING

The exposed GRE film is processed at the DSS, using a 35-mm batch processor capable of hot-processing 1000-foot rolls of film at 7 to 8 feet per minute. Developer and fixer temperature for the Lunar Orbiter processing is typically 98 to 100°F. The developer and fixer are continually agitated and percolated through filters and replenished from wall-mounted tanks as needed during processing. All processor chemicals are drained and replaced each week.

Sensitometer

The sensitometer provides standardized exposures on test film from which the correct temperature, speed, and replenishment rate necessary to obtain the proper H & D curve are established. The sensitometer electronics fire a small flash tube that passes a known amount of light through a calibrated Kodak Number 2 grey scale onto the unexposed film. Processing this known grey scale exposure and plotting the resulting densities provides the desired process-control information.

35-mm Quality Evaluation Viewer

This optical instrument is used for precision dimensional and density measurements on 35-mm film. It consists of a film-transport system, binocular microscope, densitometer, and a precision two-dimension measuring system. The base contains a fluorescent tube for examination by transmitted light. An additional spotlight provides top lighting for examination of the film surface. Longitudinal measurements to ± 0.0005 inch and lateral measurements to ± 0.001 inch may be made on this instrument. Magnifications of 10, 20, 30, and 40 diameters are available with the microscope. A Kodak Model 1 visual comparison densitometer is mounted on the instrument for convenient measurement of film densities. This densitometer is supplemented by a MacBeth TD-100 electronic densitometer.

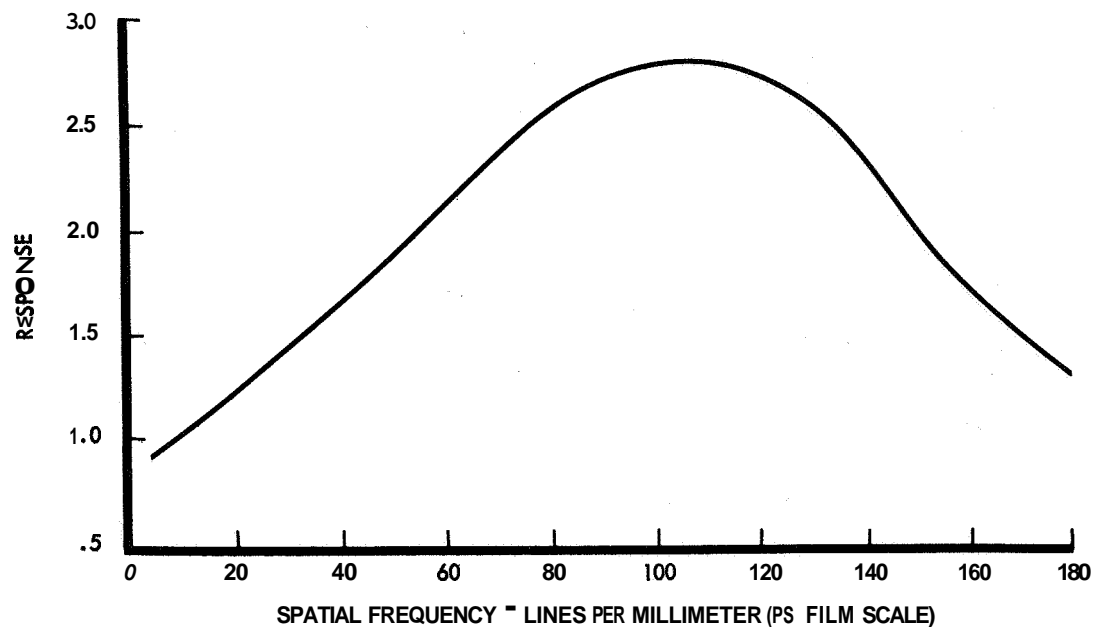


Figure 2.5-55: MTF of GRE Amplifiers with 3:1 Peaking

MICRODENSITOMETER TRACES ACROSS SUCCESSIVE SCAN LINES OF 35-MM FILM EXPOSED BY A STEADY VIDEO VOLTAGE LEVEL INPUT TO GRE
 MICRODENSITOMETER SLIT APERTURE: 10 X 200 MICRONS
 SCALE: 62.5 MICRONS PER INCH

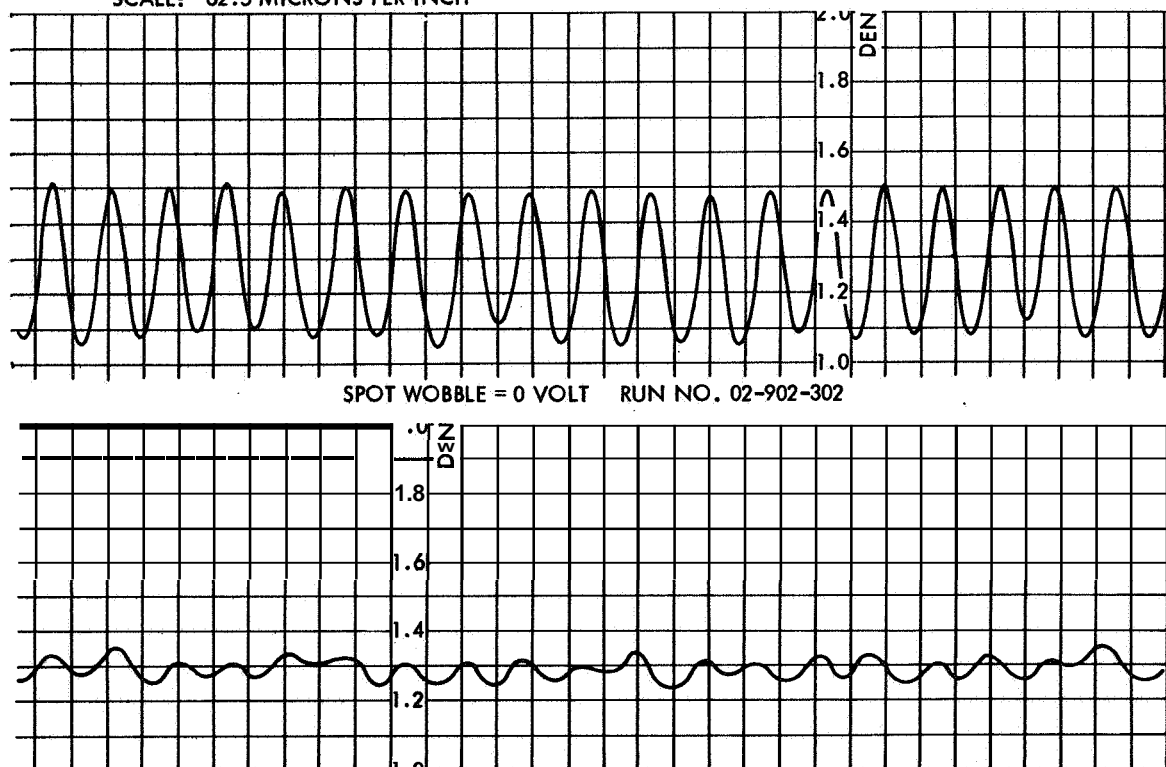


Figure 2.5-56 Spot Wobble

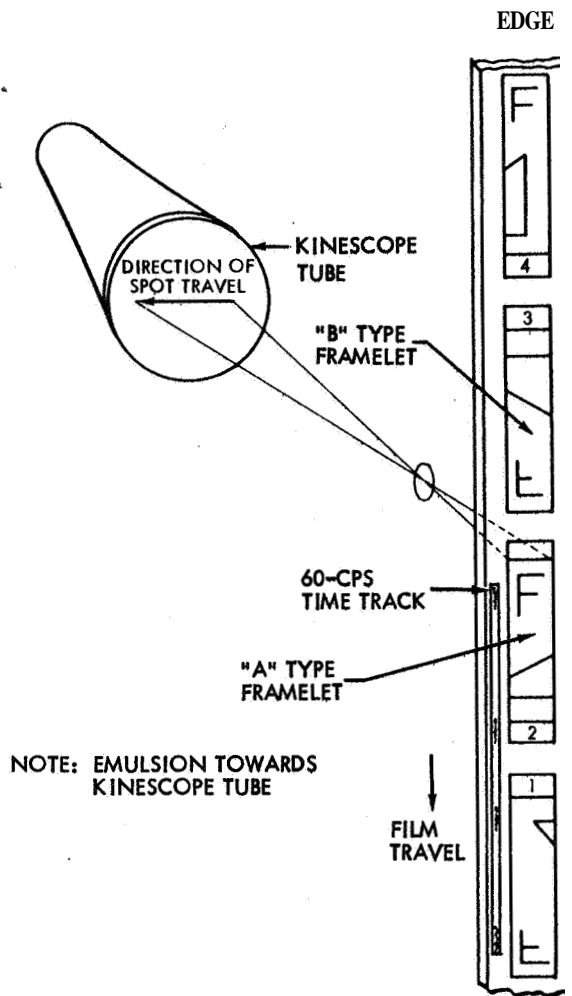


Figure 2.5-57: Geometry of Kinetube-line Image Production

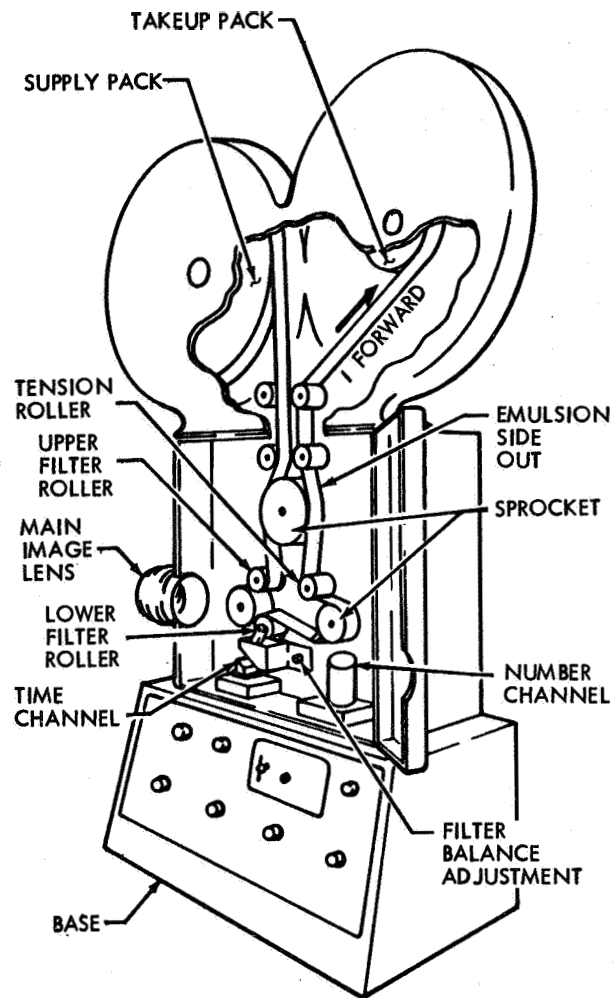


Figure 2.5-58 GRE Camera and Magazine Film-Threading Diagram

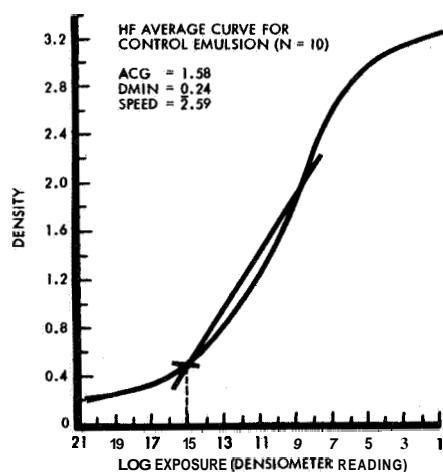


Figure 2.5-59: H & D Curve for 35-mm Processor Control SO-349

at each site, which affords more rapid, accurate reading of density step-wedges.

H&D Curve for 35-mm Processor Control

Adjustment of ground equipment for proper tonereproduction is keyed to the EG & G sensitometer at each location. Calibrated step-wedge exposures are put on the SO-349 film by means of the sensitometers, and 35-mm film processing is controlled to maintain the desired characteristics of the H&D curve shown in Figure 2.5-59. Primary control measurements are: (1) average contrast gradient (defined as the slope of the line between the 0.5 and 2.0 density intersections), (2) minimum density, and (3) speed (where speed is defined as the log-exposure value at 0.5 density). Having confirmed the H&D curve, the log E scale shows that a log exposure of 2.59 on SO-349 emulsion from the kinetube trace will produce the correct density on GRE film for black level (0.5 density). As shown for this control emulsion, 1.54 will produce the correct density on GRE film for white level (2.0 density).

2.5.5.5 RECONSTRUCTION CONDITIONING—GRS

GRE Signal Waveforms

With the processing curve determined, a series of density measurement tests identifies the correct combination of kintube bias and gain required to produce proper densities for specified GRE input voltages. When correctly adjusted, stairstep and bar test signals—diagrammed in Figure 2.5-60—will produce film densities of 0.5 ± 0.05 and 2.0 ± 0.1 . To adjust the gain in repeatable fashion, an electroluminescent panel is used to calibrate the photomultiplier that monitors the kintube. The photomultiplier output for a known light input is thus established, and the photomultiplier output relative to this value is used to set kintube bias and gain repeatably for correct black-and-white level exposures.

By exposing processing-wedges from the sensitometer and test signals from the GRE on the ends of the GRE operational film, it is possible to determine—in conjunction with the pre-exposed edge data on the flight film—whether a tone reproduction discrepancy is in the ground reconstruction electronics, ground processing, or in the spacecraft system.

Pre-Exposed Edge Data

The edge data grey scale densities as they appear on processed 70-mm film are shown in Figure 2.5-61. Step 2 of the grey scale is the same density as the background, in the area of the focus line. This background density (0.3 ± 0.05 readout density on the spacecraft film) corresponds to white level. The density range of this gray scale on spacecraft film is greater than the density range that can be transmitted through the overall system, thus the first and last steps normally are clipped by the GRE. With optimum density control, however, Step 1 will still look a little darker than Step 2. Density transfer from spacecraft film to GRE film is shown in Figure 2.5-61 as follows:

Grey Step Number	SO-243 R/O Density Range	Reconstructed Record Density Range
1	0.21-0.29	Clipped by GRE
2	0.26-0.34	1.89-2.11
3	0.34-0.42	1.64-1.82
4	0.45-0.57	1.33-1.49
5	0.61-0.73	0.98-1.13
6	0.82-0.94	0.66-0.80
7	1.05-1.21	0.50-0.60
8	1.32-1.48	0.42-0.50*
9	1.40-1.56	Clipped by GRE

* May be clipped

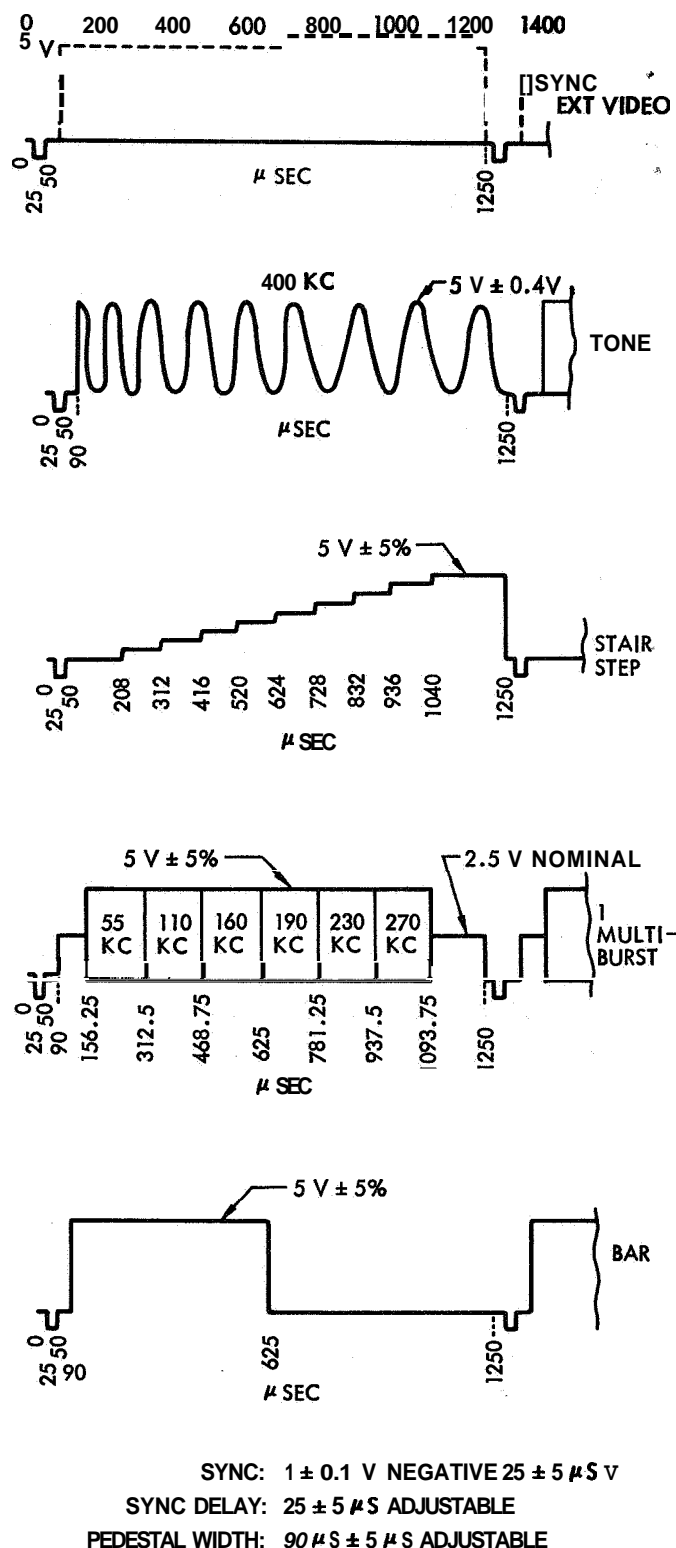


Figure 2.5-60: Composite Signal Generator Waveform Diagrams

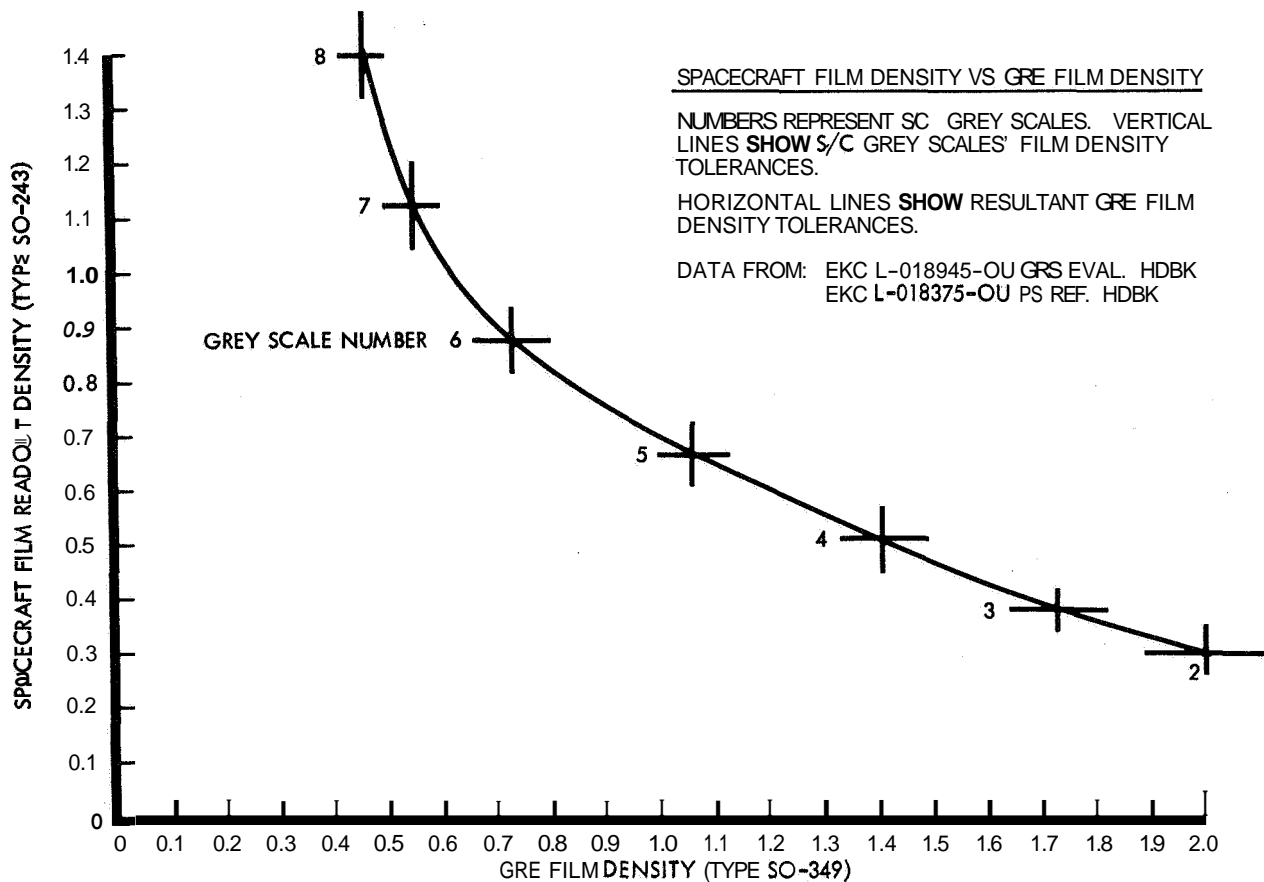


Figure 2.5-61: Spacecraft Film Density vs. GRE Film Density

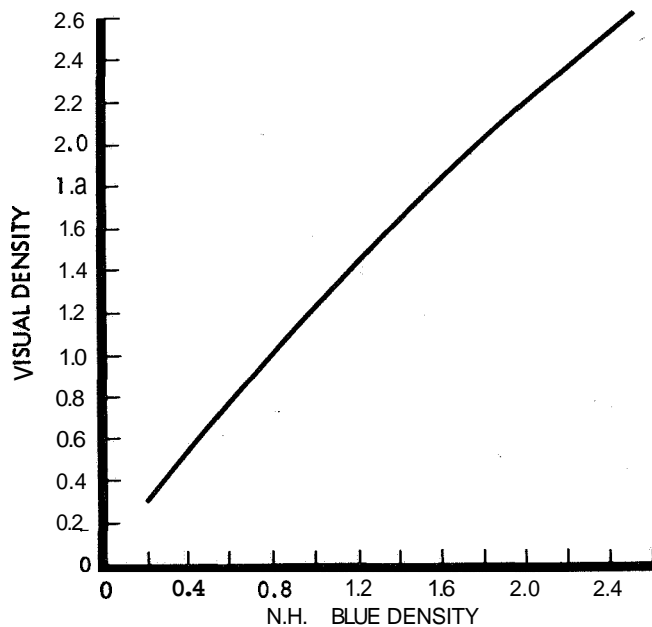


Figure 2.5-62: Relationship Between N.H. Blue and Visual Densities for Bimat Processed SO-243

Since the SO-243 film in the spacecraft is scanned by light from a P-16 phosphor, the apparent film density is dependent on transmission of the film to light of that spectral distribution. This is different from the density that the film would appear to have using standard densitometer illumination as shown in Figure 2.5-62. Hence, visual densities on the 70-mm film are converted to readout density to reflect the way in which film densities actually affect the phosphor scan readout of the SO-243 film.

Video Signal Focus Conditions

Focus of the line scan tube is adjusted by command to the spacecraft until optimum waveform is achieved. Before readout starts, the LST electrical scan is in the focus-stop position: that portion of the edge data with the diagonal lines. Gain is adjusted so that the range of 1.3 to 0.3 density on the spacecraft film corresponds to 0 to 5 volts video signal amplitude from the scanner. An image density of 1.3 or greater essentially blocks the readout light-beam to produce a zero video signal. The video gain must be adjusted until light from the beam passing through 0.3 readout density is equal to 5.0 volts. The film background readout density is $0.3 \approx 0.05$ in the focus stop position. Thus, after communications system gain calibration has been set from the sync pulse amplitude, spacecraft gain is set so that 0.3 readout density in the focus stop position is equivalent to a 5.0-volt video level. Focus conditions are illustrated in Figure 2.5-63.

Modulation Transfer Function of GRE Camera Lens and Film

System resolution of targets on GRE film is not appreciably degraded by the GRE camera lens or the GRE film. At 76 lines per mm—corresponding in a nominal 610-mm photograph to 1-meter resolution on the lunar surface—modulation transfer function, Figure 2.5-64, shows a 93% response; at the same point on SO-349 or 5374 film, it is approximately 99%, as shown in Figure 2.5-65. Due to the system magnification factor of 7.2 diameters, this degradation is actually only 10 lines per mm on the GRE film. The lines-per-millimeter scale shown is in terms of equivalent spacecraft lines per millimeter. A normal focus and resolution test of the GRE, using the composite signal generator, requires that the cycles of a 400-kHz tone signal be clearly resolved. This is equivalent to 174 lines per millimeter on the spacecraft film or twice the frequency of the specified system resolution pattern (76 lines per mm).

2.5.5.6 PHOTO REASSEMBLY

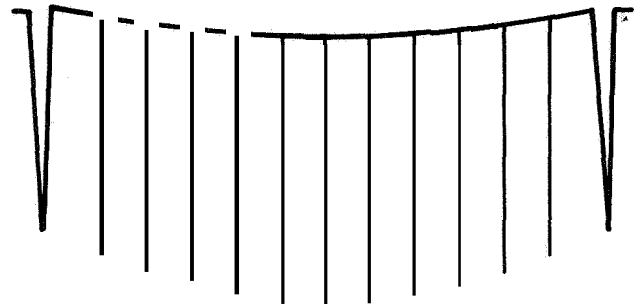
All 35-mm film developed at the DSS is sent to Eastman Kodak at Rochester, New York for reassembly and reproduction into the negatives, positives, and transparencies required for final data analysis and reporting. Reassembly is performed in the reassembly printer.

Reassembly Printer

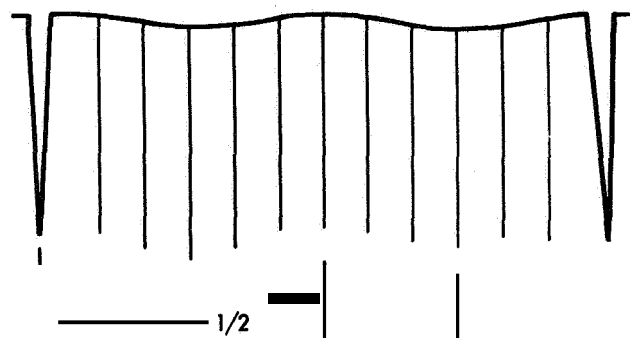
The reassembly printer produces a 16-cm record on 24.2-cm film by conventional photographic process printing from the 35-mm GRE film. Since the framelets of the 35-mm film are alternate, every other framelet must be transferred to the printer. This is done using two rear-illuminated exit gates. The film is fed upward through the A gate, and the process proceeds downward through the B gate. The film emulsion faces the lens in the A gate, and the base side of the film is in the B gate. Two flash tubes, triggered from the reassembly printer reference line in the edge data, fire almost simultaneously to print both A and B framelets. Tilt data for the reassembly subframe is again from the framelets.

AS VIEWED AT THE D.S.I.F. GRE VIDEO MONITOR
OSCILLOSCOPE

MAXIMUM FOCUS



OPTIMUM FOCUS



MINIMUM FOCUS

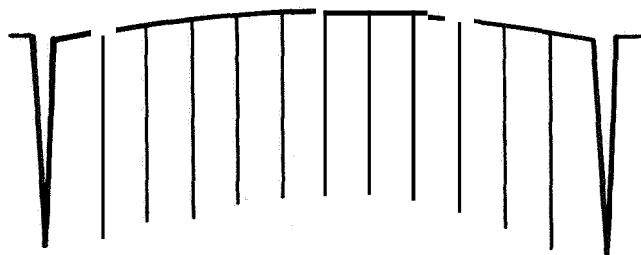


Figure 2.5-63 Video Signal Focus Conditions

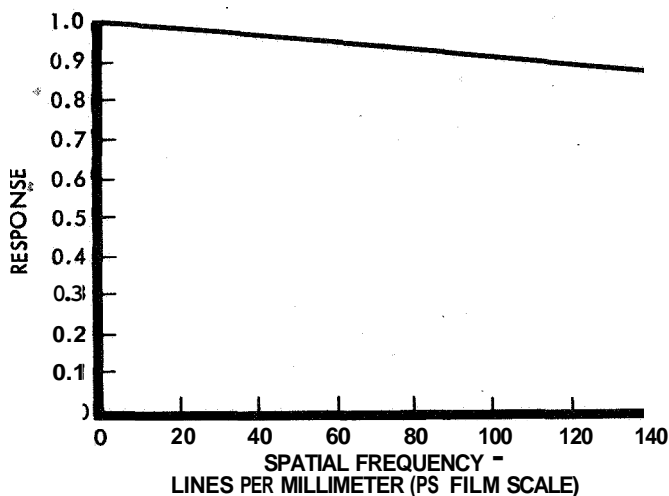


Figure 2.5-64: Modulation Transfer Function of GRE Camera Lens

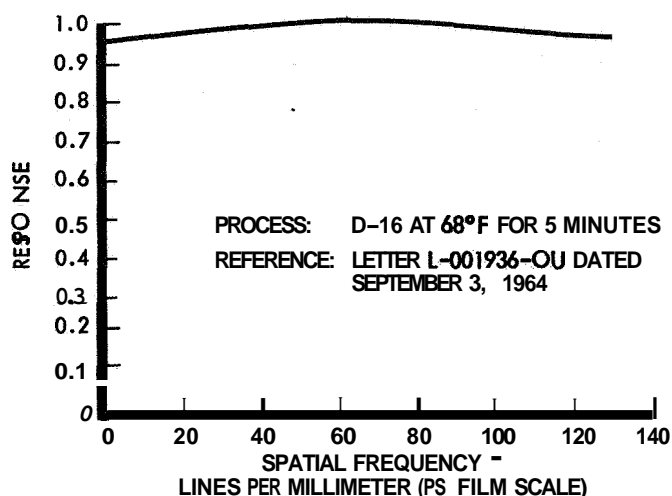


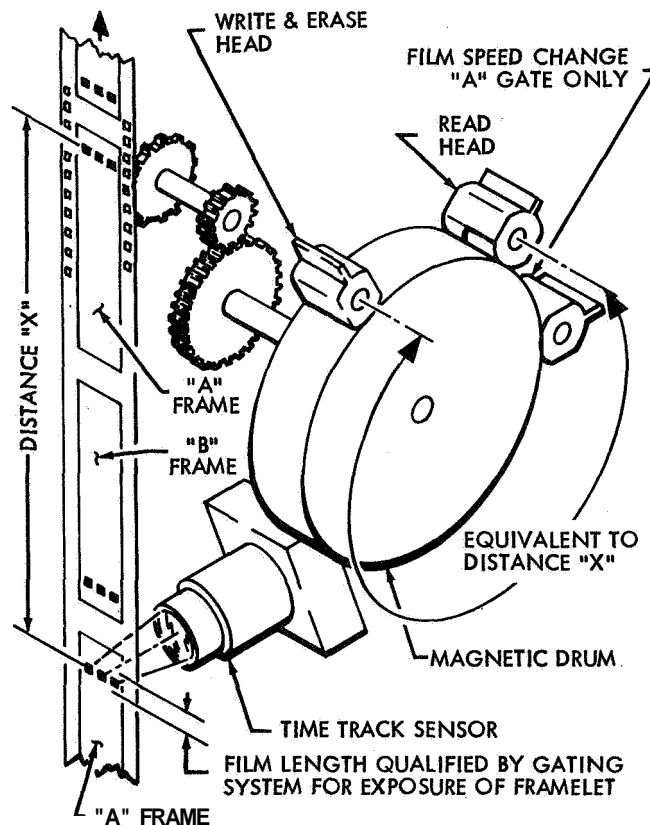
Figure 2.5-65 Modulation Transfer Function of Eastman Television Recording Film Type 5374

The framelet image is projected onto the 24.2-cm film by a 28-cm-focal-length Goertz Artar $f/11$ lens via two first-surface folding mirrors. Adjustment is provided in the lens mount as well as in the 35-mm film gate to control magnification and focus. There are identical projection systems for each gate. In the reassembly printer gate, only 1.83 cm of the image width is projected.

A reassembly subframe may contain up to 14 framelets. To print the framelets adjacent and parallel to each other, the 24.2-cm film carriage moves laterally with respect to the optical axis. Both A and B framelets are printed at each carriage position, except in the first and last position where only one framelet is printed; thus eight carriage positions are required to print 14 framelets. At least two subframes are required to reassemble a photo from the 80-mm lens, and at least seven for a photo from the 610-mm lens. The last two framelets of a subframe are repeated as the first two framelets of the next subframe for ease of reassembly.

An opaque mark placed on the primary record film cues the reassembly printer. As the primary record film advances, interruption of a light beam passing through the film produces an electrical signal to start the printing sequence. After a 14-framelet printing sequence, when the mark for the next subframe is detected, the primary record is moved backward the length of two framelets and the sequence continues.

The primary record film advances continuously during a printing run. Nominal velocity is 15.24 cm per second between framelets, slowing to 3.31 cm per second for each exposure by an electronic flash tube. The A and B gates have independent flash tubes and sensing systems for film positioning. In addition, two metering systems gate their respective reference-lines sensors and vary the film advance speed. The metering system diagrammed in Figure 2.5-66 consists of a magnetic drum, geared to run in synchronization with the film, on which a magnetic mark is placed at the time the xenon flash tube is fired. This mark, after a 270-degree drum rotation, produces a trigger that slows the film drive to 3.31 cm per second. This mark is again sensed in time to gate the reassembly reference-line sensor on. The mark is then erased and a new mark is generated as the sensor detects the next reference line and fires the flash tube.



EASTMAN KODAK COMPANY

Figure 2.5-66: Reassembly Printer Gating System

Film Format

The film in the spacecraft is scanned physically beyond the photographic image and edge data. Distance between fiducial marks is 0.254 ± 0.00254 cm and width of the electrical scan is $0.267 \text{ cm} \pm 0.00254$ cm, requiring 1160 ± 12 microseconds. GRE film dimensions are $1.922 \text{ cm} \pm 0.00762$ cm wide, with fiducial mark spacing of 1.83 ± 0.0185 cm. The GRE film image is reduced in the reassembly printer by a factor of 0.893, making the fiducial spacing 1.64 cm on the reassembled negative. The 35-mm film edge is masked to the fiducial line by the reassembly printer and the film loses GRE identification except for the reassembly title block. Edge data from the 70-mm film, however, is printed at the bottom of each reassembled framelet.

The reassembly printer is designed to provide side-by-side gap overlap of 0.00331 cm. The vertical alignment tolerance between adjacent framelets must be such that the reassembly printer reference lines are not offset by more than 0.0254 cm. Since 1 meter on the lunar surface is 0.00864 cm (on the reassembled photo) tolerance limits from the reassembly process of about ± 0.5 -meter horizontal overlap of gap and ± 3 -meter vertical registration error are indicated.

Reassembled Film Format

System magnification from the spacecraft to GRE film is determined by the fiducial mark spacing on the LST drum. The spacing tolerance between lines is $\pm 1\%$, or $1.83 \text{ cm} \pm 0.0185$ cm on the GRE film. Fiducial mark centering tolerance in the readout process is ± 7 microseconds, or 0.01275 cm on the GRE film. In practice, scan line length (including the 2.5% overscan) and distance of the scan line from the guide edge of the GRE film are the dimensions maintained on GRE film to permit proper operation of the reassembly printer. These distances are 1.922 ± 0.00762 cm and 0.789 ± 0.00762 cm. They are measured on test film made from GRE internal test signals and are a part of routine checkout of the GREs.

The modulation transfer function of the Goertz Artar lens in the reassembly printer should be at least as flat as the camera lens out to 10 lines per mm. Kodak aerographic duplicating film Type 5427 processed in D-76 has approximately a 99% response out of 10 lines per mm (i.e., 72 lines per mm on the spacecraft film). Hence, in terms of resolution, the reconstruction and reassembly introduce practically no degradation, provided density and contrast controls are maintained.

Resolution performance of the complete readout system can be monitored from resolution bars in the pre-exposed edge data diagrammed in Figure 2.5-67. These patterns are not the standard resolution targets used in test programs to evaluate system resolution, but they do provide a good reference for determining any significant change in resolution. In typical system testing, targets up to 100 lines per mm have been resolved.

Resolution from FR-900

Very little resolution degradation is experienced by first recording the electrical signals on the FR-900 and then playing it back to the GRE. Within limitations of the reproduction processes, complimentary images of edge data are essentially identical.

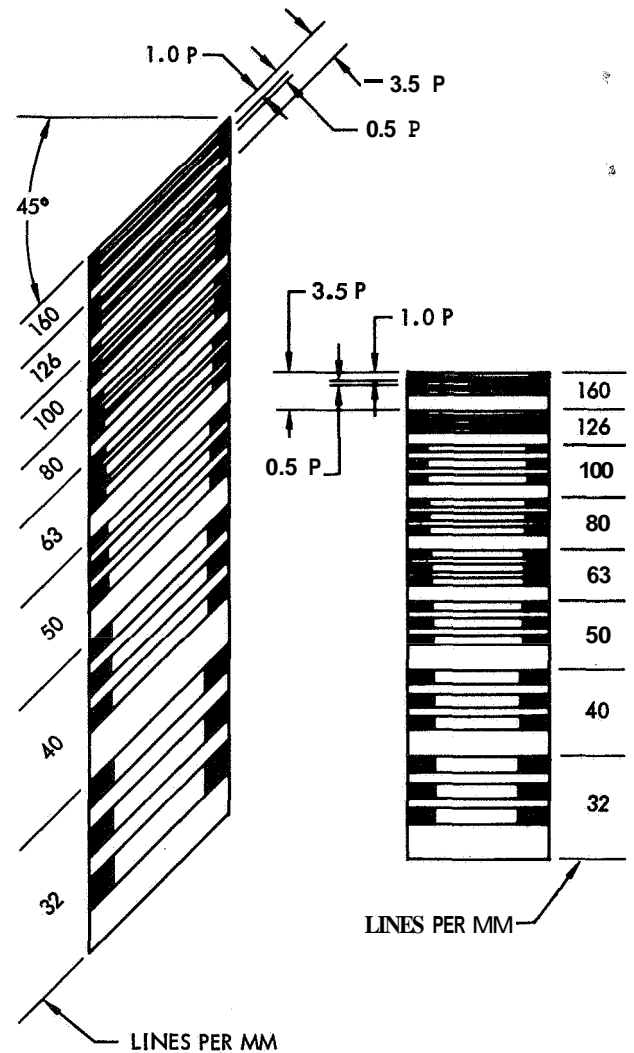


Figure 2.5-67: Edge Data Test Pattern; Horizontal and Diagonal Groups

2.5.5.7 CONCLUSIONS

Photographic reconstruction performance during Lunar Orbiter Mission I resulted in excellent medium-resolution-camera film records; the high-resolution readouts were also of excellent quality when camera operation was normal. The GRS equipment performed well, generally, at each DSS. Problems with hardware were minor and involved only component parts failures (one 12AV7 vacuum tube at DSS-41 and two R-1131-C glow modulation tubes at DSS-41 and DSS-61) during the entire mission.

The 35-mm film processor equipment proved rather troublesome in operation; however, work-around methods resulted in good-quality photo production. Experience with the GRS equipment promoted procedure changes and standardized operations for all ground stations.

2.6 LANGLEY RESEARCH CENTER OPERATIONS

NASA has established a Photo Data Assessment Facility at Langley Research Center. This facility consists of two basic elements:

- 1) Equipment for the generation of film from magnetic tape;
- 2) Equipment for evaluation and use of lunar photographs.

The Boeing Company assisted NASA in establishing the Photo Data Assessment Facility by installation and check-out of playback equipment and film generation and processing equipment and also by the procurement of the equipment necessary for film evaluation and use.

2.6.1 VIDEO TAPE LAYBACK EQUIPMENT

The equipment installed at LRC consists of a video magnetic playback subsystem and two ground reconstruction electronics (GRE), with associate test equipment. The playback subsystem employs two Ampex FR-900 video tape recorders and detection and discrimination equipment similar to that used in the three DSIF sites. The GRE are identical to those used at the DSIF, except that they have been modified to place the NASA time code on the film in lieu of 60-cycle timing used at the DSS.

The data source for the video tapes used at LRC is single FR-900 video tape recorders located at the three Deep Space Stations. These stations provided a total of 267 magnetic tapes during the first mission, including 58 tapes made during priority readout. The first tape from Goldstone and Madrid contained calibration information read out from the Goldstone test film in the spacecraft.

Output of the playback equipment, including GRE, for each original tape from the Deep Space Stations was planned to be as follows:

- 1) A duplicate copy of the original tape (10-Mc tape copy);
- 2) Tape containing only video data from the original tape (analog tape copy);
- 3) One GRE film to accompany the analog tape copy;
- 4) Two additional, lower priority GRE films for use by USGS and ACIC.

After experience in the first mission, the actual output of

the facility was modified to include all the items originally planned and in addition the following two items:

- 1) One additional GRE film for the Lunar Orbiter project office library;
- 2) Selected additional GRE films to support the screening teams that formed a part of the evaluation and use of the photo data at LRC.

As of November 10th the following data have been produced:

- 1) 10-Mc tape copies (95);
- 2) Analog tape copies (170);
- 3) GRE film, all types (854)
(from 272 original tapes).

2.6.2 VIDEO EQUIPMENT

Equipment installed at LRC to assist in photo data assessment includes the following: light tables, optical viewers of several types, automatic density plotters (Isodensitracers), and photo processing equipment. This equipment, except for the Isodensitracers, is maintained and operated by the government.

The screening of lunar photographs was directed toward several results, including Surveyor landing site selection, Apollo landing site selection, and photo site selection for future lunar orbital spacecraft.

2.6.3 PHOTOGRAPH ENHANCEMENT

A technique was developed at Langley Research Center to enhance detail in overexposed moderate resolution photographs. The technique involved the use of cascading amplifiers between the FR-900 tape playback and the GRE to obtain an amplification factor of about 2. The increased gain increased contrast in the overexposed areas sufficiently to bring out detail not otherwise evident. The gain in detail in the overexposed areas was, however, at the expense of loss in less exposed areas. Use of the enhanced photographs together with those prepared by standard procedures thus extended the range of information available for interpretation. The technique further reduced or eliminated the difficult problem of deriving information from the smeared 610-mm photographs.

2.7 HIGH-RESOLUTION FILM-SMEAR ANALYSIS

In the analysis of the image smear occurring in the high-resolution photographs, the items of prime importance were the amount and direction of smear and the displacement of the high-resolution principle point with respect to the medium-resolution principle point in the medium-resolution format. This analysis is still in progress; the final report on the problem will be released at a later date. Fifty-eight of the 211 frames have been analyzed. For the image motion compensation (IMC) smear, the measurements were taken along the velocity vector. For the film advance smear, the measurements were also taken across the velocity vector.

The displacement measurements have considerable range. The principle point of the high-resolution photograph is displaced from a low value of 1.1 mm, as projected on the medium-resolution format, to a high value of 4.3 mm. The average falls at 3.4 mm. This represents 159 milliseconds timing error and is in the direction of early triggering. Under normal operating conditions, the 610-mm-lens shutter would be actuated 40 milliseconds before the 80-mm-lens shutter.

The above measurements should be corrected for reading inaccuracies of ± 0.85 mm. This takes into consideration inaccuracies of reading the millimeter grid crater outline change due to lack of photographic control on the prints, inaccuracy in the grid itself, and positioning of the grid on the medium-resolution photographs. Assuming that this error adds to the displacement error, the resultant displacement would be 4.4 mm or 199 milliseconds. If the worst case is considered, then the total displacement is 5.15 millimeters.

To determine where the shutter is triggered in the photographic sequence, a plot of platen displacement versus time is drawn, as shown in Figure 2.7-1. On this plot, starting with the known point where shutter mechanism is initiated, the 80-mm-camera shutter position can be determined. The 610-mm-camera shutter triggering position then is determined using the displacement data. Assuming worst-case displacement of 5.15 mm, the trigger position would be coincident with the film clamp operation in the photograph taking sequence.

Film smear measurements taken fall into three categories: (1) the platen was traveling in the reverse direction and the smear is more than would have been if the V/H was shut off; (2) the V/H was off; and (3) the V/H was off but there is film advance smear. The frames with film advance smear have an average displacement of 17.57 mm or 823 milliseconds early. This is without the reading error added in. The smear in IMC direction for the sites averages out to 4.7 mm. This excludes the in-between site frames and those that have film-advance smear.

Two additional discrepancies were noted during the analysis. So far, it has been impossible to determine where high-resolution Frames 105, 118, 141, 184, and

200 were taken. The shutter was triggered early for these frames, probably about the time when V/H was turned on (this starts the film damp operation). The other discrepancy is that Frames 143 and 144 were not taken in correct sequence mode. The medium-resolution frames were taken in slow sequence mode. This fact will be further verified as more frames from Site 1-6 are anal-

This analysis supports the theory that the focal-plane shutter was triggered by "Film Clamp and Vacuum Draw Motor On" current pulse. The analysis has also revealed other discrepancies for which there is no explanation at this time. The data gathered so far is listed in Table 2.7-1.

It should be noted also that the malfunction of the focal-plane shutter in some cases resulted in an offset of the principal point of the high-resolution frames from its nominal position in the center of the corresponding 80-mm-lens frame. In a few instances, the timing error resulted in the 610-mm-lens frame being completely outside the area covered by the 80-mm lens.

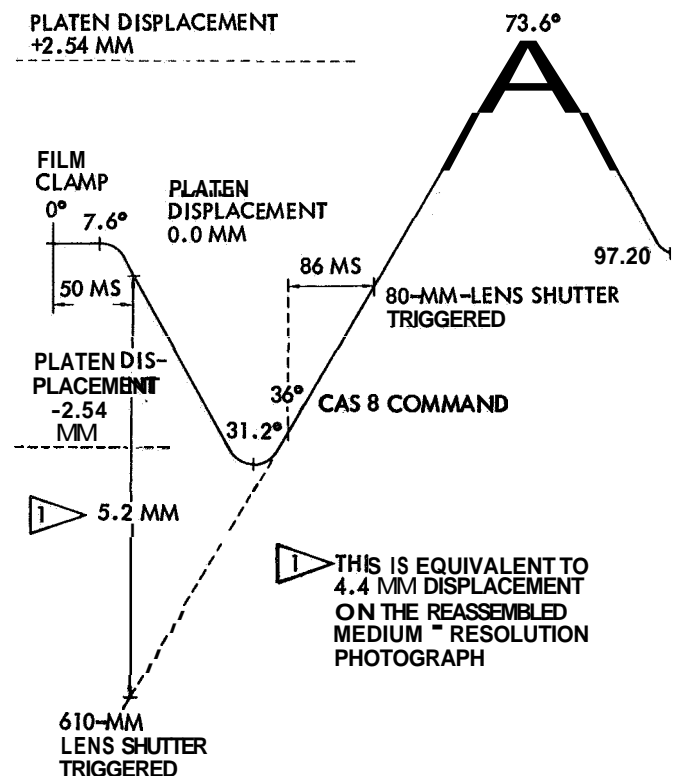


Figure 2.7-1: Shutter Trigger Positions in the IMC Cycle

FRAME NO.	SHUTTER SPEED	SMEAR (CM)	DISPLACEMENT (CM)	FRAME NO.	SHUTTER SPEED	SMEAR (CM)	DISPLACEMENT (CM)	FRAME NO.	SHUTTER SPEED	SMEAR (CM)	DISPLACEMENT (CM)
76				123	0.02	0.45	0.36	169		0.42	0.31
77				124	0.02	0.45	0.33	170		0.43	0.40
78				125	0.02	0.56	0.38	171		0.55	0.38
79				126				172		0.50	0.33
80				127	0.02	0.50	0.26	173			
81				128	0.02			174	MED. - & HI-RES. DARK		
82				129	0.02	0.45	0.29	175			
83				130	0.02	0.42	0.36	176			
84				131	0.02	0.43	0.41	177			
85				132	0.02	0.41	0.42	178			
86				133	0.02	0.43	0.35	179			
87				134				180			
88				135				181		0.20	1.82
89				136				182		0.48	0.35
90				137				183		0.55	0.35
91				138				184	HI. RES. EARLY		
92				139				185		0.55	0.32
93	0.04	0.88	0.41	140				186		0.53	0.33
94	0.04	0.85	0.36	141	HI. RES. EARLY			187		0.24	1.71
95	0.04	0.85	0.35	142				188		0.30	1.69
96				143		0.25	12.85	189			
97				144		0.47	12.65	190			
98				145				191			
99				146				192		0.50	0.36
100				147				193			
101				148				194			
102				149				195		0.55	0.34
103				150				196		0.50	0.35
104	0.02	0.42	--	151				197			
105	HI. RES. EARLY			152				198			
106				153				199			
107				154				200	HI. RES. EARLY		
108				155		0.71	0.21	201		0.51	0.34
109				156		0.46	0.24	202		0.47	0.33
110				157				203		0.55	0.40
111				158				204		0.55	0.38
112				159				205		0.41	0.43
113	0.04	0.25	0.11	160				206		0.46	0.41
114				161				207		0.45	0.38
115				162				208		0.44	0.37
116				163				209		0.46	0.33
117				164				210		0.45	0.36
118	HI. RES. EARLY			165				211		0.46	0.32
119	0.02	0.54	0.35	166				212		0.47	0.33
120		0.23	1.61	167		0.40	0.25	213		0.47	0.30
121	0.02	0.50	0.30	168		0.55	0.33	214		0.46	0.37
122	0.02	0.42	0.35					215		0.27	1.93

Table 2.7-1: Smear and Displacement Data

8/16/67

"The aeronautical and space activities of the United States shall be conducted so as to contribute . . . to the expansion of human knowledge of phenomena in the atmosphere and space. The Administration shall provide for the widest practicable and appropriate dissemination of information concerning its activities and the results thereon."

—NATIONAL AERONAUTICS AND SPACE ACT OF 1958

NASA SCIENTIFIC AND TECHNICAL PUBLICATIONS

TECHNICAL REPORTS: Scientific and technical information considered important, complete, and a lasting contribution to existing knowledge.

TECHNICAL NOTES: Information less broad in scope but nevertheless of importance as a contribution to existing knowledge.

TECHNICAL MEMORANDUMS: Information receiving limited distribution because of preliminary data, security classification, or other reasons.

CONTRACTOR REPORTS: Scientific and technical information generated under a NASA contract or grant and considered an important contribution to existing knowledge.

TECHNICAL TRANSLATIONS: Information published in a foreign language considered to merit NASA distribution in English.

SPECIAL PUBLICATIONS: Information derived from or of value to NASA activities. Publications include conference proceedings, monographs, data compilations, handbooks, sourcebooks, and special bibliographies.

TECHNOLOGY UTILIZATION PUBLICATIONS: Information on technology used by NASA that may be of particular interest in commercial and other non-aerospace applications. Publications include Tech Briefs, Technology Utilization Reports and Notes, and Technology Surveys.

Details on the availability of these publications may be obtained from:

SCIENTIFIC AND TECHNICAL INFORMATION DIVISION
NATIONAL AERONAUTICS AND SPACE ADMINISTRATION

Washington, D.C. 20546